



HAL
open science

Plasma catalytic process for CO₂ methanation

Magdalena Nizio

► **To cite this version:**

Magdalena Nizio. Plasma catalytic process for CO₂ methanation. Catalysis. Université Pierre et Marie Curie - Paris VI, 2016. English. NNT : 2016PA066607 . tel-01612734

HAL Id: tel-01612734

<https://theses.hal.science/tel-01612734v1>

Submitted on 8 Oct 2017

HAL is a multi-disciplinary open access archive for the deposit and dissemination of scientific research documents, whether they are published or not. The documents may come from teaching and research institutions in France or abroad, or from public or private research centers.

L'archive ouverte pluridisciplinaire **HAL**, est destinée au dépôt et à la diffusion de documents scientifiques de niveau recherche, publiés ou non, émanant des établissements d'enseignement et de recherche français ou étrangers, des laboratoires publics ou privés.

Université Pierre et Marie Curie

Ecole doctorale 391 : Sciences Mécaniques, Acoustique, Electronique et
Robotique de Paris

IRCP, UMR 8247 (CNRS-Chimie ParisTech)/Equipe Procédés, Plasmas, Microsystèmes

Institut Jean Le Rond d'Alembert, CNRS, UMR 7190, Sorbonne Universités, UPMC, Univ. Paris 6

Plasma Catalytic Process for CO₂ Methanation

Par MAGDALENA NIZIO

Thèse de doctorat en : Chimie - Génie des Procédés

Dirigée par CAVADIAS Simeon et DA COSTA Patrick

Présentée et soutenue publiquement le 06 octobre 2016

Devant un jury composé de :

Mme. FECHETE Ioana	Chercheur Associée, HDR Université de Strasbourg	Rapporteur
M. KHACEF Ahmed	CNRS Ingénieur de Recherche HDR, CNRS - Université d'Orléans	Rapporteur
M. AMOUROUX Jacques	Professeur Emérite des Universités, Chimie ParisTech / UPMC	Examineur
Mme. AREFI-KHONSARI Farzaneh	Professeure des Universités UPMC Sorbonne Universités	Examineur
M. GARIN François	Directeur de Recherche Emérite Université de Strasbourg	Examineur
M. CAVADIAS Simeon	Professeur des Universités UPMC Sorbonne Universités	Directeur de thèse
M. DA COSTA Patrick	Professeur des Universités UPMC Sorbonne Universités	Directeur de thèse

Acknowledgments

When the defined nature of obtaining a PhD requires the individual to perform work, it can never be successfully finished without the help and support of an entire network of people. From staff, faculty, colleagues, friends, and family, one needs all of these people to the end a PhD study. I would like to take this opportunity to sincerely thank all of people that have helped me over this journey.

First and foremost, heartfelt gratitude is due to my supervisors, Professor Simeon Cavadias and Professor Patrick da Costa, for allowing me to pursue a research area about plasma catalytic process for CO₂ methanation. They gave me incentive and support to perform this research. They provided enough freedom for me to investigate and explore my dissertation topic independently, while still providing enough guidance to keep me from losing my way. I extremely appreciate all the professional and personal advice. Thanks for your constant attention, for teaching me, for trusting me, for being patient and listening me, for transmitting me your knowledge, love and passion towards catalysis and plasma and for a hundred thousand other reasons. Both of you have given over the years, an exceptional example of what it means to be a good leader and mentor.

In addition to my advisors, my dissertation committee members Professor Jacques Amouroux who the first to promote the idea that CO₂ should be considered as raw material and rather than only a waste product from combustion processes. For the past few years he has been frequently invited to give lectures and participate in many conferences around the world to point out that carbon dioxide is a major raw material for sustainable development and energy storage. Thanks to the enormous amount of work and commitment Professor Amouroux gave to the CEOPS project it was launched and financed by EU. He has also offered his time and support to enable me to complete my research project. I am profoundly grateful for his readiness to meet and discuss any hindrance I experienced throughout my research, offering his invaluable knowledge to help me along the way. This project has been significantly enhanced by the amazing team of faculty at my disposal.

I would like to express my gratitude to the organization which partially provided funding my doctoral degree: the European programme called CEOPS (CO₂-loop for Energy

storage and conversion to Organic chemistry Processes through advanced catalytic Systems). This program has made it possible for me to obtain some great results for my thesis.

Very special thanks to the UPMC University (ED 390 - Génie des procédés et technologies avancées and ED 391 - Sciences Mécaniques, Acoustique, Electronique et Robotique) for giving me the opportunity to carry out my doctoral research and for their financial support.

Furthermore, I would like to extend my thanks to the other members of the committee, for Professor Arefi-Khonsari Farzaneh, Doctor HDR Fehete Ioana, Doctor HDR Khacef Ahmed and Directeur de Recherche Emérite Garin François offering their time to read my thesis and the precious advice on this work.

An equally heartfelt of thanks to Maria Elena Galvez, who has provided me a functional and enormously helpful understanding in the catalytic aspects of my research. Her enthusiasm and willingness in helping me plan my experiments really inspired me to give my best.

I would also like to thank Stéphanie Ognier, for all her cooperation, active participation in the project, for great help of experimental set-up and the operation of instruments, advice on calculations and her kind support during my research work.

I would like to thank Professor Michael Tatoulian, director of the 2PM team, for giving me the possibility of carrying out this project in his laboratory, his invaluable assistance and overall support. His guidance has been invaluable and will continue to serve me well throughout my career.

Special thanks to Professor Carlos Henriques and Dr Teresa Andreu, my workmates from the CEOPS project, for their friendship and interest of my work.

Additionally, I would like to thank fellow graduate PhD student Radoslaw Debek. He was gracious enough to offer his time to fabricate the catalysts used in my experiments. Without his readiness to help I would not have been able to test the effect of catalysts in my plasma system, and for that I am very thankful.

A huge “Thank you” to Rafik Benrabbah, Bradley Da Silva, Alexandre Ma, for teaching and helping me during the first month I arrived to the department and at the end of my PhD.

Special thanks to Bruno Pelat, for his help in the laboratory and with the characterization instruments. Bruno has always kept an open door, willing to help with any technical problem I might have.

I would like to thank Frederic Rousseau, Cédric Guyon, Daniel Morvan, Isabelle Mabilite and Guillaume Schelcher for their kind support, for providing valuable suggestions and for being very nice to me.

When I joined to the Procédés, Plasmas, Microsystèmes (2PM) team in Chimie ParisTech and the laboratory Jean Le Rond d'Alembert (UPMC) located in Saint-Cyr-L'Ecole, I was introduced to a group of intelligent and accomplished people. For those who were senior students when I arrived and have since become doctors and others staff faculty, Erik Martinez, Mengxue Zhang, Dhia Ben Salem, Diane Gumuchian, Simeon Léoment, Rao Xi, Maxime Cloutier, Olivier Lasage, Ines Hauner, Charlotte Rasser, Julien Wengler, Safwan Al Ayoubi, Jonathan Cramer, Aurélien Lepoetre, Charles Cavaniol, Dorota Matras, Stuart Cameron, Sandrine Duong, Acacio Mendes, Adrien Albarazi, Muhammad Kashif, Gianlong Wang, Elza Rodrigues, Johnny Abboud, Maya Daou, Alexis Matynia, Agnes Jocher, George Xie, Jean-François Krawczynski, Jerome Pequin, Jérôme Bonnety, Guillaume Legros, thank you for creating a nice environment where we are all encouraged to help and learn from one another. You were all willing to help me become accustomed to the many various aspects of experimental research when I was just a 'newbie' and I appreciate your kindness. Also, I would like to thank the other kind people that helped me in the lab and so on.

Also students contributed with their research practicals to this work, which I would like to thank them very much for. It is difficult to mention all, I would like to particularly mention Mateusz Krzak, Massimiliano Manca and Semen Marsov.

Additionally, I would like to thank Jean Le Rond d'Alembert (UPMC) technical staff for helping me in various ways, especially Dominique Busquet.

Many thanks go out to the administrative staff of both laboratory from Evelyne Mignon, Fatiha Abdennebi, Nathalie Ouvry for all of their hard work behind the scenes.

I would like to express my special thanks of gratitude to my English teacher and friend, Barbara Dulba, who helped me along the way and spent many hours on reading and checking this thesis, I am really thankful.

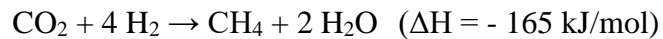
In my personal life, I would like to thank my family and close friends. They have been with me long before I began the PhD program and will continue to give support long after. I would not be where I am today without the determination and character inculcated in me by my parents. Thank you for all that you have done and all that you continue to do.

Of course I cannot forget my lifelong friends, Magdalena Makuch, Monika Bzdryra; Dominka Jagielska, Malgorzata Adamowska-Teyssier, Anna Obszyńska, Joanna Skrobacz and Veronica Olsen. Thank you for your irreplaceable and unconditional friendship.

Lastly, my deepest thanks belongs to my best friend and special person in my life, Sebastian. You have kept me balanced and reasonable during this way and I am extremely grateful to have you in my life. Thank you for being the unique person that you are.

Abstract

The limited resources of oil and natural gas, together with an increasing energy demand, has been forcing us to seek more and more efficient and cleaner energy production alternatives. Hydrogen has been recently considered as a promising energy carrier. However, there are several inherent problems with the utilization of H₂, from its transportation to its distribution. Transformation of the H₂ molecule by fixing into a carbon-containing compound, i.e. CH₄, will offer the possibility of using the conventional transportation network. Indeed, the Sabatier reaction, which is highly exothermic, involves the reaction of carbon dioxide and hydrogen gas in order to produce methane and water:



This process, called methanation, represents a feasible approach contributing to the reduction of the CO₂ emissions in our atmosphere, through a closed carbon cycle involving the valorization of CO₂, i.e. from capture.

Currently, this reaction is performed in the presence of a Lewis acid catalyst at atmospheric pressure and in a temperature range between 200-600 °C. At a temperature below 200 °C, the conversion of CO₂ to CH₄ is close to zero. While at a temperature above 350 °C, the secondary reaction, i.e. the reverse water gas shift reaction, with formation of CO becomes predominant. Consequently, the methane selectivity decreases and the main products of this reaction are CO and H₂. The water (Lewis base) present in the reaction products blocks the active sites of the catalyst. That is why, one of the ways to desorb water from the surface of the catalyst resides in the increase of the reaction temperature. However, this solution may result in the deposition of carbon and to the catalyst deactivation (the catalyst time of stream is generally estimated between 5000 and 7500 hours). Therefore, it is important to find an adapted process for the production of methane at atmospheric pressure and at a relatively low temperature.

Compared to the conventional processes currently used at temperatures higher than 450 °C, which exhibits a conversion of CO₂ to CH₄ around 80 % and a methane selectivity higher than 95 %, the desired process should display the same conversion and selectivity at low temperatures. The choice of an adapted reactor and an accurate catalyst for this process is of great importance. The catalyst should be active, selective, stable, low-cost and easy to elaborate.

In this work, production of methane is performed by the coupling of a plasma reactor (DBD - dielectric barrier discharge) with a catalyst system. DBD catalytic reactors require very low consumption of electricity power, less than 12 kJ/mole of CH₄ and, at the same time, they meet all the requirements for a large volume methane production.

Desorption of water at low temperatures (100-160 °C) is achieved through the use of non-thermal plasmas which enable the increase of the catalyst time of stream. According to the literature, a catalyst can behave as either an acid or a base of Lewis. Thus, CO₂ can be adsorbed on a Lewis base site through the carbon while oxygen can be adsorbed to a Lewis acid site; leading to the production of a water molecule. The use of catalysts activated by DBD plasmas can eliminate all the drawbacks encountered in the typical Sabatier reaction (heating the catalyst leading to the deposition of carbon) and can enhance the methanation reaction at low temperatures with a good yield. This is the reason why new catalysts and process conditions are continuously being investigated in order to maximize the methane selectivity at low reaction temperatures and at atmospheric pressure.

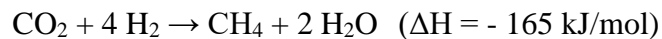
Since the reaction is exothermic, the catalyst structure and composition have an influence on the kinetic of the reaction. Ceria-zirconia oxides have recently been considered as promising catalyst supports in the preparation of active and selective catalytic systems for CO₂ methanation.

The nickel-based catalysts supported on ceria-zirconia mixed oxides (Ce_xZr_{1-x}O₂) and also hydrotalcite, zeolites and mesoporous ceria-zirconia composites have been selected for CO₂ methanation. These materials show different porosity and a large specific surface area as well as a good thermal stability. The catalysts were doped with cerium oxide to provide the storage and mobility of oxygen. Therefore, the proposed catalytic systems help ensure a good thermal and electrical conductivity both in the adiabatic and isothermal conditions. In this system, the activation of catalysts by plasma is paramount. The electrical energy supplied to the catalyst via a high voltage sinusoidal current (14 kV) produces streamers, which are responsible for the positive or negative polarization of catalytic sites. The polarization leads to the adsorption of reactants and desorption of the reaction products (mainly water) at low temperatures (<200 °C); without polarization, the temperatures are higher (between 300 and 420 °C).

The results obtained in the adiabatic conditions at low temperatures, ranging between 100-150 °C, in the presence of catalysts activated by plasma are promising. Indeed, the conversion of CO₂ to CH₄ is about 85 % with selectivity close to 100 % (reaction conditions: 20 vol% CO₂, 80 vol% H₂). The same conversion in the absence of the plasma activation of the catalyst is observed at 350 °C. At low temperatures (120-150 °C) and without plasma, conversion is almost close to zero. This low consumption energy system helps reduce the cost of production of synthetic methane together with an extended life of the catalyst. The technological approach presented in this thesis could be used on an industrial scale. Indeed, the flexibility of the production system allows the use of electrical energy produced off-peak (<30 €/MWh) or from the excess production coming from renewable sources. For this reason, not only does that process help to produce synthetic methane but it also significantly reduces carbon dioxide emissions in the atmosphere.

Résumé

Combiné à une demande en énergie croissante, les ressources limitées de pétrole et de gaz naturel nous obligent à rechercher des alternatives plus propres et de plus en plus efficaces à la production d'énergie. L'hydrogène (H₂) a récemment été considéré comme un vecteur énergétique prometteur. Cependant, il existe plusieurs problèmes liés à l'utilisation de H₂, depuis son transport jusqu'à sa distribution. La transformation de la molécule de H₂ peut s'effectuer par la synthèse d'un composé contenant du carbone, à savoir du méthane (CH₄), offrant ainsi la possibilité d'utiliser le réseau de transport classique. En effet, la réaction de Sabatier, qui est fortement exothermique, implique la réaction du dioxyde de carbone (CO₂) et du dihydrogène afin de produire du méthane et de l'eau:



Ce procédé, appelé méthanation, représente une approche réalisable contribuant à la réduction des émissions de CO₂ dans l'atmosphère, à travers un cycle fermé du carbone impliquant la valorisation du CO₂.

Actuellement, cette réaction s'effectue en présence d'un catalyseur de type acide de Lewis à pression atmosphérique et dans un domaine de température compris entre 200 et 600 °C. A une température inférieure à 200 °C, la conversion du CO₂ en CH₄ est quasi-nulle. Tandis qu'à une température supérieure à 350 °C, une réaction secondaire, la réaction du gaz à l'eau ou réaction de Dussan, impliquant la formation du monoxyde de carbone (CO) devient prédominante. Par conséquent, la sélectivité du méthane diminue et les produits principaux issus de cette dernière sont le CO et l'hydrogène. L'eau (base de Lewis), présente dans les produits de la réaction, bloque les sites actifs du catalyseur. Par conséquent, une augmentation de la température de réaction permettrait de désorber l'eau de la surface du catalyseur. Cependant, cette solution envisageable conduirait à un dépôt de carbone et par la suite, à la désactivation des catalyseurs (dont la durée de vie est généralement comprise entre 5000 et 7500 heures). Il est donc primordial de trouver un procédé permettant de produire le méthane à pression atmosphérique et à une température relativement basse.

Par rapport aux procédés conventionnels opérant à des températures supérieures à 450 °C, le procédé désiré devra conduire à la même conversion du CO₂ en CH₄ (> 80 %) et à la même sélectivité (> 95 %) mais à des températures plus basses. Le choix d'un réacteur et

d'un catalyseur, pour ce procédé, est important. Le catalyseur doit être actif, sélectif, stable, peu coûteux et facilement mis en forme. C'est dans cette optique que s'inscrit cette thèse avec la production du méthane réalisée par un couplage plasma DBD (décharge à barrière diélectrique)/catalyseur. Ce procédé nécessite une très faible consommation de puissance électrique inférieure ainsi qu'une faible dépense énergétique pour la production de CH₄ (12 kJ/mol). Dans le même temps, ce procédé présente toutes les exigences pour une production de grands volumes de méthane.

La désorption de l'eau à basse température (120-160 °C) est réalisée grâce au plasma non thermique permet ainsi de travailler à une plus faible température et d'augmenter la durée de vie du catalyseur. D'après la bibliographie, un catalyseur peut se comporter en tant qu'un acide ou une base de Lewis. Par conséquent, la molécule de CO₂ peut donc s'adsorber sur un site basique à travers une liaison carbone tandis que l'oxygène peut s'adsorber sur un site acide, conduisant ainsi à la production d'une molécule d'eau. L'application des catalyseurs activés par plasma DBD permet d'éliminer tous les inconvénients rencontrés lors la réaction typique de Sabatier (chauffage du catalyseur conduisant au dépôt de carbone) et de réaliser cette réaction à basse température avec un bon rendement. C'est la raison pour laquelle de nouveaux catalyseurs et les conditions opératoires du procédé sont sans cesse à l'étude afin de maximiser la sélectivité au méthane à des basses températures et à pression atmosphérique.

Etant donné que la réaction est exothermique, la structure et la composition du catalyseur vont influencer la cinétique de la réaction. Les oxydes de Cérium-Zirconium ont récemment été considérés comme des supports de catalyseurs prometteurs pour la préparation de systèmes catalytiques actifs et sélectifs pour la méthanation du CO₂.

Les catalyseurs à bases de nickel supportés sur des oxydes mixtes de Cérium-Zirconium (Ce_xZr_{1-x}O₂) mais également supportés sur des hydrotalcites, des zéolites ou encore sur des oxydes mésoporeux ont été sélectionnés pour notre procédé. En effet, ces matériaux présentent des porosités différentes ainsi qu'une grande surface spécifique et une bonne stabilité thermique. Ces catalyseurs ont été dopés par l'oxyde de cérium afin d'assurer le stockage et la mobilité de l'oxygène. Les systèmes catalytiques proposés dans cette thèse permettent ainsi de garantir une bonne conductivité thermique et électrique tant dans les conditions adiabatiques que dans les conditions isothermiques. Dans un tel système, l'activation du catalyseur par plasma est primordiale. L'énergie électrique fournie au catalyseur via un courant sinusoïdal à

haute tension (14 kV), produit des 'streamers', responsables de la polarisation positive ou négative des sites catalytiques. La polarisation conduit à l'adsorption des réactifs et à la désorption des produits de la réaction (essentiellement de l'eau) à basse température (<200 °C). Sans polarisation, les températures sont plus élevées et sont comprises entre 300 et 420 °C.

Les résultats obtenus dans des conditions adiabatiques à basses températures (comprises entre 120 et 150 °C), sont prometteurs. La conversion du CO₂ en CH₄ est d'environ 85 % avec une sélectivité proche de 100 % (le rapport des gaz initiaux étant de 20%vol. pour CO₂ et de 80%vol. pour H₂). Cette même conversion en l'absence de catalyseur activé par plasma, est observée à 350 °C. A basses températures (120-150 °C) et sans plasma, la conversion est presque nulle. Ce système à basse consommation d'énergie permet donc de diminuer le coût de production du méthane synthétique avec une durée de vie du catalyseur prolongée. L'approche technologique présentée précédemment pourrait donc être utilisée à l'échelle industrielle. En outre, la flexibilité du système de production permet d'utiliser l'énergie électrique produite aux heures creuses (<30€/MWh) ou encore d'utiliser l'excédent de production provenant des ressources renouvelables. Ce procédé permet non seulement de produire le méthane synthétique mais également de diminuer significativement les émissions de CO₂ dans l'atmosphère.

Contents

Acknowledgments	2
Abstract	6
Résumé	9
Chapter 1: Methanation Reaction and Plasma	18
1. Introduction	18
2. Properties, Thermodynamics and Reactivity of CO ₂	25
2.1. Current Uses of CO ₂	30
3. Literature Review	31
3.1. Methanation and Catalysis	31
3.1.1. The Factors of Choosing Catalysts for CO ₂ Methanation	35
3.1.2. Catalysts Poisoning and Deactivation Phenomena.....	38
3.2. Reactor Aspects	44
3.2.1. Fixed bed Reactors	45
3.2.2. Fluidized Bed Reactors.....	53
4. Reaction Mechanisms	55
4.1. Proposed Reaction Mechanisms for the CO ₂ Methanation Involving the Conversion of CO ₂ to CO Prior to the Methanation Process	56
4.2. Proposed Reaction Mechanisms for the CO ₂ Methanation Involving the Direct Hydrogenation of CO ₂ to CH ₄ Without Forming CO as an Intermediate.....	59
5. Hybrid Plasma-Catalytic Methanation	60
5.1. Introduction to Plasma	60
5.2. Applications of Plasma	63
5.3. Different Types of Plasma	64

5.3.1.	Plasma Generation	65
5.4.	Types of Discharges	70
5.4.1.	Streamers	71
5.4.2.	Plasma From Constant DC Potential	73
5.4.2.1.	Corona Discharges	73
5.4.2.2.	Glow Discharges	75
5.4.2.3.	Arc Discharges	76
5.4.3.	Plasma From AC Potential	76
5.4.3.1.	Dielectric Barrier Discharge (DBD)	77
5.4.4.	Plasma From Radio Frequency Discharges	78
5.5.	Plasma-Catalysis Process	79
5.5.1.	Different Plasma-Catalyst Configurations.....	81
5.5.2.	Interaction Between Plasma and Catalysts	83
5.6.	Plasma-Catalytic Methanation	84
6.	Conclusions	89
Chapter 2: Experimental Set-up and Diagnostics		91
1.	Dielectric Barrier Discharge Methanation Setup Description.....	91
1.1.	Reactor System	93
1.2.	Temperature Measurement	94
1.3.	Plasma Generation System	95
1.3.1.	Energy or Power Measurement	95
1.3.2.	Gap.....	100
1.4.	Product Collection System.....	100

2.	Diagnostics	100
2.1.	Optical Emission Spectroscopy - In Situ Diagnostics	101
2.2.	Description of Gas Chromatography	102
2.2.1.	Calibration of Gas Chromatograph.....	105
2.2.2.	Calculation of Products	106
2.3.	Technical Properties of Fourier Transform Infrared (FTIR) Spectroscopy.....	106
2.3.1.	Vibrational Modes of CO ₂ and CH ₄	107
3.	Elaboration and Characterization of Catalysts	109
3.1.	Preparation of the Nickel Catalysts.....	109
3.1.1.	Synthesis of the Ni/Ce _x Zr _{1-x} O ₂ Catalysts	110
3.1.2.	Calcination.....	110
3.2.	Preparation of the Hydrotalcite Catalysts	110
3.3.	Reduction of Catalysts	112
3.4.	Catalysts Characterization	112
3.4.1.	Hydrogen Temperature Programmed Reduction (H ₂ -TPR).....	113
3.4.2.	Temperature Programmed Desorption of CO ₂ (CO ₂ -TPD).....	113
3.4.3.	X-Ray Diffraction (XRD).....	114
3.4.4.	Brunauer-Emmett-Teller (BET) Surface Area	114
3.4.5.	High-Resolution Transmission Electron Microscopy (HRTEM).....	115
4.	Experimental Results.....	115
4.1.	Preparation of the Reactor for Experiments.....	115
4.2.	Blank Test	116
4.3.	Tests in Presence and in Absence of Plasma	116

Chapter 3: A Screening Study	118
1. Historical Background of the Project	118
1.1. Concept and Scientific Objectives	119
1.1.1. Context and Concept	119
1.1.2. Scientific and Technical Objectives	121
2. Catalysts on Different Zeolites and Mesoporous Based Structures for DBD Plasma Catalysis.....	124
2.1. Zeolite Based Catalysts.....	125
2.1.1. Preparation and Characterization of Ni/USHY Catalysts.....	126
2.1.2. Preparation and Characterization of Ni-Ce/USHY Catalysts.....	129
2.1.3. Catalysts Optimisation.....	130
2.1.3.1. Drying Method (Oven vs. Microwave Irradiation).....	130
2.1.3.2. Effect of Pre-Reduction Temperature	132
2.1.3.3. Effect of the Acidity/Basicity of the Support	134
2.1.3.4. Effect of the Presence of EFAL Species.....	136
2.1.3.5. Effect of the Si/Al Ratio of the Zeolite.....	137
2.1.3.6. Final Formulation.....	139
2.1.4. Catalysts Testing.....	141
2.1.4.1. Catalytic Tests of the CO ₂ Hydrogenation, Under Classic Thermal Conditions (IST).....	141
2.1.4.2. Results in a Hybrid Plasma-Catalytic Methanation of CO ₂	145
2.1.5. Conclusions	147
2.2. Mesoporous Nickel-Ceria-Zirconia Based Catalysts.....	148
2.2.1. Preparation and Characterization of Mesoporous Ni/Ce _x Zr _{1-x} O ₂ Catalysts.....	148
2.2.2. Catalysts Testing.....	151

2.2.2.1. Catalytic Tests of CO ₂ Hydrogenation, Under Classic Thermal Conditions (IST)	151
2.2.2.2. The Results of Hybrid Plasma-Catalytic Methanation of CO ₂	153
2.2.2.2.1. GC Chromatograms	153
2.2.2.2.2. FTIR Spectra	154
2.2.2.2.3. Action of Plasma	156
2.2.3. Conclusions	158
Chapter 4: Hybrid Plasma Catalytic Process Using Ni Supported on Ceria-Zirconia Mixed Oxide Catalysts	160
1. Introduction	160
2. Catalyst Preparation and Characterization	162
3. Catalysts Testing	168
3.1. Blank Test	168
3.2. Catalytic Activity Towards Methanation in Absence of Plasma (Plasma Off)	169
3.3. Hybrid Plasma Catalytic Methanation	170
3.3.1. Evolution of the Active Ni Phase During the Methanation Reaction	172
3.4. In Situ Diagnostics - Optical Emission Spectroscopy (OES)	174
3.4.1. Optical Emission Spectra for DBD Plasma Discharge in the Empty Reactor	174
3.4.2. Optical Emission Spectra for DBD Plasma Discharge With Catalyst	176
3.4.3. Influence Plasma Parameters	178
3.5. Reaction Mechanism Proposal	179
3.5.1. Introduction	179
3.5.2. Plasma-Enhanced Water Desorption	184
3.5.3. Plasma-Enhanced Catalysis	185
3.5.4. Methanation of CO ₂ (Plasma catalysis)	187

3.5.4.1. Isothermal Conditions: Temperature Range Between 250-450 °C at Atmospheric Pressure	193
3.5.4.2. Adiabatic Conditions: Results at Room Temperature at Atmospheric Pressure	194
4. Conclusions	195
Chapter 5: Hydrotalcite Catalysts for Hybrid Plasma Methanation Process	196
1. Introduction	196
2. Catalyst Preparation and Characterization	198
3. Catalysts Testing	201
3.1. Activity Towards Methanation in the Absence of Plasma (Plasma Off).....	201
3.2. Hybrid Plasma-Catalytic Methanation (Plasma On).....	203
4. Conclusions	204
References	206
General Conclusions and Perspectives	218
Appendix A	221
Appendix B.....	223
Appendix C	226
Appendix D	233

Chapter 1: Methanation Reaction and Plasma

1. Introduction

Energy generated by renewable energy is crucial to different aspects of global human development, such as employment, ecosystems and environmental protection. As the demand for energy continues to increase worldwide, overcoming energy barriers is a key step in the further development of civilization [1]. Moreover, economic development (chemical industry, power plants) is practically dependent of fossil fuels, which are non-renewable energy sources [1-3]; and yet fossil fuels constitute still more than 85 % of the world energy consumption. Since the industrial revolution, the consumption of fossil fuels has accounted for the majority of anthropogenic CO₂ emissions [4], resulting in environmental pollution and very presumably in an increasing global warming effect [1].

Reducing carbon dioxide emissions has been a serious concern for many years. Carbon dioxide is very important greenhouse gas, which are emitted into the atmosphere from fossil fuels combustion and anthropogenic activities. The yearly emissions of CO₂ have grown between 1970 and 2004 by about 80 % from 21 to 39 gigatons. The growing concentration of CO₂ in the atmosphere increased the impact on the environment by forcing a climate change. Nowadays, 20 % of the overall CO₂ emissions come from the energy generation [5]. Renewable sources have been the most popular option for the use of clean energy and reduction of carbon dioxide emissions. In spite of the growing adaptation of energy from renewable sources, green fuels cannot compete versus mature technologies of fossil fuels in categories of price. Several petrochemical companies are considering biomass and natural gas fuel sources as alternatives of renewable feedstock. The mitigation of greenhouse gas emissions is also an interesting challenge in investigating new concepts and new opportunities for catalysis and industrial chemistry. Recently, different carbon capture and storage technologies (CCS) have been developed for a significant reduction of CO₂ emissions into the atmosphere [6]. These technologies are mainly adequate to capture CO₂ from large industrial sources, such as fossil fuels fired power plants. However, only with such efforts it is not possible to reduce and control CO₂ emissions [7]. Also the availability of sufficient storage capacity to capture carbon dioxide is also still an open question. Little attention has been paid by the industry and scientific circles in utilization of CO₂ because of its high thermodynamic stability. For the reduction of

greenhouse gas emissions, various strategies have been proposed that include promoting the energy end-use efficiency, supporting the use of renewable energy resources as well as the set up for a sustainable transportation and waste management [8]. One effective approach to diminish the CO₂ accumulation into the atmosphere is to recover carbon dioxide from flue gases and its recycling by converting it into useful chemicals [9, 10]. For the long term goals, the conversion of CO₂ should be used as an alternative to petrochemistry and as a bridging technology towards the development of a sustainable energy supply and consequently, a sustainable industrial development [1, 11]. The process for the CO₂ valorization has been known for many decades and consists in converting it into chemical products such as: the synthesis of salicylic acid [2, 12], the synthesis of NaHCO₃-Na₂CO₃ (Solvay process) [13] and the synthesis of urea [14]. Moreover, in 1970 [2], the catalytic conversion of CO₂ to synthesize methanol from syngas enriched with CO₂ was first developed [1]. The valorization of CO₂ by its conversion into other chemicals was discussed [1-4]. Then, a hopeful approach for the valorization of CO₂ was the catalytic conversion of CO₂ into fuels: MeOH, DME, CH₄ (synthetic natural gas-SNG) and syngas [1]. The conversion of CO₂ to CH₄ by catalytic hydrogenation has been recognized as a very promising process. The need for renewable energy storage has generated much interest in the fixation of carbon dioxide through the CO₂ methanation.

In this review, focus is given on the CO₂ methanation that involves the catalytic hydrogenation of carbon oxides in order to provide an efficient alternative to conventional natural gas [15]. Moreover, the infrastructure for handling CH₄ is well adopted [1]. The development of appropriate catalysts for the conversion of CO₂ has been under intensive study by researchers around the world [1, 16-21]. Nevertheless, supported nickel catalysts are the most studied for CO₂ methanation due to their high ability to dissociate CO₂. Their higher activity and selectivity for methane have been ascribed to various factors, such as the nature of the support and metal, amount of metal and its dispersion [1]. However, these catalysts overcome several drawbacks, including sensitivity to metal site poisoning, sintering, coke deposition, and deactivation [1, 22, 23].

Indeed, it is well known that during the CO₂ methanation, the presence of water in the products leads to the sintering of Ni particles, which results in a deactivation of the catalysts. Likewise, the secondary reactions favour the CO and H₂ formation at higher temperatures (>300 °C). In order to overcome all the previously mentioned drawbacks, a hybrid combination

of catalysts coupled to a Dielectric Barrier Discharge (DBD) plasma can be applied. J. Amouroux et al. [24] studied a process for the carbon dioxide reduction to methane by a DBD plasma activated catalyst. They showed that under adiabatic conditions, a DBD plasma was able to greatly improve the conversion of CO₂ at low temperatures. A DBD plasma which produces a variety of active species, can be efficient for assisting catalytic methanation. The latter was applied to the CO methanation [25]. Jwa et al. [26] evaluated the CO methanation activity of Ni-zeolite catalysts and found that a DBD plasma can enhance the rate using a coupled plasma catalytic process.

The main greenhouse gases, which can be indicate are: water vapour (H₂O), carbon dioxide (CO₂), methane (CH₄), nitrous oxide (N₂O), hydrofluorocarbons (HFCs), perfluorocarbons (PFCs), and sulphur hexafluoride (SF₆). Moreover, CO₂ contributes to about 77 % to the world's greenhouse gas emissions (excluding water vapour) into the atmosphere in 2004 [27].

Many industrial manufacturing processes release carbon dioxide to the atmosphere, e.g. from the manufacturing of gas synthesis and combustion processes. Thus, the vented CO₂ molecule causes an increased concentration in the atmosphere. Global warming is caused by this accumulation of CO₂ in the atmosphere. These emissions should be monitored if the problem of global warming needs to be controlled.

The two main sources of CO₂ emissions within the industrial sector are manufacturing processes of industrial products where CO₂ is obtained as a by-product and from energy supply by the combustion of fossil fuels. Valorisation of CO₂ emissions represents a main stake of competitiveness for large CO₂ emitters, generally for the cement industry.

Despite increasing investments in low-carbon energy alternatives and the progressive introduction of renewable energy resources, the consumption of fossil fuels is still assumed to significantly grow due to increasing worldwide energy and electricity demands caused partially by the emergence of new economic powers in the world. As the overall carbon footprint of the predicted demand would exceed 40 Gt/year of CO₂ emissions by 2030 in comparison to 30Gt/year in 2010 [9]. From a CO₂ valorisation standpoint, scientific and industrial authorities are urged to suggest new schemes for producing and recycling carbon from fossil fuels for the energy market and chemical industry, in order to contribute to the reduction of environmental impacts. CO₂ transformation into added value products will promote the transition from carbon

fossil sources to low carbon foot-print ones. To this end, the intensive industries such as cement industry (large emitters of CO₂), represent a non-exploited source of carbon. In 2009, the worldwide production of cement was 3048 Mt with 1.5-2 Gt of CO₂ emissions representing roughly 5 % of anthropogenic global CO₂ emissions.

Cement production processes emit large quantity of CO₂ (0,723 tCO₂ per ton of cement) coming from two main stages:

- during pre-heating, the major part of the decomposition of limestone CaCO₃ into lime CaO and CO₂ named "calcination" is responsible for 60-65 % of total CO₂ emissions,
- the clinkerisation step involves combustion of various fuels which generates additional CO₂ emissions (35-40 %).

The flue gas produced in a cement plant is released to atmosphere at 80 °C and 110 °C at atmospheric pressure through only one chimney stack, such chimney vents all CO₂ emissions from the plant. The flow rate and concentration (15-25 %) of the CO₂ at the chimney stack are relatively constant over time compared to fossil fuel power plants. Actually, cement plants generally run at full load, facilitating the capture step. The associated flow rate for cement work usually ranges from 200 000 to 500 000 Nm³/h.

For the most of recycling processes, the CO₂ flow has to be purified and concentrated. After the capture stage, the concentration of CO₂ is higher than 90 %, ready for geological storage or to be recycled into added value chemicals.

Increased concentrations of greenhouse gases in the atmosphere increases the greenhouse effect that has an adverse effect on climatic changes. Carbon dioxide emissions from anthropogenic sources should be mitigated. More effective conversion and utilization of carbon dioxide is a potential solution to reduce these emissions.

In 2016, the analysis of world energy-associated carbon dioxide emissions with the consumption of fossil fuels indicates that coal is the largest source of carbon dioxide (13.5 billion metric tons), followed by liquid fuels (12.0 billion metric tons) and natural gas (8.0 billion metric tons) [28] (Fig. 1). In addition, the global CO₂ emissions from fossil fuels combustion increase from nearby zero in 1870 to 32.0 billion metric tons in 2016 and are expected to increase up to 42 billion metric tons in 2035 [28]. In order to avoid CO₂ emissions,

different measures such as recovery, removal and storage have been proposed. Moreover, carbon capture and storage needs large amounts of energy for its capture, transportation and sequestration. The utilization of carbon dioxide in chemical conversion processes may become an important option for sustainable development, mitigation of carbon emissions and reversal of the global warming process.

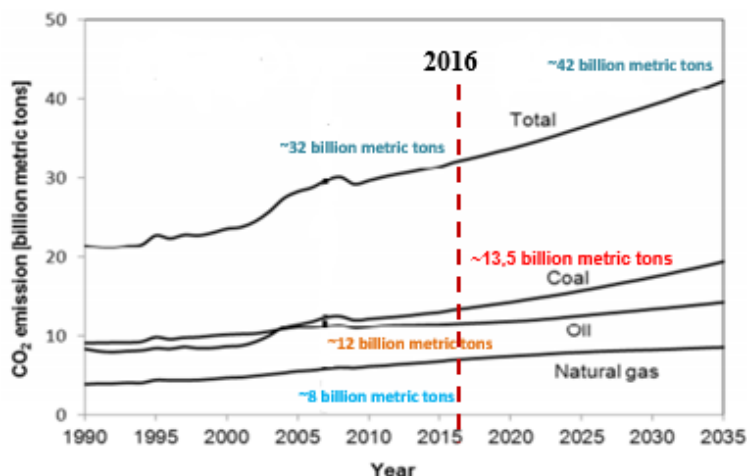


Fig. 1. The world energy-associated carbon dioxide emissions by the type of fuel (adapted and modified from [28]).

The utilization of CO₂ as a renewable raw material for the production of useful chemicals is an area of great interest. There are several reasons for producing chemicals from CO₂ whenever it is possible. CO₂ is a cheap, non-toxic and non-flammable feedstock that can often replace toxic chemicals such as phosgene. Therefore, it is a totally renewable feedstock compared to coal as the production of chemicals from CO₂ can lead to totally new materials such as polymers. New routes to existing chemical products could be more efficient and economical than current methods. The production of chemicals from CO₂ could have a small but positive impact on the global carbon balance [29].

Issues may appear on a number of promising new technologies that could contribute to the carbon dioxide emission reductions. All of them will have to overcome hurdles of economics and associated environmental impacts. Performance, cost, safety and low environmental impacts are some of the barriers that were identified to be able to prevent new technologies from becoming widely commercially used.

Until recently, CO₂ has not been used in its entire way of utilization. The use of selective reaction pathways and efficient catalysts are needed to favor the reaction rate. Surely, the chemical industry can only make some direct contribution towards the reduction of overall CO₂ emissions. Current estimations shows that, the chemical industry could contribute to convert around 1 % of the global CO₂ emissions into chemical products [6]. Table 1 reports the utilization of CO₂ in different chemical conversion processes.

Table 1. Industrial process utilization of CO₂ as a raw material for synthesis of organic compounds in 2006 [30].

Industrial processes that utilize CO₂ as raw material	World capacity per year [million tons]	Amount of fixed CO₂ [million tons]	Balance [%]
Chemical synthesis:			
Salicylic acid	0.07	0.025	0.04
Urea	143	105	87.61
Cyclic carbonates	0.08	0.04	0.05
Poly (propylene carbonate)	0.07	0.03	0.04
Fuel synthesis:			
Methanol	20	2	12.25
Synthetic natural gas	-	-	-
Other fuels	-	-	-

Table 1 shows that the amount of CO₂ utilized today for the production of organic chemicals and fuels (methanol) is small (around 100 million of tons) compared to today's global CO₂ emissions of around 30 billion of tons. Only around 10 % of the global crude oil consumption is used today in the chemical industry. It is often used as liquid fuels such as gasoline, diesel and heavy oil. Thereby, an effective use of CO₂ with regards to a visible reduction of the global emissions of CO₂ can be reached, if the CO₂ (e.g. separated from flue

gases) is utilized for fuels, for example, by methanation process. This reaction occurs at high temperatures where CO₂ is converted with H₂ into CH₄ and water and is known as the Sabatier reaction:



Several undesirable parallel and side reactions may also occur:

- the reverse water gas shift reaction:



- the Boudouard reaction:



- the Bosch reaction:



- the CO methanation reaction:



Carbon dioxide can be used as a reactant or in a gas co-feed in different non-catalytic chemical processes and heterogeneous or homogeneous catalytic processes; as well as in other reactions like photochemical, photo-catalytic reduction and electrocatalytic conversion. Most of the processes are subjects of research at the laboratory scale, and only a few processes have reached a large-scale production.

Figure 2 is an easy way to show the range of reactions for CO₂. The latter can be used as the main molecule in reactions and also used as a source of either carbon or oxygen [31].

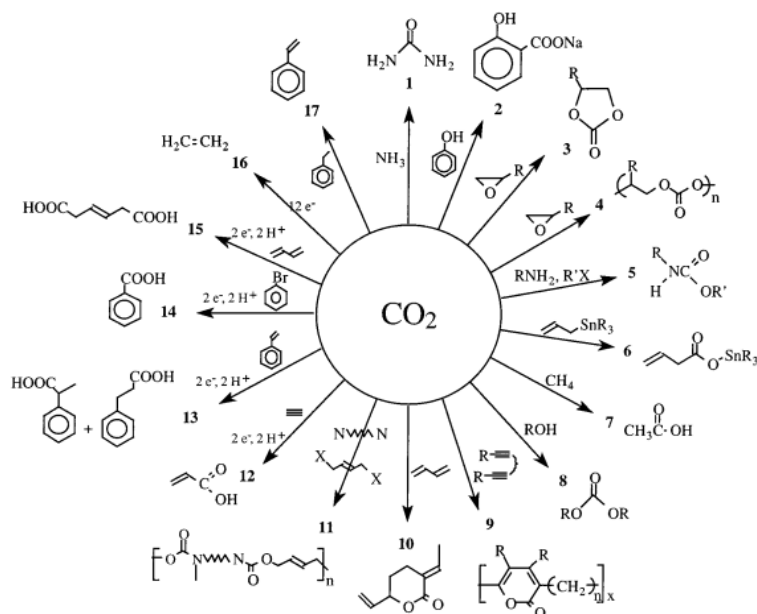


Fig. 2. Illustration of transformations of CO₂ [31].

This chapter offers a general idea about carbon dioxide valorization processes and reaction using CO₂ as a raw material. The catalytic methanation as well as the information about catalysis, reactors and reaction mechanisms for the CO₂ methanation will be presented. This part is also an introduction to plasma and plasma-catalytic processing of CO₂.

2. Properties, Thermodynamics and Reactivity of CO₂

Recently, there has been an increasing interest for reactions using carbon dioxide as a starting raw material [32]. Indeed, as it is an inexpensive and nontoxic material, and in view of the grandness of its supply, carbon dioxide represents a possible potential source for carbon feedstock for the manufacture of chemicals and fuels as an alternative to the current prevalent use of petroleum-derived sources [32]. An overview of the properties and reactivity of carbon dioxide is presented in the subsequent sections of the present chapter.

Due to the kinetic and thermodynamic stability of CO₂, the methanation reaction is extremely exothermic because of the high concentration of oxidized carbon formed in the feed gas [1, 33]. As shown by the Gibbs-Helmholtz equation: $\Delta G^\circ = \Delta H^\circ - T\Delta S^\circ$, the chemical reactions are powered by the difference between the Gibbs free energy values of the reactants

and products of the chemical reaction. In order to transform CO₂ into useful products, a large energy input and optimized reaction conditions as well as active catalysts are required. As CO₂ is an inert molecule, the carbon atom in CO₂ is in its most oxidized state, meaning that its chemical transformation is thermodynamically highly not favourable [1, 34]. As a raw material, the CO₂ molecule is in its lowest energy state, thereby constituting a major barrier in the fixing of industrial processes for the conversion of CO₂ [1].

The structure of a carbon dioxide molecule being linear, it is a thermodynamically stable molecule with a measured bond strength of $D = 532$ kJ/mol [32]. The various physical and chemical properties of carbon dioxide are presented in Table 2 here below. As shown in Table 2, the heat of formation (ΔH°) and the Gibbs free energy of formation (ΔG°) of carbon dioxide are the two most important properties. Therefore, the ΔH° and ΔG° values are the most important criteria in order to estimate the thermodynamic feasibility of a reaction.

Table 2. Physical and Chemical Properties of Carbon Dioxide.

Property	Value and Unit
Heat of formation at 25 °C	-393.5 kJ/mol
Entropy of formation at 25 °C	213.6 J/K.mol
Gibbs free energy of formation at 25 °C	-394.3 kJ/mol
Sublimation point at 1 atm	-78.5 °C
Triple point at 5.1 atm	-56.5 °C
Critical temperature	31.04 °C
Critical pressure	72.85 atm
Critical density	0.468 g/cm ³
Gas density at 0 °C and 1atm	1.976 g/L
Liquid density at 0 °C and 1 atm	928 g/L
Solid density	1560 g/L
Specific volume at 1atm and 21 °C	0.546 m ³ /kg

Latent heat of vaporization at the triple point (-78.5 °C) at 0 °C	353.4 J/g
	231.3 J/g
Viscosity at 25 °C and 1atm	0.015 cp
Solubility in water at 0 °C and 1 atm at 25 °C and 1 atm	0.3346 g CO ₂ /100 g-H ₂ O
	0.1449 g CO ₂ /100 g-H ₂ O

After analyzing the Gibbs free energy of the exothermic hydrogenation of CO₂, the majority of the related reactions are found to be thermodynamically unfavourable. Indeed, since the ΔG° values are more positive than the corresponding ΔH° values, they are less favourable. As a consequence, only a few reactions have both negative ΔG° and ΔH° values. Values of $\Delta G < 0$ either correspond to the reaction of hydrogenation or to reactions with products containing C-O bonds. Favourable values of ΔG in the hydrogenation reaction are related to the formation of water. As hydrogen must be produced at the cost of the input energy, the CO₂ mitigation cannot be achieved by any of these reactions [1]. Table 3 here below summarizes the values of the enthalpy and the Gibbs free energy, calculated by the ASPEN software [3, 35, 36], for the exothermic reaction in the CO₂ hydrogenations [1].

Table 3. Values of the enthalpy ($\Delta H < 0$) and the Gibbs free energy for the exothermic reaction in the CO₂ hydrogenations [1].

Reactions in the CO₂ hydrogenations	Enthalpy (ΔH°) $\Delta H < 0$	Gibbs free energy (ΔG°)
$\text{CO}_{2(g)} + \text{H}_{2(g)} \rightarrow \text{HCOOH}_{(l)}$	-31.0 kJ/mol	+34.3 kJ/mol
$\text{CO}_{2(g)} + 2 \text{H}_{2(g)} \rightarrow \text{HCHO}_{(g)} + \text{H}_2\text{O}_{(l)}$	-11.7 kJ/mol	+46.6 kJ/mol
$\text{CO}_{2(g)} + 3 \text{H}_{2(g)} \rightarrow \text{CH}_3\text{OH}_{(l)} + \text{H}_2\text{O}_{(l)}$	-137.8 kJ/mol	-10.7 kJ/mol

$\text{CO}_2(\text{g}) + 4 \text{H}_2(\text{g}) \rightarrow \text{CH}_4(\text{g}) + 2 \text{H}_2\text{O}(\text{l})$	-259.9 kJ/mol	-132.4 kJ/mol
$2 \text{CO}_2(\text{g}) + \text{H}_2(\text{g}) \rightarrow (\text{COOH})_2(\text{l})$	-39.3 kJ/mol	+85.3 kJ/mol
$2 \text{CO}_2(\text{g}) + 6 \text{H}_2(\text{g}) \rightarrow \text{CH}_3\text{OCH}_3(\text{g}) + 3 \text{H}_2\text{O}(\text{l})$	-264.9 kJ/mol	-38.0 kJ/mol
$\text{CO}_2(\text{g}) + \text{H}_2 + \text{CH}_3\text{OH}(\text{l}) \rightarrow \text{HCOOCH}_3(\text{l}) + \text{H}_2\text{O}(\text{l})$	-31.8 kJ/mol	-25.8 kJ/mol
$\text{CO}_2(\text{g}) + \text{H}_2 + \text{CH}_3\text{OH}(\text{l}) \rightarrow \text{CH}_3\text{COOH}(\text{l}) + \text{H}_2\text{O}(\text{l})$	-135.4 kJ/mol	-63.6 kJ/mol
$\text{CO}_2(\text{g}) + 3\text{H}_2(\text{g}) + \text{CH}_3\text{OH}(\text{l}) \rightarrow \text{C}_2\text{H}_5\text{OH}(\text{l}) + 2\text{H}_2\text{O}(\text{l})$	-221.6 kJ/mol	-88.9 kJ/mol
$\text{CO}_2(\text{g}) + \text{H}_2(\text{g}) + \text{NH}_3(\text{g}) \rightarrow \text{HCONH}_2(\text{l}) + \text{H}_2\text{O}(\text{l})$	-103.0 kJ/mol	+7.2 kJ/mol
$\text{CO}_2(\text{g}) + \text{CH}_4(\text{g}) \rightarrow \text{CH}_3\text{COOH}(\text{l})$	-13.3 kJ/mol	+58.1 kJ/mol
$\text{CO}_2(\text{g}) + \text{CH}_4(\text{g}) + \text{H}_2(\text{g}) \rightarrow \text{CH}_3\text{CHO}(\text{l}) + \text{H}_2\text{O}(\text{l})$	-14.6 kJ/mol	+74.4 kJ/mol
$\text{CO}_2(\text{g}) + \text{CH}_4(\text{g}) + 2 \text{CO}_2(\text{g}) \rightarrow (\text{CH}_3)_2\text{CO}(\text{l}) + \text{H}_2\text{O}(\text{l})$	-70.5 kJ/mol	+51.2 kJ/mol
$\text{CO}_2(\text{g}) + \text{C}_2\text{H}_2(\text{g}) + \text{H}_2(\text{g}) \rightarrow \text{CH}_2 = \text{CHCOOH}(\text{l})$	-223.6 kJ/mol	-115.0 kJ/mol
$\text{CO}_2(\text{g}) + \text{C}_2\text{H}_4(\text{g}) \rightarrow \text{CH}_2 = \text{CHCOOH}(\text{l})$	-49.1 kJ/mol	+26.2 kJ/mol
$\text{CO}_2(\text{g}) + \text{C}_2\text{H}_4(\text{g}) + \text{H}_2(\text{g}) \rightarrow \text{C}_2\text{H}_5\text{COOH}(\text{l})$	-166.6 kJ/mol	-56.6 kJ/mol
$\text{CO}_2(\text{g}) + \text{C}_2\text{H}_4(\text{g}) + 2 \text{H}_2(\text{g}) \rightarrow \text{C}_2\text{H}_5\text{CHO} + \text{H}_2\text{O}(\text{l})$	-171.1 kJ/mol	-44.4 kJ/mol
$\text{CO}_2(\text{g}) + \text{C}_6\text{H}_6(\text{l}) \rightarrow \text{C}_6\text{H}_5\text{COOH}(\text{l})$	-21.6 kJ/mol	+30.5 kJ/mol
$\text{CO}_2(\text{g}) + \text{C}_6\text{H}_5\text{OH}(\text{l}) \rightarrow \text{mC}_6\text{H}_4(\text{OH})\text{COOH}(\text{l})$	-6.6 kJ/mol	+46.9 kJ/mol

Hydrogenation reactions of CO_2 with a $\Delta\text{H} > 0$ can be executed [1, 3, 35, 36]. These reactions are associated with highly positive ΔG° values that are not favourable and which can be found in Table 4 here below [1].

Table 4. Values of the enthalpy ($\Delta H > 0$) and the Gibbs free energy for the hydrogenation reactions of CO_2 [1].

Reactions in the CO_2 hydrogenations	Enthalpy (ΔH°) $\Delta H > 0$	Gibbs free energy (ΔG°)
$\text{CO}_{2(\text{g})} + \text{CH}_2=\text{CH}_{2(\text{g})} \rightarrow \text{CH}_2\text{CH}_2\text{O}_{(\text{l})} + \text{CO}_{(\text{g})}$	+152.9 kJ/mol	+177.3 kJ/mol
$\text{CO}_{2(\text{g})} + \text{C}_{(\text{s})} \rightarrow 2 \text{CO}_{(\text{g})}$	+172.6 kJ/mol	+119.9 kJ/mol
$3 \text{CO}_{2(\text{g})} + \text{CH}_{4(\text{g})} \rightarrow 4 \text{CO}_{(\text{g})} + 2 \text{H}_2\text{O}_{(\text{l})}$	+235.1 kJ/mol	+209.2 kJ/mol
$\text{CO}_{2(\text{g})} + \text{CH}_{4(\text{g})} \rightarrow 2 \text{CO}_{(\text{g})} + 2 \text{H}_2(\text{g})$	+247.5 kJ/mol	+170.8 kJ/mol
$\text{CO}_{2(\text{g})} + 2 \text{CH}_{4(\text{g})} \rightarrow \text{C}_2\text{H}_{6(\text{g})} + \text{CO}_{(\text{g})} + \text{H}_2\text{O}_{(\text{l})}$	+58.8 kJ/mol	+88.0 kJ/mol
$2 \text{CO}_{2(\text{g})} + 2 \text{CH}_{4(\text{g})} \rightarrow \text{C}_2\text{H}_{4(\text{g})} + 2 \text{CO}_{(\text{g})} + 2 \text{H}_2\text{O}_{(\text{l})}$	+189.7 kJ/mol	+208.3 kJ/mol
$\text{CO}_{2(\text{g})} + \text{C}_2\text{H}_{4(\text{g})} \rightarrow \text{C}_2\text{H}_4\text{O}_{(\text{g})} + \text{CO}_{(\text{g})}$	+178.0 kJ/mol	+176.0 kJ/mol

Usually, the CO_2 conversion is accompanied by the production of CO. The reaction enthalpies for the production of the same product from either CO or CO_2 are comparable [1]. However, in most cases, CO is favoured compared to CO_2 [1, 3, 35, 36].

The reactivity of the carbon dioxide molecule and the potential means of promotion of its reactivity might be anticipated. Indeed, this is due to its linear symmetry and the overall non-polar nature of the molecule with a presence of the π -electron density of the double bonds and the lone pairs of electrons on the oxygen atoms and also the electrophilic carbon atom [32].

As a consequence, since the CO_2 molecule is a very stable one, a lot of energy must generally be supplied to trigger the desired transformation. Reactions on carbon dioxide often require high temperatures, active catalysts, with energy coming from electricity or from photons [32]. Thus, the reactions involving carbon dioxide are generally endothermic, and therefore, consume energy. For instance, considering reactions for the steam reforming of methane and CO_2 reforming of methane, the latter requires about 20 % more energy input when compared

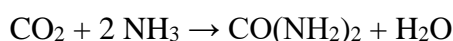
to steam reforming. However, both reactions are useful for industrial applications as they produce synthesis gas with different H₂/CO molar ratios.

When carbon dioxide is used as a single reactant, it requires more energy. However, since its Gibbs free energy is of -394.4 kJ/mol, it becomes thermodynamically more feasible when carbon dioxide is used with another reactant that has a higher Gibbs free energy. For example, methane, carbon (graphite), and hydrogen are some co-reactants that have higher (less negative) Gibbs energy. As an example, if we consider the dissociation of carbon dioxide to carbon monoxide where CO₂ is used as a single reactant and reduction of CO₂ by H₂ where CO₂ is used as a co-reactant. Moreover, the heat of reaction is less in the case where CO₂ is used as a co-reactant [3].



2.1. Current Uses of CO₂

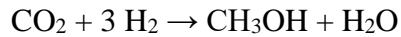
The current largest use of CO₂ resides in the synthesis of urea, which is a much used fertilizer. About 110 megatons of CO₂ are used yearly for this chemical synthesis [31]. The chemical reaction involved for the production of urea is known as:



CO₂ is likewise used to produce salicylic acid, which is found in pharmaceuticals and cyclic organic carbonates [31]. What is more, salicylic acid is produced by the reaction of sodium phenolate with CO₂ to produce sodium salicylate. The formed sodium salicylate is then converted into salicylic acid by the addition of sulphuric acid. Sodium sulphate is obtained as a by-product while aspirin is produced from salicylic acid. The reaction path involved in the production of salicylic acid and aspirin can be written as:



Methanol, used as a chemical reagent or as a fuel, is produced by the reaction of carbon dioxide and hydrogen in the presence of a catalyst. Furthermore, methanol can also be dehydrated to form gasoline-like fuels [31]. The chemical reaction involved in the production of methanol from CO₂ and H₂ is:



Other applications include the utilization of carbon dioxide in refrigeration systems, carbonated beverages, fire extinguishers, inert gas-purging systems and blasting systems for mining coal. In addition, it has to be noted that supercritical carbon dioxide is a known solvent for promoting difficult chemical reactions [31].

3. Literature Review

Amongst the different technologies aimed at the reduction of CO₂, the methanation of carbon dioxide (CO₂) is one of the methods that leads to the production of methane (CH₄). The carbon dioxide reduction through the Sabatier reaction was discovered in the 1910s. Technologies which include a possible reduction of CO₂ offer valuable advantages for protecting the environment by effectively recycling CO₂, based on the catalytic methanation. Producing methane by using carbon dioxide as a reactant would have the effect of keeping CO₂ from entering atmosphere. Indeed, its consumption leads to the production of natural gas which in turn can produce electricity to meet growing power needs.

The following part is an introduction to the research being conducted on the CO₂ methanation.

3.1. Methanation and Catalysis

The methanation of carbon dioxide is an exothermic reaction with a volume contraction:



According to Le Chatelier's principle, high pressures and low temperatures shift the equilibrium to the product side. However, though the latter reaction is thermodynamically

favoured, the reduction of the fully oxidized carbon (CO₂) to methane is an eight electron process with significant kinetic limitations that requires a catalyst that can achieve acceptable rates and selectivity for a potential industrial use [37]. Figures 3-4 show the equilibrium composition for an initial (4:1) molar mixture of H₂ and CO₂ at 1 atm with temperatures ranging from 200 to 600 °C. As it can be seen, it seems obvious that a lower operating temperature (200-250 °C) favour a higher conversion of CO₂ to CH₄ and H₂O. A challenge in the reactor design resides in the removal of the heat produced by the exothermic reaction and thus, keep a relatively low process temperature (around 350 °C) without generating hot spots [38]. Heterogeneous catalysts simplify fast reaction rates and selectivity close to 100 % for the Sabatier reaction.

Methane is the alkane with highest H/C ratio so this feature makes methane a high energy density hydrogen carrier. Hydrogen is a chemical element with the highest mass energy density, but has low mass, high flammability and high pressure requirements for its storage. These disadvantages complicate its production, transport, storage and distribution for further usage.

Synthetic natural gas is the target product of methanation (Equation 1), where the reactants engaged in this reaction are carbon dioxide and hydrogen, which can be obtained from renewable sources leading to a balance production of methane. Exhaust gases from power plants have been utilized as a reactant for methanation [39].

Moreover, methanation is extensively used at hydrogen plants of oil refineries to remove CO from H₂-rich streams (Equation 2). Carbon monoxide methanation improves the quality of fuel cells inlet streams, avoiding CO contamination of the membranes applied in the proton exchange membrane fuel cells (PEMFC) [40].



Achieving high methane yields with a good selectivity is possible if the reaction is carried out at low temperatures. Raising the temperature, on the one hand, shifts the equilibrium towards the reactants, lessening CO₂ conversion. On the other hand, the process temperature promotes the endothermic reverse water gas shift (rWGS) reaction (Equation 3) [41], which reduces the CH₄ selectivity in favour of carbon monoxide [42]:



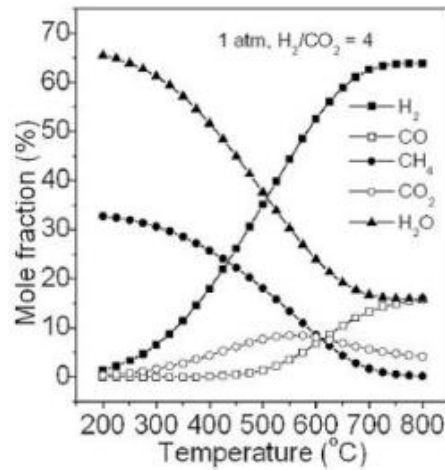


Fig. 3. Equilibrium product fraction of CO₂ methanation [43].

Figure 3 shows the methanation equilibrium composition at different temperatures. The equilibrium composition at atmospheric pressure shows that CO₂ conversion and CH₄ selectivity reach the best values at low temperature (below 350 °C). Furthermore, at temperatures above 500 °C, the CO selectivity increases in detriment of the CH₄ selectivity and yield (Fig. 3 and Fig. 4 (b and c)). Likewise, high pressure improves the reactants conversion (Fig. 4 (a)) as well as the CH₄ yield.

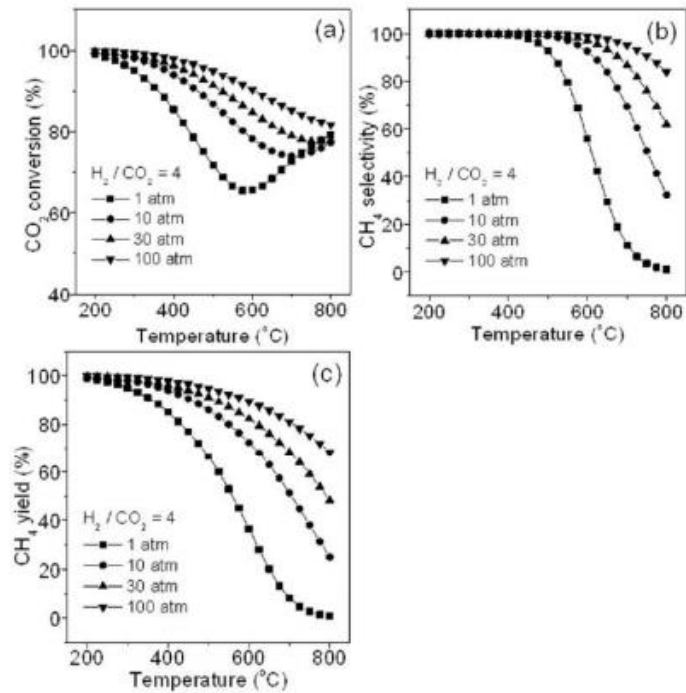


Fig. 4. Impact of pressure and temperature on CO₂ methanation: (a) CO₂ conversion, (b) CH₄ selectivity, (c) CH₄ yield [43].

An interesting challenge in the Sabatier process resides in the controlling the temperature, as the selectivity to desired products (H₂O and CH₄) is favoured at low temperatures. However, it is difficult to initiate the reaction one, because kinetic reactions are slow at low temperatures. If the reaction is started at temperatures around 350 °C, removing the heat from the exothermic reaction can be complicated. If the heat is not removed effectively, the exothermic reaction leads to a temperature increase that reduces the efficiency, and shifts to a more unfavourable selectivity.

Therefore, there still exists the need for a process that allows obtaining methane at low temperatures and at an atmospheric pressure with a high conversion rate (at least > 80 %) and high selectivity (> 95 %) and without any secondary reactions.

Several authors focused their research on the CO₂ methanation thermodynamics [26, 41-45]. The most awarded conclusions extracted from these works match with the results included in this thesis. Operation conditions should be maintained at temperatures below 400 °C in order to achieve a high CO₂ conversion and simultaneously maximize the selectivity

to methane. According to thermodynamics, the best results were expected in test runs operated at lower temperatures. Consequently, an active catalyst for methanation was decisive to achieve a good reaction rate.

3.1.1. The Factors of Choosing Catalysts for CO₂ Methanation

There are many factors that control the performance of the catalyst during catalysis and that is why the catalyst design is one of the most important features in catalysis. The performance of the catalyst is directly linked to the catalyst activity and selectivity. For a catalyst, to be of use in industry, it needs to meet steady cost, activity, selectivity, stability, recovery and reuse.

- **Particle size and surface area**

Catalyst particle size plays an important role in influencing the performance (selectivity and activity) of the catalyst. Generally, the particle sizes of the catalyst are strongly dependent on the preparation method that was used during the catalyst synthesis [46]. Usually small particles are desirable after designing the catalyst, because they result in high surface area which may lead to high activity. What is yet another advantage of having a catalyst with small particle sizes and well dispersed metal particles is that it is sometimes necessary to reduce the catalyst before commencing with any hydrogenation reactions, and, thus reducing step is achieved quickly and with facility when the particles are small and well dispersed across the support. Therefore, the reduction degree is usually high for well-dispersed small metal species across the support [47]. The usual problem encountered with large particles is that they promote carbon formation which can lead to catalyst deactivation by coking [46].

Other important aspect of the catalyst is its degree of crystallinity. The surface area of the catalyst decreases with an increase in crystallinity and that is why sometimes, when it comes to activity, the amorphous catalysts do better than their crystalline equivalent [48].

- **Metal as an active center**

The catalysts being studied for CO₂ methanation are usually made up of Group VIII, IX, X and XI transition metals. Nickel and Ruthenium based catalysts produce almost only methane, while less reactive metal components Pd, Pt, Rh, Mo, Re and Au catalyze at the same time CH₄, CH₃OH and CO (by reverse water-gas shift reaction). Whereas, Cu and Ag catalyze mainly CH₃OH [49]. Nickel based catalysts are most commonly studied, because of their high activity and low price. Sintering at reaction conditions diminishes their industrial vitality [50]. Ruthenium has been shown to be the most active metal for methanation, yet, its high cost makes it less attractive as an industrial catalyst [51]. Also of interest are multi-metallic catalysts that seek to utilize the functionality of different metals in a compatible manner. The metal loading of a catalyst can be set to dispersion, pore volume, pore size and blockage of micropores caused by the agglomeration of species leading to a reduced surface area. Although the number of active sites increases with an increasing metal loading, the dispersion of the metallic species will decrease with an increased loading [52]. As metal loading is increased a significant decrease of the BET surface area is observed, generally due to a formation of large oxide aggregates, which limits the access to the internal surface of the catalyst [53].

- **Role of a catalyst support**

Supported catalysts is composed of a support and an active metal centre, according to the definition. Support is use to achieve the highest dispersion of the catalytically active metal and to stabilise the metal centre versus sintering [54]. Supports for metal catalysts may be divided into: organic polymers and inorganic supports. Organic polymers that have been used as supports include: polystyrene, polypropylene, polyacrylates and polyvinyl chloride. Whereas, the most often encountered inorganic supports include: alumina, silica, glasses, clays and zeolites [55].

Usually, a support is present in higher amounts compared to an active metal centre. Furthermore, it should be stable under both reaction and regeneration conditions [54]. Some of the benefits for supporting the metal complexes are [55]: separation of the catalyst, thermal stability, reduced oxygen and moisture sensitivity, no solvent dependence and more easily observed corrosion effects. One of the reasons for the dominance of heterogeneous catalysis in

industry is lack of the problem of separating products from the catalyst, while, when it comes to homogeneous catalysis this is poses a serious problem. The rate of most reactions increase with an raise in temperature. Supported metal catalysts are generally stable at higher temperatures compared to homogeneous catalysts. The sensitivity of most heterogeneous catalysts to oxygen and moisture content is very low hence, compared to homogeneous catalysts, they are easier to work with. The problem related to choosing a right solvent for homogenous system is eliminated when it comes to heterogeneous systems since they do not require the catalyst to be in solution. When working with homogeneous catalysts, the problems associated with corrosion cannot be immediately seen because the reactions are carried out in a glass apparatus [55]. When it comes to heterogeneous systems the corrosion problem is generally experienced earlier, before the industrial scale operation.

By definition, the support should be neutral when it comes to reacting with both the reactants and products; nevertheless, studies have shown that some supports can react with either products or reactants, hence leading to shift on the expected selectivity. To investigate whether a support is neutral or not, various techniques can be employed. For example, the metal sites can be selectively poisoned thus revealing the role of a support or the reaction can be done in the presence of the support alone [56].

The interaction between a given metal and a support is an important aspect of the catalyst and generally, small particles interact strongly with a support resulting in high dispersion of metal across the support [46, 57].

Usually, for hydrogenation reactions, a catalyst has to be in a reduced state and this is normally done in-situ before to the reaction. The metal reduction step is strongly dependent by the intensity of metal-support interactions. If the intensity of the metal-support interaction is high, the latter will result in the difficult reduction of the metallic species, thereby further leading to a major impact on the activity of the catalyst [46].

The characteristics of the final catalyst are controlled by the internal properties of the support, the preparation route that was followed during synthesis and metal loading [58].

- **Catalyst porosity**

The porosity of the catalyst during a catalytic reaction plays a very important role. Usually, a porous catalyst is sought after because it gives more surface area. Some catalysts are more porous than others and this can lead to significant changes in their performances. Pores can be blocked or undergo structural changes during the catalytic reaction and this can result in catalyst deactivation [58].

3.1.2. Catalysts Poisoning and Deactivation Phenomena

The deactivation of catalysts is a phenomenon in which the structure and state of the catalyst change causing loss of active sites, leading to decrease in activity and selectivity over time in turn. There are many reasons for catalyst deactivation, which are divided into four main categories [59, 60] (Fig. 5).

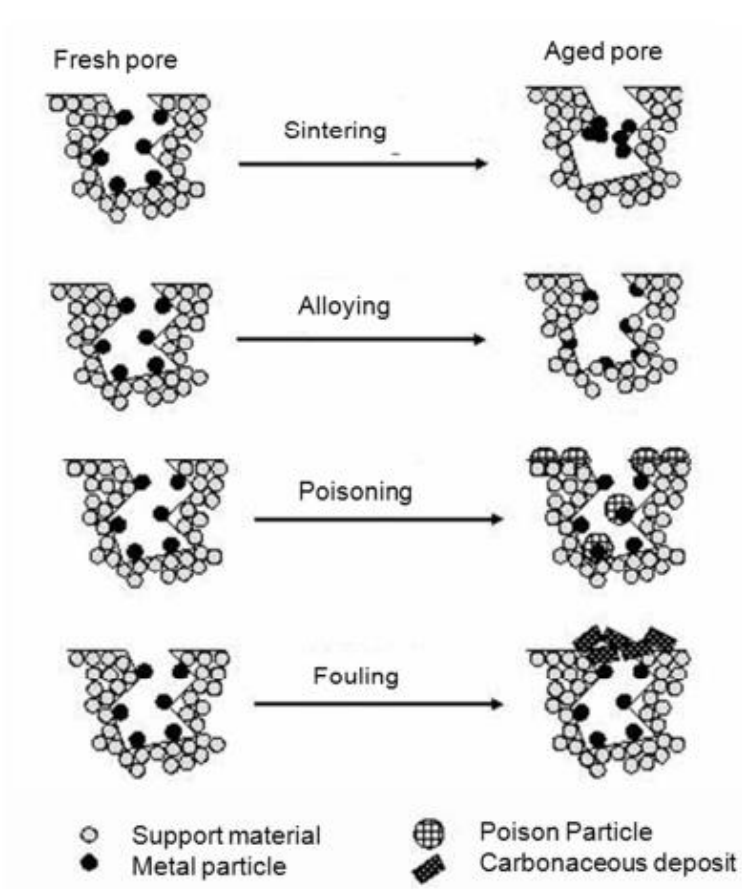


Fig. 5. Deactivation of catalyst by different mechanisms [61].

The question is what it is that may avert the idea of having a catalyst that will last forever? Economically it is not an attractive route to have a process whereby the catalyst is changed frequently. Catalyst deactivation is more important in continuous flow processes compared to batch processes, but since the problems related to waste disposal are not attractive, catalyst deactivation problems are becoming more important even in batch processes. It may be possible to recycle the catalyst at the end of its life cycle, but this is also favourable if it is economical, otherwise catalyst removal is preferred.

Catalyst deactivation link to the loss, over time, of catalytic activity or selectivity [59]. The aspect that should be looked at over catalyst design is to synthesize a catalyst with high activity, because by doing so the use of comparatively small reactors and less stringent operating conditions can be achieved. As the definition of catalyst deactivation provides that catalytic activity may not be the only aspect of interest, catalyst selectivity toward the desired product also comes into play. Then a good catalyst should hold, for some time, a desired balance between catalytic activity and selectivity [62].

When working with catalytic reactions it is important to understand the mechanisms of catalyst deactivation that occur as the reaction progresses, because in that way it is possible to have complete control over the catalyst. The mechanisms of deactivation as the catalytic reaction progresses are so many but they can be grouped into six mechanisms namely: fouling, poisoning, thermal degradation, vapour compound formation accompanied by transport, vapour-solid or solid-solid reactions and attrition and crushing [59].

- **Poisoning**

Poisoning is defined as a loss of catalytic activity due to the chemisorption of contaminations on active sites. The reaction may be called self-poisoned or self-inhibited if a reaction product is strongly adsorbed to the surface of the catalyst. A poison may be blocking an active site (geometric effect), or may change the adsorptivity of other species by an electronic effect. Poisons can also modify the chemical nature of the active sites or effect in the formation of new compounds (reconstruction) [63]. A strong poison at low temperatures may be less detrimental at high temperature [62]. Poisoning may decrease the activity but rather than influence selectivity they may even enhance it.

The poisoning of a catalyst can be classified as being selective or not. In the former case what includes preferential adsorption of the poison on the most active sites of the catalyst at low concentrations. This may come into being if there is some sort of distribution in the properties of the active sites (e.g. the acid strength) of the catalyst, and as a result the strongest active sites will be poisoned first. In the latter case of non-selective poisoning the activity loss is proportional to the concentration of adsorbed poison. In this case the catalyst surface sites are uniform to the poison and the poison chemisorption appears in a uniform manner accordingly [59, 63].

Catalytic systems, as a result the way in which they respond to some poisons, may be different. That means the resistance and susceptibility of catalysts to a given poison may vary substantially. Common poisons in hydrogenation reactions are compounds of S, Se, Te, P, As, Zn, Hg, halides, Pb, NH₃, C₂H₂ and oxygen. For instance, nickel catalyst can be oxidized by oxygen to nickel oxide, which has less activity in hydrogenation [64].

So poisoning can be favourable in increasing the selectivity of the catalyst but generally the activity is compromised. But where poisoning is useful, terms such as selectivity modifiers and selectivity promoters best describe the process [62]. For example, sulphur plays an important role as a poison in many catalytic processes such as hydrogenation or methanation [59].

- **Thermal degradation (Sintering)**

The deactivation may be an effect of the loss of the catalyst surface area because of crystallite growth of the catalytic phase or the loss of support area. Usually sintering is irreversible and occurs at high temperature where metal atoms migrate and grow to metal crystallites changing the particle size distribution. The rate of sintering increases exponentially with temperature. Sintering rate is also depends on some factors as [59]: type of metal (e.g. rate of sintering for Ni/Al₂O₃ is less than Pt/Al₂O₃), presence of promoters or contaminations (e.g. O, CaO, CeO₂, BaO reduce the rate of sintering by decreasing the atom mobility, and S, Cl, Pb, F reduce the rate of sintering by increasing the atom mobility), atmosphere (e.g. for metals, sintering is mostly rapid in oxygen atmosphere while relatively slow in hydrogen), metal dispersion (e.g. for Ni/SiO₂, metal dispersion has a strong effect on the rate of sintering for

$T > 650\text{ }^{\circ}\text{C}$), support surface area and porosity (e.g. the decreasing order of stability of Pt on different supports in vacuum is $\text{Pt}/\text{Al}_2\text{O}_3 > \text{Pt}/\text{SiO}_2 > \text{Pt}/\text{C}$). Therefore, sintering is the reason for morphological changes in the catalyst.

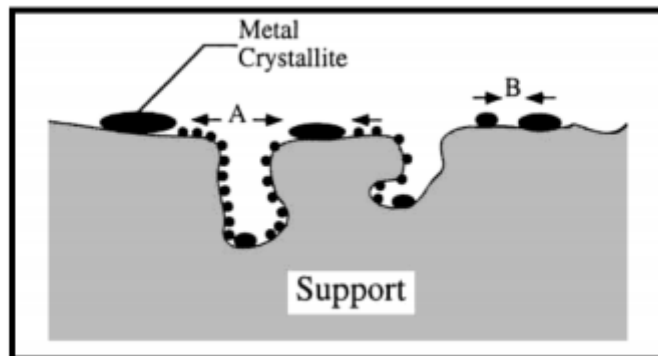


Fig. 6. Illustration of a crystallite growth due to sintering: (A) the atomic migration and (B) the crystallite migration [59].

Figure 6 shows how the position of the particle contributes to sintering because valley positions are very stable, whereas on-top positions are metastable. Sintering processes generally occur at high temperatures ($>500\text{ }^{\circ}\text{C}$) and are accelerated by the presence of water vapour [59].

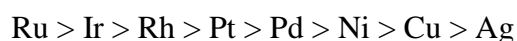
Fundamentally, sintering starts to occur when the temperature is close to the melting point because then metals start to be mobile. In order to give a prediction on the beginning of the metal sintering, Huttig and Tamman temperatures are used [62]:

$$T_{\text{Huttig}} = 0.3T_{\text{melting}}$$

$$T_{\text{Tamman}} = 0.5T_{\text{melting}}$$

When the Huttig temperature is accomplished atoms at defect sites start to become mobile, then, when the Tamman temperature is reached, atoms from the bulk will become mobile. At melting temperature the mobility will be so high because liquid phase is observed [62]. Over the catalyst life cycle many processes occur that may trigger a catalyst to surrender sintering e.g. calcinations or hot spot formation.

Despite the fact that temperature is the major driving power of sintering, other factors also affect sintering and therefore the Tamman temperature is not the best estimate to the start of sintering. Other factors which may affect sintering are: gas composition, support material, metal-support interaction, particle shape, particle size, texture, pore size and contaminations of the support or in the metal. Also, the mobility of metals is not the same and in a reduced atmosphere, the metal crystallite stability usually decreases in the following sequence [59]:



While studying sintering also the choice of the support is very important [59]. Usually, sintering rates are lower for porous supports as compared to non-porous supports. They decrease as crystallite diameter approaches those of the pores. Likewise the presence of additives may either increase or decrease atom mobility, e.g. C, O, CaO, BaO, CeO₂, GeO₂ decrease atom mobility, while Pb, Bi, Cl, F, S increase atom mobility. Structural promoters are named the additives that decrease atom mobility and reduce sintering [59].

Atom mobility may be significant for some reactions because it could be used for catalyst regeneration. For example, the redispersion of Pt in reforming catalysts [62]. Moreover the presence of water in the feed may trigger sintering. Water usually induces the metal-support interactions to be weak, hence increasing the mobility of metal atoms which may lead to sintering. The activities of hydrogenation catalysts are better when the active metals are in a reduced state. In the presence of water the metal-support interaction can be weakened, followed by oxidation of a metal [65]. But kinetically sintering is a very slow process, sintering is irreversible and prevention in this case is better than cure.

- **Fouling (coking or carbon deposition)**

Fouling is the physical deposition of species from the bulk fluid phase onto the catalyst surface and resulting in loss of activity due to blockage of active sites or pores. The product obtained by CO disproportionation is carbon while coke is usually obtained by decomposition or condensation of hydrocarbons on the catalyst surface [59]. The deactivation of catalysts by coking is common in industrial processes [65]. Probable effects of fouling by carbon (or coke) on the functioning of a supported metal catalyst are shown in Figure 7.

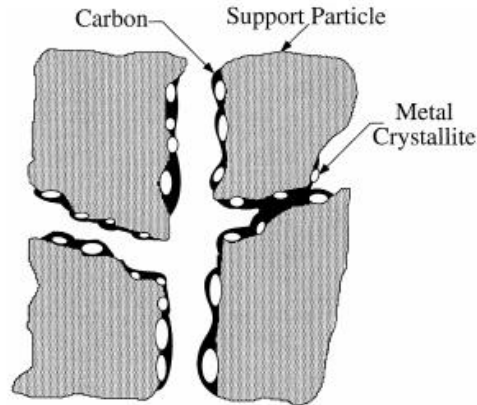


Fig. 7. Schematic diagram of fouling, crystallite encapsulation and pore plugging of a supported metal catalyst through carbon deposition [59].

Catalytic reactions including coke/carbon formation can be classified as either being coke-sensitive or coke-insensitive. In the first case, unreactive coke is deposited on active sites causing activity loss, while for coke-insensitive reactions, reactive coke precursors formed on active sites are easily removed by hydrogen (or other gas) [66].

Various mechanisms have been proposed for the formation of coke and carbon deposition. They differ, whether the catalyst is a metal or metal oxide or metal sulphide, accordingly. Therefore the chemical nature of the carbonaceous deposits depends on the mechanism of formation as well as on other factors as the temperature and pressure conditions, the chemical nature of the feed and product formed, and the age of the catalyst [63].

- **Alloying**

In alloying, combinations of two or more metals occur at high temperatures and may alter the activity and stability of catalyst. For example, the Cu-Zn alloy formation over the reduction of the catalyst in the temperature range of 230 to 500 °C with a mixture of H₂ and N₂, deactivates the catalyst and reduces its activity for the water gas shift reaction [67].

- **Mechanical failure**

Scientists who are involved in catalyst design are also needed to produce catalysts that will withstand mechanical failure. Mechanical failure of the catalyst can have many forms e.g. crushing of pellets, attrition of catalyst granules to produce powder and erosion of catalyst particles at high velocities. So a catalyst with high mechanical strength is needed to ensure resistance against the abovementioned problems [59, 62].

Some of the factors as catalyst shape and porosity, have been known to influence the mechanical strength of the catalyst. A spherical shape is most favourable, where macropores will result in reduced strength [62].

- **Leaching**

Leaching of catalyst is the deactivation route in liquid phase reactions. The reaction medium can be more corrosive and as far as metal catalysis is concerned, leaching of metal atoms depends on the reaction medium (pH, oxidation potential, properties of molecules) and on bulk and surface metal properties. Generally the loss of metal from catalysts is mainly due to support leaching. For example, alumina supports dissolve at high (higher than 12) and low pH (lower than 3) [62, 68].

3.2. Reactor Aspects

Due to the fact that the methanation reaction is highly exothermic, it is essential for the design of the reactor to have thermal control over the system. The main factor in the reactor design for this reaction is the heat removal capacity in order to avoid high temperatures and to consequently minimize catalyst deactivation. Thus, reactor must supply good heat exchange rate in order to avoid significant temperature gradients and hot spot formation. There are fundamentally two reactor types that can be used for this process: fixed bed reactors and fluidized bed reactors [69]. The heat produced during the methanation reaction has to be continuously removed from the reactor; regardless of the chosen design of the reactor. What is

more, an increase of the methane's molar gas fraction of about 1 % in the product gas causes a temperature rise of about 60 K for the CO₂ methanation [70].

The reduction of the reactive feed via a controlled dilution of the reactor inlet gas stream is an attractive way to reduce temperatures in the reactor. This can be performed by cooling down and recirculating a portion of the reactor's outlet gas stream. But, it results in some undesirable - energy losses [70].

3.2.1. Fixed bed Reactors

The adiabatic fixed bed reactor presents the simplest reactor design option. The reactor is filled with catalytic pellets, and its heat is used to increase gas temperature. With thus increased temperature the reaction rate is very high and requires a small amount of catalyst. If temperature increases the chemical equilibrium of the methane formation process shifts towards the reactants and then, the reaction comes to an equilibrium state at high temperatures which is not optimal for the CO₂ conversion. To avert catalyst destruction through thermal sintering, the adiabatic temperature might need to be limited. As the reactor feed gas can be diluted with inert gas, a surplus of one reactant or product gas recycle. Thus reactor outlet gas can be recycled and there will ensue a shift in the adiabatic temperature raise towards lower temperatures [71].

As CO₂ conversion rates are comparatively low at high temperatures (approaching equilibrium, reverse reactions become faster), a number of adiabatic reactors related in series are needed to reach the target conversion. The gas is surrendered to intermediate cooling before to each catalytic reactor, with the benefit of using simple fixed bed reactors, which have easy constructional design, through adopted to the adiabatic conditions. However, the basic limit of a series of adiabatic reactors with intermediate cooling requires that a high number of stages are needed to reach acceptably conversion; so when many reactors are necessary, such a solution becomes expensive, while using few in-series stages, the limitation to conversion could be important [71].

- **Lurgi process**

In the 1960s and 1970s, Lurgi's coal gasification process was the only technology exist for the production of synthetic natural gas at the expected quality. The methanation unit in this plant composed of two adiabatic fixed bed reactors, where the gas recycling was in the first reaction step (Fig. 8).

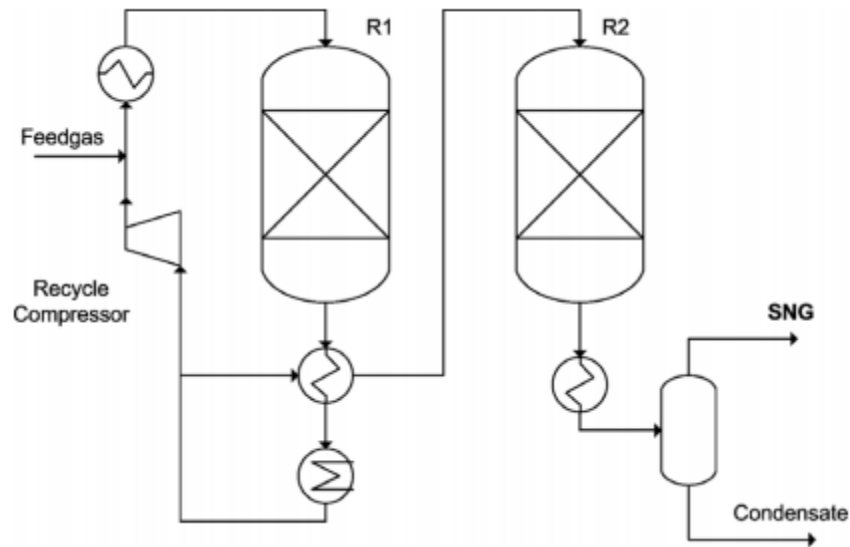


Fig. 8. Schematic diagram of Lurgi process with adiabatic fixed bed methanation reactor [69].

Two catalysts were used in the plants of Sasolburg (South Africa) and Schwechat (Austria): 20 wt.% Ni/Al₂O₃ and after a special methanation catalyst developed by BASF with higher nickel content [69]. In Table 5 the operating conditions are showed.

Table 5. Conditions in the pilot plant of Lurgi process [69].

	Feed gas	Fixed bed reactor R1		Fixed bed reactor R2	
		Inlet	Outlet	Inlet	Outlet
Temperature (°C)	270	300	450	260	315

Gas flow rate (wet), (m³_{N/h})	18.2	96.0	89.6	8.2	7.9
H₂	60.1	21.3	7.7	7.7	0.7
CO	15.5	4.3	0.4	0.4	0.05
CO₂	13.0	19.3	21.5	21.5	21.3
CH₄	10.3	53.3	68.4	68.4	75.9
C₂⁺	0.2	0.1	0.05	0.05	0.05
N₂	0.9	1.7	2.0	2.0	2.0

- **TREMP process**

TREMP stands for Topsøe's Recycle Energy efficient Methanation Process. It is a heat recovery idea, which produces high pressure superheated steam [69]. The ADAM I and ADAM II plants were expanded at the Nuclear Research Center at Jülich. These pilot plants included two processes: EVA - relied on the endothermic steam catalytic reforming of methane, as well as ADAM - the exothermic methanation process [72]. Moreover, ADAM I, had a capacity of 600 m³(STP)/h of synthesis gas and operated during 1500 hours since 1979 [73]. While, ADAM II, had a capacity of 9600 m³(STP)/h of synthesis gas and operated during 4500 hours since 1980 [72].

- **ADAMI**

For high temperature methanation Adam I was the first pilot plant. It was put in operation in the 1979s. It consisted of three adiabatic fixed bed reactors. The synthesis gas was provided by the reforming plant EVA I, where the inlet pressure of the first reactor was 28 bars and the temperature was 300 °C. Further, the product gas of the first reactor was cooled to 260-330 °C which corresponded to the inlet temperature of the second reactor. Next, the gas was cooled, fed to the third stage reactor and in the end, the gas was dried [72]. The process conditions are presented below in Table 6.

Table 6. Operating conditions for test run ADAM I [72].

	From EVA I	Recycle blower	1st stage		2nd stage	3rd stage	Product ADAM I dry
			in	out	Out	out	
Gas (m ³ (STP)h ⁻¹)	441	521	962	832	282	271	149
Pressure (bar)	27	33.4	26.85	26.70	26.6	26.5	26.5
Temperature (°C)	17	193/239	306	651	485	343	16
H ₂ O (mol%)	0.07	28.70	15.58	28.70	39.57	44.96	0.0
CH ₄ (mol%)	9.83	34.68	23.29	34.68	43.15	46.79	85.01
CO (mol%)	10.38	1.81	5.74	1.81	0.04	0.00	0.00
CO ₂ (mol%)	8.93	4.79	6.69	4.79	2.47	0.71	1.29
H ₂ (mol%)	67.59	25.70	44.90	25.70	9.97	2.63	4.78
N ₂ (mol%)	3.19	4.32	3.80	4.32	4.80	4.90	8.92

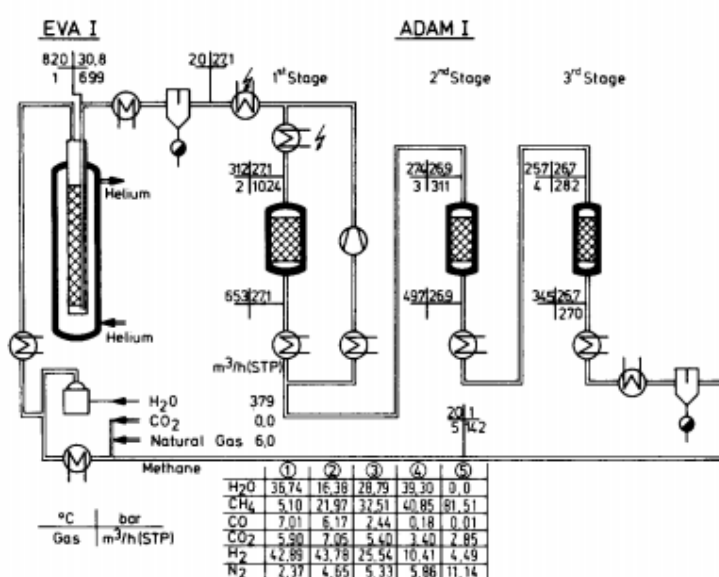


Fig. 9. The results combining EVA I/ADAM I [74].

- **ADAM II**

Adam II consisted of three adiabatic fixed catalytic methanation reactors. First, the synthesis gas was provided by EVA II and then, part of the product gas of the first reaction was recycled like in ADAM I to reach the temperature of 650 °C [72]. The temperature profiles in the catalytic beds shown in Figure 10.

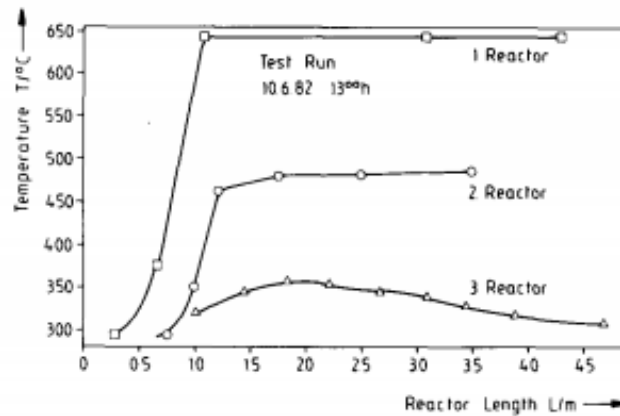


Fig. 10. Temperature profiles of ADAM II for the three stages [72].

A flow diagram of the plant with its mass balances are shown at Figure 11:

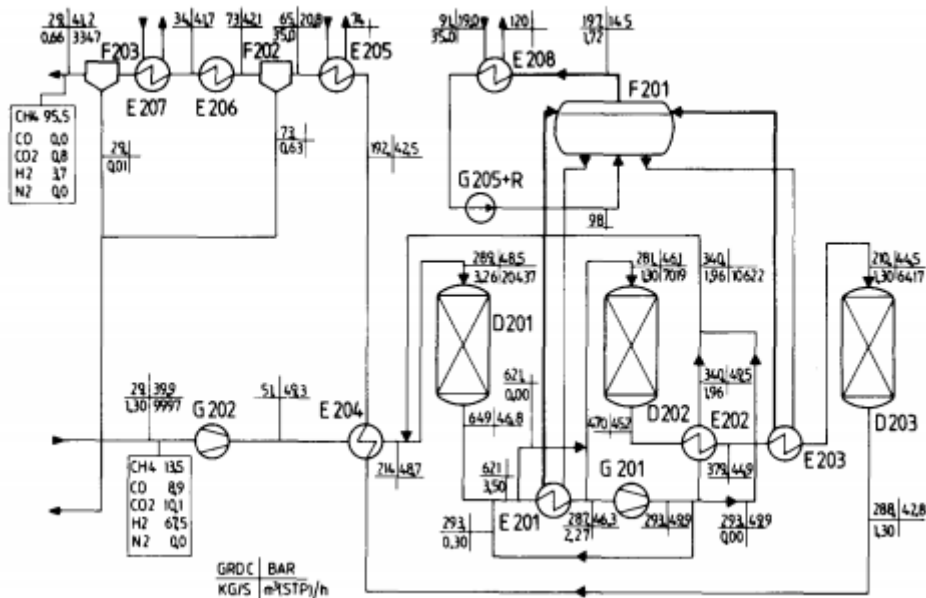


Fig. 11. Illustration of ADAM II [72].

The synthesis gas coming from EVA II was preheated in E204 to the temperature of 214 °C. Then introduced in the first reactor (D201). Half of the volume of the product gas from the first reactor was recycled to the inlet over blower G201. The rest of the product gas was cooled in E201 and fed into the second reactor (D202). The product of the second reactor was cooled (E202 and E203) and then send into the third reactor (D203). The third reactor was a counter current cooled reactor. Moreover, there were heat exchanger tubes arranged through the catalyst bed. These types of reactors are interesting when a determined product gas composition is needed. Final product is cooled and dried to a product gas rich in methane (95.5 %) [72]. The actual TREMP process consists of 4 reaction steps and product gas recycling in the first reactor remains to prevent high temperatures [75]. What is shown in Figure 12 is the temperature profile in the four reactors.

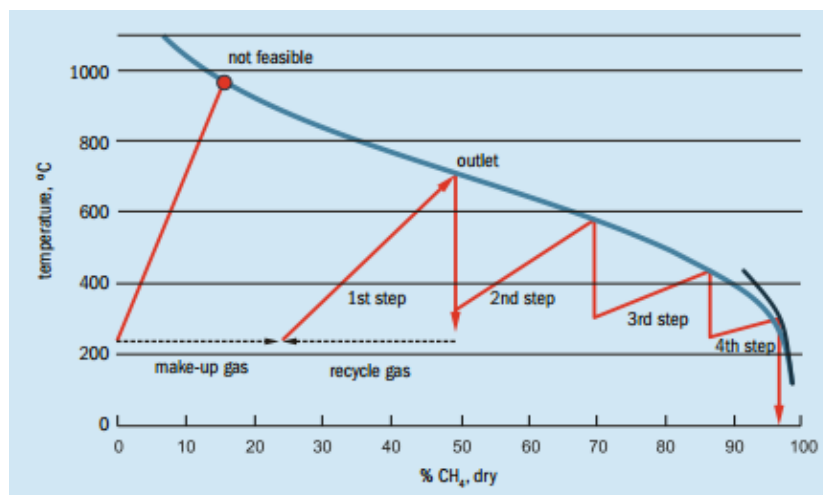


Fig. 12. Schematic diagram of temperature profiles in TREMP process [75].

The first adiabatic reactor is loaded with a non-Ni catalyst and a Ni catalyst (MCR-2X), which lets an inlet temperature of 220 °C without leading to a loss in activity (Fig. 13), in order to maximize the difference in temperature between the inlet and outlet of the reactor and to maximize the heat recovery process [75].

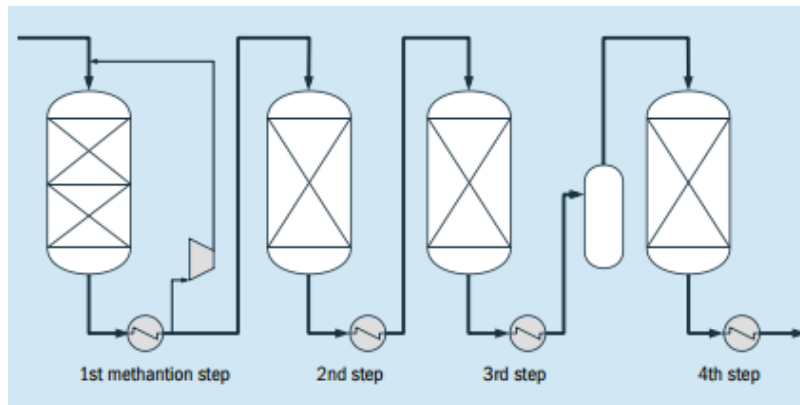


Fig. 13. Illustration of TREMP methanation process [75].

- **IRMA-cooled reactor**

The boiling water at the outlet contained a 10 % of steam and was feed into a steam drum. The steam condensed in the heat exchanger (E201) and the water was fed back to the reactor by forced circulation (P201) [27].

IRMA had a capacity of 600 m³(STP)/h of synthesis gas and worked in Jülich during 1100 hours since 1981. This methanation process consisted in an internally counter current cooled reactor, where the synthesis gas from the reformer plant EVA I was heated to an inlet temperature of 250-300 °C before being flown into the reactor R201 (Fig. 14). The tubes were cooled externally with boiling water at 100 bar (311 °C) and the process gas temperature at the outlet of the tubes was the same as the temperature of the inlet cooling water. The boiling water at the outlet contained 10 % of steam. Then, the steam condensed in the heat exchanger (E201) and the water was fed back to the reactor by forced circulation (P201) [72].

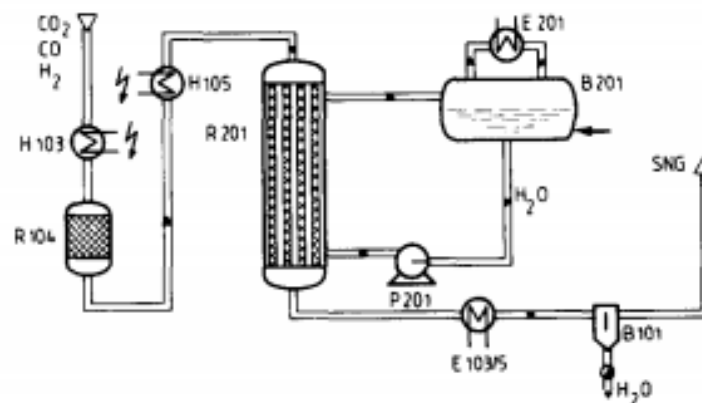


Fig. 14. Schematic diagram of pilot plant with IRMA reactor [72].

What is more, the operation condition at 28 bars presented a maximum in temperature in the reactor of less than 650 °C and a pressure loss of 3.5 bar (8m reactor length) for a gas flow of 395 m³ (STP)/h for 2 tubes [72]. The temperature profile for different gas flows in the reactor is presented in Figure 15.

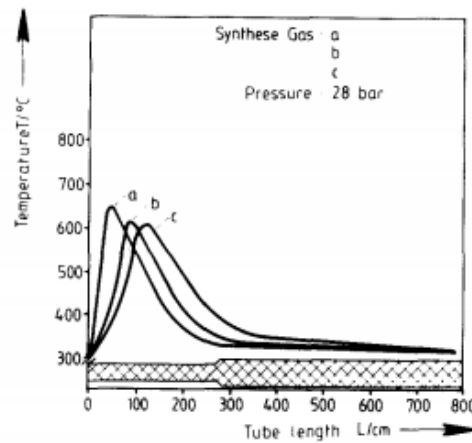


Fig. 15. Temperature profiles measured in IRMA for three different gas flows of synthesis gas [72].

- **KOMBI-process**

The process consisted in the combination of ADAM and IRMA technologies. The synthesis gas flow was divided into two flows, where one part flowed over an IRMA reactor and the other part was first mixed with the product of IRMA reactor and then send to an adiabatic reactor (Fig. 16). The idea of this process was to eliminate the recirculation in the first reactor. At 660 °C the product gas at the outlet of the adiabatic reactor was cooled down and fed to a IRMA reactor. The product gas was then cooled and dried [72].

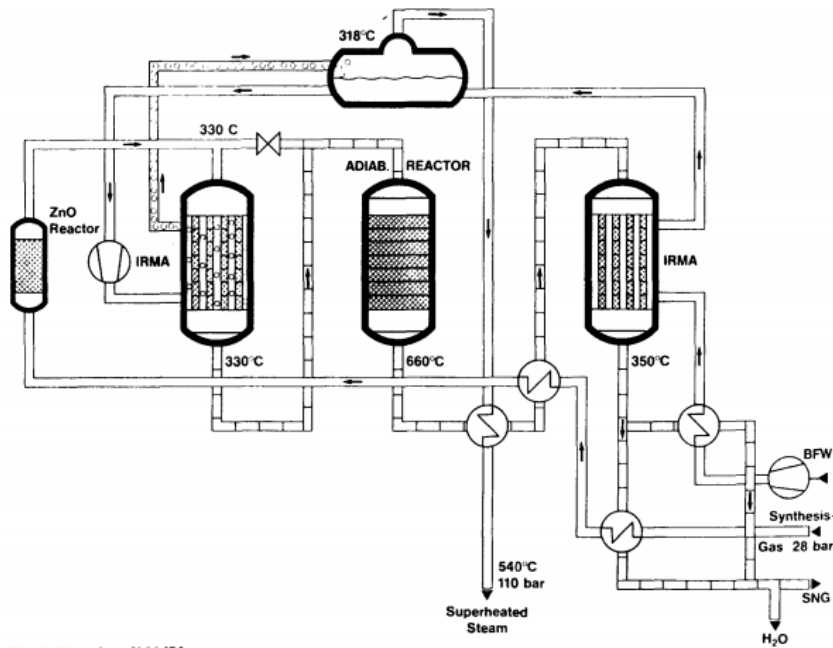


Fig. 16. Schematic diagram of COMBI-process [72].

3.2.2. Fluidized Bed Reactors

The methanation reaction in fluidized bed reactors, takes place within a fluidized bed of catalyst particles. High mass, heat transfer and almost isothermal conditions can be achieved due to a very good mixing of gas and solid catalyst particles in the fluidized bed. Another advantage of the fluidized bed reactors is the good process control. But if this reactor is chosen, we will be faced with problems of abrasion and entrainment of catalyst particles in the gas flow [76].

In fluidized bed reactors heat and mass transfer is known to be higher than in fixed bed reactors. The continuous mixing of fluidized solids gives us a chance to work at almost isothermal conditions [42]. Other benefits of this technology are the possibility of removing, adding, recycling and regenerating catalysts during operation.

- **Bureau of Mines**

This project consisted of one fixed bed and two fluidized bed methanation reactors which operated for more than 1000h. The first fluidized bed reactor reached a difference of

100 °C in temperature between inlet and outlet. The fluidized bed reactor had three gas inlets. Figure 17 shows the temperature profile in this multiple-feed fluidized reactor. Both blocks operated in a temperature range of 200-400 °C and pressures up to 20.7 bars. The multiple-feed reactor achieved conversions up to 95 % and included two regeneration cycles [69].

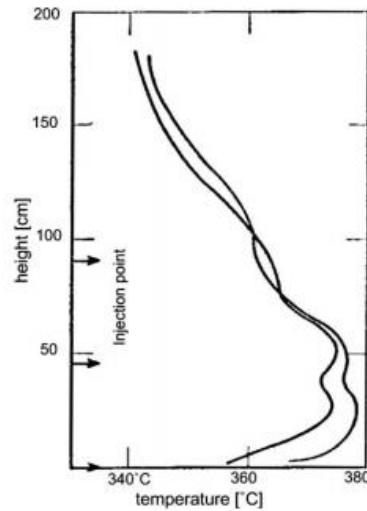


Fig. 17. Temperature profile from Bureau Mines [69].

- **COMFLUX process**

During 1975 and 1986, the Thyssengas GmbH and University of Karlsruhe concentrated on a fluidized bed methanation reactor to produce SNG. A pilot plant reactor (Fig. 18) of 0.4 m of diameter was set up and operated between 1977 and 1981 [37]. Table 7 shows the operating conditions.

Table 7. Operating conditions of COMFLUX pilot plant [69].

Temperature	300-500°C
Pressure	20-60 bar
H₂/CO ratio	Up to 4
Recycle/feed ratio	Up to 2
Gas velocity	0.05-0.2 m/s
Bed diameter	0.4 m
Bed height	2-4 m
Particle size	50-250 μm
Catalyst mass	200 kg

In 1981, a pre-commercial plant, which contained between 1 and 3 tons of catalyst, was expanded [69]. That plant had a capacity of 8000 m³(STP)/h. The operating conditions of the reactor were 60 bars with a range of temperatures of 350-550 °C [72]. The technology ceased to be developed any further when the price of oil decreased in the middle 80s [69].

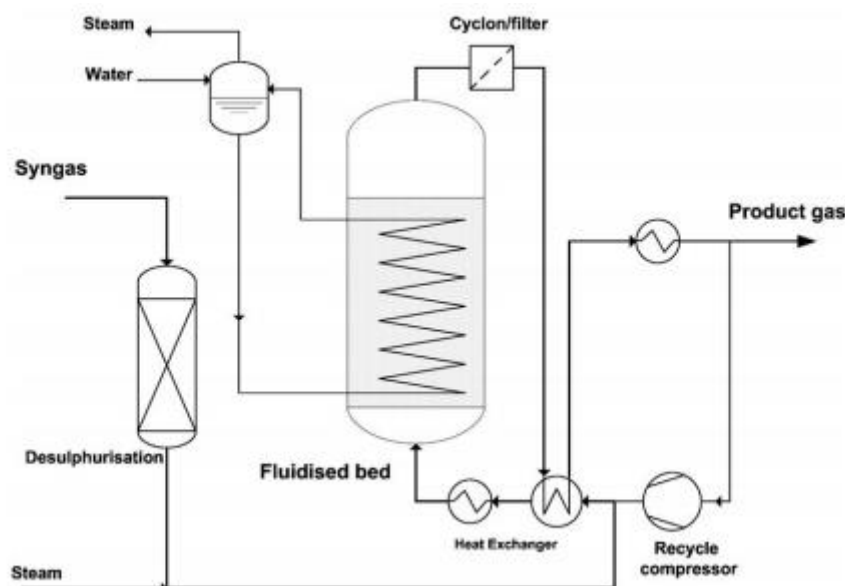
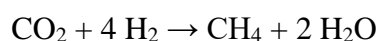


Fig. 18. Schematic diagram of COMFLUX pilot plant [69].

4. Reaction Mechanisms

Catalytic hydrogenation of CO₂ to CH₄, also called the Sabatier reaction, is an important catalytic process:



The methanation of CO₂ is thermodynamically favourable ($\Delta G_{298\text{K}} = -130.8 \text{ kJ/mol}$). However, the reduction of the fully oxidized carbon to methane is an eight-electron process with significant kinetic limitations that requires a good catalyst which can achieve acceptable rates and selectivity [37]. Extensive studies have been performed on metal-based catalytic systems on the hydrogenation of CO₂ to methane.

In spite of the fact that the methanation of CO₂ is a relatively simple reaction, its reaction mechanisms are quite difficult to establish as various opinions debate on the nature of the intermediates formed during the methane formation process. Therefore, the understanding of

such mechanisms has represented an important challenge for the CO₂ valorisation. Following analysis of several studies, it can be concluded that during the CO₂ methanation, two types of mechanisms appear [1]: a first one implying CO as intermediate (Fig. 19), in which CO₂ is converted to CO before the methanation [77-81]. The second mechanism concerns the direct methanation of CO₂ (Fig. 19) without the formation of CO as an intermediate [1, 82, 83]. It has to be noted that even for the CO methanation, no clear consensus was reached on its kinetics and mechanisms. Nevertheless, it has been proposed that the rate-determining step resides either in the formation of the CH_xO intermediate and its further hydrogenation or either in the formation of surface carbon during the CO dissociation and its interaction with hydrogen [79, 82-84].

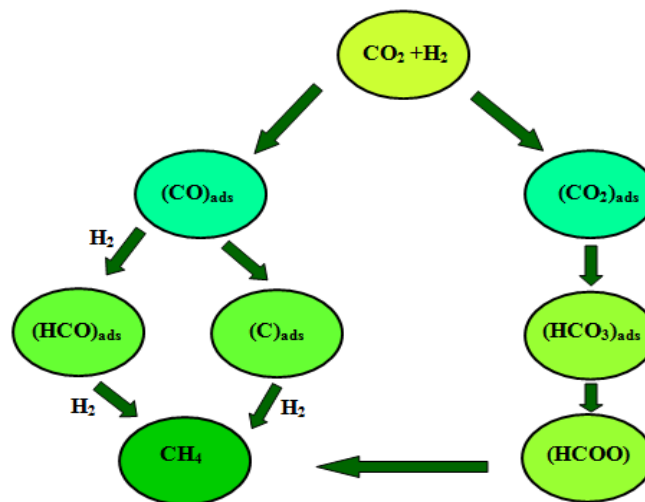


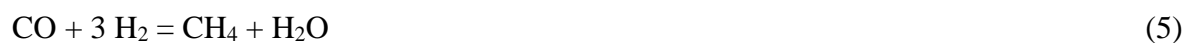
Fig. 19. Global reaction mechanisms of the CO₂ methanation (adapted from Fecheté) [1].

4.1. Proposed Reaction Mechanisms for the CO₂ Methanation Involving the Conversion of CO₂ to CO Prior to the Methanation Process

According to the nature of catalysts and their reaction conditions, the methanation mechanism is difficult to determine. Indeed, based on several papers from the literature [77-81], it is admitted that carbon monoxide is a critical intermediate for the carbon dioxide methanation [1]. More precisely, the methanation of CO₂ consists of the reduction of CO₂ to CO as described by the following equation:



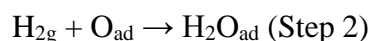
Then, followed by the conversion of CO into methane (or other alkanes) [1]:



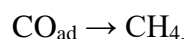
In this case, the mechanism is the same that the one for the CO methanation [1, 85, 86]. Indeed, the equilibrium for Equation 4 is slightly unfavourable at reaction temperatures ranging between 200 and 400 °C. This reaction path being unlikely, one way to overcome this issue is to require that at these temperatures the methanation of carbon monoxide (Equation 5) proceeds at significantly faster rates than the carbon monoxide production. If carbon monoxide was consumed as rapidly as it formed, no carbon monoxide would be observed in the reactor exit stream [1, 87]. Another mechanism, first suggested by Doehlemann et al. [88], points out the CO₂ dissociation into CO_{ad} and O_{ad}:



and then, the adsorbed oxygen atoms reacts with molecular hydrogen in a single step:



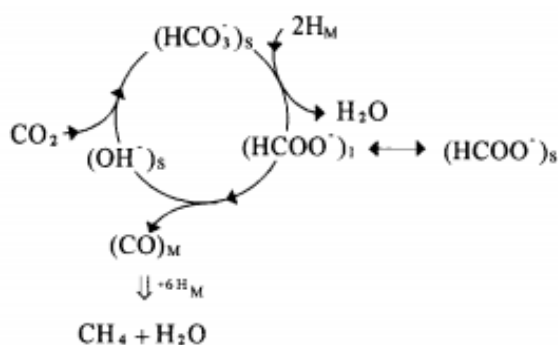
forming water, while the adsorbed CO gets transformed into methane [1]:



However, this mechanism assumes that the second step is the rate-controlling step for the CO₂ methanation. In the CO₂ methanation using Rh/Al₂O₃ as a catalyst [89], the CO₂ dissociation into carbon monoxide and oxygen on the surface of the catalyst was also observed in Diffuse Reflectance Infrared Fourier Transform (DRIFT) studies. The Rh-CO (2048 cm⁻¹), Rh³⁺-CO (2123 cm⁻¹), and Rh -(CO)₂ (2024 and 2092 cm⁻¹) bands confirmed the formation of adsorbed CO and CO₂ adsorbed as Rh-(CO)₂ and CO associated with oxidized Rh are the most hydrogen-reactive species [1].

The presence of CO as a key intermediate in the methanation of CO₂ was proved by the steady-state transient (SST) studies using a Ru/TiO₂ catalyst [1, 78]. At the interface between the metal and support, the presence of formate, resulting from its reaction with carbonate species, was also observed as an intermediate for the formation of CO [1]. A reaction mechanism (Fig. 20) is proposed including the formation of the formate through a carbonate

specie. What is more, single crystals of Ni have been proposed as a model catalyst for the CO₂ methanation [1, 90, 91]. The dissociation of CO₂ on Ni(100) [80] proved that CO₂ is first converted to CO and then to carbon before hydrogenation. The authors observed that the activation energy and reaction rate for CO₂ methanation were very close to the values obtained for the formation of CH₄ (88.7 kJ/mol) from CO (72.8-82.4 kJ/mol) under the same reaction conditions [1]. The formed CO was then dissociated into C and O atoms on the metal sites before being further hydrogenated into methane by the dissociated H₂ that remained on the metal particles [1, 81, 92]. Moreover, when a Ni(111) surface was tested using atom superposition and electron delocalization-molecular orbital theory, the dissociation of CO was found to be the rate-determining step. However, the elementary steps of the CO₂ methanation reaction consisted in two mechanisms: the carbon formation and the carbon methanation. For the first one, it has been found that the calculated activation energies were respectively of 1.27 eV (~120 kJ⁻¹) for CO₂ dissociation, 2.97 eV (~290 kJ·mol⁻¹) for CO dissociation and 1.93 eV (~190 kJ·mol⁻¹) for 2 CO dissociation. For the carbon methanation mechanism, the following activation energies were reported in the literature: 0.72 eV (~72 kJ·mol⁻¹), 0.52 eV (~50 kJ·mol⁻¹) and 0.50 eV (~48 kJ·mol⁻¹) respectively for methylidyne, methylene and methane [1, 93].



S: the support; M: the metal; I: the metal-support interface.

Fig. 20. Proposed reaction mechanisms for the CO₂ methanation [78].

4.2. Proposed Reaction Mechanisms for the CO₂ Methanation Involving the Direct Hydrogenation of CO₂ to CH₄ Without Forming CO as an Intermediate

The direct methanation of CO₂ without CO as an intermediate has also recently been reported [1, 82, 83]. Optional mechanisms for the CO₂ methanation on different catalysts consisting in the methanation of CO₂ through carbonates and formates, which are directly hydrogenated into CH₄ [1, 78, 79, 84, 94-96]. First, the CO₂ is dissociated directly into CO [1, 44, 97, 98]. The CO₂ methanation on Pd-MgO/SiO₂ catalysts [96] has shown that the MgO support initiates the reaction as magnesium carbonate species were observed on the surface of the catalysts [1]. Moreover, Pd as the active phase of the catalysts, dissociated molecular hydrogen and promoted the hydrogenation of the carbonates and others carbon atoms [1, 37]. These results demonstrate the synergy between the basic support and the active phase. Indeed, the CO₂ molecule, which is an acidic one, is activated by the basic sites of the MgO support that lead to the formation of magnesium carbonate whereas the metallic sites of Pd dissociate the hydrogen. Also methoxy groups were observed during the CO methanation mechanism [1, 99].

A Ni/CeO₂ catalyst showed the highest CO₂ conversions at low temperatures (300-400 °C) with a CH₄ selectivity close to 100 % [1, 100-102]. A better performance of the CeO₂ support was attributed to its higher ability to adsorb the CO₂ molecules, followed by its ability to reduce the molecules into CO and further convert the CO into CH₄. Temperature-programmed reduction (TPR) experiments on Ru catalysts demonstrated that the reaction of hydrogen with carbon monoxide lead to the production of CO₂ and water, without the production of methane. Therefore, it has been concluded that the CO gaseous phase is not a reaction intermediate during the CO₂ methanation with Ce_{0.95}Ru_{0.05}O₂ catalyst [1, 93].

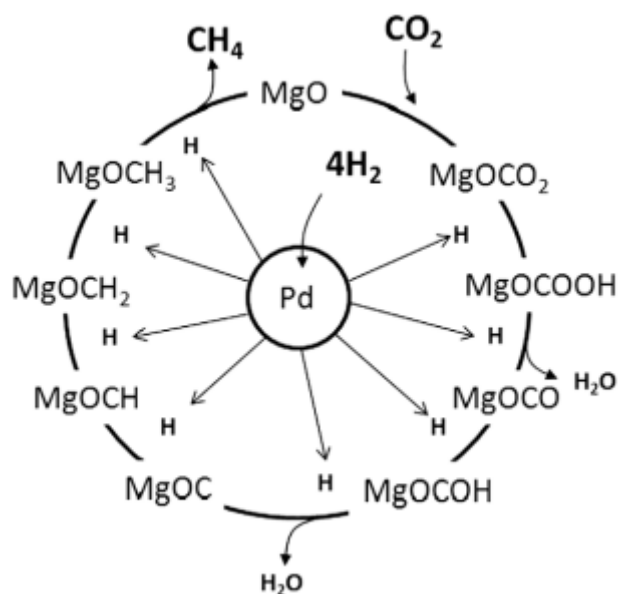


Fig. 21. A potential bi-functional mechanism for Pd-Mg/SiO₂ [37].

5. Hybrid Plasma-Catalytic Methanation

Plasma processing offers another applicable clue to the climate change challenge. Plasma discharges can be chosen to produce concrete operational conditions of characteristic temperatures and charged species densities within the discharge that promote a given set of chemical reactions. It is necessary to first understand the essential properties of plasma in order to identify the proper plasma discharge for a given process from a wide selection of types of plasma sources. This chapter section will give a short overview of plasmas and show the main physical processes that take place in a plasma. Hybrid plasma catalyst systems will be showed to present the advantages and uses of catalyst material when combined with plasma systems. Especially how catalysts may benefit CO₂ dissociation efficiency. Finally, conclusions will be given summarizing the potential of plasmas for CO₂ methanation.

5.1. Introduction to Plasma

Plasma is defined as a partially or wholly ionized gas. Therefore any gas can potentially become a plasma when energy is applied to create a significant density of electrons and ions [103]. The average charge summed over the negatively charged species (electrons and negative ions) and positive ions are give plasmas the characteristic of quasi-neutrality [104]. Plasma is

naturally available across the universe and contains ~ 99 % of the visible cosmos, including the solar corona, solar wind and nebula [104]. Plasma is also current in the top region of the Earth's atmosphere (at levels > 100 km) [104] where interactions with cosmic radiation result the dissociation of atmospheric gas molecules. It is known as the ionosphere. Natural and artificial plasmas appear over a wide range of pressures, temperatures and electron number densities. Figure 22 shows this variety in terms of their characteristic electron temperatures and number densities.

Laboratory plasmas can be classified into two categories [103]:

- i. high-temperature plasmas,
- ii. low-temperature plasmas.

Likewise can be divided into local thermal equilibrium (LTE) plasmas and non-LTE plasmas. Heavy particles in plasmas (ions, atoms) are energetic particles because are at a much lower temperature than the electrons which are characterized by much higher temperatures. High temperature serves to equilibrate high temperature of the electrons with ion temperature in a high-temperature plasma, thus establishing LTE. In non-LTE plasma, this thermal equilibrium is not steady. LTE discharges are generally used for high-temperature applications (welding). Non-LTE plasmas are usually used for low-temperature applications (plasma deposition) [103]. In laboratory plasma can be generated in various conditions from very low vacuum pressures (10^{-9} torr) up to atmospheric pressure and above. With heavy particle, (ions and neutral species) temperatures range from room temperature up to thousands of degrees Celsius. Plasma can generate temperatures that overstep those of traditional chemical processes, thus it make plasmas attractive for chemical and other industrial applications. Plasma can also increase the efficiency and intensity of chemical reactions because can create a significant concentration of excited and chemically active species. This would be unavailable in conventional chemistry [104].

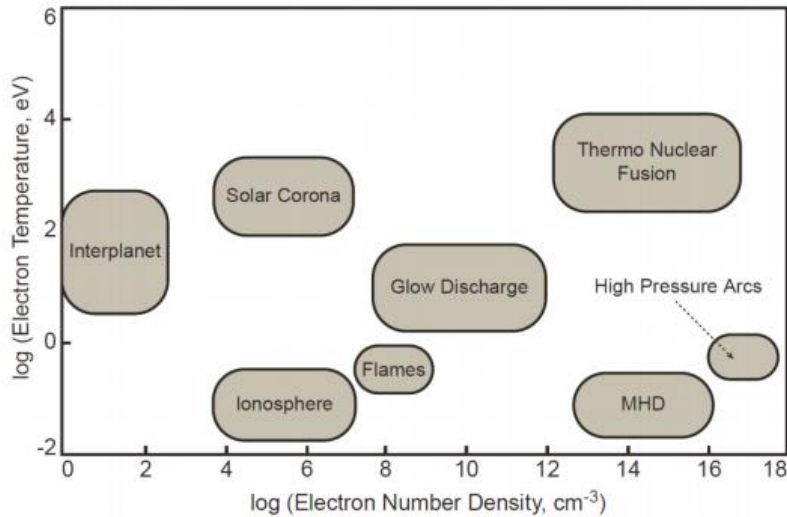


Fig. 22. Classification of plasmas in reference of electron temperatures and number densities [104].

The most important parameters which characterizes a plasma is the temperature of plasma species and number density of electrons. Usually, energy is transferred to electrons over acceleration by an applied electric field, which in turn is transferred to heavy particles through collisional processes. With an equilibrium temperature determined by collisions processes, the electron temperature can be higher than heavy particle temperatures. If the collision frequency is too low, electron and heavy particle temperatures may never equilibrate [104].

With gas temperatures more than 3,000 K, plasma in which the electron temperature (T_e) approaches the heavy particle translational temperature (T_0) is defined as thermal plasmas. And the plasma is called as a non-thermal plasma when $T_e \gg T_0$. Generally for non-thermal plasmas, the temperature relation is as follows: $T_e > T_v > T_r \approx T_i \approx T_0$. T_e is usually close to unity measured in units of electron volts or eV (equivalent to 11,600 K) with the gas temperature (T_0), close to room temperature [104].

Density is another characteristic of plasma particles. For a plasma to exist there must be a significant number density of charged species, but plasma does not need to be fully ionized. The ratio of charged species density to neutral species density approaches one in a completely ionized plasma. It is called the ionization degree and is indicated by the following equation [104]:

$$X = n_e / (n_e + n_0) \tag{6}$$

n_e - number density of electrons [m^{-3}]

n_0 - number density of neutrals [m^{-3}]

Plasma discharges commonly used to study plasma-chemical systems are recognized as weakly ionized and the ionization degree is around 10^{-7} - 10^{-4} , which means the neutral particle number density is several orders higher than the charged particle number density [104]. A thermal plasma has a high degree of ionization so is almost completely ionized. A non-thermal plasma is generally weakly ionized with an ionization rate less than 10^{-2} . The density of the ions (n_i) is another important parameter which has the same value as n_e [104]. The plasma in the DBD reactor utilized in this work is weakly ionized.

Mostly plasmas seem to be quasi-neutral, even if there may happen variations in ionization degree in various plasmas. It results from some basic electrostatic principles. Any charge separation that takes place between electrons and positive ions will generate an internal electric field, indeed accelerating the electrons in the direction of the ions and reducing any charge separation that may exist [104].

So to sum, free charges make plasma electrically conductive, internally interactive and strongly sensitive to electromagnetic fields [105]. Thus plasma offers three major features [104]:

- ability to achieve very high temperatures and high densities in comparison to traditional chemical processes,
- plasmas produce high concentrations of energetic and chemically active species as radicals, ions, electrons, atoms and photons,
- they can keep the bulk temperature low (room temperature) and simultaneously be non-equilibrium providing high concentrations of active species.

5.2. Applications of Plasma

Applications of plasma are found in many areas today. Some laboratory techniques have been expanded for a generation of plasma discharges, since the first studies into electrical arcs. Plasmas are used in a plurality of applications where such checking is required and when special sources of energy are needed, because plasmas are conductive and respond to electric and magnetic fields [103].

The first significant industrial application of plasma: the synthesis of ozone (O_3) from an O_2 silent discharge for water purification was studied by Siemens in the 1850s [106], but as the first, Langmuir named this phenomenon as a „plasma” in the 1920s [107]. Understanding

of the plasma chemistry is still missing in numerous cases, despite the fact that of these plasma technologies are relatively advanced [108]. Plasma technologies have progressed to contain a wide range of applications and some of them are mentioned below [103]:

- a) *Lasers* (CO₂ laser discharges for cutting);
- b) *Lighting* (fluorescent lamps);
- c) *Pollutant remediation* (destruction of volatile organic compounds (VOCs) from diesel exhausts);
- d) *Surface modification* (plasma hardening of metallic components for cars);
- e) *Thin film deposition* (anti-reflective coatings for lenses);
- f) *Plasma display panels* (area flat-screen televisions);
- g) *Chemical synthesis* (O₃ generation or synthesis of acetylene (C₂H₂)).

5.3. Different Types of Plasma

In order to better understand plasma, it is important to base their categories on their special characteristics, since there is a significant number of various types of plasma. For CO₂ methanation we are taking atmospheric pressure process, into consideration. There are two main types of atmospheric-pressure plasmas classified in terms of the electron temperatures: thermal and non-thermal (which are also known as equilibrium and non-equilibrium plasmas respectively).

- **Thermal plasmas**

In thermal plasma also named as hot plasmas, applied energy and time for equilibration has resulted in a plasma discharge that can be determined by a single temperature at all points of its space. For thermal plasmas the electron and bulk gas temperatures along with energy content are very high and electron and particle (neutrons, protons, etc.) temperatures are the same [104]. These plasmas is also characterized by higher power and higher density as well as low selectivity of chemical processes and are partially ionized but sufficiently conductive. As examples of thermal plasma we can give the sun, plasma torch and arc discharge [104].

- **Non-Thermal Plasma**

Non-thermal plasma also called cold plasma is characterised by multiple temperatures related to various plasma species. This plasma refers to a plasma state that is not in thermal equilibrium. The equilibrium is not reached as the electron number density is not enough high when compared to other heavy particles to achieve sufficient energy transfer between the electrons and the heavy particles [109]. Ionization and chemical processes in these plasmas are established by electron temperature and are not so sensitive to thermal processes and temperature of gas. Generally the electron temperature of cold plasmas is about 11600 K (1 eV) but the gas temperature is usually about room temperature (300 K) [104].

A lot of applications have been found for this plasma due to their low gas temperatures, high electron temperature and numerous chemically active species and radicals such as atomic oxygen O or hydroxyl OH. These active species have the potential to drive chemical reactions processes while keeping the gas temperature low. Non-thermal plasma is usually created as a result of direct electron impact ionization at low pressures or low powers or in pulsed discharge systems and also characterized by high chemical selectivity. As an example of cold plasmas we can indicate corona discharge, dielectric barrier discharge and glow discharge [104].

Cold plasmas can be also classified by their generation mechanism [110]. Moreau [111] was given mechanism of cold plasma formation in detail. Mechanisms comprise, but are not limited the following types [110]:

- dielectric barrier discharge,
- corona discharge,
- glow discharge,
- radio frequency discharge,
- microwave discharge.

5.3.1. Plasma Generation

Various possibilities exist in igniting a plasma. Collision of particles, electromagnetic radiation or strong electric field are examples that can generate ions beside the thermal energy.

For the formation of non-thermal plasmas, the application of an external electric field between two electrodes surrounded by a volume of gas is the most widely used method. The plasma can be ignited at atmospheric pressure and above or at low pressures (1-10³ Pa) [104].

The breakdown voltage (V_b) which is dependent on the gas pressure (p) and on the distance between the electrodes (d), determines the minimum voltage required to breakdown a gas in order to form a plasma discharge [112]. This relationship was developed by Friedrich Paschen in 1889 and is called the Paschen's Law, in which a and b are constants that are dependent on the gas type. In Figure 23 are shown the ignition voltages (V_b) as a function of the product of $p*d$ for various gases being calculated by the following Paschen formula [112]:

$$V_b = a * (p*d) / \ln(p*d) + b \quad (7)$$

The constant a depends on the gas type and represents the minimal ionization energy [112]:

$$a = (E/p)_{\min} = (V_b / p*d)_{\min}$$

E - electric field (V/m)

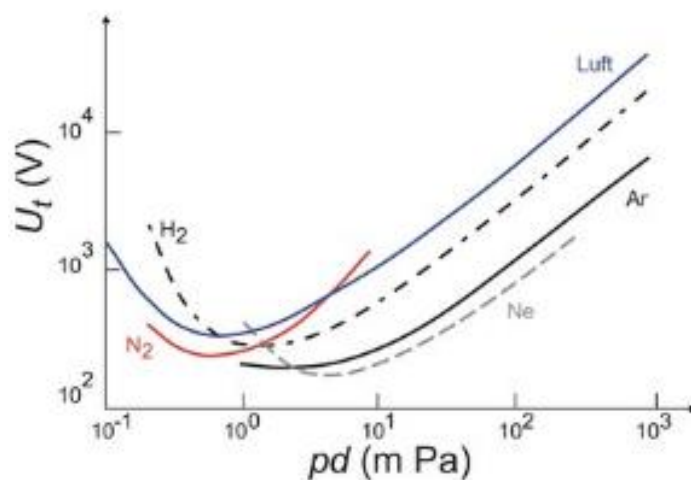


Fig. 23. Paschen curves for various gases [112].

All gases have a characteristic minimum for the ionization voltage and on both sides of the minimum the curves rise continuously as shown in Figure 23. The slopes on the left side of the maximum can be explained by a reduced gas pressure, as the mean free path of an electron increases and the number of collision decreases. In reality, the energy of the electrons is high enough to ionize the particles but there is a low probability of an electron-particle collision. In

order to ignite a plasma, a higher voltage is required but this is not possible for too low values of $p \cdot d$ [112].

The opposite is observed on the right side of the Paschen minimum. The number of collisions increases and the free mean path decreases because here the particle density is very large. The electrons cannot achieve the required ionization energy. In comparison to carbon dioxide or methane, helium has a lower Paschen minimum, because its cross section is lower, resulting in a larger mean free path of the electrons. Therefore, sometimes the inlet flow during an experiment is diluted with helium or argon for an easier ignition of the plasma [112].

The source creating plasma are secondary electrons being generated through primary electrons through a collision of a neutral particle with primary electrons; electrons getting their energy via electric fields. Thus, a particle with a low ionization energy will be ionized at lower electric fields [112]. The current flow will sharply increase due to an intensive avalanche of electrons in the discharge gap between the electrodes, at a point where the breakdown voltage is achieved. High energy electrons will collide with gas molecules causing the formation of new “active” plasma species (excited molecules and atoms).

During the collisional processes that occur between the charged and the neutral species, only a small portion of the energy is transferred, due to the relative sizes of the species involved. In most weakly ionized plasmas, electrons are the primary energy carrier and are accountable for transferring energy to heavy particles by collisions. The degree of ionisation in plasma is determined as the ratio of the density of charged particles to the density of neutral species, usually in the range of 10^{-7} - 10^{-14} [104]. Table 8 shows the collision processes [106].

Generally, two classes of collisions occur: elastic and inelastic ones can be differentiated. In elastic collisions, there is no change in the internal energies of the colliding particles between the charged particles (typically a very light electron) and the neutral (a heavy particle) ones. When an electron succeeds in transferring energy and changes the internal structure of neutral through ionization or excitation, this collision is named inelastic [104].

Table 8. The main plasma processes (A and B represent atoms and M a temporary collision partner) [106].

Electron/Molecular Reactions	
Excitation Dissociation Attachment Dissociative attachment Ionisation Dissociative ionisation Recombination Detachment	$e^- + A_2 \rightarrow A_2^* + e^-$ $e^- + A_2 \rightarrow 2 A + e^-$ $e^- + A_2 \rightarrow A_2^-$ $e^- + A_2 \rightarrow A^- + A$ $e^- + A_2 \rightarrow A_2^+ + 2 e^-$ $e^- + A_2 \rightarrow A^+ + A + e^-$ $e^- + A_2^+ \rightarrow A_2$ $e^- + A_2^- \rightarrow A_2 + 2 e^-$
Atomic/Molecular Reactions	
Penning dissociation Penning ionisation Charge transfer Ion recombination Neutral recombination	$M + A_2 \rightarrow 2 A + M$ $M^* + A_2 \rightarrow A_2^+ + M + e^-$ $A^\pm + B \rightarrow B^\pm + A$ $A^- + B^+ \rightarrow AB$ $A + B + M \rightarrow AB + M$
Decomposition	
Electronic Atomic	$e^- + AB \rightarrow A + B + e^-$ $A^* + B_2 \rightarrow AB + B$
Synthesis	

Electronic	$e^- + A \rightarrow A^* + e^- , A^* + B \rightarrow AB$
Atomic	$A + B \rightarrow AB$

Some of the parameters that determine a collisional process are the collision cross-section along with the mean free path and collision frequency [104]. In order to generate plasma electrically without initially free charges present is not possible. If the particles of the neutral gas are recognized to be a rigid sphere of radius r and their density n , the kinetic theory of gases determines the cross section for the collision (δ) and the mean free path (λ) as in the following equations [104]:

$$\delta = \pi r^2$$

$$\lambda = 1/\delta n$$

The collision frequency (ν) which is the average number of collisions per second and the mean time between collisions (τ) are defined as:

$$\nu = v_{av}/\lambda$$

$$\tau = 1/\nu$$

where v_{av} is the average velocity of the molecules in the gas and is defined as:

$$v_{av} = (kT/M)^{1/2}$$

where M is the mass of the molecule and k is the Boltzmann constant. The mean free path is inversely proportional to the pressure in the system if the temperature of the gas is constant [104]:

$$\lambda = ct/p$$

ct - constant depending on the gas

p - pressure in the gas

5.4. Types of Discharges

Various methods are employed to generate plasma, each generates plasmas with specific properties that make them attractive for a specific application. These methods can be divided into three groups: constant DC potential field, pulsed DC or alternating current (AC) potential and high frequency radiation.

Depending on the gas pressure, the electrode gap and the electrode configuration, several discharge regimes can be featured. They can be classified according to their current-voltage characteristics. In Figure 24 are shown the voltage/current characteristic of a discharge and the corresponding circuit diagram. This diagram is divided into three parts: the dark, glow and arc discharge and consists of an external voltage source, the plasma, a resistance, devices to measure the current and the voltage across the plasma zone. First, when breakdown occurs a self-sufficient glow discharge is generated between electrodes. The obtained discharge is limited in its current by the resistance of the circuit. The current limitations establish the kind of discharge that exists in system. Depending on current [112]:

- very low power: non-thermal-dark discharge;
- moderate power: non thermal-glow
- high power-thermal arc.

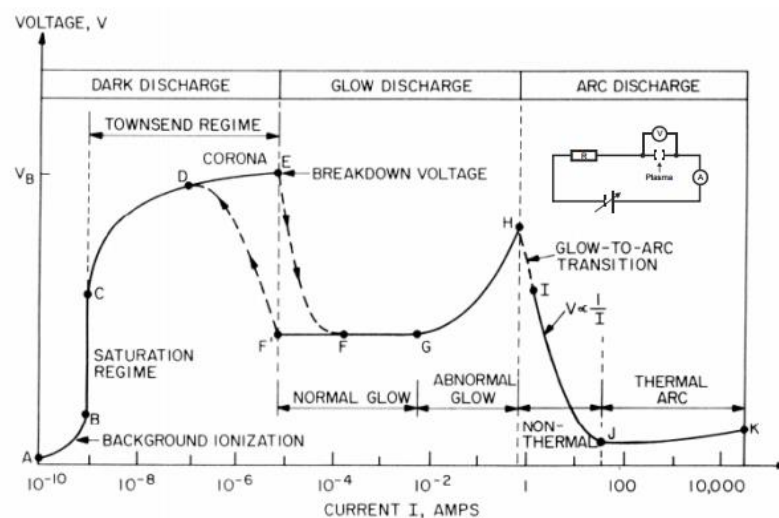


Fig. 24. Voltage-current characteristic of the DC low pressure electrical discharge [112], where: A-background ionization, B-saturation regime, C-begin of the Townsend regime, D-corona discharge, E-electrical breakdown, F to G-normal glow discharge, G to H-abnormal discharge, H to I-glow to arc transition, I to J-non thermal arcs, I to K-thermal arcs.

The dark discharge (invisible to the eye) is divided into the background ionization (A to C) and the Townsend (C to E) regimes. The free charge carriers in the former are produced via background ionization due to cosmic rays. The charged particles are accelerated to the oppositely charged electrode after some voltage is applied. An increase of the voltage between the plasma electrodes happens because not all ions and electrons can recombine to form the neutral particles. When the current increases after changing the voltage at the adjustable power-supply from A to C, the potential difference between the plasma electrodes increases, because the resistance in the plasma area increases. The current approaches a limit after reaching point C. The electric field becomes high enough to accelerate the free electrons to an energy being higher than the ionization energy of the particles. Secondary electrons are made before the primary electrons reach the anode, and the resistance in the plasma area decreases. The recombination process is dominant in the region C to E so this part is named the dependent discharge in the Townsend regime. The secondary electrons are accelerated in the electric field and if the mean free path is long enough, the electrons can ionize other particles. At point E the voltage is called ignition voltage and is high enough to generate many electrons to ignite the plasma. Between E and H the plasma is in the glow discharge region. The plasma is luminous there and the electron number density and energy are high enough to excite molecules and atoms in the visible region. An example is plasma TVs or the yellow light of the street lights (sodium vapour lamp). Because the resistance in the plasma zone decreases, the voltage decreases after igniting plasma at point E and increasing the current. At point G, the normal discharges change over to the abnormal glow discharge. The potential difference between the plasma electrodes increases again and electrons are emitted thermally out of the electrode. Higher than point H is created for currents an arc discharge which is used for electric arc welding [112].

5.4.1. Streamers

Starting from the cathode, a streamer is formed from an intensive primary electron avalanche (Fig. 25a). Due to the polarization of charges inside it, a space charge field is related with this avalanche. This electric field rises with the avalanche growth. Before creation of streamer, the avalanche has to reach a certain amplification. A weakly ionized region can be

made due to amplification of the electric field, as soon as the space charge field is comparable or exceeding the applied external field. Thus, streamer is initiated [112].

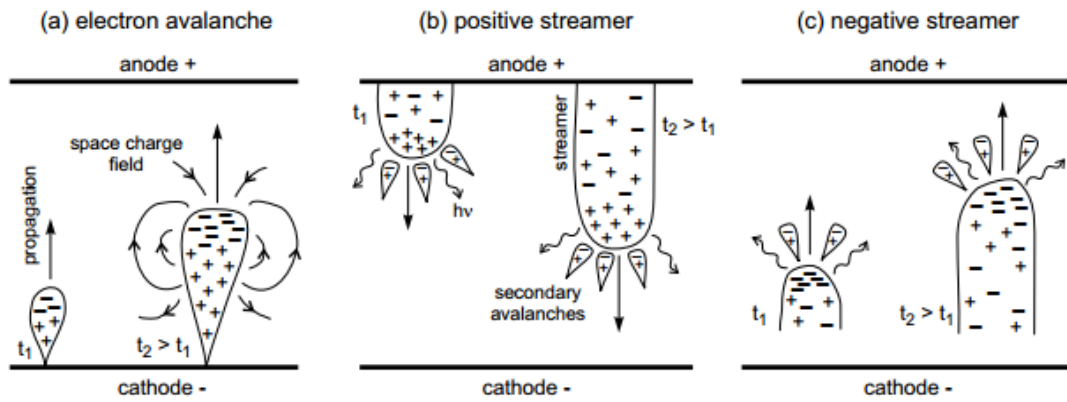


Fig. 25. Breakdown mechanisms leading to a spark discharge [112].

Streamer grows and propagates, following a zigzagging and branched path due to the random nature of the propagation mechanism. The speed of this propagation is high, reaching 10^6 m/s and depending on the gap distance and voltage; the propagation can be directed towards both the anode or the cathode [112].

In moderate gaps and with moderate voltages, the avalanche-to-streamer transition appears only when the basic avalanche has crossed the gap and reached the anode. Next, the streamer starts from the anode and grows towards the cathode. This kind of streamer is called positive. The streamer growth is caused by secondary avalanches, created close the positive head of the streamer (Fig. 25b) [112].

In large gaps and with strong gap voltages, the space charge field of the primary avalanche can be high enough to create the streamer even before reaching the anode. So the avalanche-to-streamer transition occurs in the gap and the streamer propagates towards both electrodes at the same time. This kind of streamer is called negative (Fig. 25c). Here, the electrons of the primary avalanche create a negative head for the streamer [112].

The discharge phase begins when the electrode gap is closed by streamer. If we accept that a streamer is full well conducting, the head of a positive streamer is at the same potential as the anode. When the streamer head is coming close to the cathode, all the potential fall is

located over a very short distance, the distance between the cathode and the streamer head. The electric field is so intense in this region that electrons are emitted in large number from the cathode and from atoms close the cathode. Once the gap is closed by streamer, these electrons, multiplied at huge intensity, are accelerated towards the anode in the initial streamer channel, leading to a strong ionization. The creation of a true spark channel is thus likely caused by this back streamer, which strongly increases the degree of ionization in the original streamer channel [112].

5.4.2. Plasma From Constant DC Potential

Plasma generation from constant DC potential is realized by applying DC voltage across two electrodes. The electrodes are supported at potential difference high enough to ionize gas molecules that are situated between the electrodes. Some examples of this type of plasma are shown below.

5.4.2.1. Corona Discharges

Corona discharges appear when the field at one or both electrodes is stronger than in the surrounding gas. They can occur at atmospheric pressure near curved regions such as projecting points, edges of wires, corners or thin wires where there is a significant electric field. Coronas have often been seen at high voltage transmission lines or lightning rods. A corona discharge can be created by applying either continuous or pulsed DC voltage between two electrodes. A continuous flow of gas is occupies the area between the electrodes where the corona is created [104, 113].

Depending on the relative polarity of the electrodes corona discharges can take on several forms. The various types of corona discharge are shown in Figure 26 for a point-to-plate electrode configuration. Positive corona is formed at a pointed anode and negative corona is formed at a pointed cathode. The initial breakdown of the gas produces a burst pulse in a positive corona, which is limited to the area immediately surrounding the electrode. It requires an increase in voltage to create additional charged species, which leads to the formation of streamers because the discharge is space-charge limited [113].

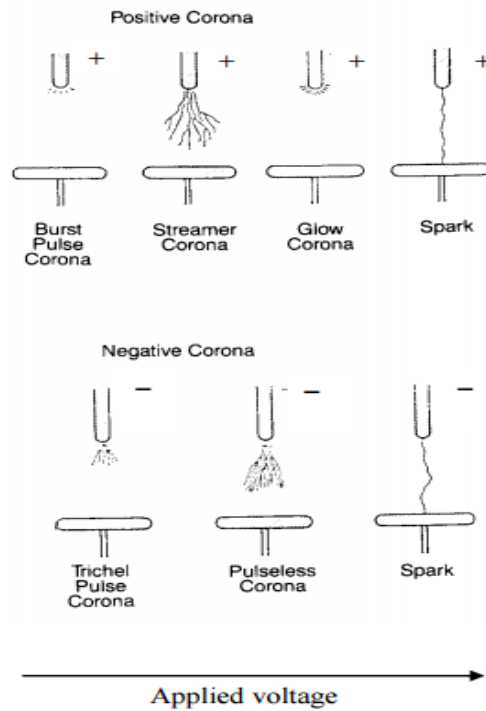


Fig. 26. Illustration showing various forms of corona discharges in a point-to-plate electrode configuration [113].

In positive and negative corona, high current flow will result in complete breakdown and the formation of a single spark discharge that bridges the discharge gap. A spark discharge is limited to a narrow channel and produces an unsteady current. The spark is generally noisy and causes local heating in the channel in which it is formed and is therefore not a desired effect. The use of short DC pulses, typically of nanosecond duration can overcome the problem of undesirable spark formation. By switching between plasma pulses and plasma afterglow, the current flow can be controlled. This improves the energy efficiency of the process and allows for operation at higher powers [113].

Applications of corona include ozone production and photocopying and also has been used to remove NO_x and SO_x from flue gas [114]. Corona is used in fuel reforming to investigate the dry reforming, steam reforming and partial oxidation of methane [104, 110, 115].

5.4.2.2. Glow Discharges

Glow discharge is by far the most well-known of all the plasma gas discharge types. Glow discharges are low-pressure (<10 mbar) processes that take place between flat electrodes in a tube or reactor and shows higher degree of ionization than dark discharge and has more efficient volume than arc discharges. They are popular because they work at low current (10^{-6} to 10^{-1} amps) and moderate voltages. The low pressure can effect in high field and high energy electrons that produce intense glows, hence the name [116-119]. A small fraction of ions and electrons are generated over breakdown process when a high electrical potential is applied to the electrodes. Generally the plasma in the glow discharge is quasi-neutral, so the number of electrons and negative ions is equal to number of positive ions in all regions, besides the “cover” regions. Altogether, a glow discharge consists of the three regions: cathode layer, positive column and anode layer. Electrons are driven towards anode and ions driven towards cathode while ionizing the neutrals that they collide with. Cathode layer is dominated by positive ions as the electrons are repelled from cathode and consists of sub-regions, namely: Aston dark space, cathode glow, cathode dark space, negative glow and Faraday dark space. Positive column occurs if electrodes are separated enough from each other, so that cathode and anode layers do not overlap. The excited species start emitting photons when the electron energy reaches enough energy under the electric field. The electric field in this region depends only on the gas type, pressure and the diameter of the tube, and the electric current in the positive column is established by external resistance or the load [104, 105]. Anode layer is dominated by electrons and negative space charges. There is an anode dark space and anode glow sub-region in the anode layer and the ionization is about three orders of value smaller than that in the cathode layer [104, 105].

A simple glow discharge with its regions across the length of its discharge is shown in Figure 27, and these regions are determined by the light emission patterns of plasma components in those locations. Just PC, FS and NG are visible at atmospheric pressure due to small length scales of the near electrode covers. Glow discharge makes a foundation for neon lamps and plasma TV screens and aside from illumination purposes, glow discharge has been explored for its potential in hydrocarbon reforming, particularly in the conversion of methane in to syngas [116, 118].

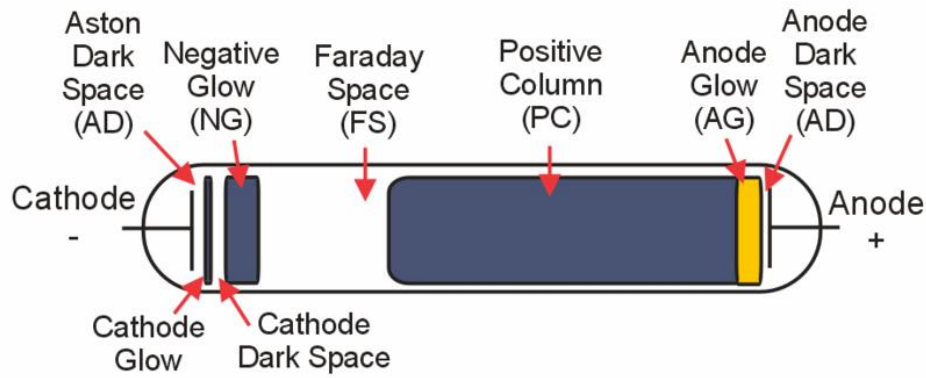


Fig. 27. Schematic diagram of glow discharge regions [120].

5.4.2.3. Arc Discharges

The arc discharges, characterized by high current (~ 100 A), low voltage (several to tens of volts) and a bright light emission. The gas is highly ionized and forms an equilibrium plasma, the fraction of ionized atoms is on the order of 10^{-3} to 10^{-1} . The gas phase and the electron temperature are both of the same order, 10^4 K. The arc discharge is different from the glow discharge in the electron emission mechanism from the electrode. In arcs, electrons are emitted by thermionic processes, due to the heating of the cathode. Arc discharges have been studied as a means of improving combustion [104].

5.4.3. Plasma From AC Potential

The plasma from a AC potential come from application of the electrical potential across two electrodes. One of the electrodes is covered with a dielectric material which accumulates charge once breakdown occurs. This build-up of charge alters the field and stops the current for a time. Discharge finally occurs and current is resumed in agreement with the oscillating potential. The duration of the current pulse relates to the pressure, properties of the gases and the dielectric material applied. These discharges are accidentally distributed in space and time. This type of plasma generation are known as barrier discharges [106].

5.4.3.1. Dielectric Barrier Discharge (DBD)

The dielectric barrier discharge (DBD) also named as silent discharge (due to an absence of noisy spark formation) is a very colorful discharge and it is comprised of multiple micro discharges [104]. It is a strongly non-thermal plasma that can be done at atmospheric pressure. It is driven by a sinusoidal AC voltage in the frequency range from 0.05-500 kHz [121] and able to form stable discharges in a range of various gases at relatively high discharge powers. DBD is highly non-equilibrium plasmas that supply high density active species (radicals, energetic electrons and ions) but still has moderate gas temperature. Siemens developed a process to generate ozone from oxygen or air in a DBD reactor and reported the first experimental researches in 1857 [122]. A new feature of Siemens discharge apparatus was the fact that electrodes were put outside the chamber and did not come in contact with the plasma [123].

The DBD reactor consists of two electrodes (with one or two dielectric barriers) set up in the discharge gap. Common dielectric materials with high relative permittivity are quartz, glass, enamel, ceramic, silica glasses and teflon. Therefore, to operate a DBD reactor an alternating voltages are required and the electric field in the discharge gap has to be high enough to cause a breakdown. In Figure 28 some possible DBD configurations are illustrated including planar, cylindrical and surface discharges. In general, one electrode is grounded while the other electrode is supplied with an alternating current [121].

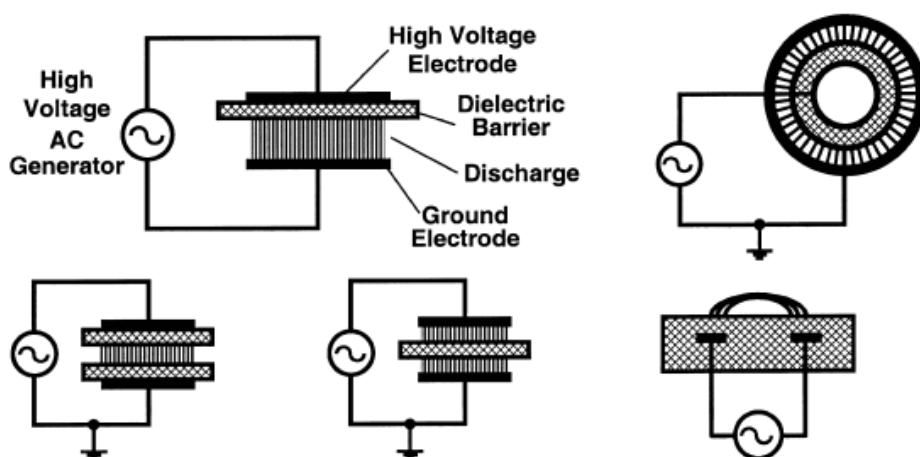


Fig. 28. Diagrams of planar, coaxial and surface DBD configurations [121].

A coaxial design is used in the experimental setup in this work. From 0.1 mm to several centimetres can vary the spacing in the discharge gap. The DBD is a non-uniform plasma discharge because it consists of many tiny breakdown channels called microdischarges or filaments. They cover the entire surface of the dielectric material and extend across the discharge gap. The dielectric barrier reduces the flow of current leading to suppressed microdischarges, leaving significant charge deposition on the dielectric surfaces. The microdischarges are reformed at the point where the breakdown voltage is reached in the next half cycle of the AC voltage sine wave, as the polarity of the electrodes is changing fast. This leads to the continuous formation of nanosecond microdischarges at a frequency which is twice that of the applied frequency [121]. Generally the current density in the filaments is 100-1000 A cm⁻², the electron density is 10¹⁴-10¹⁵ cm⁻³ and typical electron energies are in the range 1-10 eV. The microdischarges are accidentally distributed via the surface of the dielectric and the position of the formation is dependent on the residual charge distribution on the dielectric surface [124].

Non-thermal plasma is used to pump CO₂ lasers and to generate excimer radiation in the UV and VUV spectral regions. DBD has been used to explore the production of syngas or hydrogen by fuel reforming of hydrocarbons and alcohols [25, 125]. This kind of plasmas are also being used for plasma displays and for production of methanol from methane/oxygen mixtures, various thin-film deposition processes [126], and the remediation of exhaust gases. The advantage of the dielectric barrier discharge over other discharges is the option to work with a non-thermal plasma at atmospheric pressure and the relatively straightforward scale-up to larger dimensions.

5.4.4. Plasma From Radio Frequency Discharges

Through inductive coupling of the gas to the impinging radiation, plasma is generated by high-frequency radiation. Usually within the range 1-10³ Pa, radio frequency (RF) electromagnetic fields can be used to generate weakly ionised plasma at low pressures [127]. The properties of the RF discharge will change as the collision frequency increases at higher pressures, leading to a discharge approaching a thermal regime when close to atmospheric pressure [106]. Generally these discharges work at frequencies within the range 1-100 MHz

corresponding to wavelengths within the range 300-3 m [127]. Homogeneous plasmas can be formed by this method [106]. RF discharges are especially beneficial for applications that need the electrodes to be outside of the discharge region, hence preventing contamination with metal vapours given off at the electrodes [106]. Capacitively coupled plasmas (CCPs) and inductively coupled plasma (ICPs) are the two main types of RF discharge and in Figure 29 are shown typical reactor designs for each of these configurations [104, 127].

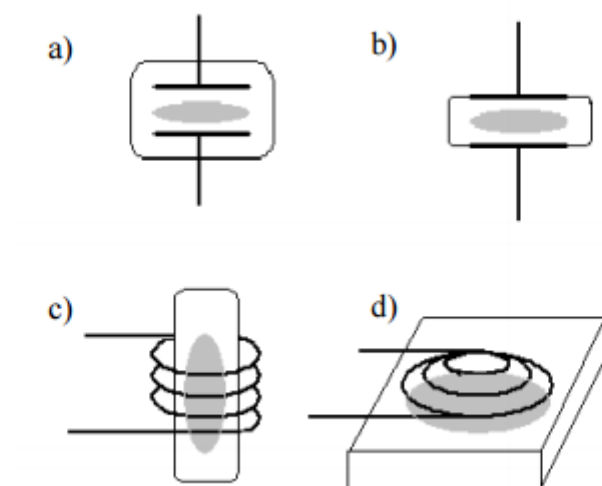


Fig. 29. RF discharges electrode configurations, where: a) CCP with the electrodes inside the gas chamber, b) CCP with the electrodes outside the gas chamber, c) ICP with the discharge located inside an inductive coil and d) ICP with the discharge located adjacent to an inductive coil [104].

5.5. Plasma-Catalysis Process

The use of catalyst material combined with plasma to enhance plasma-chemical reactions will be described in this section. An introduction to catalysis will be given first, followed by a description of different plasma/catalyst systems. Finally, the interaction between plasma and catalysts will be discussed.

Catalysts are substances that accelerate reaction rates and increase chemical selectivity, allowing chemical processes to occur at temperature and pressure conditions under which they would not be able to proceed otherwise. Heterogeneous catalysis is a process by which the catalyst is immediately changed when reactants and products adsorb on the surface of the

catalyst [128]. Firstly the reactants adsorb on the surface, becoming activated by interaction with the catalyst, which causes a quick and selective transformation of the reactants into adsorbed products. Next the products desorb from the surface, leaving the catalyst in its original state until the process starts again. The selectivity may also be manipulated through catalyst by increasing the rate of the rate-determining step of a desired stoichiometric reaction and catalysts can help reach a specific effect of products [128]. By lowering the activation energy or energy barrier of the reaction, a catalyst is able to increase the reaction rate of a process. This is realized by providing a surface on which adsorption and dissociation can occur. As that can more easily transform reactants into products. How the activation energy (E_{act}) can be affected by the presence of catalyst material is shown in Figure 30. Leads to an exothermic reaction given by a negative ΔH , as is the case here [128].

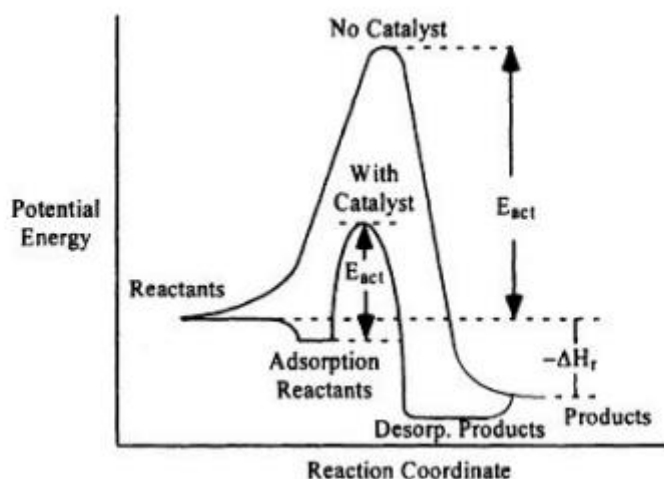


Fig. 30. Illustration of catalytic and no catalytic effects on activation energy [128].

The reaction rate is a function of temperature and concentration. Catalyst can increase the reaction rate by increasing the number of reaction sites or by decreasing E_{act} (which results in an increase in the number of collisions that result in reactions). Adding a support for the catalyst species is one of the mechanisms for increasing the number of available catalytic sites. It can be done by maximize the catalyst surface area using high-surface-area porous oxide materials as carriers, such as Al_2O_3 , TiO_2 or SiO_2 [128].

Physisorption and chemisorptions are kinds of adsorption that can occur on a catalytic site. Adsorption take place when a chemical bond is formed between the adsorbing species and the adsorbing surface. Chemisorption take place at relatively higher temperatures and the

adsorbate and adsorbent create chemical bonds at the surface. Physisorption is comparatively weak, relying on attractive Van der Waals forces between adsorbate and adsorbent. This appears as the condensation of gas molecules on a surface at low temperatures, with a typical Van der Waals layer separating the two species [128]. Physisorption and chemisorptions processes are shown in Figure 31.

The use of plasma in combination with heterogeneous catalysis can give an attractive solution, as it combines low temperature activity, fast response and compactness of the plasma reactors with the high selectivity of catalytic reactions.

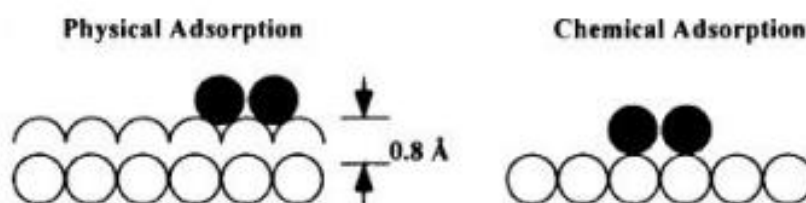


Fig. 31. Schematic diagram of physical and chemical surface adsorptions [128].

5.5.1. Different Plasma-Catalyst Configurations

As shown in Figure 32 when catalysts are combined with plasmas, they are usually incorporated into a non-thermal plasma, in either single-stage or two-stage configurations. Plasma can be used to supply energy for catalyst activation and it can also provide the reactive gas species needed for reactions on the catalyst surface. In a single-stage system, the catalyst is placed directly into the plasma discharge; what allows direct interaction between the plasma and catalyst. The catalyst is in contact with the discharge and also in contact with the short-lived active species such as excited atoms and molecules, radicals, photons, and electrons [129]. In a two-stage plasma-catalyst system, the catalyst is positioned either downstream or upstream of the plasma discharge. The active species are end products and long-lived intermediates resulting from the plasma or catalytic treatments in plasma pre-processing and post-processing accordingly. The discharge may affect catalyst performance and the catalyst may affect discharge performance because of the direct interaction of catalyst placed inside the discharge zone with the plasma. Plasma will supply a gas stream enriched with radicals and excited species, which can speed up thermal catalysis of the reactants and thus increase the energy

efficiency of the process [130]. Plasma-treated catalyst may also result in reduced metal particle size and higher metal dispersion, both leading to higher catalyst reactivity and longer durability. The catalyst can also affect the plasma. When catalyst is placed inside the discharge in the form of a packed-bed reactor where there are many contact points between pellets and pellets/electrodes, the electric field can become enhanced depending on the dielectric constant of the pellet material. An increased electric field can lead to higher ionization and dissociation events. When catalyst is placed after the discharge zone, the main role of the plasma is to change the gas composition before it reaches the catalyst, either providing chemically active species [130].

The catalyst material is usually introduced in the form of pellets, honeycomb monoliths, foam and coating of the electrodes or reactor walls [130]. Generally, lifetimes of vibrationally excited species have been reported as 1-100 ns at atmospheric pressure. It is too short, therefore vibrational species would not be involved in reaction mechanisms involving a two-stage plasma-catalysis configuration [131].

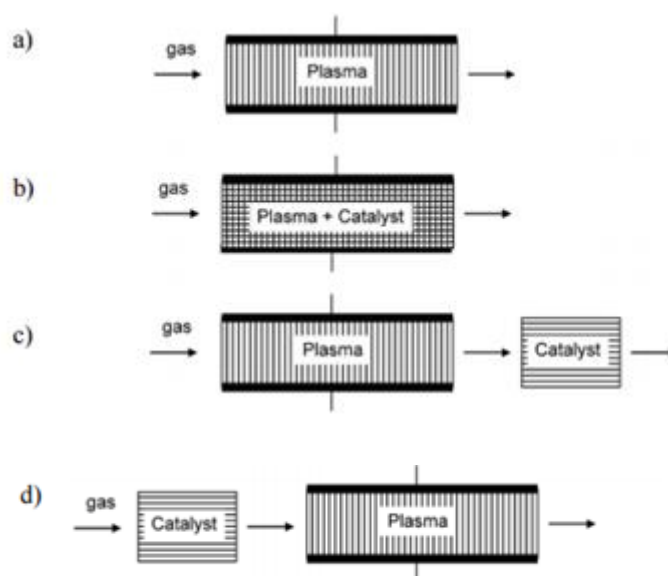


Fig. 32. Illustration of various plasma-catalyst configurations, where: (a) is a only plasma system, (b) is a single-stage arrangement, (c) is a two-stage arrangement with plasma pre-processing and (d) is a two-stage process with plasma post-processing (adapted from [129]).

Dielectric barrier discharges (DBD) have repeatedly been studied for experimental plasma/catalyst systems, for example, one investigation has reported the effects of adding of

porous $\gamma\text{-Al}_2\text{O}_3$ packed into a pulsed corona discharge [132]. With the plasma reactor alone, CO_2 conversion was only 3 % and with the addition of the catalyst, the CO_2 conversion increased to 16 % under the same operating conditions. With the optimization of the plasma source and with the right catalyst, high energy efficiency could be achieved with a high conversion degree.

In this thesis, plasma-catalysis concern to the single-stage process, where the catalysts are packed directly into the discharge gap of a coaxial DBD reactor.

5.5.2. Interaction Between Plasma and Catalysts

When the catalyst is placed directly in the plasma discharge the chemical and physical features of the plasma and catalyst can be changed. Chen et al. [130] considers each of these effects. The gas discharge promotes catalysis, while the catalysts enhances the nonequilibrium of plasmas. Such a plasma modified catalysis would cause an important modification in chemisorptions and desorption, and hence in the activity and selectivity of the catalyst. This action of plasma on a catalyst has been used to prepare efficiency catalyst for conventional catalysis. Kizling and Jaras reviewed the use of plasma techniques in catalyst preparation, regeneration and catalytic reactions [133].

Amplification of the average electric field strength can take place if the dielectric properties and morphology of the selected catalyst are right, resulting in an enhanced efficiency of the chemical reactions occurring in the discharge. The physical properties of the plasma discharge can be changed by catalyst surfaces. Also various discharge modes can be generated such as filamentary microdischarges and homogeneous surface discharges. Furthermore, the plasma region can be extended if the discharge is able to expand along a catalyst surface, this could lead to greater generation of active species in the plasma volume. The presence of a catalyst in plasma regions can also increase the nonequilibrium character of gas discharge. Jogan et al. [134] have studied the reduction of CO_2 from flue gas by using an AC ferroelectric packed-bed reactor and when reactor was packed with spherically shaped BaTiO_3 pellets, the energy yield was higher than in the case of absence of these pellets. So if an external electric field (usually AC) were to be applied across the packed high-dielectric layer, pellets would be polarized and the charge would accumulate on the dielectric surface. An intense electric field

would be generated, resulting in microdischarges between the pellets. These microdischarges in the packed-bed reactor would lead to the production of energetic electrons [135].

Specific selection of catalysts could result in preferable selectivity towards desired reaction products. Surface adsorption within a plasma volume can have characteristic input to improved reaction performance. The retention time and concentration of species in the plasma discharge will be enhanced, when reactant gas molecules are adsorbed onto the catalyst surface. This could result in increased probability of reactive collisions with active species in the plasma volume.

Plasma can help catalytic surface reactions by enriching the gas stream with radicals and excited species, what is the opposite to thermal catalysis where gas molecules are mostly in the ground state when they are adsorbed onto a catalyst surface [131]. Non-thermal plasma produces ions, radicals and electronically excited species which can enhance plasma volume reactions, because their internal energies are often higher than the activation energies for thermal catalysis. For ions and radicals usually required threshold energies are in the range of 5-20 eV and for electronically excited species, threshold energies are in the range of 1-10 eV. While vibrationally excited species are produced with lower threshold energies of 0.1-1 eV and that is why the internal energies are too low to simplify plasma volume reactions. But activation energies for reactions involving vibrational species can be lowered when adsorbed to a catalyst surface. Therefore, the vibrational state can be a significant contributor to the acceleration of catalysis in a plasma system. Furthermore, the energy required for surface adsorption of radical species may be lower than for adsorption of ground state gas molecules, what can also lead to enhancements in plasma-catalysis [131].

By using non-thermal plasma many highly durable catalysts have been prepared for CO₂ and CH₄ conversions and in both catalysts and plasma combined reactions, it is expected that plasma would modify the physic-chemical properties of a catalyst in situ, after which the modified catalyst would show high performance in the plasma reaction [136].

5.6. Plasma-Catalytic Methanation

The combination of non-thermal plasma and catalysis can be recognized as an effective and promising solution to convert CO₂ and renewable H₂ into higher value chemicals at low temperatures and atmospheric pressure. Plasma-catalytic processes have potential to generate a

synergistic effect. This effect can reduce the activation energy of the reaction, to increase the conversion of reactants, and to raise the selectivity and yield toward the desired products. All of these contribute in various ways to enhancing the energy efficiency of the plasma process and activity and stability of the catalyst. Plasma processes are highly flexible and can be integrated with a renewable energy source which can provide energy for the plasma system.

Though many different metals have been used to catalyze the methanation process, catalysts, mostly based on Group VIII metals such as Ni and Ru supported on various porous materials, are of the most commonly studied required to achieve considerable methanation rates [41, 51, 137-139]. Ni-based catalysts have been widely investigated, because of their high activity and low price [50]. The interaction between the metal and support also plays a very active role in catalyst performance [52] and an important role in the active site dispersion, stability and activity [140].

Yamasaki et al. [141] studied the effect of tetragonal ZrO₂ on the catalytic activity of Ni/ZrO₂ catalyst. Actually, ZrO₂ is very interesting support due to its acidic/basic features and CO₂ adsorption abilities. Fraction of ZrO₂ was increased with increasing of Ni content which had an impact on methanation activity. Perkas et al. [142] developed Ni/ZrO₂ catalysts doped with Ce cations. Higher porous volume and size which was obtained with 30 mol% Ni loading had impact on higher catalytic activity of CO₂ methanation. It was recognized as a synergistic effect between the surface area and the doping of the rare earth elements. The surface area was increased due to the mesoporous structure in the support, which showed the insertion of the Ni particles into the pores. It was also reported that Ni-based catalysts prepared by using DBD plasma has higher metal dispersion than that prepared by calcinations method and the addition of Ce can enhance the dispersion of Ni [143, 144]. Ocampo et al. [19] evaluated CO₂ methanation activity of Ni-ceria-zirconia for the first time and revealed that Ni-ceria-zirconia exhibited excellent catalytic activity and stability during 150h on stream. Such high performances were due to the high oxygen storage capacity of ceria-zirconia oxides and the highly disperse nickel. Other studies [21] claimed that CO₂ methanation activity on Ni-ceria-zirconia was related to the particular interaction between Ni²⁺ cations and ceria-zirconia support.

Lately, hydrotalcite materials have started to attract attention for their application in CO₂ methanation and in catalysis due to the ability to exchange interlayer anions, their particular

basic features and the possibility of introducing different type of divalent (Mg^{2+} , Co^{2+} , Ni^{2+} , Mn^{2+} , Zn^{2+}) and trivalent (Al^{3+} , Fe^{3+} , Cr^{3+}) cations into their brucite-like structure [145]. Moreover, Debek et al. [145] studied the addition of Ce-species into the catalytic hydrotalcite-based structure and showed that they promoted the reducibility of the nickel species and resulted in the introduction of new strong oxygen species and intermediate (Lewis acid-base pairs) strength basic sites, which increased the CO_2 adsorption capacity of the catalysts. Promoters such as CeO_2 and ZrO_2 can elevate catalytic activity and thermal stability of Ni-based catalysts. He et al. [146] showed excellent performance at 350 °C for CO_2 methanation using Ni- Al_2O_3 -HT catalyst derived from Ni-Al hydrotalcite precursor provided highly dispersed Ni particles along with strong basic sites. The reaction started at 225 °C and the CH_4 selectivity could reach 99.5 % at 350 °C and the CO_2 conversion of 82.5 % and remained unchanged for 20h in the catalyst stability test. Fan et al. [147] studied CO_2 methanation over Ni/ MgAl_2O_4 catalysts prepared by different decomposition methods. They obtained smaller Ni particles with enhanced metal-support interaction and unique structure through DBD decomposition, which facilitated the hydrogenation of CO_2 to CH_4 . The DBD plasma decomposition was found to be beneficial for improvement in the catalytic activity.

For thermal-catalytic CO_2 hydrogenation at high temperatures between 300-500 °C a wide range of supported metal catalysts have been studied to this day. Du et al. [148] evaluated CO_2 methanation activity of Ni/MCM-41 catalysts with different amount of Ni. Reduction at high temperature (700 °C) produced stable catalyst with good activity and selectivity since most Ni species was reduced to highly dispersed Ni^0 due to the surface hitching effect. Cheng et al. [149] examined the reaction mechanisms of CO formation in the RWGS reaction over a Cu/ γ - Al_2O_3 catalyst at 500 °C. Liu et al. [150] found that Mn-based catalysts were the most promising catalysts in the RWGS reaction. Cai et al. [151] studied fractional-hydrolysis-driven formation of non-uniform dopant concentration catalyst nanoparticles of Ni/ $\text{Ce}_x\text{Zr}_{1-x}\text{O}_2$ in methanation of CO_2 and showed that a structure with Ce and Ni enriched at the surface improved the conversion of carbon dioxide. Despite the encouraging results observed for Ni-catalysts at around 300 °C and atmospheric pressure, the presence of water in the products leads to the sintering of Ni particles, which is the main reason for catalysts deactivation.

It is well known that during CO_2 methanation the presence of water in the products leads to the sintering of Ni particles, which results in deactivation of the catalysts. Likewise, the secondary reactions favor the CO and H_2 formation at higher temperatures (>300 °C). A

hybrid combination of catalysts with Dielectric Barrier Discharge plasma (DBD) may allow us to overcome all the above mentioned drawbacks. Moreover, DBD catalytic reactors require usually only very low consumption of electricity power, less than 12kJ/mole of CH₄ and, at the same time, they meet all the requirements for large volume methane production [44]. Among various plasma, DBD plasma can be effective for assisting catalytic methanation. Non-thermal plasma which produces a variety of active species such as electrons, ions and radicals has been applied to the methanation of CO [25, 152, 153]. Song et al. [25] investigated the production of synthesis gas with the use of a Ni catalyst packed in dielectric barrier discharge (DBD) reactor, and reported that the CO selectivity considerably increased with the application of plasma. J. Amouroux et al. [24] studied process for the carbon dioxide reduction to methane by DBD plasma activated catalyst. They showed that under adiabatic conditions DBD plasma was able to greatly improve the conversion of CO₂ at low temperatures. Furthermore, Jwa et al. found that non-thermal plasma could enhance the rate of catalytic methanation of CO using a coupled plasma catalytic process using a Ni-Zeolite catalyst [137]. Oshima et al. [154] reported the effect of electric field on the RWGS reaction over different La-ZrO₂ supported catalysts at low temperatures. Table 9 shows more examples of the CO₂ catalysts investigated in the literature under thermal catalytic systems and plasma catalytic systems.

But a very limited work has been carried out to investigate the CO₂ hydrogenation using plasma-catalytic processes at low temperatures up until now. In this work we investigate a hybrid plasma-catalytic methanation process in order to propose optimum low temperature conditions. A combined catalysts and DBD plasma led to the high yields necessary for these processes to become economically viable. Structural and chemical characterizations were performed on selected Ni-Ce_xZr_{1-x}O₂ and Ni-Mg-Al hydrotalcite-derived catalysts prior and after methanation reactions in order to show the viability of this process in terms of catalyst durability.

Table 9. CO₂ catalysts investigated in the literature under thermal catalytic systems and plasma catalytic systems.

Catalyst	Temp. (°C)	Feed Ratio, H ₂ :CO ₂	CO ₂ Conversion (%)	CH ₄ Selectivity (%)	CH ₄ Yield (%)
Thermal catalytic systems of CO₂ and CO methanation					
15%Ni/RHA-Al ₂ O ₃ [52]	500	4:1	63	90	58
LaNi ₄ Al [155]	400	4:1	91.50	95	-
15%Ni-2%CeO ₂ /Al ₂ O ₃ [156]	300	4:1	71	99	-
10%Ni/La ₂ O ₃ [157]	380	4:1	100	100	-
10%Ni-Ce _{0.72} Zr _{0.28} O ₂ [19]	350	4:1	75	99.10	-
5%Ni-Ce _{0.5} Zr _{0.5} O [21]	350	4:1	65.90	98.20	-
Ni ₄₀ (Zr _{0.9} Ce _{0.1})O _x [142]	350	4:1	81	100	-
5%Ni-CZ [158]	350	4:1	67.90	98.40	-
14%Ni7%CeUSY [45]	400	4:1	68.30	95.10	-
10%Ni/CeO ₂ [102]	350	4:1	90	100	-
15%Ni/SiC [159]	350	4:1	83	100	-
Ce _{0.96} Ru _{0.04} O ₂ [16]	450	4:1	55	99	-
Pd-Mg/SiO ₂ [37]	450	4:1	59.20	95.30	56.40
Plasma catalytic systems of CO₂ and CO methanation					
Ru/TiO ₂ /Al ₂ O ₃ [153]	240	1:3	78	93	-
Ni-Al ₂ O ₃ -HT [146]	350	4:1	82.50	99.50	-
Ni/MgAl ₂ O ₄ [147]	300	4:1	71.80	-	71.80
10%Ni-Zeolite [26]	220	4:1	82	-	-
15%Ni Ce _{0.9} Zr _{0.1} O ₂ SBA15 [24]	140	4:1	75.70	99	75.70
20%Ni-30%Ce/Cs-USY [24]	120	4:1	64.90	92	55.06

6. Conclusions

The proofs for climate change are huge and indisputable but the only insecurity lies in the predictions for how rapid and how severe the consequences will be known. Emissions of CO₂ will continue to increase leading to drastic effects on the environment until the world's fossil fuel dependence is not curbed.

This chapter has presented an extensive series of investigations into CO₂ methanation. From the literature, it appears that Ni is the best optional candidate from other catalysts due to its high selectivity for methane production. The role of the support dominates the catalyst design in reference to developing an efficient methanation catalyst, mainly with respect to ensuring enhanced metal dispersion and a long catalyst lifetime. As the methanation reaction is exothermic, the excessive heat of reaction induces metal sintering, which lowers the total metal surface area and leads to the poor activity observed for the classical supports. Therefore, it is essential that an efficient and low-temperature methanation catalyst with a high thermal stability and coke formation resistance should be developed. Many investigations have focused on the CO₂ methanation, but significant effort must still be made in the coming years to understand the fundamental reaction mechanisms in order to improve the activity and the selectivity of catalysts for methane. Indeed, many proposals about intermediates and mechanisms employed for the CO₂ methanation have been formulated. However, a final picture has not been drawn yet.

Plasma processing of CO₂ could assure an alternative means of CO₂ conversion to produce gaseous products such as methane. The highly energetic plasma electrons have the possibility to successfully excite and dissociate CO₂ via collisional processes, reducing anthropogenic CO₂ emissions. This plasma technology could provide a means to continue burning fossil fuels without emission harmful carbon emissions into the atmosphere.

The potential of non-thermal plasma technologies for the methanation of CO₂ has been described also in this chapter. Non-thermal plasma have many advantages over conventional catalysis, especially that they can be generated under ambient conditions and need no complex systems. There are some collisional processes that affect the energy exchange of charged and neutral species. The addition of catalyst material may help to increase conversion rate without changing the energy input and shift temperature of the process to much lower, leading to a more

energy efficient reaction than with plasma alone. During the hybrid process there is no evolution of the catalytic phases that lead us to optimistic for the scaling up of such kind of process.

Chapter 2: Experimental Set-up and Diagnostics

Carbon dioxide methanation coupled by plasma catalytic system was studied in this thesis. The effect of the plasma discharge on the conversion of CO₂ was checked with nickel supported on ceria-zirconia mixed oxide (Ce_xZr_{1-x}O₂) [19, 21] and hydrotalcite catalysts [145-147] to understand the role of the plasma and find out how efficient the plasma-catalysis is in the production of methane. The catalysts commonly used for methane production are based on transition metals supported on metal oxides [84, 160]. Even though the catalysts consisting of a noble metal, such as ruthenium or rhodium [84, 138, 160], nickel-based catalysts have been the most widely studied because nickel is cheap and shows high activity [84, 161, 162].

The tests were carried out by varying reactor temperature under plasma and non-plasma conditions at constant CO₂/H₂ ratios in the feed gas. This reaction was tested at different operation conditions in the laboratory. When introducing a catalyst into a plasma discharge, the impact that the dielectric properties of the catalyst have on plasma generation must be recognized for CO₂ methanation, also other operating parameters such as specific input energy, gas temperature and DBD configuration. The objective was to investigate a hybrid catalytic plasma system for CO₂ methanation based on a DBD plasma and catalysts. The main topics introduced in this chapter are the experimental set up of the reaction system, the procedure used in CO₂ hydrogenation to CH₄ and corresponding calculation methods. Details of the experimental aspects of this research will be presented below. These subjects will be reviewed to facilitate the interpretation and understanding of the results of this experimental work. Experimental part is composed from three chapters (chapter III, IV and V).

1. Dielectric Barrier Discharge Methanation Setup Description

Experiments were performed in Institut de Recherche de Chimie Paris and Institut Pierre-Gilles de Gennes, both of which are located in Paris, and also in the Institut Jean Le Rond d'Alembert (UPMC) located in Saint-Cyr-L'Ecole. Figure 33 shows the experimental set-up for this study, consisting of mass flow controllers (MKS Instruments, Inc.), high-voltage power supply, a hybrid plasma-catalytic reactor, a digital oscilloscope and a gas

chromatograph. What was also used for some tests was a Fourier transform infrared spectrometer (FTIR), an optical emission spectrometer (OES) and a mass spectrometer (MS, Pfeiffer Omnistar 422), which facilitated following the formation of other possibly products such as formic acid. It consists of three major systems: the reactor, plasma generation, and product collection. Copper, teflon and stainless steel tubing (1/4th and 1/8th inch) and Swagelok fittings were used for the reactor set-up.

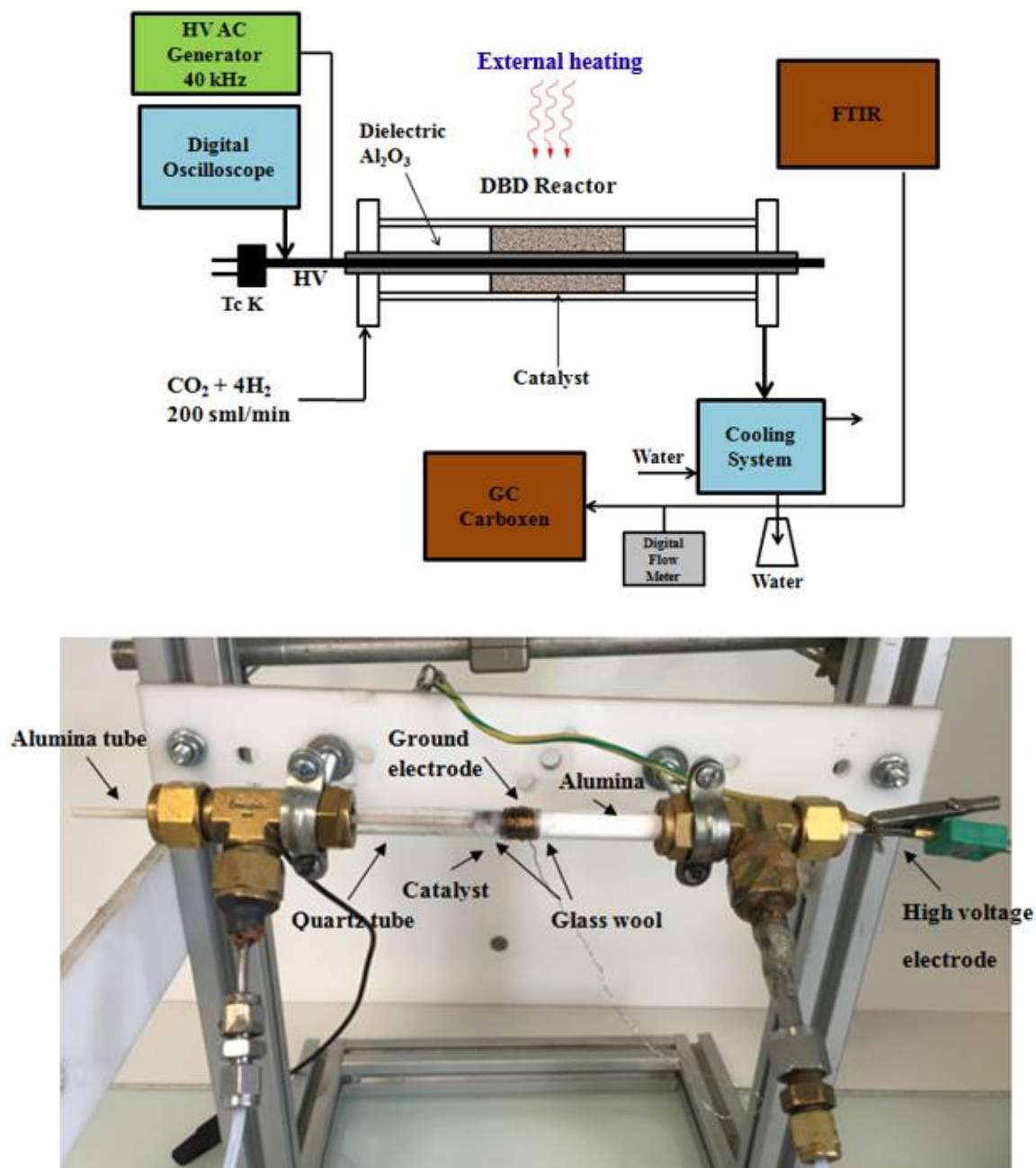


Fig. 33. Schematic diagram and picture of the experimental set-up used for plasma assisted catalytic methanation of CO₂.

1.1. Reactor System

Hybrid plasma-catalytic methanation performance of CO₂ to CH₄ was evaluated in a dielectric barrier discharge (DBD) plasma reactor operating at atmospheric pressure and consisted of two coaxial tubes (quartz and alumina tubes). Between the outer tube (∅ (diameter), 10 mm and a wall thickness, 1 mm) and the inner (∅, 3 mm) the discharge was sustained in a gap of 2,5 mm with steel foil wrapped around the outer surface of the quartz tube acting as the ground electrode. The effective length of the DBD reactor was approximately 10 mm, corresponding to the height of the steel foil. The catalysts tested were packed inside the discharge gap and held in place with quartz wool. The DBD reactor used in the present work is shown in Figure 34.

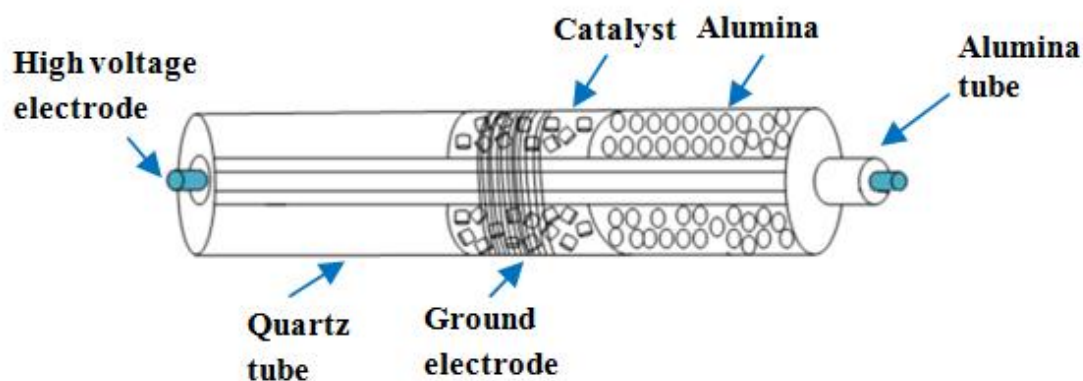


Fig. 34. Dielectric barrier discharge plasma reactor.

Plasma-assisted catalytic methanation and conventional catalytic methanation were performed at atmospheric pressure over a temperature range of 100-420 °C. To keep volume 0.6 cm³ the amount of catalyst placed at the annular space of the discharge zone in DBD reactor was approximately 300 mg (depending on catalyst density). The experiments were carried out with a packed bed of dielectric material in the reactor (alumina). To avoid any problems with the flow and catalyst, alumina was placed in the reactor (it has not any effect on the measurements, but prevents the catalyst from any movement). The feed gas containing 20 vol% CO₂ and 80 vol% of pure H₂ was passed through the reactor at a flow rate of 200 mL/min. Gas hourly space velocity (GHSV) was calculated as presented below. This variable facilitate the

evaluation of the catalyst behaviour in direct relation with the amount of catalyst. The GHSV is calculated as follows:

$$\text{GHSV} = Q_{\text{in}}/V_{\text{cat}}$$

Q_{in} - inlet volumetric flow rates

V_{cat} - volume of catalyst

Under such conditions, the Gas Hourly Space Velocity (GHSV) was found to be 20,000 h^{-1} for catalysts from the CEOPS project, 20,000 h^{-1} for hydrotalcite catalysts and 52,000 h^{-1} for the $\text{Ni/Ce}_x\text{Zr}_{1-x}\text{O}_2$ catalysts (0.3 g mass of catalyst and 0.23 cm^3 the volume). Gas flow rates were controlled by mass flow controllers (MKS Instruments) and gas mixtures were stabilised before the plasma was turned on. Temperature was kept constant with the aid of an external convection heater. The reactor could be heated up to 500 °C.

1.2. Temperature Measurement

The reactor temperature was measured with a K-type thermocouple placed close to the catalytic bed as shown in Figure 35. The use of infrared for temperature measurement was not practically with the current configuration of the reactor system. As both systems have showed the same temperature during measurement, the thermocouple was employed even though it may not have been equally accurate.

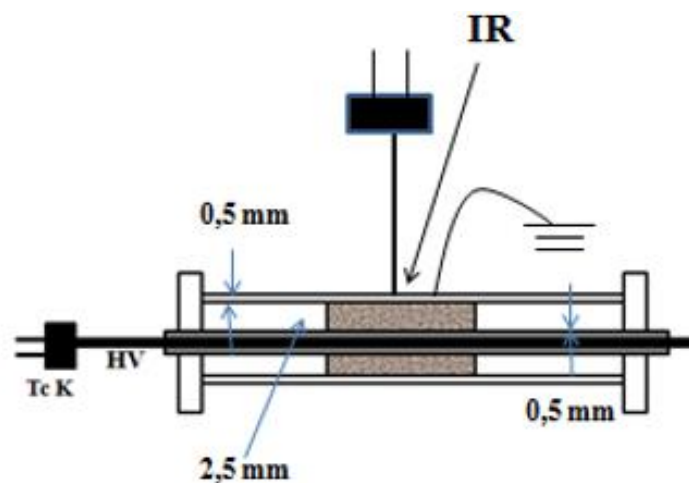


Fig. 35. System for a temperature measurement.

1.3. Plasma Generation System

An alternating current (AC) high voltage, (operating frequency: 40-41 kHz) in the range of 10-18 kV (peak to peak), was applied to the discharge electrode to create plasma. It corresponded to a power between 1-3 W over a temperature range of 100-400 °C (power calculate by using UI method) and 3-6 W over a temperature range of 100-200 °C (adiabatic conditions) and between 7-9 W over temperature range of 200-400 °C (isothermal conditions) - power calculate by using Lissajous method. The voltage-current waveforms were measured with the use of an numerical oscilloscope (LT 342, LeCroy) or a pico oscilloscope (picoTechnology, PicoScope 5000 Series) with the use of a high voltage probe (ELDITEST GE 3830-voltage measurement of up to 30 kV) and Pearson 2877 Current transformer (frequency range - 300 Hz-200 MHz) respectively.

1.3.1. Energy or Power Measurement

For determination of the discharge power in a plasma reactor we can distinguishes two possible methods. Firstly with method measures the input Voltage and the Current through the plasma reactor (UI) and then by Lissajous method.

The former (UI) measures the input voltage and the current over a resistor (the current through the plasma reactor). Characteristic waveforms for the input voltage and current in a DBD reactor, recorded using an oscilloscope is shown in Figure 36.

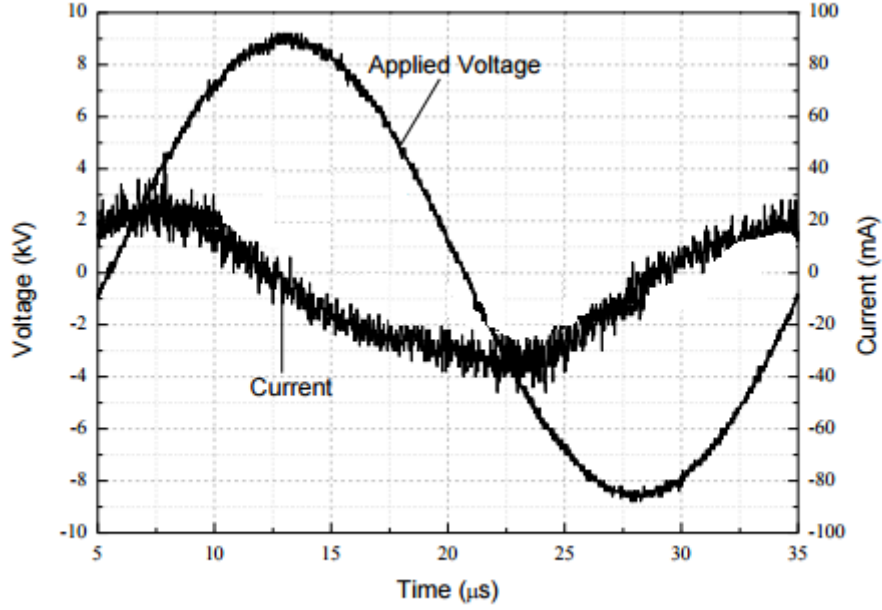


Fig. 36. Reactor voltage $U(t)$ and current $I(t)$ waveforms for a DBD.

The temporary power (P) in the reactor at any given time can be calculated by multiplying the $U(t)$ (the high voltage (HV) on the reactor) and current $I(t)$ (current flowing through the reactor (and resistor (R))). It is the simplest to understand by follow the equation as shown below:

$$P(t) = U(t) * I(t) \quad (1)$$

The current is calculated as presented underneath, where V_R is the voltage across the resistor and R is the resistance:

$$I(t) = V_R(t)/R \quad (2)$$

By integrating the discharge power over one cycle (where t_0 is the centre of the cycle) can calculated the average power over a single period (T) as shown below:

$$P = \frac{1}{T} \int_{t_0-T/2}^{t_0+T/2} P * dt = \frac{1}{T} \int_{t_0-T/2}^{t_0+T/2} U(t) * I(t) * dt = \frac{1}{T} \int_{t_0-T/2}^{t_0+T/2} \frac{U(t) * V_R(t)}{R} * dt \quad (3)$$

Due to the plasma is a series of microdischarges of short duration and the current waveform needed to capture this information accurately this method is difficult to perform [104].

The latter, Lissajous method introduced by Manley in 1943 [163] is now recognized to be the most precise method for DBD power determination. This method requires the measurement of the input voltage and the voltage (V_c) across a capacitor displayed in oscilloscope. The capacitor accumulates a charge from the current flowing over the reactor and this can be determined by measuring the voltage on the capacitor (V_c) as shown below:

$$Q(t) = C * V_c(t) \tag{4}$$

We can plot the charge versus high voltage which is known as a Q-U Lissajous figure (the area of which is equal to the discharge power) by recording the values for $Q(t)$ and $U(t)$ via a series of regularly sampled points which capture the full cycle of the AC sinusoidal wave (Fig. 37).

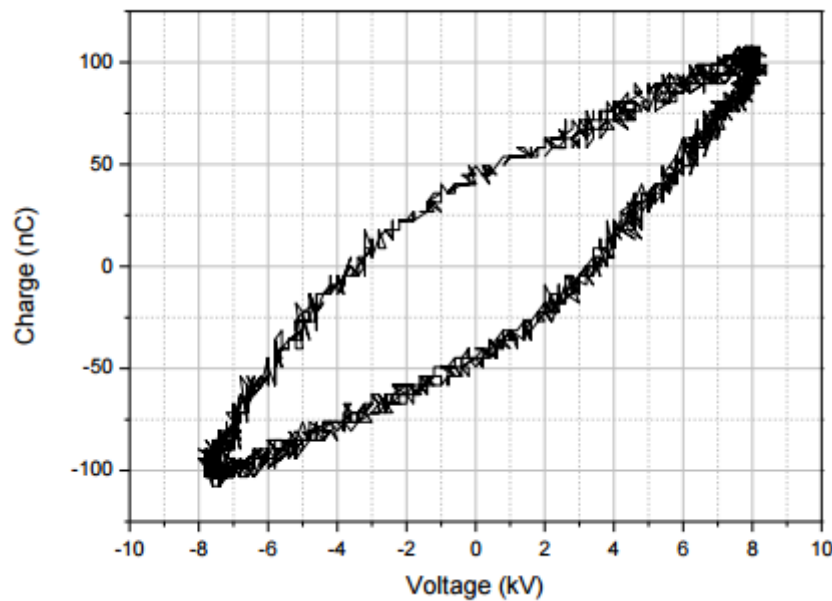


Fig. 37. Q-U Lissajous figure.

As shown below the area of the Lissajous figure can be calculated by the integration in Equation 8 [163, 164]. The benefit is that the charge is stored in the capacitor and does not require a fast transient digitiser to record it. The energy per cycle (W) can be found from Equation 3 by multiplying by T .

$$W = \int_{t_0 - T/2}^{t_0 + T/2} U(t) * I(t) dt \tag{5}$$

The current flowing over the measuring capacitor (C) is given by:

$$I(t) = \frac{dQ}{dt} = C \frac{dV_c}{dt} \quad (6)$$

From here we have:

$$Q(t) = C * V_c(t) \quad (7)$$

So the energy per cycle is:

$$W = \int_{t_0-T/2}^{t_0+T/2} U(t) * C * V_c(t) dt = \int_{t_0-T/2}^{t_0+T/2} U(t) * dQ(t) \quad (8)$$

And if we register U(t) and Q(t) as a series of n regularly sampled points via one cycle we can approximate W (energy per cycle) by a summation using trapezoidal integration as:

$$W \approx \sum_{k=1}^n \left(\frac{U_{k+1} + U_k}{2} \right) * (q_{k+1} - q_k) \quad (9)$$

So to get the power in the reactor we need to multiply by the number of cycles per second and if the voltage (U) has a frequency (f), where:

$$f = 1/T \text{ we have:} \quad (10)$$

$$P = W * f = f \sum_{k=1}^n \left(\frac{U_{k+1} + U_k}{2} \right) * (q_{k+1} - q_k) \quad (11)$$

The area of a Q-U Lissajous figure is represented by integrals in Equation 11 and 8. The gradients and positions of the lines from Lissajous figure can be used to calculate some of the electrical parameters of the discharge such as: peak-peak charge, charge discharged, transferred charge and capacitance [163, 165, 166].

A LabVIEW system was used for the measurement of the plasma power (Lissajous figures) [163]. The LabVIEW system is based on a 2-channel analogue to digital conversion (ADC) sampling method and uses Picoscope hardware (picoTechnology, PicoScope 5000 Series); this was chosen to record the waveforms for the high voltage AC sine wave (via a 1:1000 reducing probe) and the voltage across a capacitor (5 nF). Details of the method for

power calculation and functions of the LabVIEW system can be found below.

PicoScope 5000 Series connections:

- Chan A (voltage): HV via 1:1000 reducing probe,
- Chan B (current): Vc from probe capacitor.

The power was calculated from Equation 8 with the use of the numerical approximation of Equation 11:

$$P = W * f = f \sum_{k=1}^n \left(\frac{U_{k+1} + U_k}{2} \right) * (q_{k+1} - q_k) \tag{11}$$

This requires the frequency (f) of the HV supply and a single cycle of data from U(t) and V_c (t).

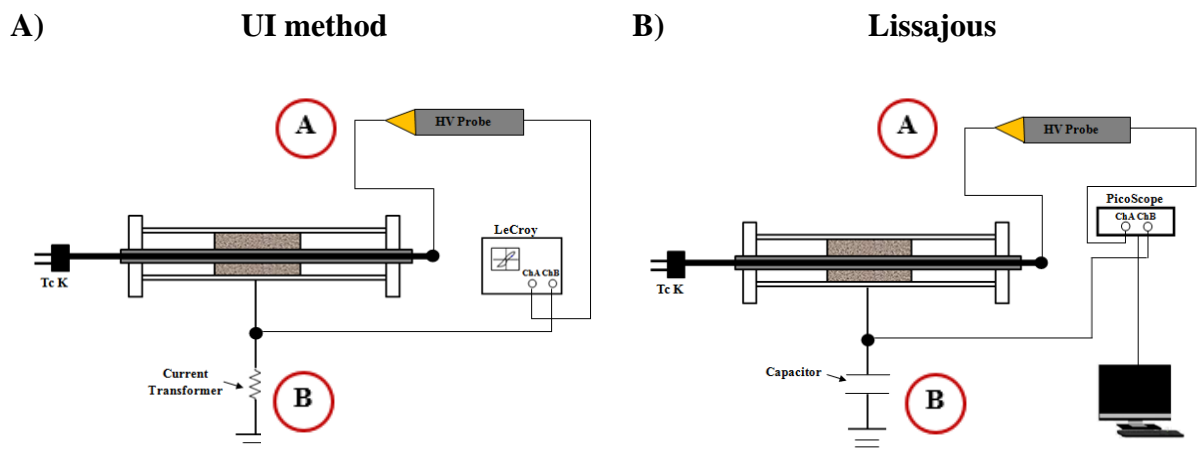


Fig.38. Circuit for measuring the discharge power of a plasma reactor: A) High Voltage and the Current method (UI); B) Lissajous method, where B, A - channels .

Figure 38 shows a typical circuit layout used during tests. The power was determined by measuring input voltage U(t) and either the current flowing through the current transformer (Fig. 38A), or the charge on capacitor (Fig. 38B).

The specific input energy is defined as the amount of energy spent per liter of reactant or product gas by the following equations:

Specific Input Energy [J/L] = [Power [W] / Flow rate [L/s]]

Power [W] - Power input at discharge,

Flow rate [L/s]] - Total input flow rate.

This parameter is an important variable that directly influences the methanation reaction. Furthermore, the latter changes along with the reactants flow rate and/or the residence time. Experiments that are reported in this study were carried out at a constant flow rate.

1.3.2. Gap

In all experiments throughout this research the discharge gap was kept constant - 2.5 mm. Increased in discharge gap will result in variation breakdown voltage and larger current, there by changing the discharge power.

1.4. Product Collection System

As reaction takes place at high temperatures, exhaust gases were cooled in order to collect the liquid products. The product stream passed through a short stainless steel tube into an unheated section of tubing that led to the collector section of the apparatus. Drops that condensed in this section fell down the tube into the condenser and collection vessel. For CO₂ methanation the liquid products contained pure water. Water formed as product was continuously removed and condensed from the product gas. The mass balance was performed at steady state (after 30 min time on stream), and the conversion rate of carbon dioxide and the methane or carbon monoxide production was calculated.

2. Diagnostics

To monitor the excited species in a gas discharge in situ method was used - Optical Emission Spectroscopy (OES) [167-171]. Spectroscopic analyses showed here were used to

find the species as: CH, CO, H α , and OH present within such plasmas in discharge (H₂, CO₂ and CO₂/H₂).

To analyze CO₂/H₂ and all gaseous products ex-situ methods were used - Gas Chromatography (GC) and Fourier Transform Infrared Spectroscopy (FTIR). Analyses were performed also for the liquids products (ultrapure H₂O). The liquids products were checked in another laboratory with the use of NMR analysis.

2.1. Optical Emission Spectroscopy - In Situ Diagnostics

Most widely used diagnostics of plasma processes, particularly for the atmospheric pressure plasma source is Optical Emission Spectrometry (OES). It is the spectral analysis of the light emanating from plasma and the least perturbing in-situ plasma diagnostic method. OES measures emissions from excited atoms and molecules. Species emission is dependent upon the concentration of species in their excited states, and is therefore a convolution of the concentration and distribution of ground state species, and the source for their excitation, for example electrons in a plasma. We can identify the neutral particles and ions present in the plasma by measuring the wavelengths and intensities of the emitted spectral lines. Setup is simple, as light is collected from the emitting source, and directed onto a diffraction grating, which separates the light into its constituent wavelengths. The light is then passed onto a detector such as a charged couple detector (CCD), and then it can be converted into an emission spectrum. The spectral fingerprint of optical plasma emission supplies information about the chemical and physical processes that take place in plasma but it also provides temporal resolution with high reliability [170, 171].

In present thesis, OES system Czerny-Turner spectrometer was used for the identification of active species within the plasma volume. This spectrometer was equipped with three gratings: 1200 grooves.mm⁻¹, 300 nm blaze, 2400 and 3600 grooves.mm⁻¹, 240 nm blaze. The diffraction grating is very important element of the monochromator as it distinguishes each different wavelength components. The emitted light was transmitted to the spectrometer through a 19 optical fiber bundle. A spectral band extending from 200 to 900 nm was used. The OES system consists of a monochromator (Acton, Model SpectraPro 2750) which has a focal length of 750 mm, grating controller and CCD detector (1024 × 1024 pixels) with an intensifier

system (Princeton instruments PIMAX) as shown in Figure 39. The software WinSpec was used for parameter control and spectra processing.

Generally, the slit width and exposure time would be significant parameters in optical measurement using OES. The minimum adjustable slit width is 10 μm , but according to the intensity of the incident light source it can be adjusted and in this research, a slit width of 100 μm was used. The signal emission was reached by averaging 10 scans to compensate energy fluctuations and the spectrum acquisition was typically made with a time of 100 ms.

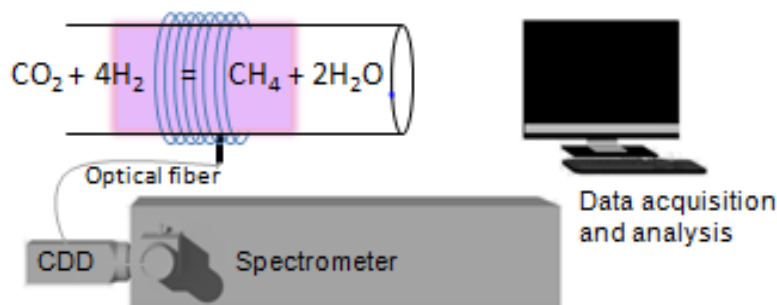


Fig. 39. Experimental setup for optical emission spectrum measurement.

2.2. Description of Gas Chromatography

During experiments in this thesis gas chromatography (GC) was used for the analysis of gas mixtures and to analyze CO_2 we used also a specific sensor. A gas chromatograph analyses the composition and concentration of sample gas by flowing it over long capillary tubes (column). Chromatography needs a „mobile phase” (including the mixture to be separated) and a „stationary phase” over which the mobile phase can be eluted. The mobile phase is generally an inert carrier gas (helium or argon), which is continuously passed over a column containing the stationary phase.

GC columns consisted of a tube containing a packing of solid support material with different liquid or solid coatings depending on the type of mixture being separated. Most GCs currently use capillary columns, which give many benefits over packed columns. The stationary phase is covered evenly on the inside of a capillary tube which eliminates problems related with irregular packing [172].

Into the column is injected the mixture to be separated. Various gas species pass over the column at various rates depending on the strength of electrostatic interactions with the walls of the column. This causes the gas mixture to be separated into individual components that reach the end of the column and are detected at different times. The component gases can be identified by comparison with chromatograms for known species (by measuring the retention time of each species in the column). Selection of right column materials and operating conditions are critical for resolution of the gas mixture, because retention times are affected by the gas concentration, flow rate and pressure, the column material and temperature [172]. The signal produced by each gas is characteristic for that gas, as it reaches the detector results in a peak on the chromatogram at a residence time. Moreover, the peak area is proportional to the gas concentration. Typical gas chromatogram is shown in Figure 40.

The concentrations of relevant compounds were analyzed by a gas chromatograph - an IGC 120 ML, Delsi Intersmat equipped with an analytical column (Carboxen), using helium as a carrier gas. Gas products were analyzed during experimental runs by taking gas samples from the exit stream with a gas-tight syringe and injecting into the GC. Gas sample analysis required approximately 20 minutes. Composition of product gases, including the unreacted gases analyzed by GC-TCD, are depicted below, numbers 1-6 denote the retention time (RT, min) for every component detected, for which He is used as reference as shown in Figure 40:

- (1). hydrogen (H_2) (RT \approx 1.5)
- (2). oxygen (O_2) (RT \approx 4)
- (3). nitrogen (N_2) (RT \approx 5)
- (4). carbon monoxide (CO) (RT \approx 6.5)
- (5). methane (CH_4) (RT \approx 12)
- (6). carbon dioxide (CO_2) (RT \approx 15.5)

The product compositions were determined from the peaks area, corresponding at retention time of the various components, compared to the peaks area of standard gas.

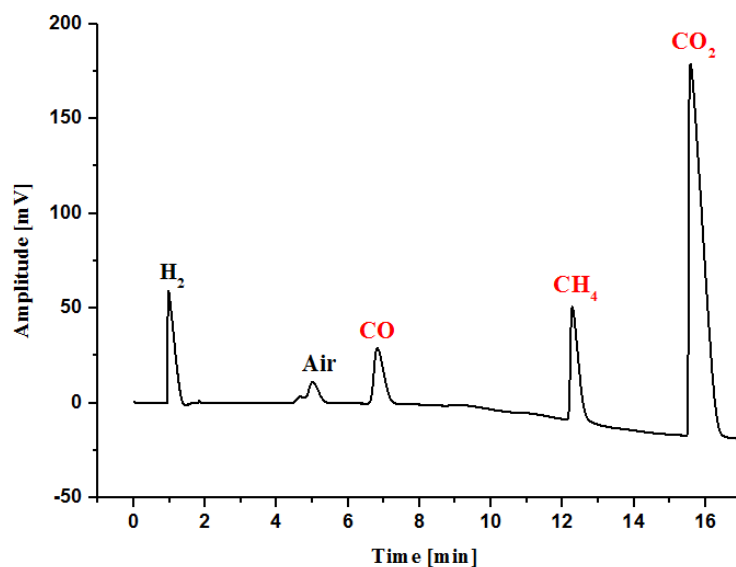


Fig. 40. Gas chromatogram obtained using Carboxen column in an IGC 120 ML, Delsi Intersmat GC.

Gas sample components were detected using an Thermal Conductivity Detector (TCD). Thermal conductivity (TCD) is a commonly used detector in gas chromatography. This detector can be used for the detection of any gases that are different in thermal conductivity to the carrier gas. As depicted in Figure 41, a detector consist of some filaments in a Wheatstone bridge system: the column effluent (R3) and reference gas (R4) enter cells containing analytical filaments. Remaining filaments that complete the bridge (R1 and R2) have fixed resistances so the change in voltage through the bridge is proportional to the change in resistance when a constant current is applied. The resistance of the analytical filament varies depending on the temperature, which is affect by the thermal conduction of the gas being detected. The voltage over the bridge is measured and the signal is reinforced to provide the GC response signal. Electrically heated tungsten-rhenium or platinum wires are generally used for the analytical filaments [172]. The filaments often have a non-linear response and require individual calibration for each type of gas being analysed. During the design of practical measuring devices, it was found that the overall amount of heat transferred is not given by the thermal conductivity of the medium alone, but that the molar heat capacity and other factors also play a significant role.

While flame ionization detector (FID) can ensure very good resolution, TCD is a good detector for initial studies with an unknown sample. As it responds to all compounds, thanks to

the fact that all compounds (organic and inorganic), have a various thermal conductivity from helium. Moreover, the TCD is also used in the analysis of permanent and inorganic gases (argon, oxygen, nitrogen, carbon dioxide, carbon monoxide) because it responds to all these substances. Whereas the flame ionization detector cannot detect compounds which do not contain C-H bonds.

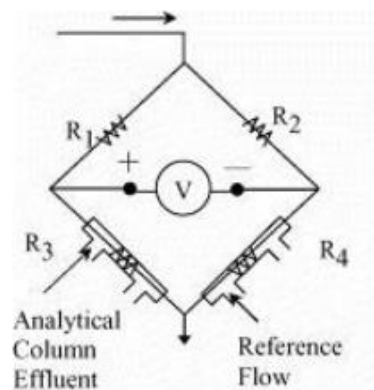


Fig. 41. Illustration of a thermal conductivity detector [173].

The gases that were detectable included all of the hydrocarbon reactants (methane) and the permanent gas products (carbon monoxide, carbon dioxide). Oxygen and argon were neither reliably separated nor detected by this system. Argon would be used as the plasma medium as it will easily maintain a plasma at relatively low power. Moreover, with addition of Ar, a more stable discharge was obtained, and according to some authors Ar or He activates the catalyst.

2.2.1. Calibration of Gas Chromatograph

The gas analysis takes place in the gas chromatograph (IGC 120 ML, Delsi Intersmat), it is calibrated for 5 different gases using a gas calibration standard (SCOTTY 48) and using pure gases. This standard contains 1 mol% each of CO₂, CH₄, CO, H₂ and O₂ in 95 mol% of N₂. Gas sample was injected to the gas chromatograph using glass syringes (Dynatech Precision Sampling, Series 5 mL) of 0.5, 1, 1.5, 2, 3, 4 and 5 mL. Using five or three different volumes allows five-point/three-point, linear calibrations for each gas. In Appendix A, the calibration of the equipment is given briefly.

2.2.2. Calculation of Products

To calculate CO₂ conversion (X_{CO₂}) and the selectivity of CH₄ (S_{CH₄}), the products were collected after half hour of steady-state operation at each temperature. The calculation of product selectivity for CO₂ methanation was based on the carbon in the CO₂ converted for CH₄ and CO and was defined as follows:

$$X_{CO_2} = 100 \times ([CO_2]_{ini} - [CO_2]_{product}) / [CO_2]_{ini}$$

where [CO₂]_{ini} and [CO₂]_{product} are respectively the concentrations of CO₂ in the gas entering and existing in the reactor,

and selectivity to methane:

$$S_{CH_4} = 100 \times ([CH_4]_{product}) / ([CO_2]_{ini} - [CO_2]_{product})$$

and CO yield:

$$Y_{CO} = 100 \times ([CO]_{product}) / ([CO_2]_{ini} - [CO_2]_{product})$$

If there was a problem with mass balance the calculation of product selectivity for CO₂ methanation was defined as follows:

$$X_{CO_2} = 100 \times ([CO_2]_{ini}) / ([CO_2]_{product} + [CH_4]_{product} + [CO]_{product})$$

$$S_{CH_4} = 100 \times ([CH_4]_{product}) / ([CH_4]_{product} + [CO]_{product})$$

2.3. Technical Properties of Fourier Transform Infrared (FTIR) Spectroscopy

Fourier Transform Infrared (FTIR) spectroscopy is a technique that can be applied to the analysis of solids, liquids or gases. It is an effective tool used for the detection and characterization of different types of molecules. Moreover, this technique remains an impressive approach as it is cheap (equipment and reagents), does not require high grade solvents or expensive internal standards. Further, equipment is widely available in standard laboratories and the method is suitable for routine analyses [174].

Spectra are commonly plotted as the absorbance as a function of the wavenumber (1/wavelength). They contain absorption peaks which appear at wavenumbers corresponding to various modes of vibrations of bonded atoms present in the sample molecules. The absorption wavenumber depends on the relative mass and the geometry of the atoms. Resonance between vibrations depends on molecule conformation and further modulates the spectra. Then, IR spectra contain a wealth of information on both the chemical structure of molecules and on their conformation [175]. The intensity of the signal on the IR spectrum is proportional to the concentration of that species, making FTIR spectroscopy appropriate for both qualitative and quantitative analyses.

There must be an interaction between IR radiation and a changing dipole moment, in order for absorptions to be IR active. Homonuclear diatomic molecules (H_2 , N_2 and O_2) have no changing dipole moment as the molecule vibrates and are therefore IR inactive. Polyatomic molecules have a few fundamental modes of vibration that can give complex absorption spectra.

For this thesis, the functional group inference was detected by Fourier Transform Infrared (FTIR) spectrometer. The FTIR spectra were recorded within the range of $4000-400\text{ cm}^{-1}$ with 60 scans at 4 cm^{-1} resolution to maximize the signal to noise (S/N) ratio. Typically, 60 scans were collected for one spectrum, and the results were presented as absorbance spectra. Fourier transform infrared (FTIR) spectroscopy was performed to determine the type of adsorbed species at different temperature and gas compositions. The FTIR experiments were conducted with CO_2/H_2 gas mixtures.

2.3.1. Vibrational Modes of CO_2 and CH_4

For a molecule with N atoms, the whole number of coordinates required to specify the position of all atoms is $3N$. They are said to have $3N$ degrees of freedom. Since three coordinates are needed to specify the centre of mass of the molecule, three degrees of freedom can be subtracted for translation of the total molecule in space. Moreover, three more degrees of freedom can express the rotation of the molecule about its axes, leaving $3N-6$ vibrational modes for non-linear molecules. Whereas, linear molecules can rotate about only two axes and have two rotational modes, leaving $3N-5$ vibrational modes.

As carbon dioxide is a linear molecule, therefore has $3(3) - 5 = 4$ vibrational modes, two of which are degenerate resulting in the three modes as presented in Figure 42. The symmetric stretch is IR inactive caused a lack of changing dipole moment, while the antisymmetric stretch and bending modes are IR active. The bending vibration has a degenerate mode which is perpendicular to the motion (Fig. 42c). Therefore, the IR spectrum of CO₂ will contain two fundamental vibrational bands at 2349 cm^{-1} and 667 cm^{-1} [176]. These vibrational transitions are imposed with rotational lines caused by the simultaneous vibration and rotation of the molecules but in polyatomic molecules such as CO₂, it may happen that two vibrational levels belonging to various vibrations may be accidentally degenerate.

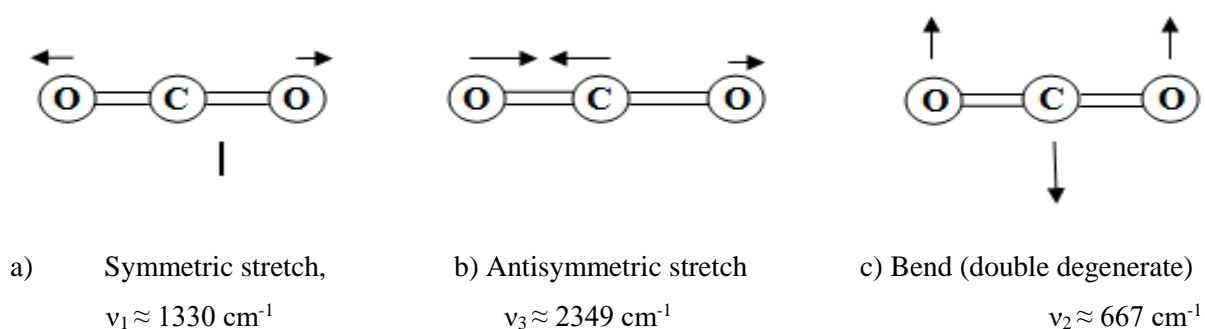
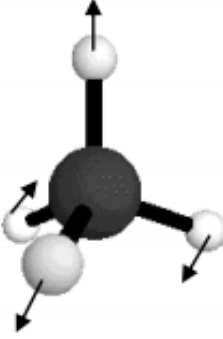
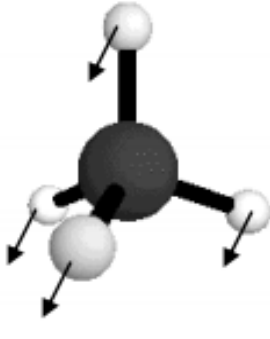


Fig. 42. Vibrational modes for the IR absorptions of CO₂ (adapted from [177]).

Methane is a non-linear molecule and has $3(5) - 6 = 9$ modes of vibration. Of these nine modes, two are triply degenerate modes which shows a vibrational bands on the IR spectra at 3020 cm^{-1} and 1306 cm^{-1} ; as presented in Table 9. Others three vibrational modes correspond to symmetric motions and they are IR inactive (ν_1 and ν_2).

Table 9. Vibrational modes for the IR absorptions of CH₄ (adapted from [178]).

Symmetric stretch, $\nu_1 \approx 2914\text{ cm}^{-1}$	Symmetric deformation (double degenerate),

	$\nu_2 \approx 1526 \text{ cm}^{-1}$
	
Asymmetric stretch (triplly degenerate), $\nu_3 \approx 3020 \text{ cm}^{-1}$	Asymmetric deformation (triplly degenerate), $\nu_4 \approx 1306 \text{ cm}^{-1}$

3. Elaboration and Characterization of Catalysts

Two types of catalysts were used during this study: Ni-Ce_xZr_{1-x}O₂ catalysts and hydrotalcite catalysts. Both are described below.

3.1. Preparation of the Nickel Catalysts

For the purpose of the study, three catalysts were prepared, namely: 15NiCZ1090, 15NiCZ5842 and 15NiCZ8515. The nickel supported on ceria-zirconia mixed oxide (Ce_xZr_{1-x}O₂) catalyst was prepared in a conventional wet impregnation method. Commercial ceria-zirconia mixed oxide (Ce_xZr_{1-x}O₂) with different Ce/Zr ratios: Ce_{0.1}Zr_{0.9}O₂, Ce_{0.58}Zr_{0.42}O₂ and Ce_{0.85}Zr_{0.15}O₂ (Rhodia Solvay) were used a support. The targeted nickel loading of all the catalysts was 15 wt.% [19, 21, 151, 179].

3.1.1. Synthesis of the Ni/Ce_xZr_{1-x}O₂ Catalysts

A Ni/Ce_xZr_{1-x}O₂ catalyst was prepared by the wet impregnation method. The ceria-zirconia mixed oxide (5 g) catalyst supports were impregnated with an aqueous solution of nickel nitrate hexahydrate (Ni(NO₃)₂·6H₂O, Aldrich) (3.8 g) as metal precursor. The nickel solution was added to the support under vigorous stirring at room temperature. Water was then evaporated at 60 °C with continuous stirring. The resulting impregnated solid was then oven dried overnight at 100 °C and subsequently calcined at 550 °C for 4h in air.

3.1.2. Calcination

The above three catalysts were calcined in a stream of air at 550 °C for 4h with a heating rate 10 °C/min. Table 10 shows the steps that were followed during the calcination process.

Table 10. Temperature ramping details followed during the calcination process.

Step No.	Temperature ramp/°C	Duration/h
1	20-550	0.53
2	550-550	4
3	550-20	2

3.2. Preparation of the Hydrotalcite Catalysts

The universal procedure applied to synthesize the hydrotalcites involved co-precipitation and in case of selected samples, by adsorption of transition metal species from aqueous solution of [Mⁿ⁺(EDTA)]⁽⁴⁻ⁿ⁾⁻ chelates, calcination and reduction/activation in the stream of hydrogen in order to obtain metallic nickel supported catalyst. Figure 43 shows the schematic procedure of the catalyst preparation.

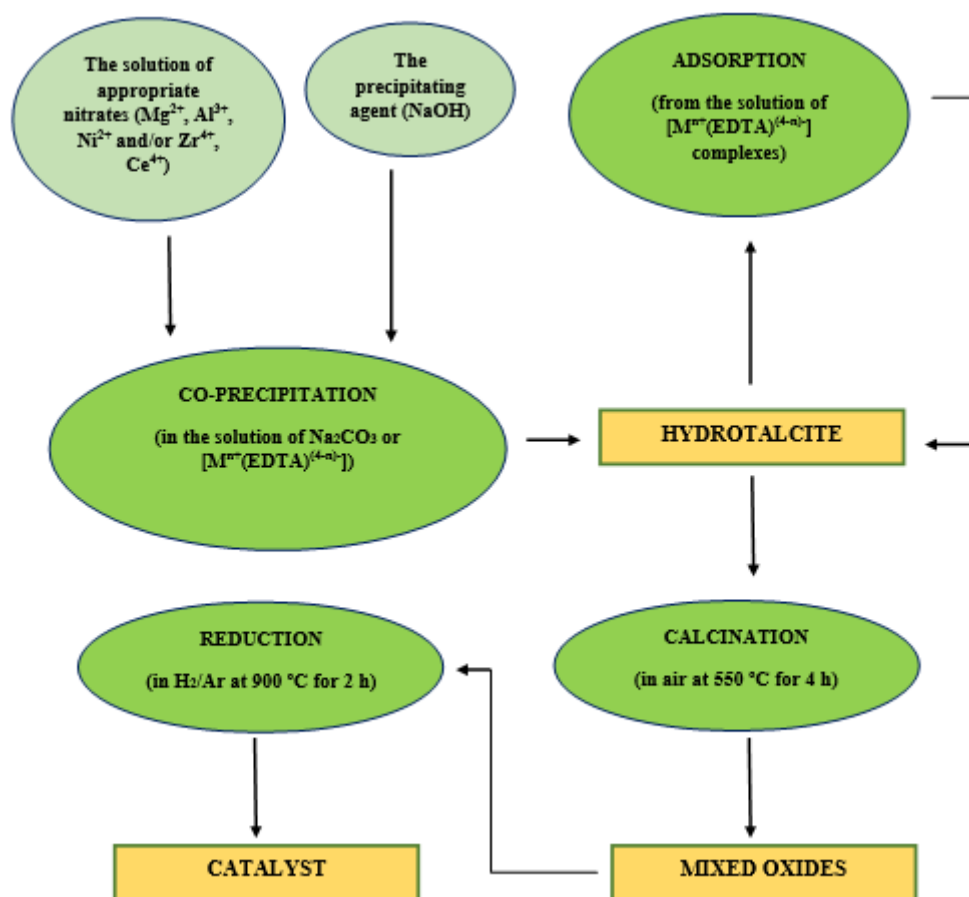


Fig. 43. Schematic procedure of the catalyst preparation [180].

The Ni-containing Mg-Al hydrotalcites were synthesized through co-precipitation method at constant pH from an aqueous solution of appropriate nitrates (Ni(NO₃)₂·6H₂O, Mg(NO₃)₂·6H₂O, ZrO(NO₃)₂·xH₂O - Sigma Aldrich) of total cations concentration equal to 1M. The precipitating agent was 1M solution of NaOH (POCH). These two solutions were added simultaneously to the 0.05 M solution of sodium carbonate. The flows of different solutions were adjusted in order to maintain constant pH equal to 10. The co-precipitation was carried out under constant stirring at 65 °C. The obtained mineral suspension was aged at 65 °C for 1h and subsequently washed with warm distilled water (ca. 50-60 °C) and filtered until neutral pH of the filtrate was registered. The synthesized materials were dried in air overnight at 80 °C and finally ground into fine powders.

Nickel was introduced into hydrotalcite structure at the co-precipitation stage. The obtained nickel containing hydrotalcites possessed fixed value of M²⁺/M³⁺ equal to 3. The

nickel content was changed by the substitution of 25 % of magnesium cations by nickel cations in the brucite-like layers, with respect to naturally occurring Mg/Al hydrotalcite ($\text{Mg}_6\text{Al}_2(\text{OH})_{16}\text{CO}_3 \cdot 4\text{H}_2\text{O}$).

The effect of Ce and or Zr was examined. Ce^{3+} cations were introduced into hydrotalcite structure via adsorption method. The amount of Ce^{3+} corresponded to 3 wt.% of the weight of the HT-MgAl hydrotalcite powder. Zirconium species were introduced into brucite-like layers at the co-precipitation stage. The molar ratio of $\text{Al}^{3+}/\text{Zr}^{4+}$ was equal to 9, while molar ratio of $\text{M}^{2+}/\text{M}^{3+}$ was equal to 3 [145, 180].

The resulting hydrotalcites were subsequently calcined at 550 °C for 4h. Four different catalysts were prepared: HT-25Ni, Ce-promoted: HTNi-Ce, Zr promoted: HTNi-Zr, and Ce-Zr-promoted: HTNi-CeZr.

3.3. Reduction of Catalysts

Catalyst is only activated when the metal oxide of the catalyst is reduced to metal with hydrogen at high temperature [181]. Temperature-Programmed Reduction (TPR) method provides information regarding the most suitable conditions for proper catalysts reduction. In accordance to this, before methanation test a $\text{Ni}/\text{Ce}_x\text{Zr}_{1-x}\text{O}_2$ catalysts were pre-reduced in a H_2 stream for 2h with a total gas flow of 40 mL/min at temperature 470 °C corresponding to the higher temperature used for process evaluation. Whereas, a reductive pretreatment for hydrotalcite catalysts was maintained in a 10% H_2/Ar stream for 2h with a total gas flow of 100 mL/min at temperature 900 °C [145, 182].

3.4. Catalysts Characterization

The main goals of the catalyst characterization work were to set the nature of the active centres for the methanation reaction. The knowledge about the catalyst features helps in improved catalysts and in modifying the preparation method with the aim of optimizing the

catalytic performances. To characterize the catalysts the following techniques were used, all of which have been described with details in Appendix B.

3.4.1. Hydrogen Temperature Programmed Reduction (H₂-TPR)

Temperature programmed reduction (TPR) was applied in order to compare the redox properties and the interaction strength between the support and the active phase particles of catalysts.

Hydrogen temperature programmed reduction (H₂-TPR) profiles were obtained on a BEL Japan BELCAT-M instrument interfaced with a computer. The experiments were carried out for 50 mg of catalyst powder under a stream of 25 mL/min of 5% vol. H₂/Ar gas mixture. The H₂ consumption was recorded while the temperature was raised up from 100 °C till 950 °C with a heating rate of 7.5 °C/min. Prior to each TPR experiments, the catalysts had been pre-heated at 400 °C under helium flow for 1h and then cooled down to 100 °C in order to clean the catalysts surface from adsorbed gases and water. The H₂ consumed was monitored by a TCD detector. The TPR profiles were analyzed via ChemMaster V.1.4.2 software where the H₂ consumption for each peak was calculated as well as the total H₂ consumption.

3.4.2. Temperature Programmed Desorption of CO₂ (CO₂-TPD)

The chemisorption ability of CO₂ can be used to study the basicity of catalyst in this technique. Thus, the higher temperature of CO₂ desorbed from the catalyst the higher basicity of the catalyst.

Temperature programmed desorption of CO₂ was carried out in a flow system (BEL Japan BELCAT-M equipped with a TCD detector) using a 10% vol. CO₂/He gas mixture. About 50 mg of catalyst was loaded in a quartz U-tube and flushed at 500 °C for 1h in He flow and cooled to 80 °C. Then, they were exposed to a gas mixture of 10% vol. CO₂/He for 1h at 80 °C in order to adsorb CO₂. Helium was then flown for 15 min in order to desorb the physically adsorbed CO₂. Temperature programmed desorption (TPD) of CO₂ was carried out heating the

samples at 10 °C/min up to 950 °C under He flow. The desorbed CO₂ was measured with the aid of the TCD detector.

3.4.3. X-Ray Diffraction (XRD)

X-ray diffraction pattern of the catalysts prepared in this study were analysed with a Empyrean diffractometer from PANalytica with Cu-K α radiation equivalent to 0.154059 nm operated at 45 kV and 40 mA. The catalyst powder was added to the sample holder where it was flattened with a glass slide until a smooth surface was achieved. The diffraction data was recorded in the 2 θ range of 3-90° with a step size of 0,01°. The average crystallite size was calculated with the Scherrer equation (1, Appendix B) [183]:

$$D = \frac{K\lambda}{\sqrt{(B^2 - b^2)} \cos(2\theta/2)} \quad (12)$$

K - shape factor (0.9),

λ - X-ray wavelength (0.15406 nm),

B - the peak width for a diffraction line at angle 2 θ ,

b - the instrument peak broadening,

$\sqrt{(B^2 - b^2)}$ - is the peak width for corrected instrumental broadening.

3.4.4. Brunauer-Emmett-Teller (BET) Surface Area

The specific surface area was determined by physisorption of N₂ at 77 K using a BELSORP-mini II measurement system equipped with a thermal conductivity detector (TCD). Prior to the analysis, samples were degassed at 110 °C for 3h with a constant N₂ flow to remove all adsorbed moisture from the catalyst surface and pores. The BET method was used to calculate the specific surface area.

3.4.5. High-Resolution Transmission Electron Microscopy (HRTEM)

High-Resolution Transmission electron microscopy observations of the reduced and used catalysts were performed using a JEOL JEM 2011 transmission electron microscope equipped with a LaB₆ filament, operating at 200 kV.

4. Experimental Results

The experiments that have been done can be categorized into two types: blank test (without catalysts) and tests with catalysts under plasma-on and plasma-off. These experiments were performed in two range of temperature: low (under adiabatic conditions) and high (under isothermal conditions). During the tests with plasma under adiabatic conditions the process started at room temperature and after the discharge increased temperature. Due to the exothermicity of the reaction, reactor temperature also increased and was stabilized between 90-270 °C depending on the thermal conductivity of the whole system. Under isothermal conditions, the reactor was heated by an external heat source in the case of experiments with and without plasma.

The following section describes the steps in which the tests were carried out.

4.1. Preparation of the Reactor for Experiments

The procedure which describes preparation of the reactor for tests was presented below in points:

- 1) Quartz wool was used at the bottom of reactor in order to prevent any movement of alumina,
- 2) to avoid any problems with the flow and catalyst, alumina was placed in the reactor (it has not any effect on the measurements, but prevents the catalyst from any movement),
- 3) quartz wool was added to prevent mixing of the catalyst with alumina,
- 4) the catalyst (0,6 cm³) was placed and if there was a problem with the flow, because the catalyst had a high density, catalyst was mixed with quartz balls,

5) the catalyst was covered with quartz wool, to prevent from any movement of catalysts during the measurement.

4.2. Blank Test

The blank test was done for the studied temperatures range (90-420 °C). Results obtained during blank tests in methanation of CO₂ versus temperature under adiabatic and isothermal conditions in the absence of catalysts, without and under plasma.

4.3. Tests in Presence and in Absence of Plasma

Plasma - assisted catalytic hydrogenation and standard catalytic hydrogenation were studied for a temperature range of 90-420 °C. The influence of the most important reaction parameters, i.e. influence of frequency and voltage, temperature was studied at moderate temperatures (320, 370 and 420 °C in isothermal conditions and 90-220 °C in adiabatic conditions). In the range of 220-420 °C the reactor usually worked in isothermal conditions (the reactor was heated by external heat source) and a better conversion of CO₂ for the case of plasma and catalyst when comparing to catalyst alone was observed. A higher conversion was achieved at low temperature, at around 200 °C.

Before starting the reaction, all mass flow controllers were calibrated in the range of flow necessary for the desired feed conditions (CO₂ - 40 mL/min and H₂ - 160 mL/min). The experiments for the plasma-catalytic hydrogenation of CO₂ were performed at atmospheric pressure in a continuous flow apparatus equipped with DBD plasma quartz reactor. The catalytic reactor was placed in the middle of the quartz tube, consisting of a fixed-bed of particle catalyst, corresponding to the total volume of 0.6 cm³. The effective length of the plasma-catalytic reactor was approximately 10 mm. Then the catalyst was reduced in a H₂ stream for 2h with a total gas flow of 40 mL/min at 470 °C. After reduction, the reactor was adjusted to the desired reaction temperature (room temperature) under the same gas flow. Once the temperature became stabilized, the reacting gas flow rates were adjusted using mass flow controllers and send through the reactor. The feed stream passed to the fixed bed reactor. Experimental method ensure proper mixing of the feed gases. Reaction temperature was kept

constant and controlled with the use of an electric and an external convection heater (TRIAC ST, Leister Technologies AG) and a temperature control system.

The reaction temperature was measured with a K-type thermocouple placed close to the catalytic bed after the plasma zone. Exhaust gases were passed through the thermo scientific refrigerated circulating water bath (Haake C10 K10) in order to collect the liquid products. Energy was supplied by a Calvatron SG2 high voltage 40-41 kHz AC supply (applied voltage was between 11-18 kV peak to peak). Electrical characterization was made measuring voltage (using a high voltage probe), power and frequency by a 500 MHz numerical oscilloscope (LeCroy LT 342) or with a pico oscilloscope (picoTechnology, PicoScope 5000 Series). Then, gas products were analyzed during experimental runs by taking gas samples (5 mL) from the exit stream with a gas-tight syringe and injecting into the GC according to the procedure outlined above.

Chapter 3: A Screening Study

1. Historical Background of the Project

This work coincided with the launching of a new European programme called CEOPS (CO₂-loop for Energy storage and conversion to Organic chemistry Processes through advanced catalytic Systems). CEOPS was a 3 years European project funded under the NMP (Nanosciences, nanotechnologies, materials and new production technologies), theme of the European Union 7th Framework Program. The project, that started on 1st February 2013, was devoted to the development of a sustainable approach for the production of methanol, which is well known as a precursor of fine chemicals products from CO₂ via an easy transportable vector: methane. This approach should enable the decentralization of methanol production leading to the emergence of distributed, small and flexible production units of fine chemicals. This vision paves the way for several novel and sustainable production schemes.

The technological work being based on the development of advanced catalysts and electro-catalytic processes, advanced catalysts for application in three promising electro-catalytic processes (Dielectric barrier discharge plasma catalysis, Photo-activated catalysis and Electro-catalytic reduction) were investigated in order to increase their efficiency overtime.

The CEOPS project consists in 10 partners from 6 EU member states with a high level of expertise in their respective scientific and technological fields spread all over Europe: CEA (Commissariat à l'Énergie Atomique et aux Énergies Alternatives, France), C.T.G. SPA (Italy), IST (Instituto Superior Técnico, Portugal), OMNIDEA (OMNIDEA LDA, Portugal), FCT/UNL (Faculdade de Ciências e Tecnologia/Universidade de Nova de Lisboa, Portugal), GSER (GDF SUEZ Energy Romania SA, Romania), IREC (Fundació Institut de Recerca de l'Energia de Catalunya, Spain), E-MRS (European Materials Research Society, France), CCB (Chemie Cluster Bayern GmbH, Germany), UPMC (Université Pierre et Marie Curie-Paris 6, France).

1.1. Concept and Scientific Objectives

1.1.1. Context and Concept

The rapid growth witnessed in the atmospheric CO₂ concentration has been currently confirmed as the most important environmental problem facing humanity. This focused attention had the merit of speeding up applied research on the subject, which finally led to the discovery of multiple new alternatives for CO₂. Despite increasing investments and developments in low-carbon energy alternatives and the progressive introduction of renewable energy resources, consumption of fossil fuels is still expected to grow substantially, due to increasing worldwide energy and electricity demands partially caused by the emergence of new economic powers in the world. As a consequence, the overall carbon footprint of the expected demand would thus exceed a 40 Gt/year of CO₂ emissions by 2030 versus 30 Gt/year in 2010 [184]. Valorisations of the CO₂ emissions constitute a complementary strategy to the CO₂ geological sequestration that will contribute to the reduction of the environmental impacts. The CO₂ transformation into added value products will promote the transition from carbon fossil sources to low carbon footprint ones. Intensive industries (e.g. cement industry), as large emitters of CO₂, represent a non-exploited source of carbon. In order to maintain the competitiveness of such industries, captured CO₂ can be valorised and converted into high value chemical products. From a fine chemicals standpoint, methanol is a major intermediate molecule for the chemical industry which represents fine chemical products bearing an average cost of 400 \$/ton metric. Industrially, methanol is synthesised from fossil fuel by steam reforming methane followed by the hydrogenation of CO. The market transition to the production of sustainable products has generated a demand for high-value products such as low carbon footprint methanol. Methanol is an important and versatile building block, which can play the role of chemical storage molecule for energy and be used for the synthesis of products such as acetic acid, formaldehyde, olefins, but also ephedrine or caffeine.

The concept of the CEOPS project (Fig. 44) relied on the development of two chemical pathways based on:

- **Sub-system A:** Upstream, CO₂ to methane conversion realised with advanced catalysts to promote the efficiency of CO₂→CH₄ electro-catalytic process (pathway A) at the point of CO₂ emission (cement works). Methane acts as an easy storable and transportable carbon vector

(from intermittent sources).

- **Sub-system B:** Downstream, the direct conversion of methane to methanol is done at the point of fine chemicals production with advanced catalysts to promote the efficiency of the direct pathway (pathway B) instead of using the current pathway consisting of a steam reforming of CH_4 , which represents 60-70 % of cost production of current methanol, followed by the CO hydrogenation reaction.

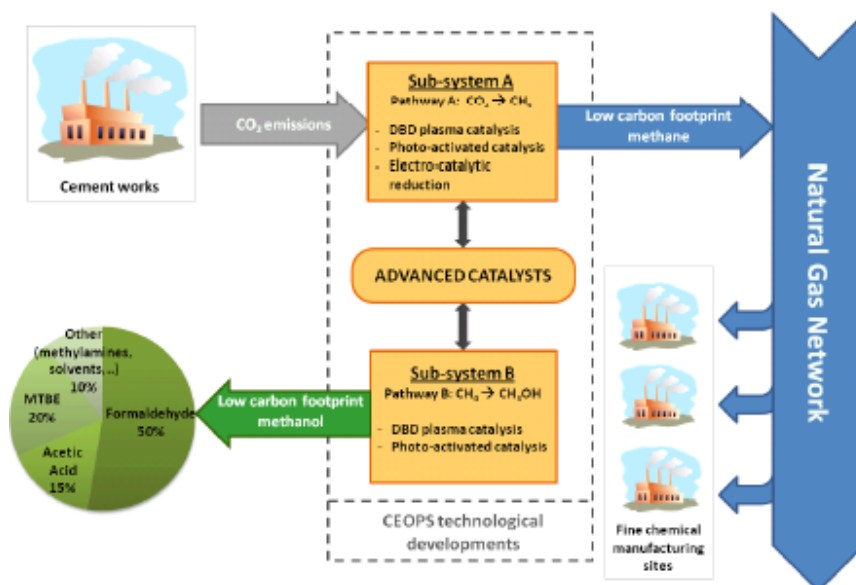


Fig. 44. General CEOPS project concept.

While large CO_2 emitters and fine chemicals producers are currently and geographically dispersed throughout Europe, the CEOPS concept proposed to use of the existing wide natural gas network via the injection and transportation of an intermediate product: methane. Indeed, whereas CH_4 is easily transported, the instability of CH_3OH makes its transportation by truck more hazardous. Furthermore, methane already benefits from the extended and existing European natural gas network infrastructure, so its distribution will prevent additional CO_2 emissions (rail and road transportation). This sustainable approach will thus enable the decentralisation of methanol production which will favour the emergence of distributed, small and flexible production units of fine chemicals.

Moreover, the flexibility of CEOPS production scheme, in a low consumption period (less than a threshold price of energy/MWh) or with a surplus of renewable energy production should ensure the competitiveness of the concept.

The CEOPS project was focused on the development of advanced catalysts and electro-catalytic processes. Specific catalysts were developed and evaluated to overcome the current limitations of thermal catalysis for each chemical pathway. These limitations were:

- the ageing of catalysts mainly due to water generated during the CO₂ hydrogenation to CH₄ that limits the catalyst time of stream to 5000-7500 hours.
- the low conversion rate and selectivity of the direct reaction from methane to methanol.

1.1.2. Scientific and Technical Objectives

Both pathways (CO₂ to CH₄ and CH₄ to CH₃OH) have been developed by thermal catalysis for several years. However many drawbacks such as low catalysts efficiency (conversion rate and selectivity) and deactivation, which are not compatible with industrial requirements, still remain. As a consequence, the CO₂ to CH₄ reaction is not competitive at an industrial scale and the CH₄ to CH₃OH conversion is achieved industrially in two steps. CEOPS was developed and evaluated efficient advanced catalytic materials for application in three promising electro-catalytic processes in order to radically increase their conversion rates and selectivity overtime.

The performances of the studied catalyst and process schemes were benchmarked, while the most efficient and durable scheme for both pathways were selected on the basis of conversion rate, selectivity and energy (electricity) consumption.

The project was structured with 4 scientific and technical objectives which are described in Figure 45 as follows:

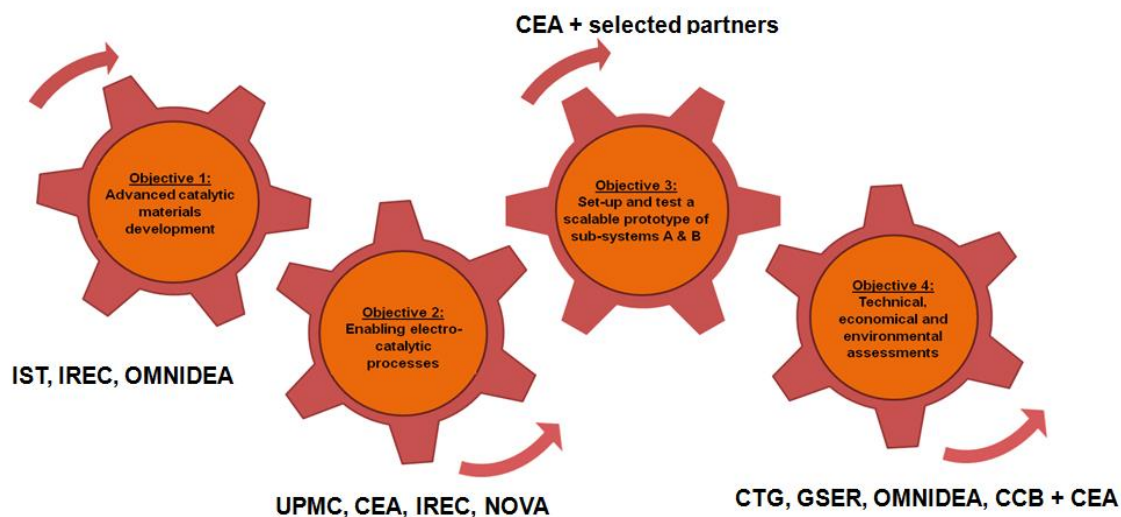


Fig. 45. Objectives of the CEOPS project.

Objectives:

1. **Advanced catalytic materials development.** Catalysts were developed in order to increase the conversion rate and selectivity:

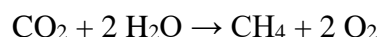
- Nano-structured zeolite in combination with metal oxides and mesoporous metal oxides for DBD plasma catalysis,
- Nano-structured TiO₂ (nano-tubes) and mesoporous tungsten oxides and beta zeolites for photo-activated catalysis,
- Multi-functional cathode materials with bimetallic nanoparticles for CO₂.

2. **Enabling electro-catalytic processes.** Electro-catalytic processes were developed to promote the sustainable production of fine chemicals from emitted CO₂.

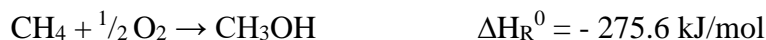
Pathway A: The chemical pathway starts by water electrolysis followed by the CO₂ hydrogenation.



and the overall reaction is the sum of those two:



Pathway B: The partial oxidation of methane to methanol.



The performance objectives set by the project for the competitiveness of both pathways was expressed in terms of conversion rate, selectivity and electricity consumption as shown in Table 11 here below.

Table. 11. Objectives for the competitiveness of both pathways.

	Pathway A	Pathway B
DBD plasma catalysis	CO₂ hydrogenation: Conversion rate > 65 % Selectivity > 90 % Electricity consumption (<12kJ/mole _{CH₄}) [185]	Conversion rate > 30 % Selectivity > 50 % Electricity consumption (<5kJ/mole _{CH₄})
Photo-activated catalysis	CO₂ reduction to CH₄: Conversion rate > 65 % Selectivity > 90 % Electricity consumption (<1,64 MJ/mole _{CH₄}) [185]	
Electro-catalytic reduction		NA

These electro-catalytic processes were developed in lab-scaled reactors, incorporating catalysts (objective 1) as follows:

- **DBD plasma catalysis** was implemented in a fixed bed reactor for mechanisms studies. The plasma created active species nearby the catalyst surface and improved kinetics by both surface reaction. Desorption of by-products were liable to deactivate catalysts active sites during operation. In turn, this led to higher and stable efficiency overtime.
- **Photo-activated catalysis**. The photon activation of catalysts promoted low electricity consumption and an enhancement of the conversion rate and selectivity.
 - ✓ *Photo-electro-catalytic* technology was implemented in a photo-electrochemical (PEC) cell with an innovative photo-anode.

✓ *Photocatalytic* technology was implemented in a fixed bed reactor.

• **CO₂ electro-catalytic reduction** was developed with ionic liquid which can be also used for the CO₂ capture instead of current amine based solvents. The electro-reduction reactor integrated multifunctional cathode materials to overcome the fast deactivation of catalysts.

3. *Set-up of a prototype for sub-systems A and B.* The most efficient and durable catalytic scheme was selected for each pathway. Catalysts and processes were scaled up to a prototype scale. The same performance indicators and targets (Objective 2) were addressed at the prototype level. This prototype allowed the evaluation of thermal balance, electricity consumption and catalytic efficiency.

4. *Techno-economic and environmental assessments.* Based on the above evaluation, the economic and environmental competitiveness of the CEOPS process routes from industrial CO₂ emitters to fine chemical customers was finally determined in terms of:

✓ techno-economic performances assessments.

✓ environmental impact assessments for the industrial CO₂ valorisation and “renewable” methanol market evaluation of the need for low carbon footprint methanol in chemistry and the CO₂ policy at European level.

✓ comparison of the competitiveness and the overall efficiency of the low carbon footprint methanol with the one produced today from fossil source with the current technology (thermal catalysis).

2. Catalysts on Different Zeolites and Mesoporous Based Structures for DBD Plasma Catalysis

For the CO₂ methanation, nickel-based catalysts cover the larger part of published works. Under thermal testing, the presence of water as a reaction product, leading to metal sintering, has been claimed as the main reason for the deactivation of catalysts. Another major problem of the Ni-based catalysts is their deactivation at low temperatures due to the interaction of the metal particles with CO and subsequently formation of mobile nickel carbonyls. Furthermore, no specific catalyst was developed for an optimum synergy with a plasma induced

reaction system. The development of processes and catalysts able to promote the water desorption for the methane synthesis was a crucial point, in order to minimize the catalyst deactivation, together with an increasing low temperature activity/CH₄ selectivity for plasma-induced systems. The bi-functional character of foreseeable catalysts favoured the use of specific catalytic functions for the hydrogen and for the CO₂ activation.

In this task, catalysts were developed for both pathways (CO₂ → CH₄ and CH₄ → CH₃OH). This chapter shows results obtained for different catalysts for the CO₂ methanation. For the CO₂ conversion to CH₄, two DBD catalysts 20%Ni-30%Ce/Cs-USY and Ce_{0.9}Zr_{0.1}O₂-15% Ni SBA-15 presented a synergy with a DBD plasma below than 200 °C for the CO₂ hydrogenation with a conversion rate of about 80 %. At low temperature (< 200 °C) with the zeolite based catalyst, a 60 % of conversion with 99 % in the methane selectivity was obtained, with a plasma power consumption of 32 kJ/mol. In the present market conditions and current regulations, methane will be produced at a cost of 135 €/MWh_{HCV}, inclusive of the investment costs, considering an electricity average price of 42 €/MWh. The electricity price per MWh to make methane competitive is close to 3 €/MWh. At the current stage, the environmental impacts of pathway A and pathway B are larger than the impacts of currently available technologies. This is mainly due to the large energy demand and the current electricity mix in the EU. An energy mix of 100 % of renewable energy could become an environmentally favourable alternative to methane and methanol from other sources.

Results obtained for all tested catalysts are given in Appendix C.

2.1. Zeolite Based Catalysts

Zeolite-based catalysts were achieved over the use of bi-functional systems composed of zeolites and metal species. It has to be noted that IST has worked on the preparation and characterization of catalysts. Taking into account the presence of water as a reaction product, a particular zeolite structure, considering the high stability presented under highly severe conditions, was used: the US (ultra-stable) Y zeolite (USY) that presents a FAU (Faujasite) structure. Samples, with a controlled type of active sites (metals, metal oxides and acid sites) provided by zeolites, took not only advantages of the zeolite ability to stabilize various metal species, but also from the zeolite confinement effects (zeolite cages, channels and channels intersections that really act like nano-reactors, boosting the catalysts activity) were prepared.

Besides foreseeable parameters optimization (as the acidity/basicity of the zeolites, Si/Al ratio, metal species contents) other variables such as the Ni reduction temperature before catalytic testing or the effects of the presence of rare-earth-Ce-oxides, were evaluated to maximize the synergy with the plasma, allowing catalysts tuning.

A few catalysts based on Ni and Ce supported USY-zeolites were prepared for the CO₂ conversion into methane. The introduction of metal species was conducted by an incipient wetness impregnation technique, followed by calcination.

Different loadings of Ni (2-14 wt.%) and Ce (3-15 wt.%) were introduced into the samples. All the prepared catalysts were then characterized by elemental analysis, nitrogen adsorption, hydrogen temperature programmed reduction (H₂-TPR), UV-Vis spectroscopy and X-Ray diffraction (XRD). Furthermore, they were catalytically tested under thermal heating in order to verify their suitability for the reaction, in terms of CO₂ conversion and CH₄ selectivity. The stability of the catalysts was evaluated by submitting the catalysts to 10 hours of reaction at 400 °C. In some catalysts, TEM analysis of Ni particles size was done.

2.1.1. Preparation and Characterization of Ni/USHY Catalysts

All catalysts were based on ultra-stable FAU structure (USHY form), taking into account the good resistance of this particular structure to water vapour presence at high temperature. Ni was introduced by an incipient wetness impregnation technique in which the Ni obtained content varied between 2 and 14 wt.%.

Different parameters were studied such as: the Ni loading, the addition of Ce (activity and selectivity promoter) and the introduction of alkaline (Cs, Na) or alkaline-earth (Mg) cations. Different zeolite properties were also evaluated: their acidity/basicity (sodium content), the influence of the presence of extra-framework aluminium species, the global Si/Al ratio type of structure compensating cation (Na, K, Mg, Cs).

Ultra-stable HY zeolites (Si/Al=6.5 and 40) were impregnated with Ni (5-14 wt%) solutions prepared from Ni nitrate, with right concentrations, using an incipient wetness impregnation technique. All catalysts were then dried at 120 °C overnight and calcined under airflow at 500 °C, during 2h (10 °C/min rate).

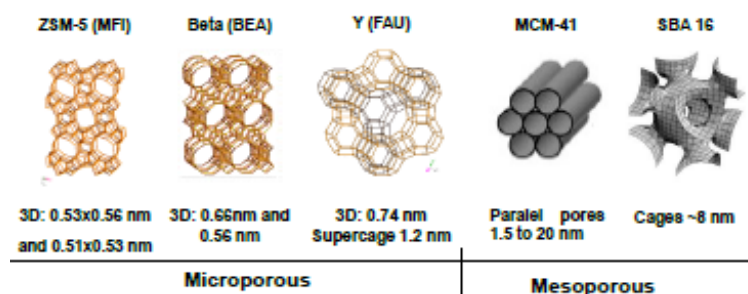


Fig. 46. Various zeolite structures used as supports.

Before reduction, catalysts were characterized by an UV-Vis Diffuse Reflectance Spectroscopy (Cary 5000 UV-Vis spectrophotometer) and X-Ray Diffraction (Bruker D8 Advance XRD).

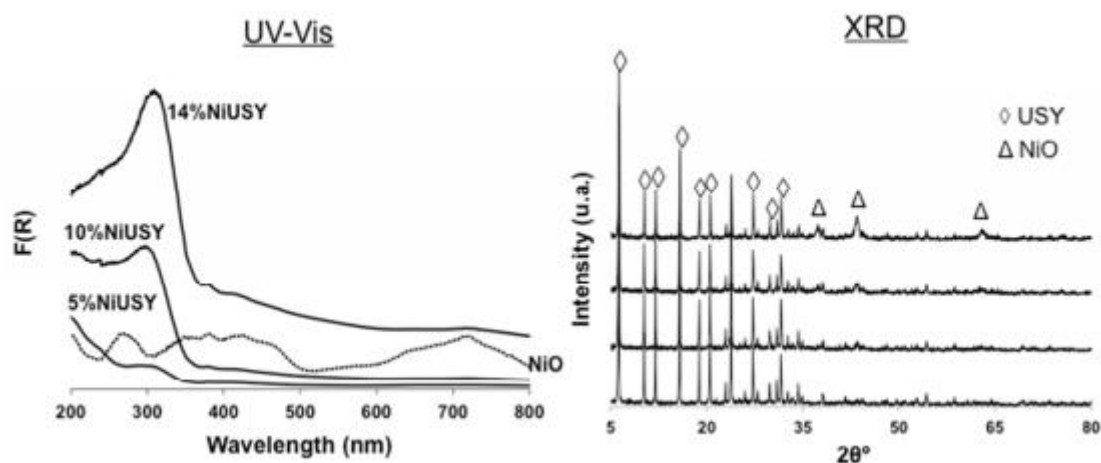


Fig. 47. Characterization results of non-reduced as prepared and calcined Ni/USHY by UV-Vis DRS and XRD done by IST (Portugal).

As show in Figure 47, both techniques reveal the only presence of NiO (bands at 300, 390, 429 and 725 nm (UV-Vis DRS - (Diffuse Reflectance Spectroscopy)) and diffraction peaks at 37°, 43° and 63°.

Furthermore, the prepared catalysts were characterized by Hydrogen Temperature Reduction (H₂-TPR) as shown in Figure 48, with gas flow of a mixture consisting of 5% H₂ vol. in Ar and a heating rate of 10 °C/min, from RT to 900 °C. Hydrogen consumption (received by a TCD detector) was plotted against temperature, allowing to identify different metal reduction processes, which could be correlated to various metal species or to metal species located in different positions inside or outside zeolite framework.

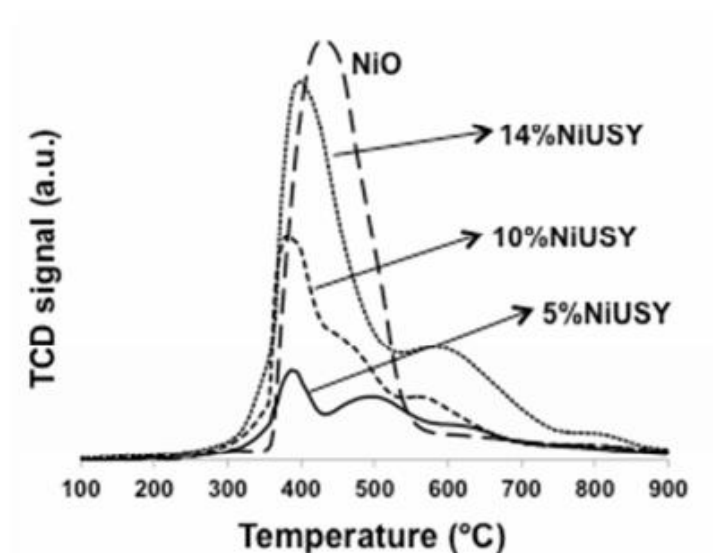


Fig. 48. Characterization results of non-reduced as prepared and calcined Ni/USHY catalysts by H₂-TPR done by IST (Portugal).

This technique included the detailed analysis of catalysts reduction processes:

- the process observed at 400 °C was assigned to the reduction of NiO on the zeolite outer surface as it is identical to the reduction temperature of bulk NiO reduction,
- Ni²⁺ on zeolite supercages was observed at 500 °C,
- Ni²⁺ on sodalite cages was observed at 600 °C,
- Ni²⁺ on zeolite hexagonal prisms was detected at 800 °C.

Nitrogen adsorption was used to establish both the microporous volume (V_{micro}) and the external surface ($S_{\text{ext.}}$) of prepared catalysts (Table 12).

Table 12. Microporous volume and external surface area set by N₂ adsorption.

Sample	V_{micro} (cm ³ /g)	$S_{\text{ext.}}$ (m ² /g)
USY	0.286	17
5%NiUSY	0.280	13
10%NiUSY	0.210	14
14%NiUSY	0.222	14

The obtained results reported in Table 12 show a significant decrease of the external surface with an increasing Ni catalysts loading, which seems to confirm that the NiO location

on zeolite crystallites lies in the external surface, after calcination of catalysts, thus, confirming H₂-TPR results.

2.1.2. Preparation and Characterization of Ni-Ce/USHY Catalysts

Based on the previous results and in order to assess the effect of adding Ce to Ni/USY catalysts, the 5% Ni/USY sample was used as the catalyst.

Therefore, catalysts containing 5 wt%. of Ni, previously prepared, were further impregnated with 3-15 wt%. of Ce (cerium nitrate solutions, with adequate concentrations, were used), using the incipient wetness impregnation technique. All catalysts were then dried at 120 °C overnight and calcined under an air flow at 500 °C, during 2h (at a 10 °C/min rate).

Before reduction, catalysts were characterized using the UV-Vis diffuse reflectance spectroscopy (DRS) and H₂-TPR (Fig. 49).

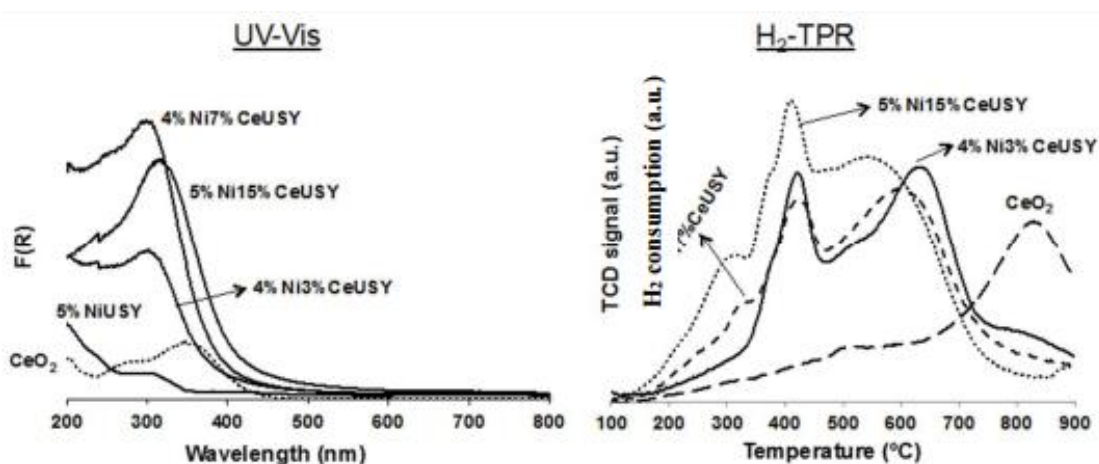


Fig. 49. Characterization results of non-reduced as prepared and calcined 5% Ni-Ce/USHY, by UV-Vis DRS and H₂-TPR done by IST (Portugal).

UV-Vis DRS analysis showed that both Ce³⁺ and CeO₂ were detected (bands at 260 and 310 nm, accordingly), being the last of main Ce species detected in these catalysts.

Hydrogen TPR showed two main reduction processes:

- at 400 °C, the reduction of NiO was detected.
- at 600 °C, a reduction processes assigned to CeO₂ was observed. The latter occurred at a lower temperature than bulk CeO₂, which can be explained either by the activation of

hydrogen by the Ni particles (reduced at a lower temperature), or eventually by the formation of small Ce particles, strongly interacting with the zeolite structure.

2.1.3. Catalysts Optimisation

Several aspects have to be considered for the optimization of Ni and Ni-Ce containing USY zeolite-based catalysts. Among these, the most relevant ones for the final optimised catalyst are based on the:

- drying method (oven vs. microwave irradiation).
- effect of pre-reduction temperature (470, 550, 600 and 700 °C).
- effect of the acidity/basicity of the support.
- effect of the presence of EFAL (Extra-Framework Aluminium) species in the zeolite structure.
- effect of the Si/Al ratio of the zeolite.

Catalysts were then characterised by H₂-TPR, UV-Vis DRS spectroscopy and (in some cases) by TEM, and compared to conventional heated catalysts.

The methodology used for the optimisation of the catalysts involves the study of these parameters following an independent evaluation method. Most of this study was performed over 5 wt%. of Ni/USY, in order to avoid thermodynamics limitations existing at high conversion levels.

2.1.3.1. Drying Method (Oven vs. Microwave Irradiation)

These tests were carried out with 5% NiNa-USY catalyst. A standard drying method was compared with two MW procedures (using various equipment). A standard calcination step was always done afterwards. UV-Vis DRS and H₂-TPR results (obtained with calcined samples) are presented in Figure 50.

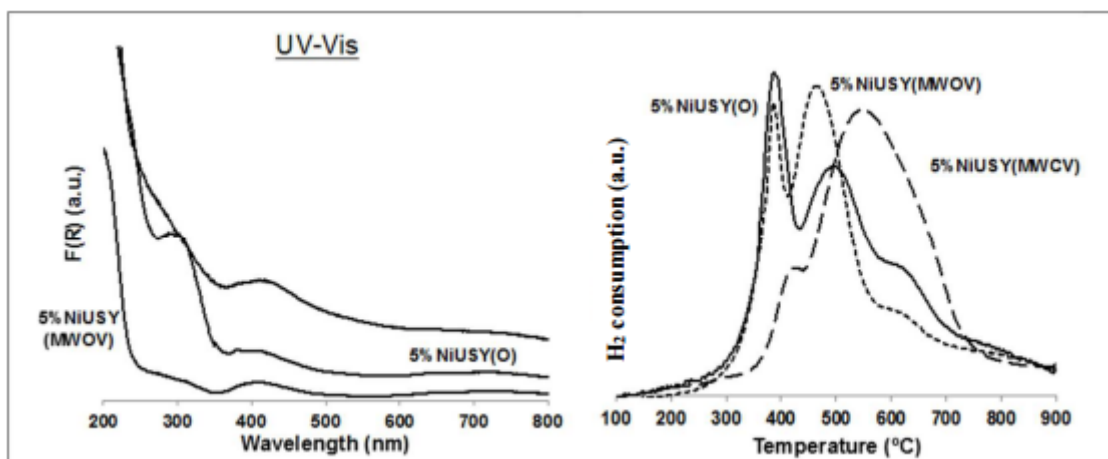


Fig. 50. Characterization results of 5% NiNa-USY dried in an oven or under microwave radiation, by UV-Vis DRS and H₂-TPR (O-oven dried; MWOV-micro-wave dried in open vessel; MW-CV: microwave dried in closed vessel) done by IST (Portugal).

Using the UV-Vis DRS spectroscopy, NiO species were detected at 300, 380 and 420 nm, while bands at 410, 650 and 740 nm were assigned to Ni²⁺ octahedral species.

Temperature programmed reduction under H₂, allowed the detection of a shift of the maximum reduction temperature in the samples dried under micro-wave radiation. This probably indicates that in these cases, a higher Ni species fraction is located deeply inside the zeolite structure (more difficult to reduce).

The catalytic evaluation for the CO₂ methanation is depicted in Figure 51.

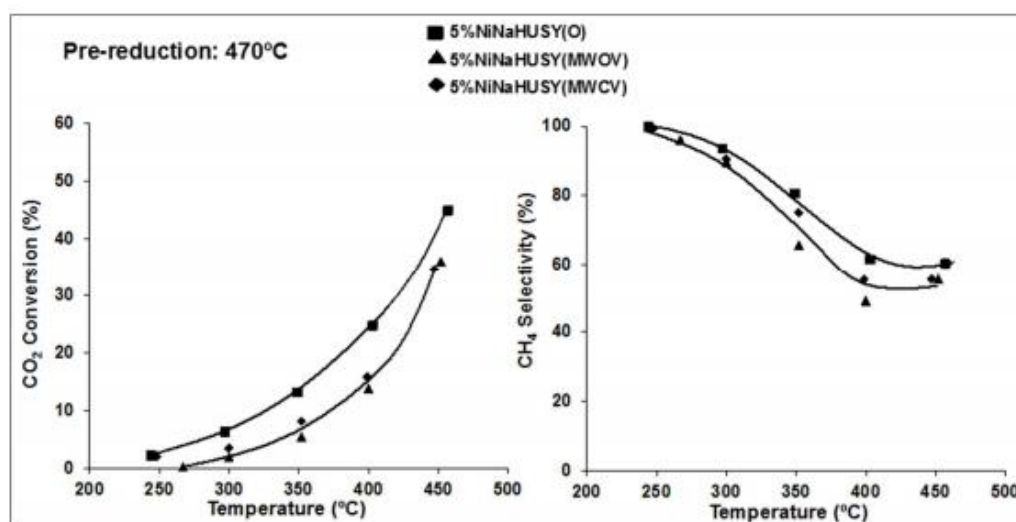


Fig. 51. CO₂ hydrogenation to methane, obtained under conventional heating, for 5 %NiNa/USY catalyst, (O-oven dried; MWOV-micro-wave dried in open vessel; MW-CV: micro-wave dried in closed vessel) done by IST (Portugal).

When the pre-reduction step is performed at 470 °C, the catalyst dried in the oven presents higher CO₂ conversions and CH₄ selectivity (probably due to the higher fraction of reduced Ni species at this temperature).

2.1.3.2. Effect of Pre-Reduction Temperature

This was evaluated with a 5 %NiNa-USY catalyst (standard preparation) by reducing it, earlier to CO₂ methanation, at 470 °C, 550 °C, 600 °C and 700 °C. Catalytic results under conventional heating are depicted in Figure 52.

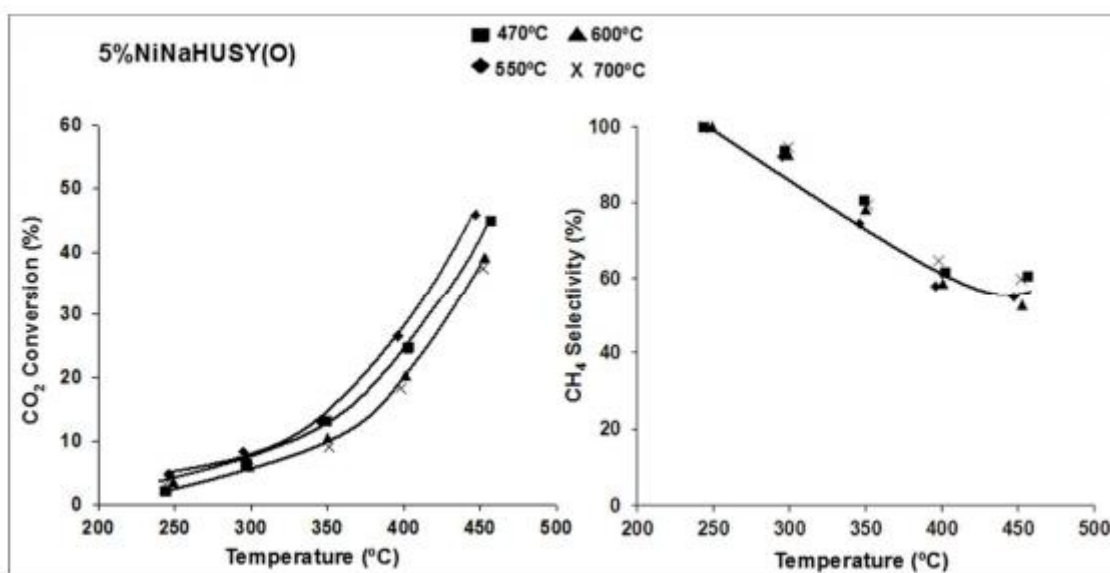


Fig. 52. CO₂ hydrogenation to methane, obtained under conventional heating, for 5 %NiNa/USY catalyst, after different pre-reduction temperatures done by IST (Portugal).

The evolution of conversion with the reduction temperature follows the order:

$$550\text{ °C} > 470\text{ °C} > 600\text{ °C} \cong 700\text{ °C}.$$

The increase of activity observed for the samples reduced at 550 °C, compared to those reduced at 470 °C is probably due to the increase of the amount of reduced Ni species along with the reduction temperature (Fig. 53).

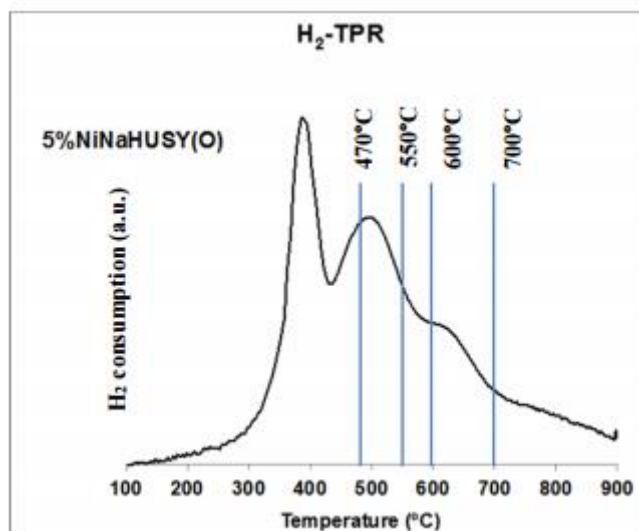


Fig. 53. H₂-TPR of 5% NiNa-USY (O), where the used maximum reduction temperatures are shown, (470, 550, 600 and 700 °C) done by IST (Portugal).

The decrease in the catalytic activity, observed for samples reduced at higher temperatures (600 and 700 °C) is probably due to the sintering of Ni particles, favoured at high temperatures. As shown in Figure 54, an increase in the Ni crystallites size is observed when the reduction temperature increases from 470 to 700 °C [45].

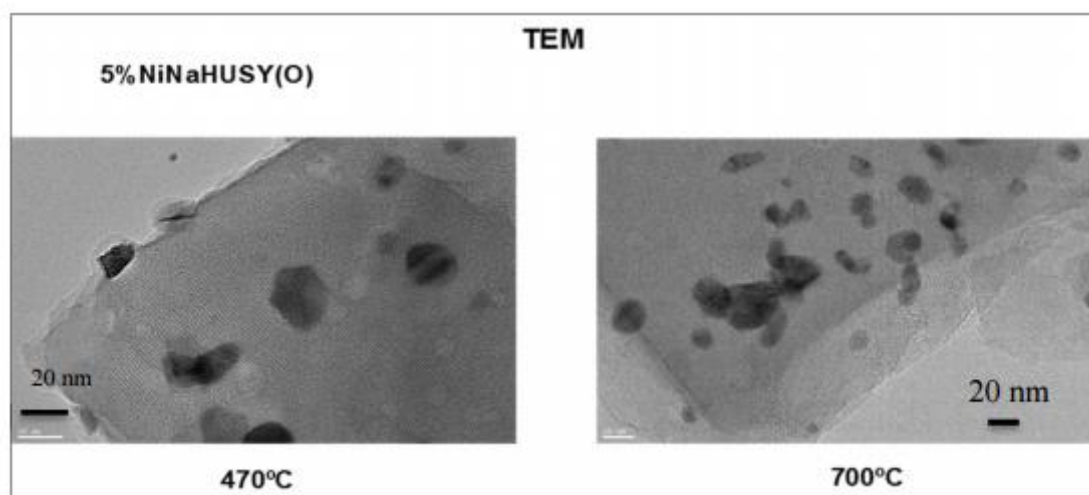


Fig. 54. TEM analysis of oven-dried 5% NiNa-USY catalyst, at 470 and 700 °C done by IST (Portugal).

2.1.3.3. Effect of the Acidity/Basicity of the Support

The acidity of the catalyst, feature that has been claimed to take a role in the CO₂ activation, was tuned with the objective of maximizing the synergy with the plasma for a higher conversion and selectivity. The acidity level will control the conductivity of the catalyst and was generated and modified by ion-exchange with alkaline metals, in order to regulate the Brønsted acid sites concentration and by modifying the concentration of extra framework aluminium (EFAL) responsible for the Lewis acid sites formation.

In order to assess this issue, two zeolites were prepared from the base sample (2.1 wt% of Na): one “acidic sample”, obtained by ion-exchanging with NH₄NO₃, followed by calcination under dry air (“H form”) and a “basic form” obtained by ion-exchanging with NaNO₃ (increasing sodium content), followed by calcination under dry air.

Sodium content of samples is advisable in Table 13. In all samples, 5 wt% Ni/USY catalyst was impregnated.

Table 13. Sodium content of 5wt% Ni/USY zeolite samples prepared to assess the effect of the acidity/basicity of the support.

Sample	Na wt.%
Reference 5wt.%Ni/USY	2.10
“Acidic” catalyst (H form)	0.11
“Basic” catalyst (Na form)	3.10

UV-Vis DRS and H₂-TPR analysis of these samples are depicted in Figure 55.

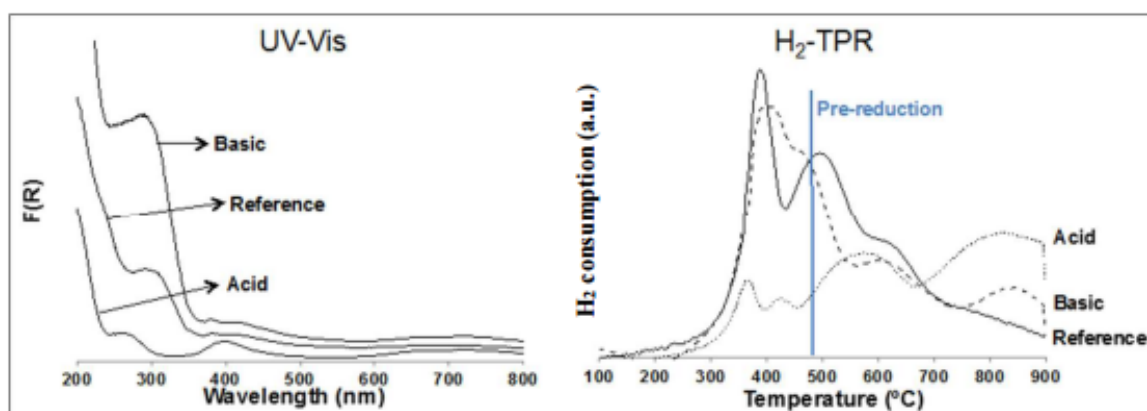


Fig. 55. UV-Vis and H₂-TPR of parent, acidic and basic samples of 5wt%Ni/USY zeolite done by IST (Portugal).

Acid catalyst (H form) presents both NiO and octahedral Ni²⁺ species (bands at 300, 410, 650 and 740 cm⁻¹), while in the reference sample (2.1wt% Na) and basic sample (3.1wt% Na), only NiO (bands at 300, 390, 429 and 725 nm) can be observed.

Acid catalyst presents two main nickel species reduction processes (at 600 and 800 °C) while the reference and basic samples present two reduction processes at 400 and 500 °C, indicating that Ni is mainly located on the external surface and in zeolite supercages. Like in the previous results, it was possible to establish a correlation between Ni species reduction temperature and their location (external, reduced at lower temperatures or internal, reduced at higher temperatures) in zeolite structure.

The catalytic results for the CO₂ methanation, under conventional heating, are depicted in Figure 56.

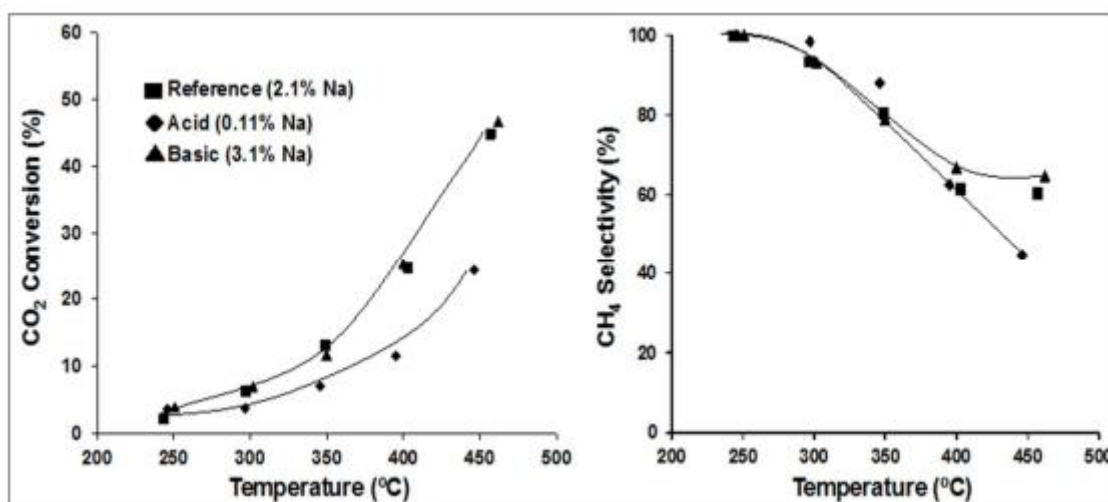


Fig. 56. CO₂ hydrogenation to methane, obtained under conventional heating, for 5wt%Ni/USY catalysts, with different Na content (acidity/basicity assessment) done by IST (Portugal).

From this figure, it can be observed that a low Na content (acid sample) gives both a lower CO₂ conversion and CH₄ selectivity. This seems to be related to the various reducibility of the Ni species in more basic or acid samples. Consequently, an acidic character of the zeolite support presents a negative effect on both activity (a smaller fraction can be reduced at 470 °C) and selectivity to CH₄.

2.1.3.4. Effect of the Presence of EFAL Species

The subsistence of EFAL (Extra-Framework Aluminium) species in a zeolite structure usually arises from delamination that can be originated by thermal treatments in the presence of water or even from operation conditions (water is a product of methanation reaction). The presence of EFAL species, indicating a delamination process can also indicate a possible failure of the zeolite framework. Moreover, it is well known that the presence of Lewis acid sites can enhance the strength of remaining Brønsted acid sites. In order to assess this point, two Y zeolite structures presenting an identical global Si/Al ratio but containing a different Si/Al_{IV} ratio were used. These ratios were calculated from the unit cell parameter (Breck-Flanigen equation) corresponding to “real” Si/Al ratio of the zeolite framework (method disclosed in D. Breck, Zeolite Molecular Sieves [186]), based on data from XRD. Both catalysts present a similar Na content which are reported in Table 14.

Table 14. EFAL content of USY zeolite samples.

Sample	Si/Al ^a	Si/Al _{IV} ^b	EFAL	Na(%)
Reference	2.80	3.80	13	0.11
Dealuminated USHY	2.80	9.10	35	0.10

a- obtained by chemical analysis

b- obtained by a Breck-Flanigen type equation: $N_{Al}^{framework} = D(a-A)$, with **A** and **D** constants and **a** the lattice constant

UV-Vis DRS and H₂-TPR analysis of these samples are depicted in Figure 57.

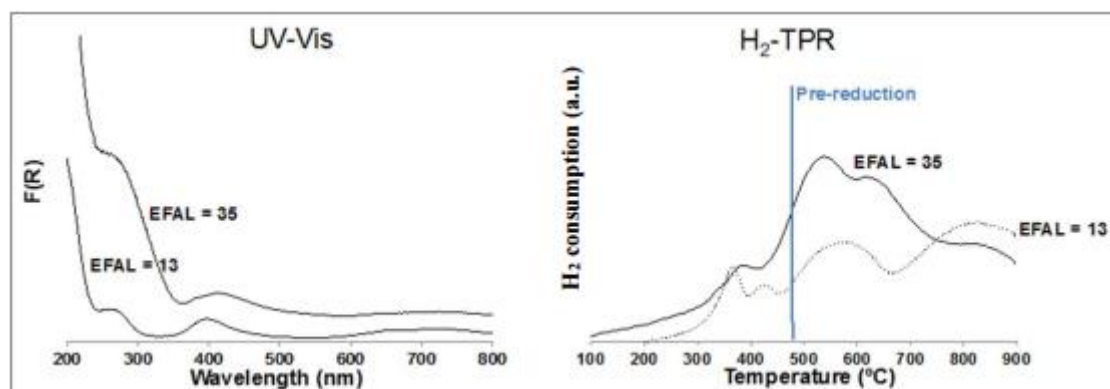


Fig. 57. UV-Vis and H₂-TPR of 5%Ni-USY zeolite catalysts, with various EFAL content done by IST (Portugal).

For EFAL=13, the sample presents UV-Vis bands at 300, 410, 650 and 740 nm, assigned to octahedral Ni²⁺ species and NiO. On the contrary, the EFAL=35 sample only presents NiO species (300, 390, 429 and 725 nm).

From H₂-TPR, it is possible to conclude that a higher amount of Ni species is reducible until T_{red.}=470 °C for the EFAL=35 sample.

As depicted in Figure 58, these results can explain the better catalytic performance of the EFAL=35 sample both to the CO₂ conversion and CH₄ selectivity.

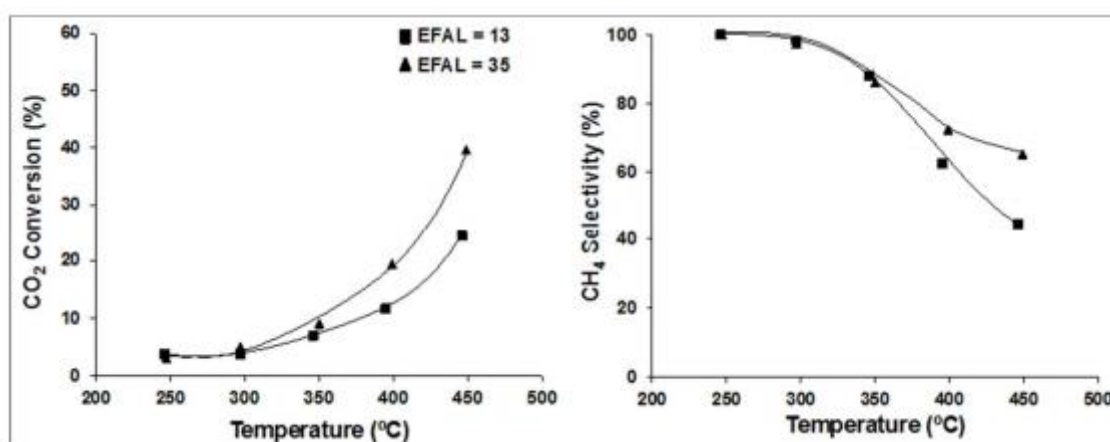


Fig. 58. CO₂ hydrogenation to methane, received under conventional heating, for 5% Ni-USY catalysts, with different EFAL content done by IST (Portugal).

2.1.3.5. Effect of the Si/Al Ratio of the Zeolite

The Si/Al ratio of zeolites is often considered as a key factor that allows to determine its catalytic behaviour for a given reaction. Therefore, a comparison of three different Si/Al ratios for USY zeolites, all containing 5 wt.% of Ni, was performed (Table 15).

Table 15. Si/Al ratios of different 5 wt% Ni-USY zeolite samples.

Sample	Si/Al ^a	Si/Al _v ^b	Na (%)
Reference Si/Al=2	2.8	3.8	0.110
Sample Si/Al=15	15	16	0.015
Sample	40	38	0.015

Si/Al=40			
-----------------	--	--	--

a - Global Si/Al, determined by elemental analysis

b - Framework Si/Al, calculated from the unit cell parameter (Breck.Flanigen equation) and IR

UV-Vis DRS and H₂-TPR analysis of these samples are depicted in Figure 59.

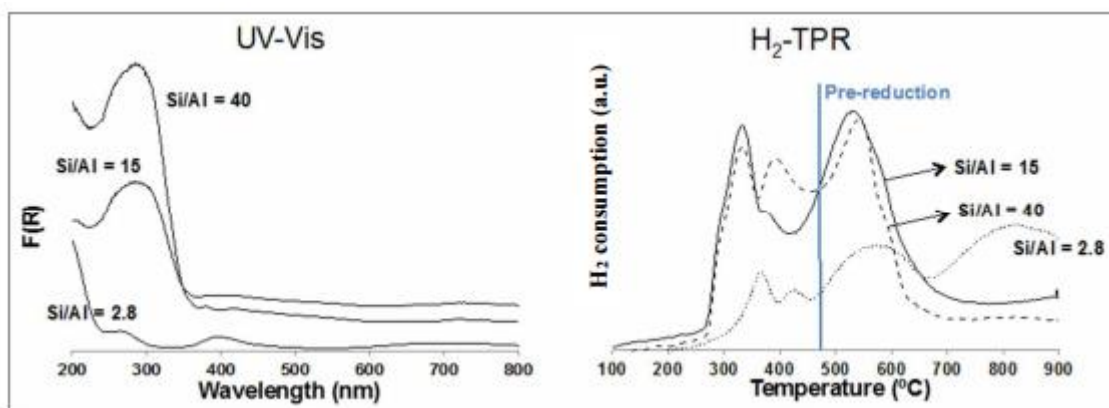


Fig. 59. UV-Vis and H₂-TPR of 5% Ni-USY zeolite catalysts, with different Si/Al ratios done by IST (Portugal).

The low Al/Si=2.8 wt% - Ni catalyst sample (with a higher content on Al, corresponding to a higher number of acid sites), presents octahedral Ni²⁺ species, together with NiO (bands at 300, 410, 650, 740 nm), while samples with a higher Si/Al ratio only present NiO (bands at 300, 390, 429 and 725 nm).

H₂-TPR shows that the fraction of Ni species, reducible at T ≤ 470 °C, increases with the Si/Al ratio.

These results can explain the better catalytic performance following the present order: Si/Al=40 > Si/Al=15 > Si/Al=2.8, presented in Figure 60, both to CO₂ conversion and CH₄ selectivity. Therefore, this indicates better performances with an increasing Si/Al ratio.

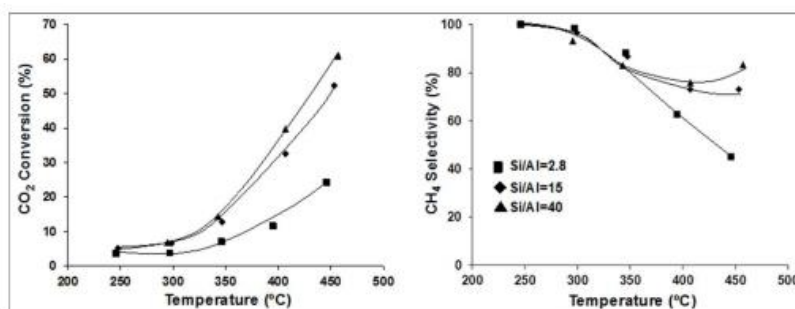


Fig. 60. CO₂ hydrogenation to methane, obtained under conventional heating, for 5% Ni-USY catalysts, with different Si/Al ratio done by IST (Portugal).

2.1.3.6. Final Formulation

In order to obtain a Ni/zeolite-based catalyst, the final formulation took into account the main results of the previous optimization and characterization, including results from the conventional heating methanation.

Overall, the main aspects that were considered were: high contents of Ni and Ce (obtained by incipient wetness impregnation), a high Si/Al ratio, and presence of an alkaline cation (obtained by ion-exchange). The only point that has not been yet possible to accomplish is related to the positive effect of EFAL species. Indeed, the latter were not present in the used Si/Al=40 USY zeolite, as it is very difficult to obtain a crystalline of a FAU structure with a high Si/Al ratio, in the presence of comparable amount of EFAL species.

The conventional heating methanation (Fig. 61) exhibited a better behaviour for the 30%Ce14%NiCs USY (Si/Al=40) sample that was also chosen as the sample to be tested with a DBD plasma.

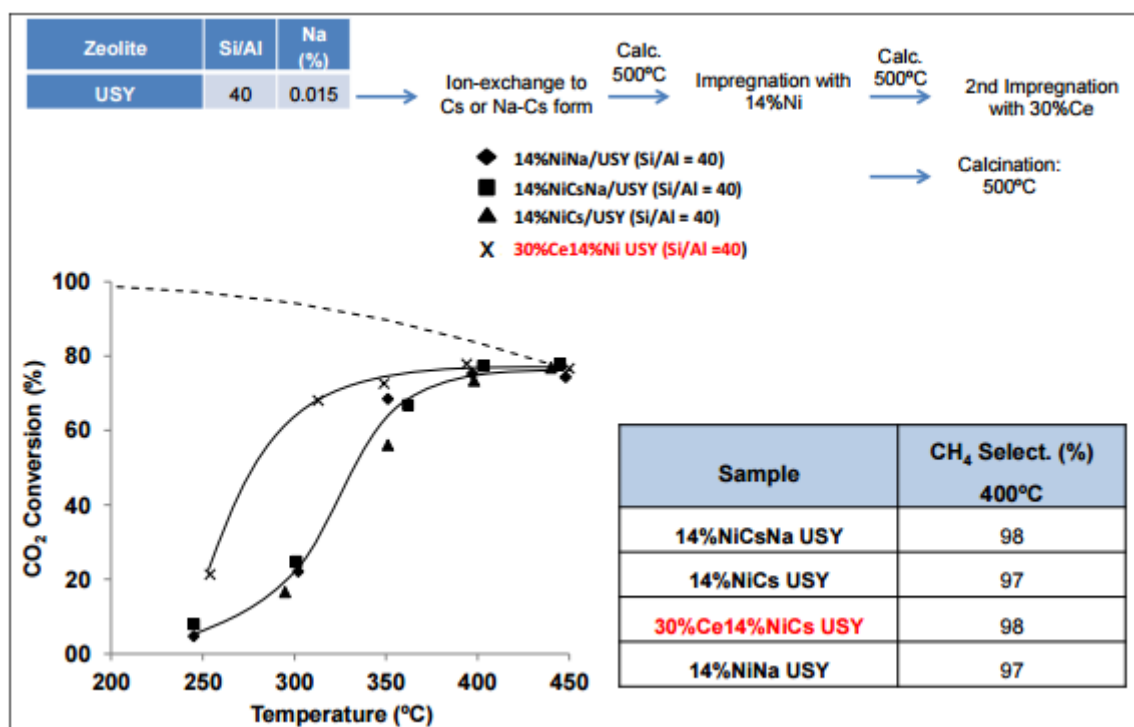


Fig. 61. Preparation methodology and catalytic results, obtained under conventional heating for optimized Ni/zeolite-based catalysts done by IST (Portugal).

In Table 16, a comparison between results obtained in literature and final formulation catalyst has been made. In order to draw conclusions on the behaviour of zeolite-based catalysts that can perform the CO₂ methanation reaction, the performances of the most active and selective zeolite-based catalysts (including the final formulation catalyst) were compared to those obtained for the catalysts found in references [16, 19-21, 37, 52, 148, 187]; all samples being tested under thermal catalysis.

Table 16. Published results on thermal catalytic systems of CO₂ methanation.

Sample [16, 19-21, 37, 52, 148, 187] and this work	T (°C)	pCO ₂ (atm)	H ₂ : CO ₂	GHSV (h ⁻¹)	Contact time* (min)	Flux Tot/Wcat (mLs ⁻¹ g ⁻¹)	CO ₂ Conversion (%)	CH ₄ selectivity (%)	CH ₄ Yield (%)
Ce _{0.95} Ru _{0.05} O ₂	450	0.13	4	61.000	0.8	12.5	55	99	55
3%Ni-MCM-41	400	0.28	2.6	-	8.0	1.6	17	96	16
6.2%Pd-3.6%Mg/SiO ₂	450	0.17	4	-	5.2	2.0	59	95	56
6.2%Pd-3.6%Ni/SiO ₂	450	0.17	4	-	5.2	2.0	50	89	45
12%Ni/ZrO ₂ -Al ₂ O ₃	360	0.22	3.5	-	5.6	2.3	73	97	71
5%Ni/La ₂ O ₂ CO ₃	300	0.20	4	-	6.1	2.1	40	89	36
15%Ni/RHA-Al ₂ O ₃	500	0.20	4	-	1.5	8.3	64	91	58
5%Ni-Ce _{0.5} Zr _{0.5} O ₂	400	0.16	4	43.000	2.0	6.1	80	~99	79
10%Ni-Ce _{0.72} Zr _{0.28} O ₂	400	0.16	4	43.000	2.0	6.1	85	~99	84
14%Ni/USY	400	0.16	4	43.000	0.5	23.9	65.5	94	62
14%Ni7%Ce/USY	400	0.16	4	43.000	0.5	23.9	68.3	95	65
14%NiCs/USY	400	0.16	4	43.000	0.5	23.9	77	98	75.5
14%Ni30%CeCs/USY	400	0.16	4	43.000	0.5	23.9	78	98	77

*Taken as the reverse of the weight hourly space velocity (WHSV)

However, the operating conditions used in these studies were very different. Therefore, this comparison was focused on the catalysts tested under operating conditions similar to those used in the present work. It can be observed that the results are not significantly different, even if the contact times used in the present study are low (in some cases four times smaller than the literature ones).

The results obtained with the IST samples point out that Ni-based zeolites could be used as catalysts to perform the CO₂ hydrogenation reaction into methane, since they present very interesting activity and selectivity levels. Indeed, the higher is the amount of Ni on the catalysts,

the better their performances are. Moreover, the addition of Ce to the Ni zeolites also leads to a further improvement of the catalysts activity and selectivity, as these catalysts seem to present a good stability. The effect of the zeolite support properties, such as the acidity/basicity, the number of extra-framework Al species and the Si/Al ratio, as well as the effect of the calcination temperature after impregnation of Ni, on the catalysts performances were studied. Important improvements of the catalysts activity and selectivity were observed by changing these parameters.

2.1.4. Catalysts Testing

2.1.4.1. Catalytic Tests of the CO₂ Hydrogenation, Under Classic Thermal Conditions (IST)

Catalysts were tested under classic thermal conditions in order to assess their capacity under DBD Plasma conditions. Experimental setup (Fig. 62) was provided with CO_x non-dispersive IR detectors and a GC chromatograph allowing the detection of CH₄. The reactor effluent passed by a water trap in order to eliminate moisture before composition analysis. Gas flows (CO₂, H₂ and N₂) were controlled by mass flow meters. The total gas flow was measured several times at each reaction temperature in order to be able to perform mass balances, i.e., the hydrogenation reaction $\text{CO}_2 + 4 \text{H}_2 \rightarrow \text{CH}_4 + 2 \text{H}_2\text{O}$ occurring with a decrease of mole number.

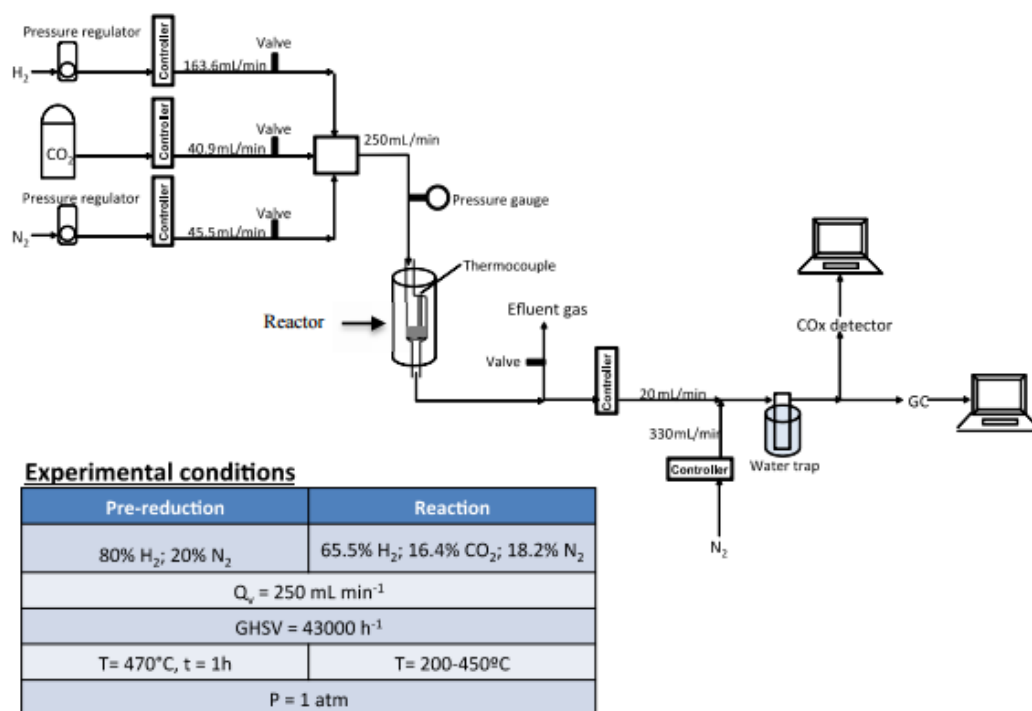


Fig. 62. Reactivity set-up and experimental conditions used for conventional heating methanation tests of Pathway A catalysts done by IST (Portugal).

The reactivity setup was provided by a tubular reactor placed inside a furnace. The reactor temperature was controlled by a thermocouple placed near the catalyst surface. Reactants and products analysis were performed via an IR specific CO_x detector, while the methane concentration was determined by Gas Chromatography. The gaseous flow exiting the reactor was continuously monitored. The used operating conditions (pre-reduction and reaction) are presented in Figure 62. The pre-reduction step was performed prior to the reaction, as Ni⁰ species are needed for H₂ activation. Ni is presented as Ni oxide, after impregnation/calcination steps as under the operation conditions (T_{red}=470 °C), not all the nickel is reduced. The obtained main results are presented in Figure 63.

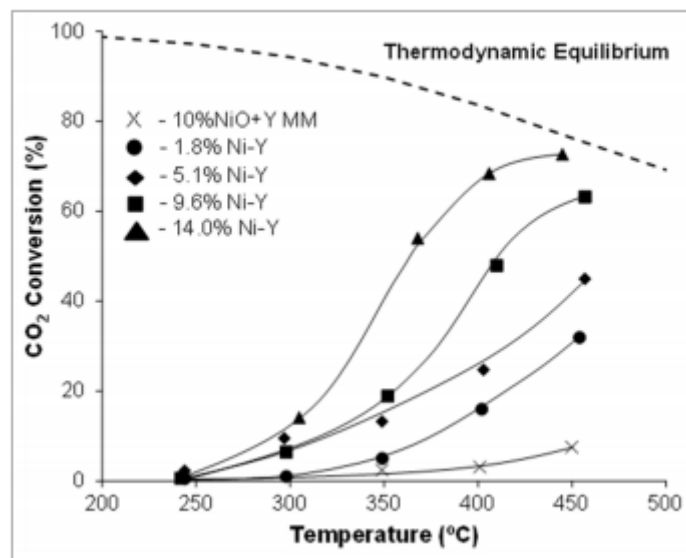


Fig. 63. CO₂ hydrogenation to methane, obtained under conventional heating, for Ni/USHY catalysts done by IST (Portugal).

Table 17 presents the CH₄ selectivity of Ni-USY catalysts at 450 °C.

Table 17. CH₄ selectivity obtained at 450 °C, for NiUSY catalysts (conventional heating).

Sample	CH ₄ Selectivity (%)
2% NiUSY	38.3
5% NiUSY	61.4
10% NiUSY	78.8
14% NiUSY	94.2

The CO₂ conversion as well as the CH₄ selectivity both increase with an increasing Ni content. This can be interpreted in terms of the increasing fraction of Ni reduced until 470 °C (pre-reduction temperature) as observed by H₂-TPR.

The positive role of Ni⁰ species, originated from “external” Ni oxides (UV-Vis DRS) was observed for the first time.

Results obtained with the Ni-Ce catalyst, under the same previous conditions are presented in Figure 64.

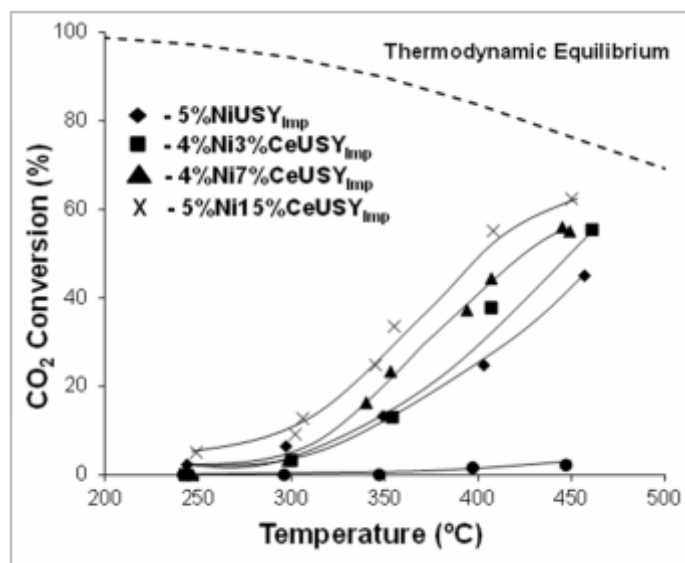


Fig. 64. CO₂ hydrogenation to methane, obtained under conventional heating, for Ni-Ce/USY catalysts done by IST (Portugal).

Table 18 presents the CH₄ selectivity of Ni-Ce/USY catalysts at 450 °C.

Table 18. CH₄ selectivity obtained at 450 °C, for Ni-Ce/USY catalysts (conventional heating).

Sample	CH ₄ Selectivity (%)
5% Ni/USY	61.4
4% Ni 3% Ce/USY	72.1
4% Ni 15% Ce/USY	75.5
5% Ni 3% Ce/USY	86.2
7% Ce/USY	1.8

Like in the Ni case, it can be notice that the CO₂ conversion as well as the methane selectivity both increase with an increasing catalysts Ce content, evidencing a synergism between Ni and Ce species.

In an attempt to verify the catalyst stability, a longer test was performed under steady-state conditions at 400 °C. The obtained results are presented in Figure 65.

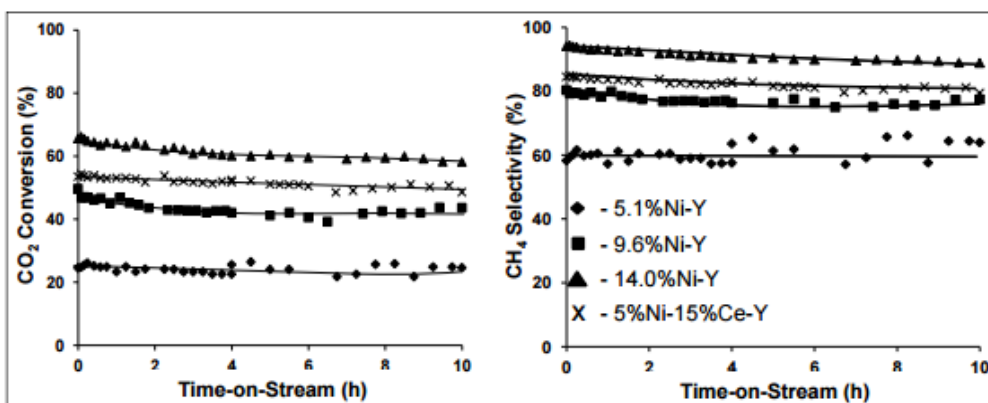


Fig. 65. Stability tests performed during 10 h at 400 °C for Ni and Ni-Ce USHY based catalysts done by IST (Portugal).

2.1.4.2. Results in a Hybrid Plasma-Catalytic Methanation of CO₂

This work investigated the hydrogenation of CO₂ into methane in a dielectric barrier discharge (DBD) plasma reactor packed with Ni-Ce/Zr based catalyst. For the present investigation, plasma-assisted catalytic hydrogenation and standard catalytic hydrogenation were studied for a temperature range of 100 to 420 °C. In the presence of only the catalyst, the CO₂ conversions were less than 2 %, suggesting that thermal activation of the catalyst was not sufficient enough to achieve a significant methanation rate for the studied temperature range. On the other hand, with DBD plasma created in the catalyst bed, a precipitous rise in the CO₂ conversion of more than 60 % was observed.

A comparison of different catalysts is presented below at moderate temperatures (320, 370 and 420 °C in isothermal conditions and 100-200 °C in adiabatic conditions). In the range of 220-420 °C, the reactor usually works in isothermal conditions (the reactor was heated by external heat source) and a better CO₂ conversion was observed in the case of plasma with catalyst when compared to catalyst alone. It has to be noted that this better conversion was achieved at a low temperature (~200 °C).

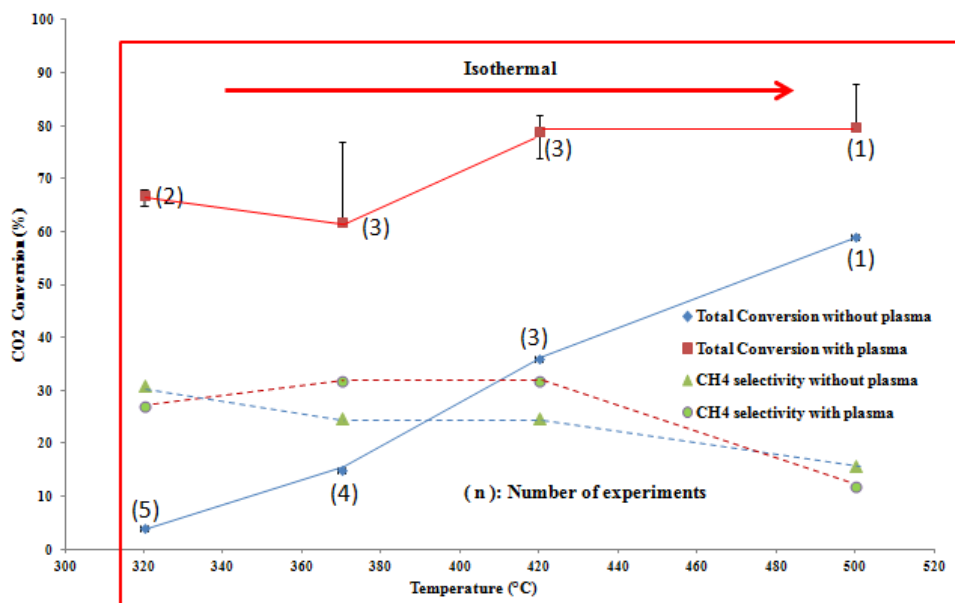


Fig. 66. CO₂ Conversion with and without plasma for tested catalyst 5%NiHNa/USY, voltage = 14 kV, f = 41 kHz.

The difference between the CO₂ conversion with and without plasma at 320-420 °C was around 30-40 %. The total conversion with plasma was close to 45-63 % with a CH₄ selectivity around 30-40 %. It can be noted that the CH₄ selectivity decreases when the temperature increases. Therefore, the studied catalyst did not work in adiabatic conditions and showed a higher selectivity to CO.

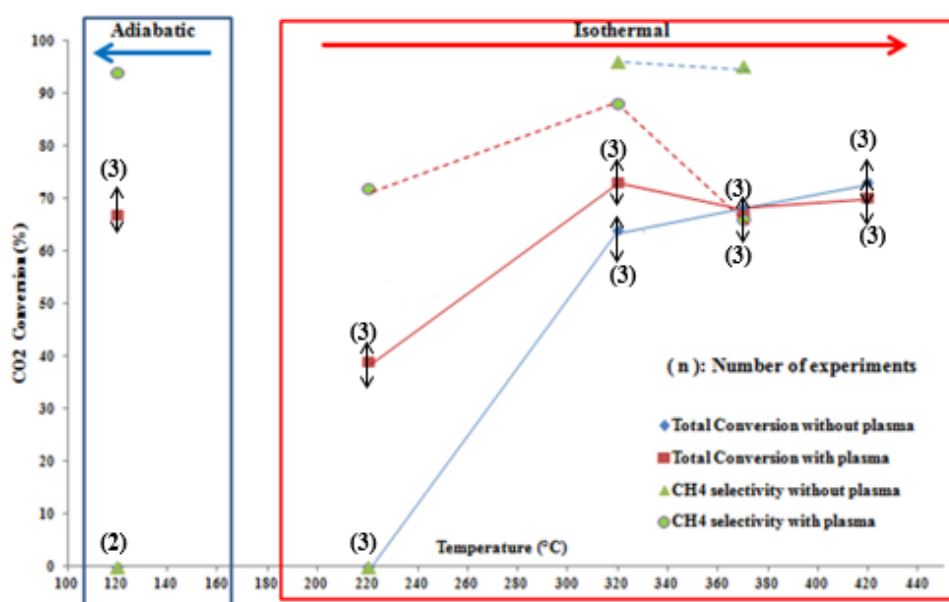


Fig. 67. CO₂ Conversion with and without plasma for tested catalyst 20%Ni30%CeCs/USY, voltage = 14 kV, f = 41 kHz.

Figure 67 show CO₂ conversions in the DBD plasma reactor packed with 20%Ni30%CeCs/USY catalyst in the presence or in the absence of plasma in a temperature range of 120-420 °C. It can be seen that under adiabatic conditions, with plasma, the process starts at room temperature; then the discharge increases the temperature. The reaction then starts and due to its exothermicity, the reactor temperature further increases and stabilizes around 120 °C.

Under isothermal conditions, within the range of 220-420 °C, the reactor was heated by an external heat source in both cases (with or without plasma). This range of temperature was explored as 350 °C is the optimum one for the Sabatier reaction in the conventional process. Without plasma in adiabatic conditions, the conversion was less than 1 % at 120 °C whereas it increased to about 70 % at 120 °C with plasma. Without plasma in isothermal conditions, the conversion was less than 1 % at 220 °C but it increased to about 70 % at 320 °C. At a higher temperature, no differences could be observed between experiments with or without the presence of plasma (the conversion was around 60 % without plasma whereas, with plasma, the conversion reached around 70 %). Surprisingly, the DBD plasma was able to improve the conversion of CO₂ to more than 70 %. Especially at a low temperature range of 120-220 °C where catalysis alone did not produce a significant methanation rate, the plasma gave rise to a sharp increase in the conversion of CO₂.

2.1.5. Conclusions

The obtained results point out to the fact that Ni-based zeolites could be used as catalysts of the CO₂ methanation reaction as they present very interesting activity and selectivity levels.

Despite the fact that catalytic evaluation was performed under DBD plasma-induced hydrogenation of carbon dioxide, catalysts were also evaluated by thermal heating. This procedure allowed for the catalytic evaluation of a large number of parameters, which is also reflected in the final results, as a direct relationship could be drawn between the catalysis results performed at IST (thermal) and the ones performed at the UPMC (DBD plasma).

The addition of Ce to Ni zeolites leads to a further improvement of the catalysts activity and selectivity. The fact that methane selectivity also increases (by lowering the CO yield) when ceria is added, means that the latter is probably also involved in the rate step regarding the CO₂ dissociation and/or hydrogen insertion in the CO_x species.

The conversion efficiencies in the presence of plasma were enhanced. The carbon

dioxide reduction at low temperatures depends on the plasma activation of the catalyst. As a consequence, in an adiabatic reactor stabilized at 120 °C, a CO₂ conversion of 60 % can be obtained.

2.2. Mesoporous Nickel-Ceria-Zirconia Based Catalysts

Mesoporous Nickel-Ceria-Zirconia based catalysts were obtained by a replication method of mesoporous silica (IREC has worked on the preparation and characterization of catalysts).

Previous works of Ocampo [19, 21] pointed out the astonishing performances of nickel based Ce_xZr_{1-x}O₂ catalysts synthesized by sol gel method in the Sabatier reaction. Such performances were attributed to their high oxygen storage capacity and to their ability to highly disperse nickel. Nevertheless, the thermal stabilization of nanoparticles is very restricted by the sol-gel method due to a coalescence phenomenon which lowers its activity. In order to overcome this limitation, the use of a hard template method in order to obtain a high-surface area and stabilized mesoporous nickel-ceria-zirconia catalysts has been proposed. This method, in which the template is removed afterwards, ensures a good control of the particle size since the template acts as a physical barrier to the coalescence of the crystals during the calcination process. This removal results in highly crystalline materials with a high surface area, for maximizing its catalytic activity. The estimate of the conventional thermal catalytic performances were done by IST in order to select the most performing formulations for further DBD plasma tests.

2.2.1. Preparation and Characterization of Mesoporous Ni/Ce_xZr_{1-x}O₂ Catalysts

Mesoporous nickel-ceria-zirconia catalysts, were obtained by a replication method of mesoporous silica. Figure 68 shows the synthesis procedure that involves the impregnation with metal precursors of a mesoporous silica scaffold (in this case, SBA-15), the calcination and synthesis of metal oxide nanocrystals at high temperature and the removal of the silica template.

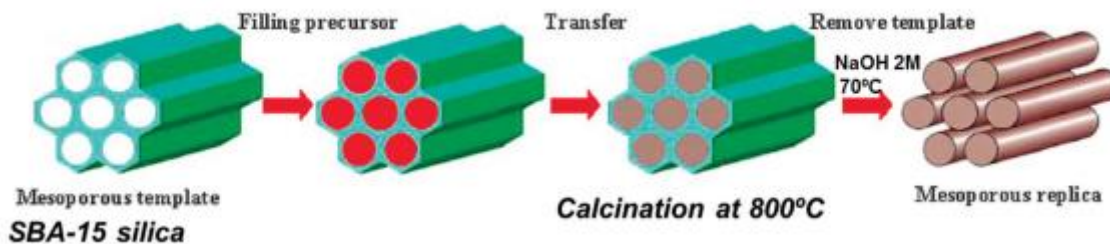


Fig. 68. Illustration of the hard template method for the synthesis of mesoporous oxides.

A SBA-15 (two-dimensional hexagonal with $p6mm$ symmetry mesoporous silica) was used. The latter was synthesised under acidic conditions using a non-ionic triblock copolymer surfactant ($EO_{20}PO_{70}EO_{20}$, Pluronic P123 from BASF) as a structure-directing agent [188]. SBA-15 was impregnated with solutions of nitrate salts of the metal precursors in two steps. Firstly, proper amounts of cerium nitrate ($Ce(NO_3)_3 \cdot 6H_2O$), zirconium oxynitrate ($ZrO(NO_3)_2 \cdot 6H_2O$) and nickel nitrate ($Ni(NO_3)_2 \cdot 6H_2O$) were dissolved in purified water or ethanol in order to make 0.1 M solutions of $Ce(NO_3)_3 \cdot 6H_2O$ and $ZrO(NO_3)_2 \cdot 6H_2O$. In the first impregnation step, 0.15 g of silica template (SBA-15) was mixed with the adequate volumes of ceria and zirconia solutions in order to obtain 1 mmol of total metal ions. The metal ratio $[Zr^{4+}]/([Zr^{4+}]+[Ce^{3+}])$ was varied between 0 to 0.2, and the nickel content between 5 and 15 %. The mixture was stirred for 30 min then dried at 50 °C and calcined at 350 °C for 4h with a heating rate of 4 °C/min. In the second impregnation step, 0.5 mmol of metal ions with the same metal ratio were added to the resulting powder, stirred, dried and calcined to 800 °C. In order to remove the silica template, products were hot-etched using NaOH. Powders were then cleaned several times in a 2M NaOH solution and stirred for 2h at 70 °C. The powder catalysts were recovered by centrifugation and washed with purified water until reaching a neutral product ($pH=7$). The latter were finally cleaned twice with ethanol and dried for 12h in air in an oven.

As seen in Table 19, for all the compositions, the catalysts had a high surface area (BET values ranging between 120 and 150 m^2/g), which decreased with the nickel loading and increased with the zirconia loading.

Table 19. BET surface area (m²/g) of mesoporous oxides.

	5% Ni	10% Ni	15% Ni
Ce	135.0	132.4	126.4
CeZr(90:10)	138.1	136.6	129.7
CeZr(80:20)	149.3	141.3	129.8

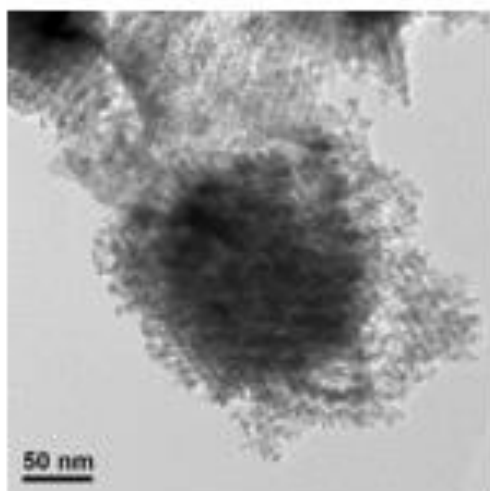


Fig. 69. TEM image of mesoporous oxide done by IREC (Spain).

The TEM image displayed in Figure 69 further corroborates the transferred porosity from the template to the mesoporous oxide, in which the structures have been preserved despite the fact that the samples were calcined at high temperatures. The morphology consists of an array of nanorods or nanowires composed for aligned nanocrystals, with a mean diameter of around 8-9 nm, and an intragap of 4-5 nm.

As indicated in Figure 70, according to the diffraction patterns obtained by XRD, all the samples crystallize on the fluorite structure (cubic) and no evidence of NiO formation were found. However, only a shift in the diffraction patterns due to the solid solution formed is observed. The cell “a” parameter values were calculated by adjusting the profile using Fullprof program [189] taking into account a single phase with a fluorite symmetry (Fig. 70, right). It can be seen that Ni²⁺ incorporation promotes cell expansion whereas Zr⁴⁺ contraction assures a high dispersion of nickel in the catalyst.

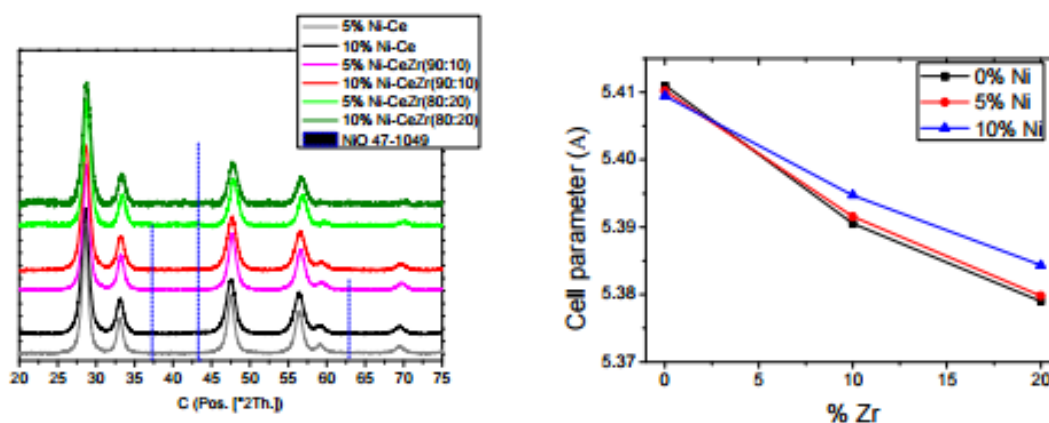


Fig. 70. Left, XRD patterns of mesoporous Ni-Ce_xZr_{1-x}O₂ catalysts, dotted lines corresponds to NiO pattern. Right, cell parameter as a function of Zr and Ni content done by IREC (Spain).

H₂-TPR results (Fig. not shown) present a sharp peak before 400 °C corresponding to the Ni²⁺ → Ni reduction, followed by a broad peak up to 500 °C corresponding to the reduction of Ni²⁺ species inserted into the ceria lattice. Peaks located around 200 °C and 700 °C corresponds to the Ce⁴⁺ → Ce³⁺ reduction.

2.2.2. Catalysts Testing

2.2.2.1. Catalytic Tests of CO₂ Hydrogenation, Under Classic Thermal Conditions (IST)

Thermal catalysis (experimental setup shown in Fig. 62) demonstrate a high conversion rate at low temperatures (300 °C) and a high selectivity (higher than 98 %) shown in Figure 71. Catalysts samples were pre-reduced at 400 °C, for 1h under 80%H₂:20%N₂ to activate the catalyst. As presented in Table 20, the highest conversion was reached with the 15wt.% Ni-Ce_{0.9}Zr_{0.1}O₂ catalyst. Therefore, this composition was chosen as the optimum.

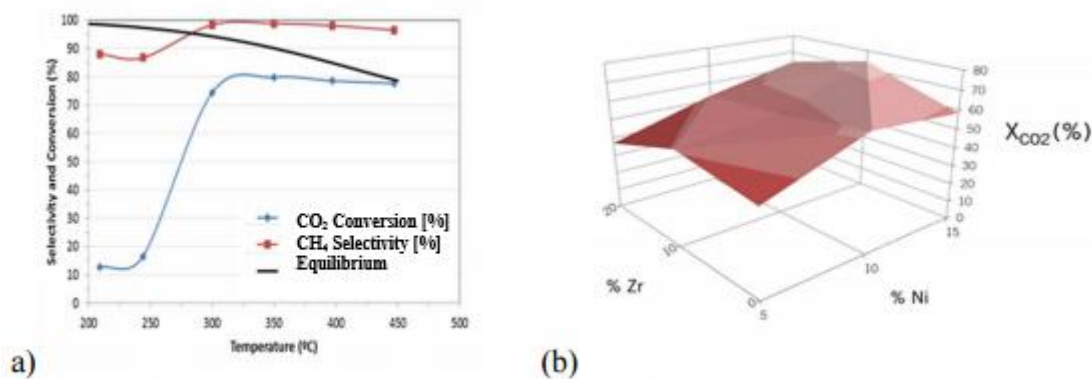


Fig. 71. (a) CO₂ hydrogenation to methane, obtained under conventional heating, for mesoporous 15wt.% Ni-Ce_{0.9}Zr_{0.1}O₂ catalyst; (b) conversion of CO₂ at 300 °C for all the samples tested, done by IREC (Spain).

Table 20. CO₂ conversion at 300 °C and 350 °C, and CH₄ selectivity obtained at 350 °C, for Ni-Ce_xZr_{1-x}O₂ catalysts (conventional heating).

% Ni	% Zr	X _{CO2} (300 °C)	X _{CO2} (450 °C)	S _{CH4} (%) (450 °C)
5	0	44	70.8	97.2
5	10	51	70.6	97.2
5	20	37	61.0	93.9
10	0	62	76.6	98.2
10	10	55	72.9	97.6
10	20	53	69.6	96.7
15	0	58	74.2	98.4
15	10	74	79.8	98.9
15	20	64	75.6	98.5

In addition, stability tests carried out during 10h, at 300 °C or 400 °C showed practically no degradation of the catalyst, which corroborates the assumption that stabilization at a high temperature inside the template can lead to nanocrystals with stable performance under the operation conditions without sintering.

Once the composition for thermal catalysis was optimized, several batches were tested with DBD plasma.

2.2.2.2. The Results of Hybrid Plasma-Catalytic Methanation of CO₂

Catalysts in a powder form were used in this part. Before each experiment, catalysts (300 mg) corresponding to a GHSV of 20 000 h⁻¹ were activated in H₂ flow for 2h at the temperature of 470 °C. Experiments were performed at 20 °C, 220 °C, 320 °C, 370 °C and 420 °C, with or without plasma. Typical voltage values used were varied between 10 to 16 kV at a fixed frequency of 40 kHz. The resulting energy was estimated in the range of 20-80 μJ/cycle, corresponding to a power between 0.8 and 3.2 W.

2.2.2.2.1. GC Chromatograms

The GC chromatograms located in Figure 72 below show results obtained for the 15% Ni Ce_{0.9}Zr_{0.1}O₂ SBA-15 catalyst (2h activation at temp 470 °C) at different temperatures with or without the use of plasma.

The results show an increase in the CO₂ conversion in the presence of plasma at different temperatures. As shown in the chromatograms, the reaction can be carried out at low temperatures (T<250 °C) but the conversion remains only close to zero %. However, at a high temperature, the difference is not so visible. As the process is performed at a high temperature (T>420 °C), a secondary reaction can occur due to the exothermicity of the process itself in which the methane selectivity decreases as well as the products are transformed into CO and H₂. The CH₄ selectivity lies between 100 and 68 %, but lowers with an increasing temperature. At 150 °C, the CO₂ conversion is about 4 times higher when plasma enhances the reaction with a selectivity of 100 %. Plasma assisted catalysis increases between 70 and 90 %, the CO₂ conversion in adiabatic conditions, depending on the nature of the catalyst.

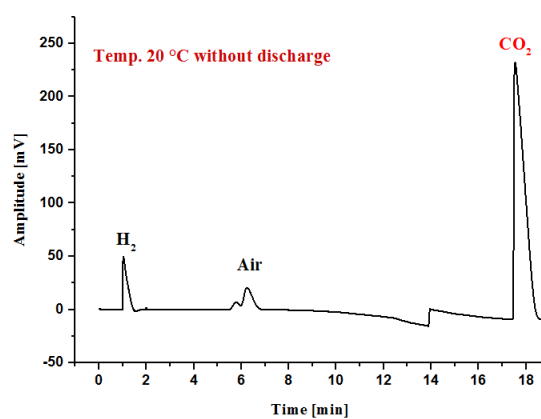
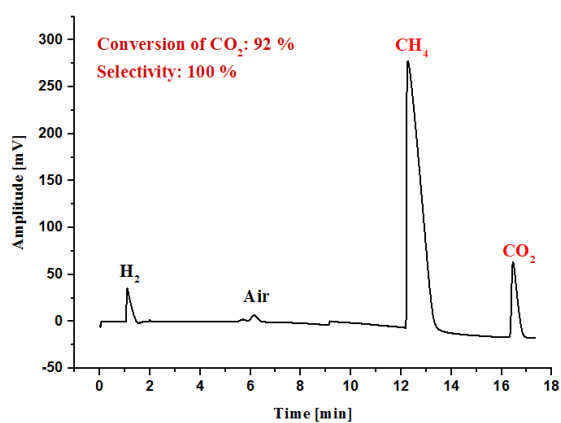
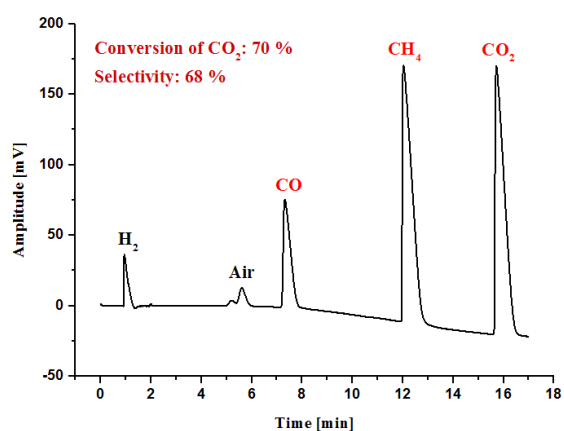
A**B****C**

Fig. 72. GC with TCD: analysis of products (A) at 20 °C without discharge, (B) at 150 °C with discharge, (C) at 420 °C with discharge.

2.2.2.2.2. FTIR Spectra

The FTIR spectra presented below in Figure 73 show the spectrum obtained for the 15% Ni Ce_{0.9}Zr_{0.1}O₂ SBA-15 catalyst during the carbon dioxide methanation reaction at different temperatures (20-420 °C) with and without the action of plasma.

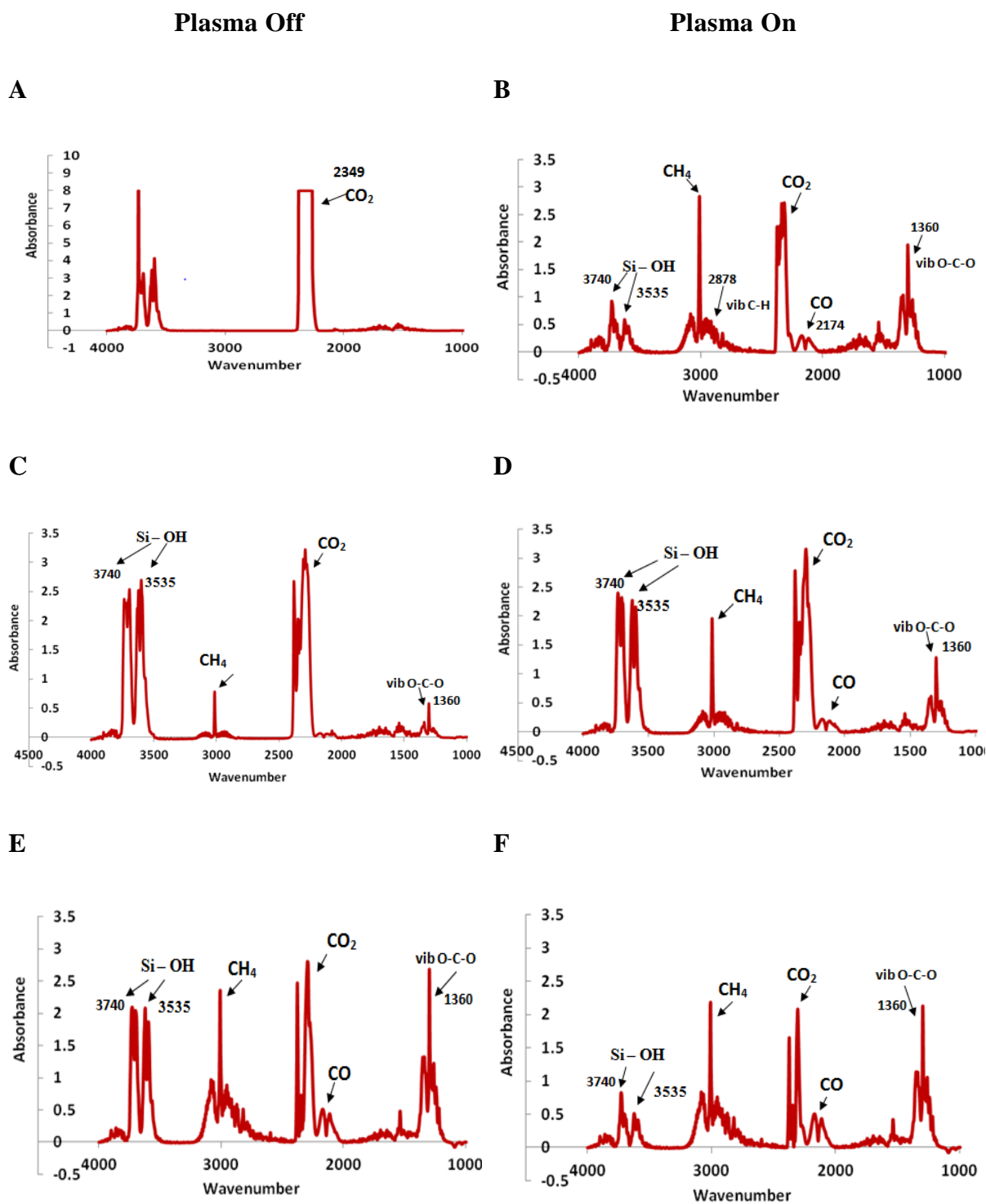


Fig. 73. Spectra obtained for the 15% Ni Ce_{0.9}Zr_{0.1}O₂ SBA-15 catalyst during CO₂ methanation with and without plasma (A) 20 °C, (B) 140 °C, (C,D) 160 °C and (E,F) 370 °C.

The band at 2349 cm^{-1} originating from gaseous CO_2 appeared with an appreciable intensity. The band located around 2174 cm^{-1} observed for the 15 % Ni $\text{Ce}_{0.9}\text{Zr}_{0.1}\text{O}_2$ SBA-15 catalyst during the carbon dioxide methanation reaction can be assigned to linearly bound adsorbed carbon monoxide (CO). The bands located at 1360 cm^{-1} (symmetric O-C-O stretching), 1382 cm^{-1} (C-H bending), 1552 cm^{-1} (asymmetric O-C-O stretching), 2878 cm^{-1} (C-H stretching) and 2952 cm^{-1} (combination of the asymmetric O-C-O stretching and C-H bending) were assigned to the stretching and bending vibrations. The bands located at 3535 and 3740 cm^{-1} can be probably assigned to the vibration of the Si-OH and adsorbed water molecules [190] in the spectrum for the SBA-15. The band located at 1238 cm^{-1} can be assigned to the stretching vibration of the Si-O-Si [140].

In the hydroxyl (OH) region, some OH groups spectra corresponding to the bands at 3605 , 3643 and 3742 cm^{-1} can be observed. These bands occur in all spectra. Many researchers [140, 190] have shown that the peak at 3740 cm^{-1} is due to silanol groups (Si-OH) coming from the zeolite. The latter may be present in defects in the structure or the exterior surface of the zeolite crystal. Therefore, it is reasonable to attribute the band located at 3742 cm^{-1} to silanol groups.

In the range of $2800\text{-}3000\text{ cm}^{-1}$, some bands can be observed. These peaks could be attributed to the characteristic absorption band of methyl symmetric C-H stretching ($2958\text{ cm}^{-1} \rightarrow \nu_{\text{as}}(\text{CH}_3)$ and $2925\text{ cm}^{-1} \nu_{\text{as}}(\text{CH}_2)$), methyl asymmetric C-H stretching ($2885\text{ cm}^{-1} \rightarrow \nu_{\text{s}}(\text{CH}_2)$) implying that some organic compounds were deposited or adsorbed on the catalyst surface. Bands located between 2700 and 2900 cm^{-1} could be respectively accounted for the aldehyde and ketone C-H stretching or methylene symmetric and asymmetric C-H stretching. Bands located at 3041 and 3174 cm^{-1} were attributed to the CH stretching.

2.2.2.2.3. Action of Plasma

The aim of this study was to convert CO_2 to methane in the presence of hydrogen. The CO_2 conversion was investigated in dielectric-barrier discharges with and without catalysts at a low temperature ($100\text{ }^\circ\text{C}$) and also at higher temperatures ranging between $220\text{-}420\text{ }^\circ\text{C}$ at atmospheric pressure. The combination of discharges and catalysts lowered the activation

energy of the reaction resulting in a decrease of the catalyst optimum temperature. The presence of the catalyst in the discharge increased the methane yield and selectivity. The carbon dioxide reduction at low temperature, i.e. 100-200 °C, depends on the plasma activation of the catalyst in an adiabatic reactor stabilized at 140 °C where CO₂ conversion of 80-90 % can be obtained.

For the 15% Ni-Ce_{0.9}Zr_{0.1}O₂ SBA-15 catalyst, the experiments under adiabatic (120-170 °C, without external heating) and isothermal (220-420 °C with external heating) conditions were performed. The results displayed in Figure 74 show a very low (less than 1 %) CO production for all temperatures (except at 420 °C) and large amounts of CH₄ and water. This catalyst was active under adiabatic (120-170 °C, without external heating), with plasma, leading only to the production of CH₄ (not CO or other C_xH_y) with conversions ranging between 75 to 90 %. Without plasma and with external heating up to 170 °C, this catalyst was totally inactive.

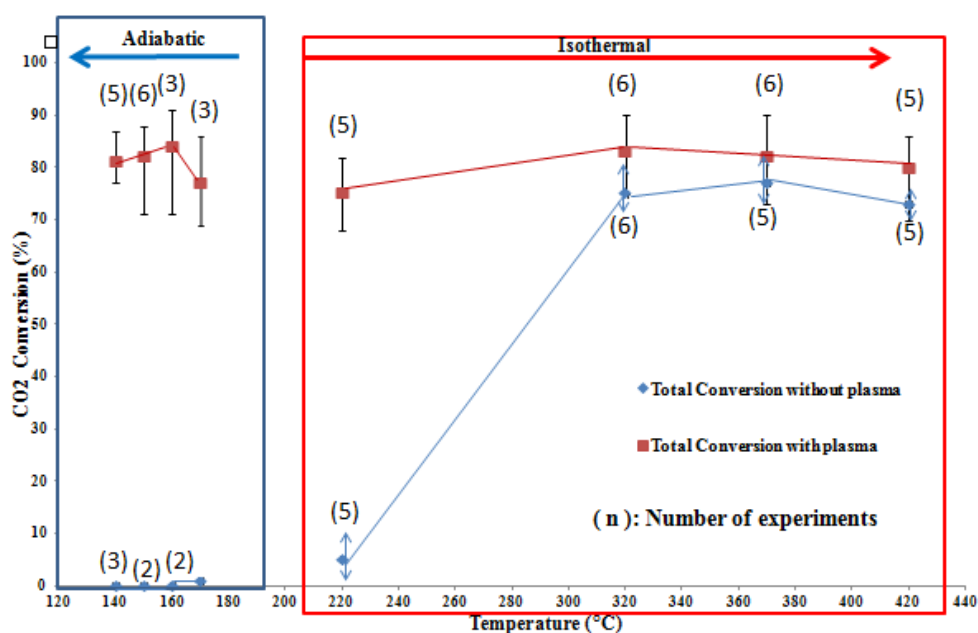


Fig. 74. CO₂ Conversion with and without plasma for the catalyst 15%Ni-Ce_{0.9}Zr_{0.1}O₂ SBA-15, voltage = 14 kV, f = 41 kHz.

As a conclusion, the process should be carried out in adiabatic conditions until a steady state is reached, which further continues in isothermal conditions. Under adiabatic conditions and with plasma, the process starts at room temperature; then the discharge increases the temperature. The reaction starts and due to its exothermicity, the reactor temperature further increases and stabilizes at a temperature below 150 °C, depending on the thermal conductivity

of the overall system. Under isothermal conditions, in the temperature range of 200-420 °C, the reactor is heated by an external heat source in both cases (plasma or without plasma). This range of temperature was explored because the temperature of 350 °C is the optimum for the Sabatier reaction in conventional processes.

Therefore, an increase of the total conversion with the plasma at 250-300 °C was expected but not at 140 °C and without external heating. For this reason, the experiments were repeated several times and confirmed the effect of the DBD plasma on the CO₂ conversion at low temperature.

2.2.3. Conclusions

Mesoporous nickel-ceria-zirconia catalysts shown a good distribution of the Ni sites. The latter was obtained on high-surface area materials and with stabilized nanocrystals, which confers to the material a good long-term operation without a degradation process due to sintering.

As a conclusion, the action of the plasma was demonstrated. In a fixed bed configuration, experiments were performed in a wide range of temperatures with plasma and catalyst and without plasma (catalyst alone). In the isothermal regime, the action of the plasma was highlighted, because the total CO₂ conversion without plasma ranged between 5-30 %, while under plasma action, the total CO₂ conversion ranged between 70 and 90 %, and increased with the temperature. When the plasma was switched off and the reactor was maintained at 150 °C by an external heating, the CO₂ conversion was less than 1 % (within the experimental error). In both examples, during the elementary pulses, due to the applied high frequency and voltage, an activation of the sites was obtained. The latter increased the desorption rate of H₂O which led to an increase of the global CO₂ conversion rate at a low temperature (<150 °C) and, simultaneously, an increase of the life stream of the catalyst. Moreover, the breakthrough of using the DBD plasma caused an increase of the CO₂ conversion rate to CH₄ in all cases. This phenomenon was observed using Ni supported on mesoporous ceria or ceria/zirconia or alternatively the Ni/Ce zeolite based catalyst for a temperature ranging between 320 and 420 °C. With all catalysts, an increase of the CO₂ total conversion was observed when plasma was operating. With some catalysts, this action occurred at a low temperature (150 °C) and without external heating in which a total conversion higher than 80 % was obtained with a CH₄

selectivity close to 100 %, in particular with all catalysts contained Ce. As a final statement, the key step of the reaction is probably the water desorption coming from the catalytic sites which are enhanced by the plasma in this range of temperature.

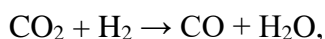
Chapter 4: Hybrid Plasma Catalytic Process Using Ni Supported on Ceria-Zirconia Mixed Oxide Catalysts

1. Introduction

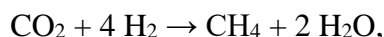
Hydrogenation of CO₂ has been intensively investigated for the last few years because it is responsible, to a great extent, for the greenhouse effect. Chemical recycling of CO₂ is very attractive because it can lead to less consumption of carbon based fossil resources [4].

The common point of CO₂ hydrogenation process is the production of water. The most important reactions are:

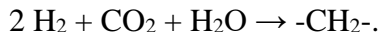
- the conversion of CO into CO₂ (intermediate step for the synthesis of liquids fuels) (RWGS):



- the methanation of CO₂ (Sabatier reaction):



- formation of hydrocarbons by the Fischer-Tropsch (WGS):



In all these cases the desorption of the water produced by the reaction, can promote hydrogenation. This can be obtained by increasing the temperature of the catalyst, but this leads to a carbon deposition on the catalyst resulting in its deactivation.

Non-thermal plasma is a technique which allows for desorption of water at room temperature. This advantageous feature of the plasma may be used to desorb water from CO₂ hydrogenation catalysts. This will be illustrated here with the Sabatier reaction.

The Sabatier reaction (Nobel Prize of Chemistry in 1912) thermodynamically is favorable ($\Delta G_{298\text{K}} = -130.8 \text{ kJ/mol}$). Nevertheless, the reduction of CO₂ (very stable molecule) to CH₄ (also very stable molecule), is a process that involves 8 electrons and requires the use of catalysts to obtain conversions and acceptable selectivities.

Ni-based catalysts have been widely investigated, because of their good compromise between high activity and low price [51]. Ocampo et al. [19] evaluated CO₂ methanation activity of Ni-ceria-zirconia and revealed that Ni-ceria-zirconia exhibited excellent catalytic activity and stability during 150h on stream. Such outstanding performance was due to the high

oxygen storage capacity of ceria-zirconia oxides together with the presence of highly dispersed nickel. Other studies [21] claimed that CO₂ methanation activity on Ni-ceria-zirconia was related to the particular interaction between Ni²⁺ cations and the ceria-zirconia support. Cai et al. [151] studied fractional-hydrolysis-driven formation of non-uniform dopant concentration catalyst nanoparticles of Ni/Ce_xZr_{1-x}O₂ in methanation of CO₂ and showed that a structure with Ce and Ni enriched at the surface improved the conversion of carbon dioxide. Despite the encouraging results observed for Ni-catalysts at around 300 °C and atmospheric pressure, the presence of water in the products leads to the sintering of Ni particles, which is the main reason for catalysts deactivation. However, conversion becomes negligible below 250 °C. At higher temperatures, (>420 °C), concomitant secondary reactions favor the CO and H₂ formation, thus considerably decreasing the selectivity towards the methane formation. A hybrid combination of catalysts with Dielectric Barrier Discharge plasma (DBD) may allow us to overcome all the above-mentioned drawbacks.

The catalysts can chemically be modified with support materials so that they have an enhanced low-temperature activity. The catalytic activity can also be improved by a physical means, such as DBD plasma. Non-thermal plasma can promote the catalytic hydrogenation of CO₂ into CH₄. In a previous study was shown that the plasma significantly increased the catalytic activity, especially at lower temperatures and pressures that the catalyst was not so active [191, 192]. In a traditional thermal catalysis, catalysts are activated by thermal energy to go over an activation barrier. While, in plasma-catalysis, catalyst is directly in contact with plasma, and reactive species (energetic electrons, free radicals, excited atoms, molecules) generated by the plasma can activate reactant molecules either in the gas phase or on the catalyst surface, possibly leading to the triggering of catalytic reactions at low temperatures. The bond strengths for gaseous CO₂ is 8 eV, respectively, but they get weak when adsorbed on the catalyst surface. The energetic electrons produced by the plasma can easily break the carbon-oxygen bond of the adsorbed carbon oxides, so the adsorbed carbon is easily hydrogenated to produce methane.

A hybrid plasma-catalytic system was used in the hydrogenation of carbon dioxide (CO₂) into methane (methanation) at atmospheric pressure and very low temperature using a dielectric barrier discharge (DBD) plasma reactor packed with Ni-Ce_xZr_{1-x}O₂ catalysts. Three catalysts were prepared by a conventional wet impregnation method, using 15 wt% of Ni loading over ceria-zirconia mixed oxides having different Ce/Zr ratios (Table 21). The physico-

chemical features of both catalysts and supports were evaluated by means of X-Ray Diffraction (XRD), Temperature-Programmed Reduction of H₂ (H₂-TPR), Temperature Programmed-Desorption of CO₂ (CO₂-TPD) and Transmission Electron Microscopy (TEM). All methods and conditions during catalyst characterization tests were described in Chapter 2 and in Appendix B. The methanation experiments in the absence or in the presence of plasma were carried out in the temperature range of 90-420 °C. The hybrid plasma 15NiCZ5842 catalyst combination was found to efficiently convert CO₂ into methane even at low temperature. Indeed, CO₂ conversions as high as 80 %, together with 100 % selectivity toward methane was measured in the presence of plasma at 90 °C. On the contrary in the absence of plasma, the same conversion and selectivity were only achieved at much higher temperatures around 300 °C, for the same catalyst.

2. Catalyst Preparation and Characterization

Three catalysts were prepared by a conventional wet impregnation method (Chapter 2), commercial ceria-zirconia mixed oxide (Ce_xZr_{1-x}O₂) with different Ce/Zr ratios: Ce_{0.1}Zr_{0.9}O₂, Ce_{0.58}Zr_{0.42}O₂ and Ce_{0.85}Zr_{0.15}O₂ were used a support. The final catalysts were respectively denoted as 15NiCZ1090, 15NiCZ5842 and 15NiCZ8515.

The physic-chemical features of both catalysts and supports were evaluated by means of BET analysis of the N₂ adsorption isotherms, X-Ray Diffraction (XRD), Temperature-Programmed Reduction of H₂ (H₂-TPR), Temperature Programmed-Desorption of CO₂ (CO₂-TPD) and Transmission Electron Microscopy (TEM). Conditions during these experiments were described in Chapter 2 and results are showed below.

The values of BET surface areas for both the Ni-catalysts and the ceria-zirconia supports, obtained from their corresponding N₂ adsorption isotherms, are shown in Table 21.

Table 21. BET surface area, Crystallite sizes of NiCZ catalysts before reduction, total H₂ consumption.

Catalyst	S _{BET} (m ² /g)	D CeZrO ₂ (nm)	D NiO (nm)	Total H ₂ consumption (mmole/g)
15NiCZ1090	67	10.6	21.5	2.34
15NiCZ5842	87	7.4	18.7	3.00
15NiCZ8515	106	5.5	29.0	2.70
CZ1090	73	8.2	-	-
CZ5842	93	7.2	-	-
CZ8515	115	4.3	-	-
15NiCZ5842 after reduction at 470 °C	86	-	-	0.63
15NiCZ5842 after hybrid plasma-catalytic test	87	-	-	1.14

Surface area is always higher for the unloaded supports pointing the pore blockage (around 8 % BET diminution) occurring to a certain extent upon the incorporation of Ni. 15NiCZ8515 shows the highest BET of this series of catalysts, since the BET surface area of the CZ8515 (Ce_{0.85}Zr_{0.15}O₂) is almost 36 % higher than the rest of ceria-zirconia supports. The addition of Ni, however, does not seem to modify the crystalline structure of ceria-zirconia support. The diffraction patterns acquired for the different catalysts and supports are shown in Figure 75.

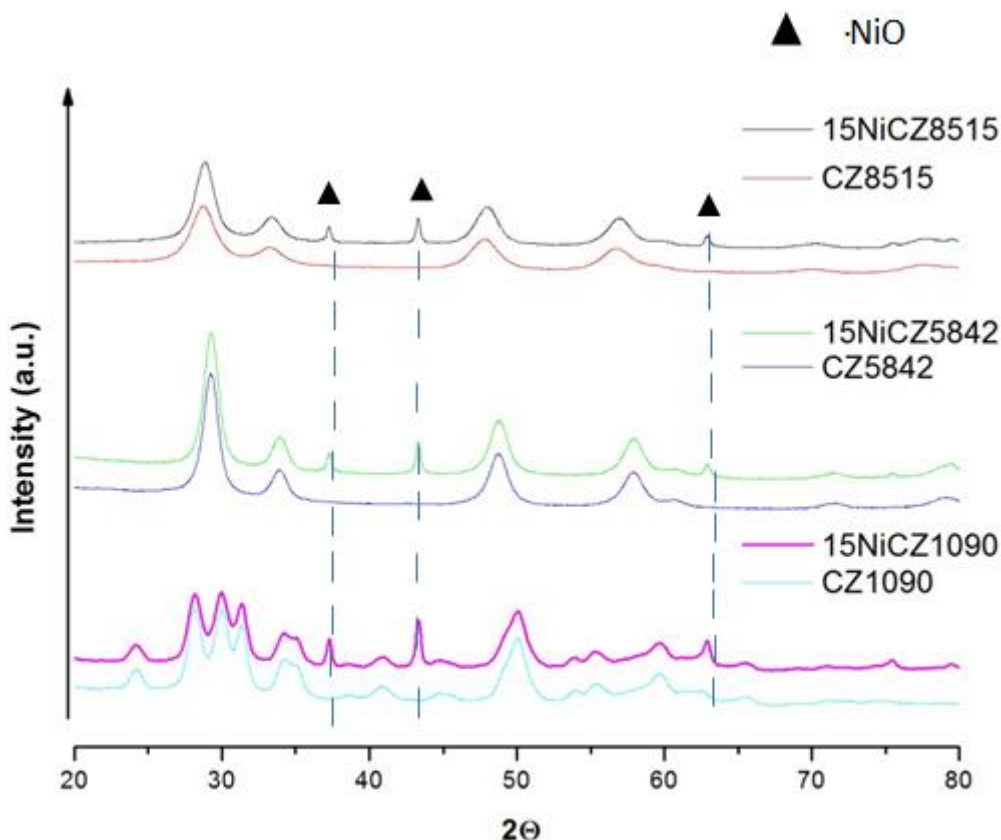


Fig. 75. X-ray diffractograms for the catalysts and the supports before reduction.

XDR patterns evidence the marked diffraction peaks corresponding to NiO particles. The crystal size of such NiO particles calculated from the diffraction patterns are shown in Table 21. NiO Crystal size varies with the type of the support. The larger particles, of around 29 nm, were found for 15NiCZ8515, corresponding to the support containing more cerium oxide. Ni is better dispersed on 15NiCZ5842 (NiO particles of 18,7 nm), which may explain the higher CO₂ conversions measured in the absence of plasma.

Figure 76 shows the hydrogen consumption profiles (H₂ TPR) of the three catalysts, as well as that of the CZ supports. In agreement with literature [21, 24, 25, 44, 45, 152, 158, 193], 15NiCZ catalysts present similar reduction profiles. The hydrogen consumption begins ca. 250 °C and ends around 620 °C. It is well known that the reduction peak between 380 and 420 °C is attributed to bulk NiO while the broad peaks appearing between 250 and 620 °C correspond to the reduction of the ceria-zirconia support. The higher the Ni dispersion the lower the temperature at which the peak corresponding to NiO appear in the TPR profiles. This is clearly observed for this series of catalysts since 15NiCZ8515 TPR profile exhibits a marked

peak of NiO reduction starting at much lower temperatures than 15NiCZ5842 or even 15NiCZ1090. The increased presence of Zr seems to be thus favouring the dispersion of Ni species on the supports surface.

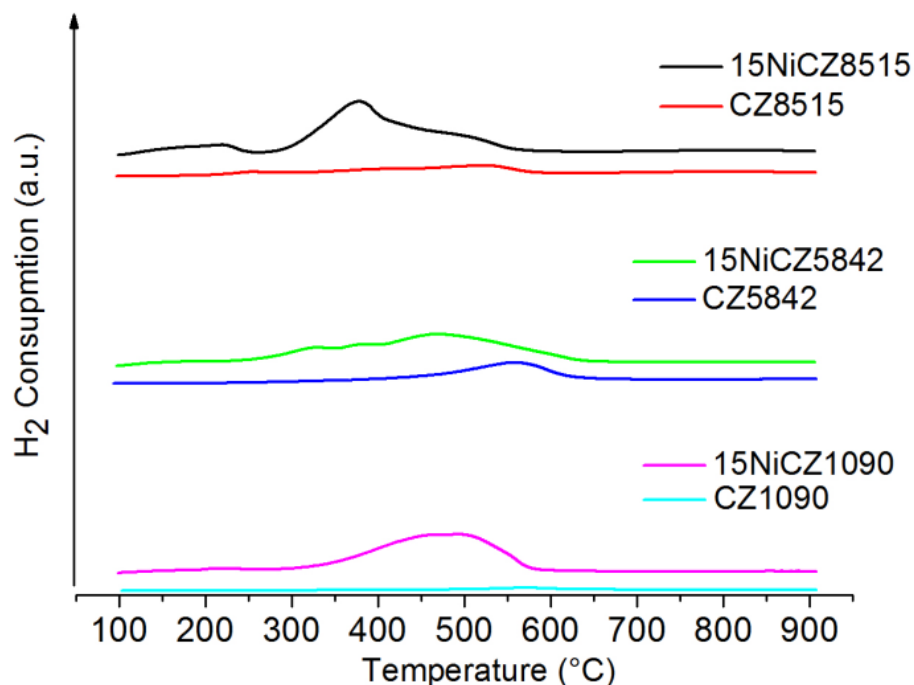


Fig. 76. TPR profiles of the different catalysts and supports.

Basic properties of the catalyst surface play an important role in the methanation process since they are required in the adsorption and activation of CO₂ [194]. They can be evaluated by the means of temperature-programmed desorption of CO₂ (TPD-CO₂). The results of TPD-CO₂ of the different materials reduced at 470 °C for 2h presented in Figure 77. The bare supports CZ showed a strong desorption peak with the maximum at approximately 120 °C. This peak can be ascribed to the presence of basic centers of low and/or medium strength (e.g. OH and O groups) [21, 195-198]. For both 15NiCZ5842 and 15NiCZ1090, the peaks corresponding to the support are present which leads to the conclusion that on these catalysis only exist weak and medium basic sites necessary to methanation reaction [21, 158]. In the case of 15NiCZ8515 catalyst a peak appears at temperatures between 450 and 700 °C. This corresponds to the strong basic site (e.g. O²⁻) [196-198]. Thus, incorporation of nickel seemed to the formation of strong basic sites and elimination the quantity of weak basic ones. This fact may point a stronger

interaction between Ni and ceria from the support, resulting in enhanced basicity of 15NiCZ8515 catalyst. According to the literature addition Ni into the ceria-zirconia improved the redox properties of the material favouring oxygen transfer, which would be required for CO₂ activation [198-200]. However, the increased presence of zirconium in the mixed oxide support may hinder the strong interaction between Ni and ceria.

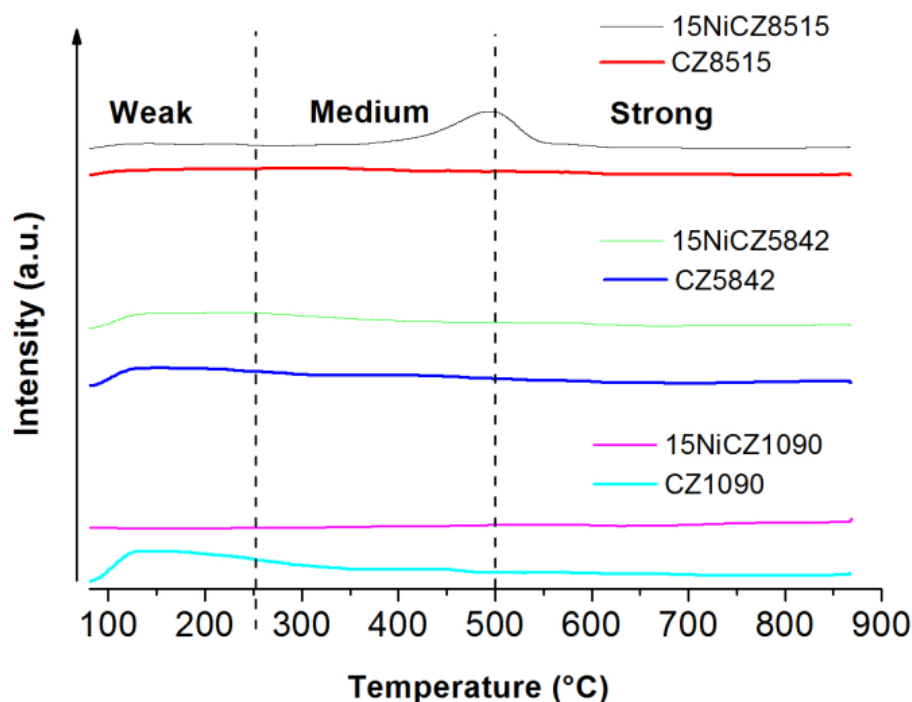


Fig. 77. TPD profiles of CO₂ adsorption on the pre-reduced catalysts and supports.

Based on the methanation reaction mechanism proposed on such materials [158, 193], it was shown that the kinetically relevant step is the adsorption of CO₂ leading to adsorbed CO and adsorbed O. Thus, on 15NiCZ5842 and 15NiCZ1090, low/ medium strength basicity is enough to initiate the reaction at sufficiently high temperatures in the absence of plasma, i.e. close to 300 °C. Furthermore, the particles of NiO and then of Ni after reduction being better dispersed on 15NiCZ5842, may contribute to achieving catalytic conversion at lower temperature than on 15NiCZ9010 or even 15NiCZ8515. The TEM images acquired for these catalysts are presented in Figure 78. For the three fresh catalysts (A,C,E), it was not possible to evidence the Ni particles on the CZ bare supports.

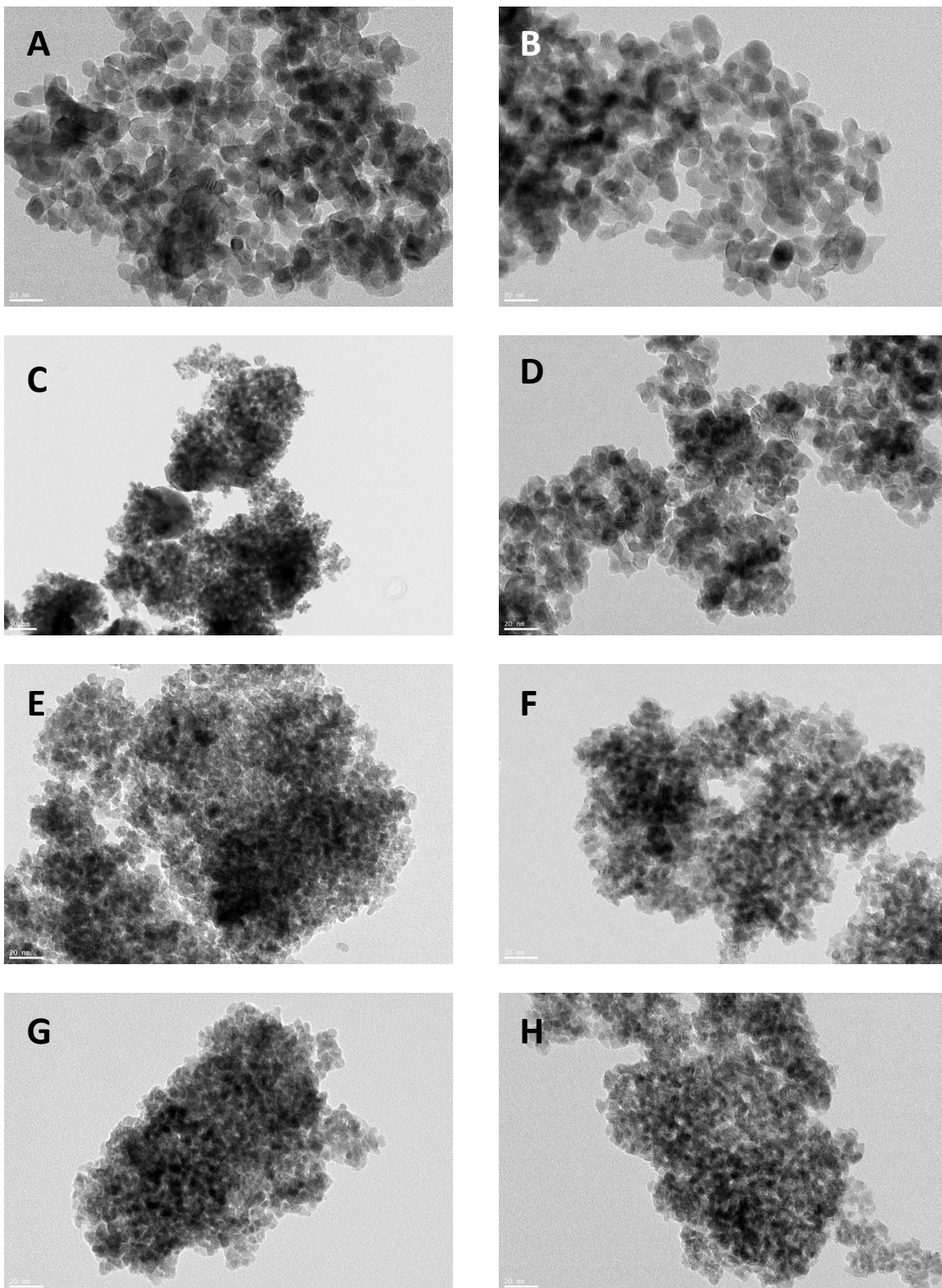


Fig. 78. TEM images of the fresh catalysts after hybrid plasma-catalytic methanation. (A, B) 15NiCZ1090, (C, D) 15NiCZ5842, (E, F) 15NiCZ8515.

However, by EDS (Fig. not shown) performed on reduced samples, it was possible to verify that the Ni⁰ is well dispersed on the supports.

3. Catalysts Testing

3.1. Blank Test

Before hybrid plasma-catalytic tests the blank test was done for the studied temperatures range. In the absence of catalysts without plasma no reaction occurs, only H₂ and CO₂ were observed. Whereas around 4-6 % CO were observed in the absence of catalysts under plasma in each tested temperature. Figure 79 shows results obtained during blank tests in methanation of CO₂ versus temperature under adiabatic and isothermal conditions in the absence of catalysts without and under plasma. During tests with plasma under adiabatic conditions the process starts at room temperature and after the discharge increases temperature. Due to the exothermicity of the reaction, reactor temperature also increases and is stabilized between 110-270 °C depending on the thermal conductivity of the whole system. Under isothermal conditions, the reactor is heated by an external heat source in the case of experiments with and without plasma.

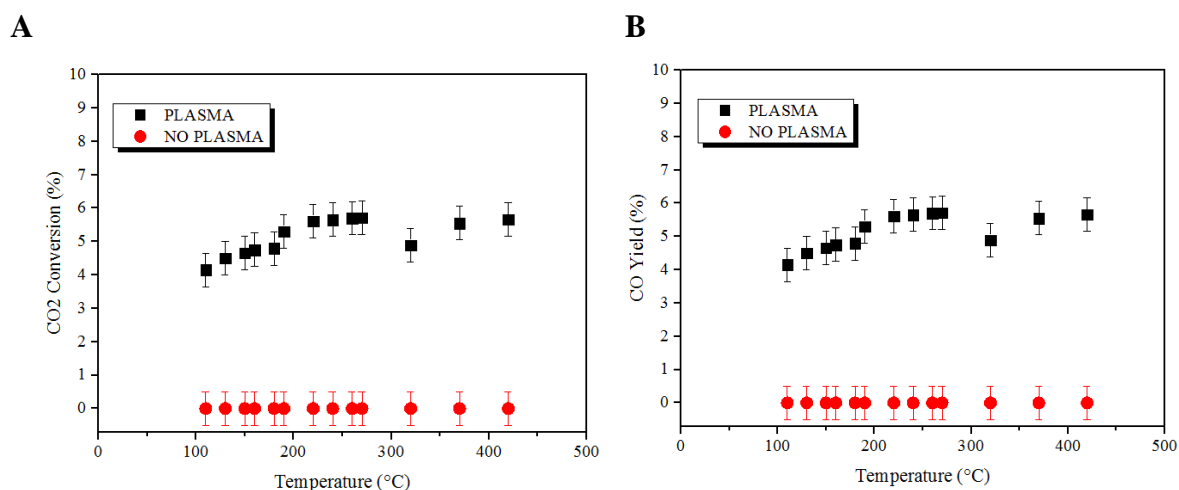
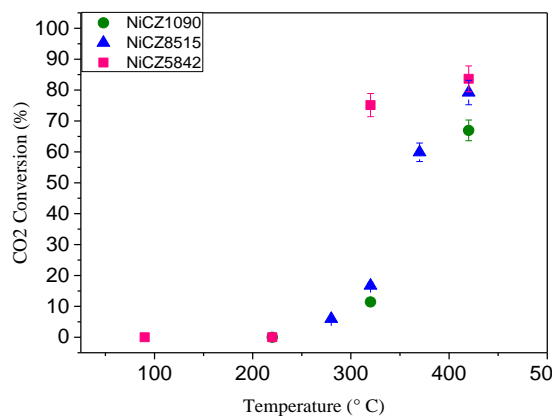


Fig. 79. Results of blank tests (A) CO₂ conversion, (B) CO yield in methanation of CO₂ versus temperature under adiabatic and isothermal conditions in the absence of catalysts without plasma and under plasma, voltage = 15 kV, f = 41 kHz.

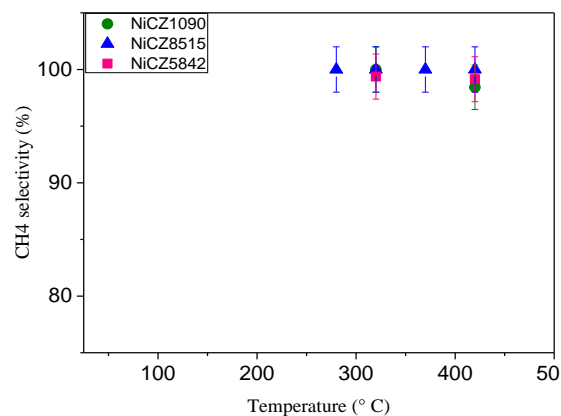
3.2. Catalytic Activity Towards Methanation in Absence of Plasma (Plasma Off)

Figure 80 contains the results obtained in the methanation tests in the absence of plasma, for the three different catalysts prepared. The thermodynamic equilibrium predicts CO₂ conversions varying from 100 to 85 %, with the temperatures increasing from ambient to 400 °C [26, 44, 45]. Methanation experiments in the absence of plasma evidenced negligible CO₂ conversion at temperatures lower than 280 °C. CO₂ conversion rapidly increases in the range 280-450 °C, reaching values close to the thermodynamic limit, especially in the case of NiCZ5842, as seen in Figure 80a. In this range of temperature, the selectivity was found to be almost 100 %, Figure 80b. Nor was formic acid nether formaldehyde were detected by MS and thus one can note that the unique secondary product was carbon monoxide with a yield lower than 2 % in the studied temperature range (Fig. 80c).

a)



b)



c)

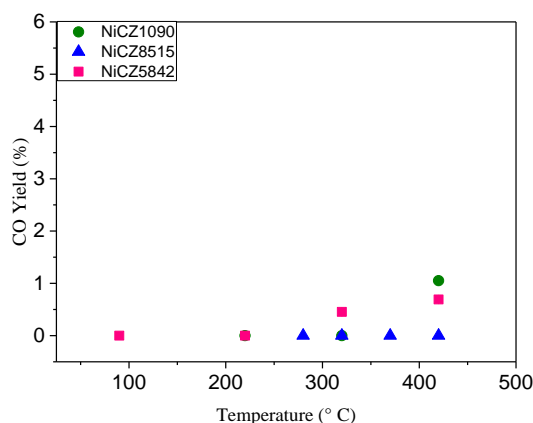


Fig. 80. (a) CO₂ conversion, CH₄ (b)selectivity and (c) CO yield versus temperature over 15NiCeZr catalytic system. Reaction conditions: 20 vol% CO₂, 80 vol% H₂, GHSV = 50,000 h⁻¹, voltage = 15 kV, f = 41 kHz.

3.3. Hybrid Plasma Catalytic Methanation

Figure 81a presents CO₂ conversions in the presence of the different catalysts and plasma in the temperature range of 90-450 °C.

Without plasma (Fig. 80), the conversion was almost zero below 250 °C, and it increased to about 85 % at 450 °C. In agreement with the literature [26] non-thermal plasma was able to greatly improve the conversion of CO to more than 97 %, almost close to the thermodynamic equilibrium conversion with a methane selectivity always higher than 90 % at temperatures lower than 260 °C. Particularly at low temperatures (T<260 °C) at which catalysis alone did not produce significant methanation rate, the plasma gave rise to a sharp increase in the conversion of CO. Indeed, our hybrid system is more active at even much lower temperature (from 90 °C) than ones previously proposed in the literature [196] based on a zeolite catalytic phase.

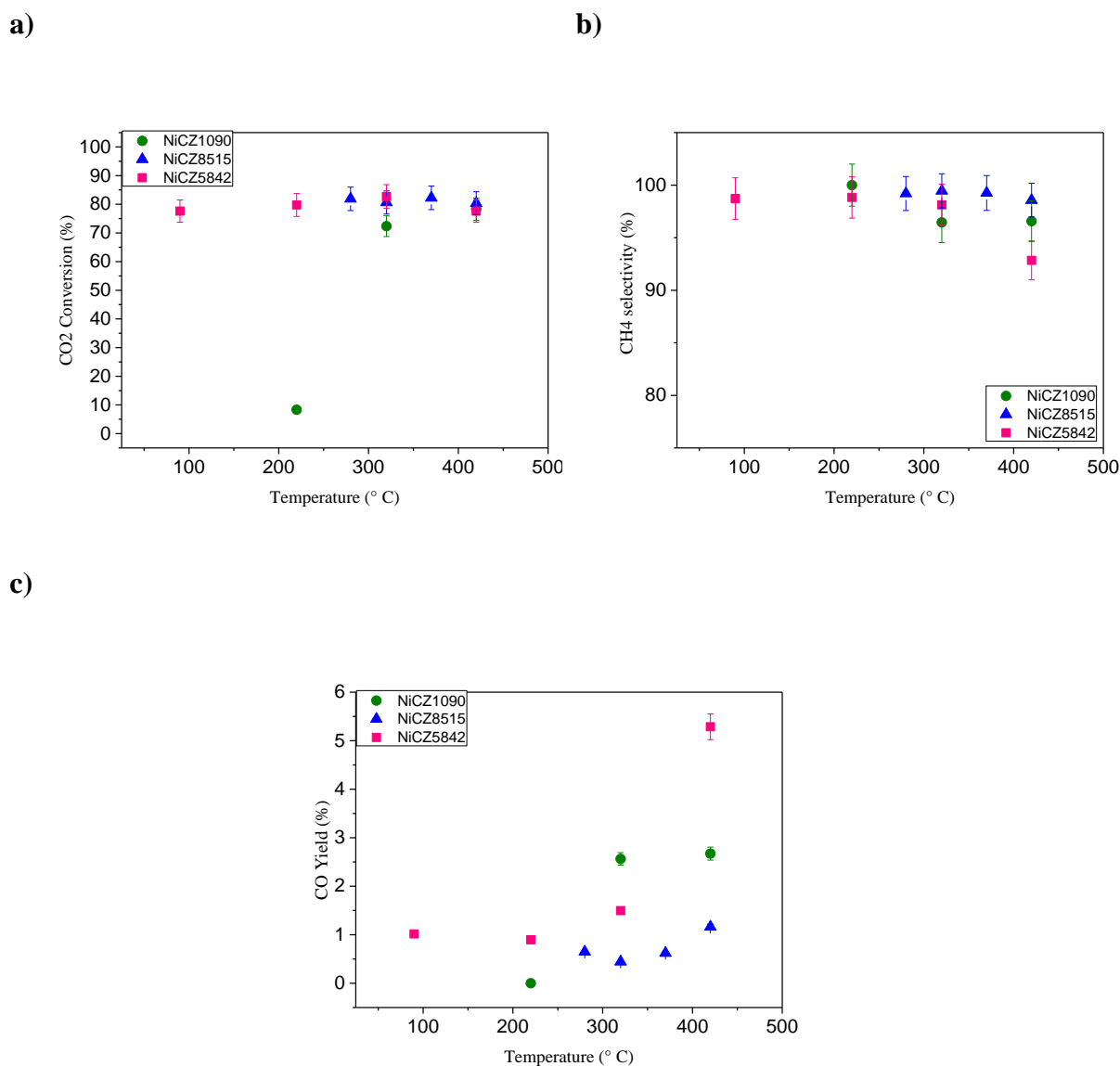


Fig. 81. (a) CO₂ conversion, (b) CH₄ selectivity and (c) CO yield versus temperature over the different catalysts in the hybrid plasma-catalytic configuration. Reaction conditions: 20 vol% CO₂, 80 vol% H₂, GHSV = 50,000 h⁻¹, voltage = 15 kV, f = 41 kHz.

According to the literature, the catalytic methanation involves the dissociation of CO₂ to CO* and O* in which * is an active site [26, 193, 201, 202]. The extent of this reaction is low at low temperatures but it is thermodynamically favourable [26]. The following steps of the methanation consist on the reaction of this dissociated species with hydrogen to produce methane. It is well known that plasma can help to dissociate adsorbed molecules, what will lead to an enhancement in the final CO₂ conversion and CH₄ yield.

Thus, at low temperature and in the presence of the hybrid system NiCZ and plasma, the formation of these adsorbed active molecules is favored in comparison to catalytic methanation alone in which this reaction does not take place for $T < 250$ °C. Moreover, since CZ bare supports are well known to act as an oxygen reservoir [203], these CO* and O* will be even more ready to react with hydrogen leading to higher conversions at low temperatures. At high temperature, the catalysts are active enough to activate the formation of CO* and O* species [21, 158, 193], and the plasma becomes inefficient and even non-recommendable since CO appears as non-negligible by-product (Fig. 81c), as moreover predicted by thermodynamics.

Let us note here that for sake of comparison, the methanation reaction was also conducted with plasma alone, i.e. in the absence of catalyst (Fig. 79) at low temperature. At 90 °C, the CO₂ conversion was found to be around 5 %, with CH₄ yield and CO yield of 0 % and 5 % respectively. This result further confirms the synergetic effect of the hybrid plasma-catalytic system.

3.3.1. Evolution of the Active Ni Phase During the Methanation Reaction

The catalytic activity of 15NiCZ5248 in the presence of the DBD plasma was tested in a long-duration methanation experiment, corresponding to 100h time on stream. The catalyst after this long duration test was submitted to further physico-chemical characterizations.

TEM analysis (Fig. 78b, d and f) evidences the absence of any morphological modification of the catalyst after this test. Moreover TPR was performed on 15NiCZ5248 before and after catalytic test and after hybrid plasma runs (Fig. 82).

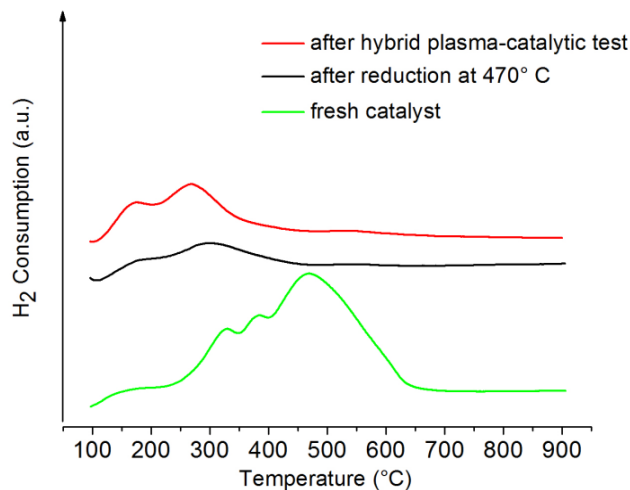


Fig. 82. Comparison of TPR profiles of the 15NiCZ5842 catalyst, fresh, after reduction at 470 °C and after the 100h duration hybrid plasma-catalytic methanation test.

Similar reduction peaks at low temperature are observed prior and after catalytic runs leading to the conclusion that during this process the Ni species are similar, however the peaks are more intense showing an increase of the active nickel species. Similar results have been presented on another catalytic system based on zeolites [26]. In order to verify that the hybrid catalytic plasma process does not affect the intrinsic basicity of the material, CO₂ TPD measurements were conducted on the 15NiCZ5842 before and after the 100h test (Fig. 83). Similar profiles of CO₂ desorption are observed. One can thus conclude that there were no changes in the basicity occurring as a consequence of the 100h duration test.

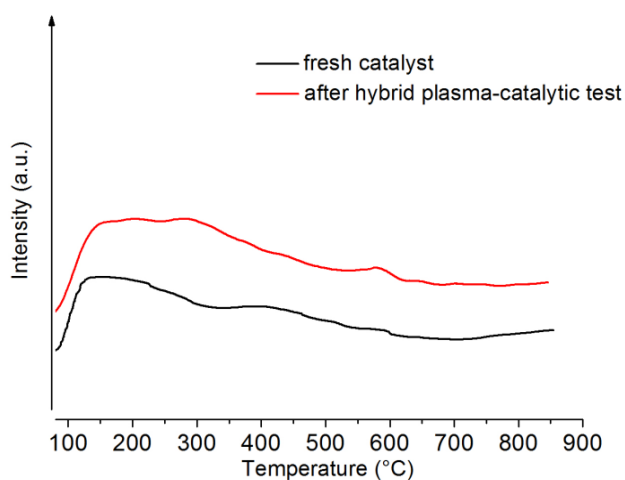


Fig. 83. Comparison of TPD profiles of the 15NiCZ5842 catalyst, fresh and after the 100h duration hybrid plasma-catalytic methanation test.

3.4. In Situ Diagnostics - Optical Emission Spectroscopy (OES)

As introduced before (Chapter 2), OES is an in situ method to monitor the excited and ionized molecules and ions in a gas discharge [167-171]. It allows the partial determination of the plasma composition without exerting any influence over it. Furthermore, OES provides essential information about the excitation state (vibrational and rotational), the electronic temperatures and the energy distribution. To better understanding of the processes in the discharge, the gas phase in the discharge was investigated with optical emission spectroscopy during the experiments. The idea was to identify and isolate differences in the spectra originating from non-catalyst and catalyst experiments.

3.4.1. Optical Emission Spectra for DBD Plasma Discharge in the Empty Reactor

In order to study the species presented in discharge (H_2 , CO_2 and CO_2/H_2), characterizations of the discharge by OES were performed in Institut Pierre-Gilles de Gennes (IPGG).

The spectra were acquired with the Czerny-Turner spectrometer system that has already been described in the experimental section (Chapter 2). It should be noted that the spectroscopic analyses showed here were not used to deduce the concentration of the different species within the plasmas, but to identify of what types of species are present within such plasmas. In this work, based on the coupled process previously proposed [182], OES information is used with the aim of identifying the contribution of plasma to the overall reaction mechanism.

The optical fibers were positioned vertically along the plasma close to the reactor wall approximately 4 mm in front of the discharge zone to avoid destruction of the fiber. The OES measurements were repeated at least three times. Identification of atomic and molecular species was done by comparing observed spectral lines with compiled lists of known lines [171].

The presence of a CO_2/H_2 plasma into the reactor without catalysts results in the formation of several excited species, i.e. CO, CH, and $H\alpha$ as shown in Figure 84.

At 283 and 297 nm, two bands of the third positive system of carbon monoxide were found, which are typical of CO-containing discharges [171, 204].

The major emission bands of CO₂ are found in the region between 380 and 440 nm. The peak at 390 nm and between 420-440 nm belongs to the CH transition [204, 205].

An H α line was observed around 656 nm [170, 171]. Generally, the molecular hydrogen spectrum has few characteristic features, producing no groups of lines or heads resembling a typical band system. The H₂ molecule radiates quite weakly throughout the entire visible spectrum.

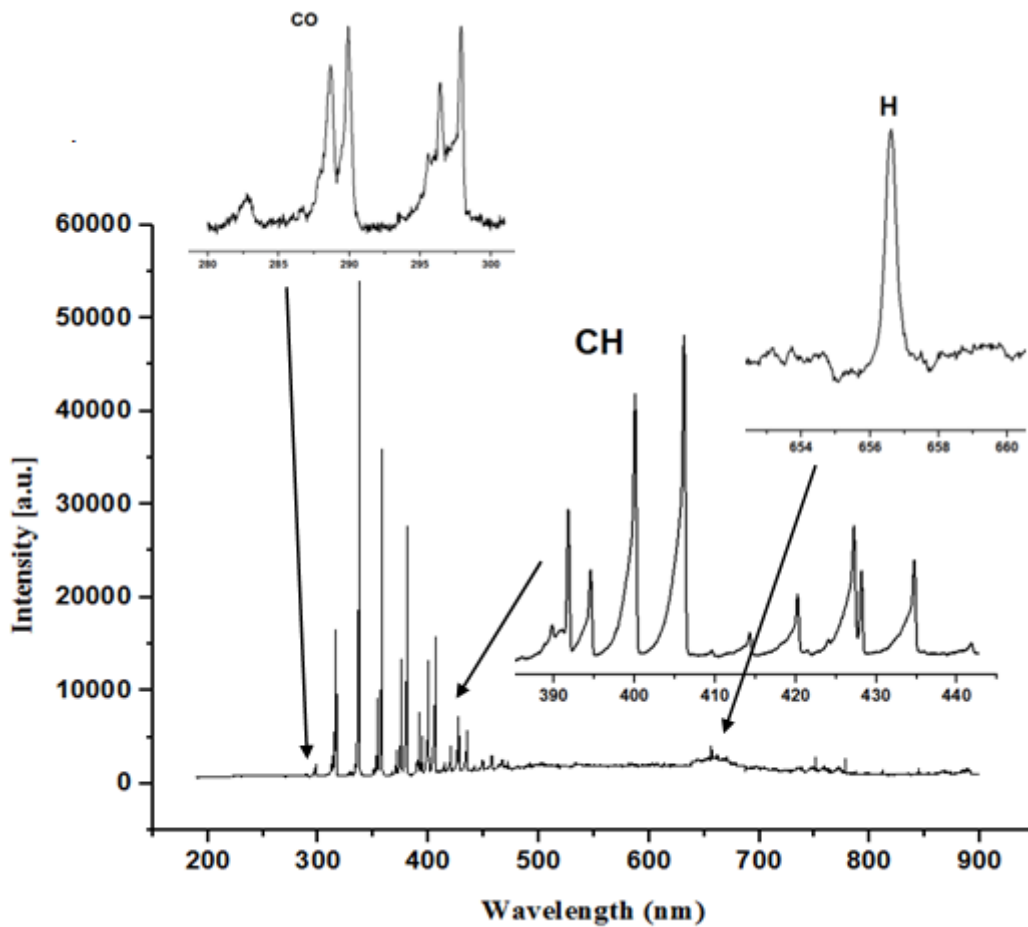


Fig. 84. Emission spectrum recording during CO₂ methanation, 100 ms acquisition time, 140 °C. Discharge conditions: gap = 2.5 mm, voltage = 14 kV, f = 41 kHz.

3.4.2. Optical Emission Spectra for DBD Plasma Discharge With Catalyst

The hydrogenation of CO₂ in the presence of a DBD plasma coupled to a NiCe_xZr_{1-x}O₂ catalyst was considered and studied using OES, as a tool for the determination of the excited species and for gaining insight into role of both plasma and catalyst into this coupled process. Figure 85 shows the OES spectra obtained under different reaction conditions: A) plasma and NiCe_xZr_{1-x}O₂ catalyst; B) plasma and the ceria-zirconia oxide (no Ni, only support).

The presence of a CO₂/H₂ plasma into the empty reactor results itself in the formation of several excited species in the gaseous phase, i.e. CO, CH and H α . The same species are observed when the plasma is combined with the NiCe_xZr_{1-x}O₂ catalyst. In presence of the plasma-support system we can observe also O species. Weak O lines can be observed at 750 and 777 nm [206]. For CO and H α species (mainly for support) we observe peaks but with low intensity. Though the ceria-zirconia support may be able to interact to a certain point with the excited species created by the plasma, the conversion of such species is only possible in the presence of the Ni-active sites present in the Ni/CeZrO₂ catalysts. Once these Ni-active sites are ready for reaction, the gaseous excited species created by the plasma react on the catalyst surface and are converted to the reaction products. Although the ceria-zirconia support favours CO₂ adsorption and dissociation and may contribute to oxygen transfer, the presence of Ni is crucial for the methanation reaction, as well as its dispersion, crystal size and reduction state. These findings are in agreement with previously published results, in a work that indeed compared different types of ceria-zirconia supports having different ceria and zirconia content [182].

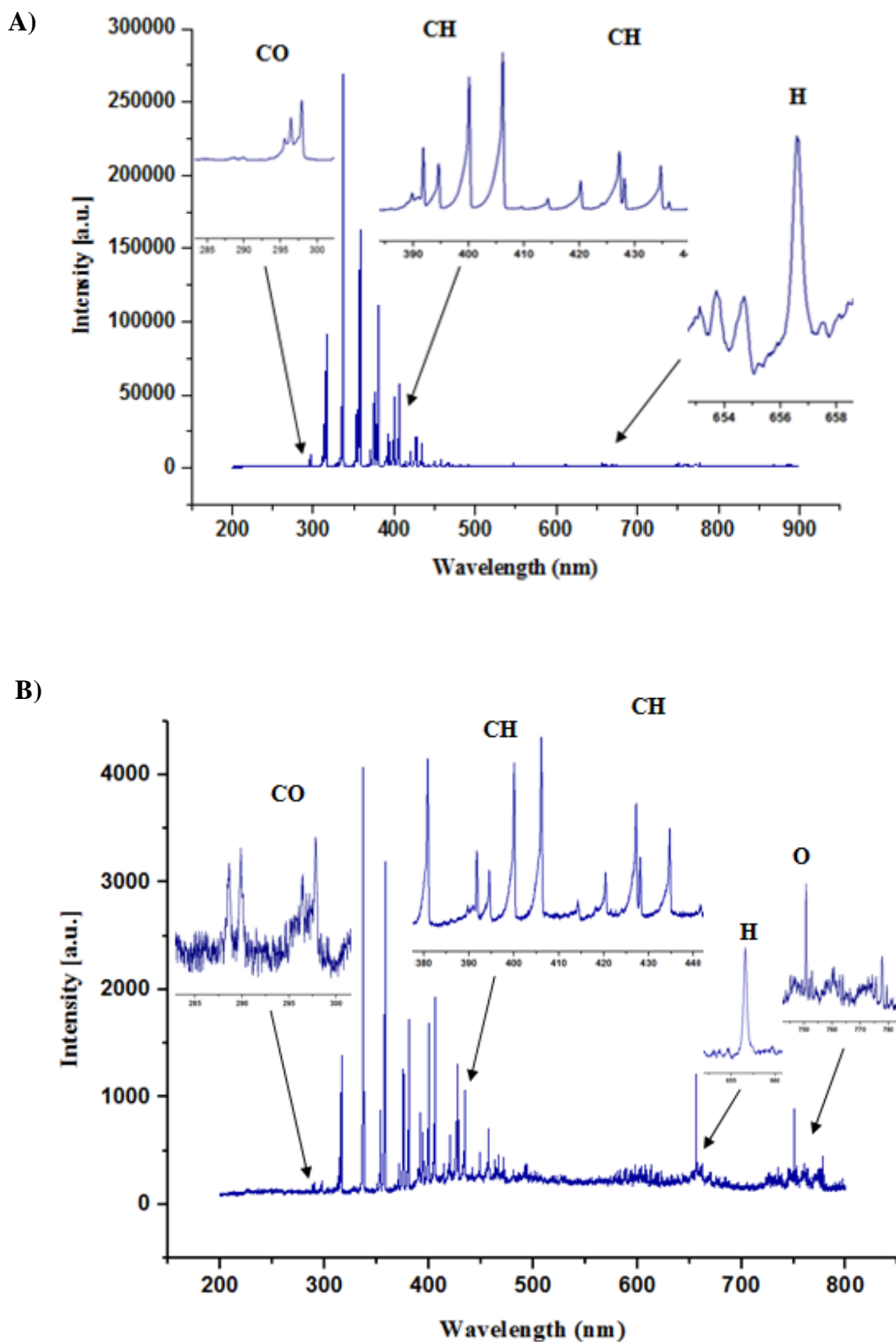


Fig. 85. Emission spectrum recording during CO₂ methanation for A) plasma and NiCeZr catalyst, B) plasma and ceria-zirconia oxide; 100 ms acquisition time. Discharge conditions: gap = 2.5 mm, voltage = 18 kV, f = 41 kHz.

The OES study of the coupled plasma-catalytic system evidenced the formation of several excited species in the CO₂/H₂ plasma. Though the ceria-zirconia support may contribute to CO₂ adsorption and dissociation, the methanation reaction involving the consumption of the gaseous excited species is only possible in the presence of the Ni-containing catalyst.

3.4.3. Influence Plasma Parameters

Figure 86 presents CO₂ conversions in the DBD plasma reactor under adiabatic conditions packed with Ni-Ce_{0.58}Zr_{0.42}O₂ catalyst in the presence of plasma for a temperature range of 28-210 °C where influence of frequency and voltage were studied. At low frequency (2-5 kHz) and at low voltage (11 kV) conversion becomes 0 %, whereas at 41 kHz with increases of voltage conversion started to be visible (small CO₂ conversion of 3 % occurs at 13 kV (110 °C)). Also temperature is not high (28-70 °C) when applied frequency and voltage is too low. Optimal conditions were found at 41 kHz-15 kV where total conversion of CO₂ was 82.61 % with selectivity almost 100 %. By increasing the voltage to 18 kV, the selectivity decreased to half (from 99 to 53 %) and production of CO began.

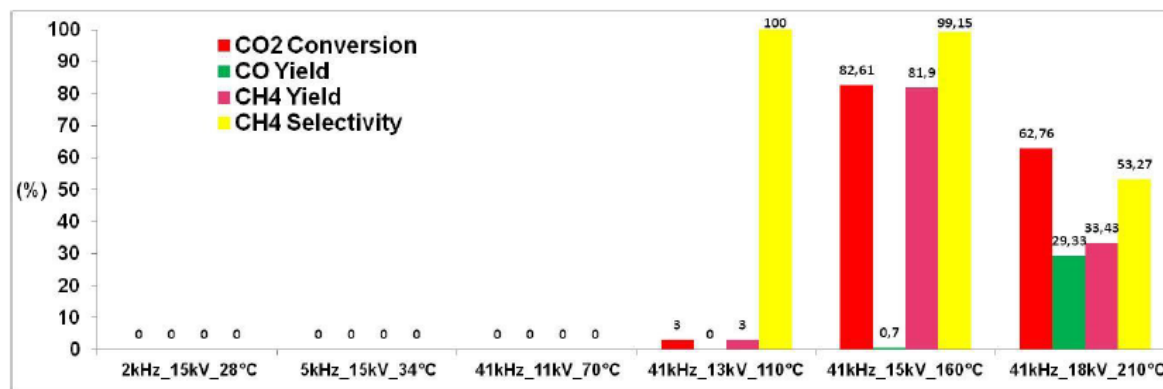


Fig. 86. Results of hybrid plasma-catalytic experiments under adiabatic conditions (CO₂ conversion, CH₄ selectivity, CH₄ yield and CO yield) in methanation of CO₂ over different plasma parameters with Ni-Ce_{0.58}Zr_{0.42}O₂ catalyst.

Optimal conditions were found at 160 °C, so test at this temperature was done with applying different frequency and power.

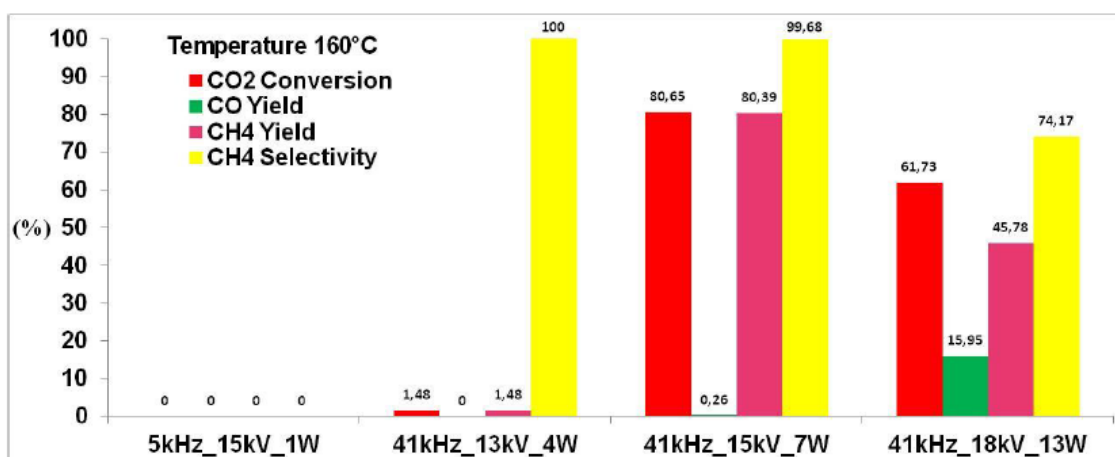


Fig. 87. Results of hybrid plasma-catalytic experiments (CO₂ conversion, CH₄ selectivity, CH₄ yield and CO yield) in methanation of CO₂ over constant temperature (160 °C) with Ni-Ce_{0.58}Zr_{0.42}O₂ catalyst.

As shown in Figure 87 results which obtained are the same as in Figure 86 so we can deduce that temperature did not have influence on CO₂ conversion to CH₄. Only CH₄ selectivity increase when higher voltage was applied (41 kHz-18 kV) because production of CO decreased from 29 to 16 %. This can be explained by the presence of hot spots. A practical challenge in reactor design is to remove heat produced by the exothermic reaction and maintain a relatively low process temperature without generating hot spots [38].

All results including specific energy and power density are shown in Appendix D.

3.5. Reaction Mechanism Proposal

3.5.1. Introduction

Prior to suggesting a methanation mechanism, under plasma conditions, a brief summary based on the literature and our experimental results is presented below.

A heterogeneous catalytic reaction generally takes place in five steps:

- Diffusion of the reactants on the surface and into the pores of the catalyst,
- Adsorption on the catalyst,
- Surface reaction of the adsorbed species,

- Desorption of the products from the surface of the catalyst,
- Diffusion of the products in the gas phase.

The difference in the methanation process between thermal catalysis and plasma catalysis is that the first one, is obtained at a relatively high temperature (300-350 °C) whereas, in the second one, the process begins at room temperature (Fig. 88). Indeed, this phenomenon can be achieved thanks to the electrons generated by the discharge and then, the temperature increases due to the exothermicity of the reaction. The maximum CO₂ conversion is obtained at 20-150 °C.

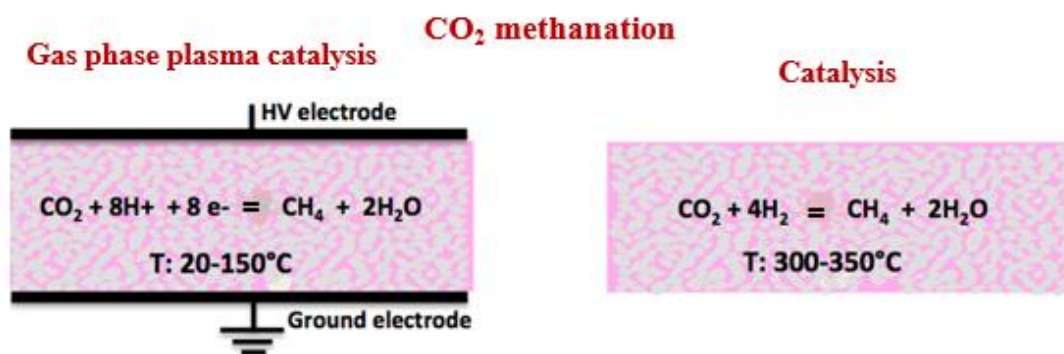
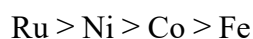


Fig. 88. Illustration of the CO₂ methanation process by thermal catalysis and plasma catalysis.

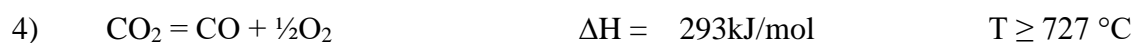
The following carbon dioxide methanation: $\text{CO}_2 + 4 \text{H}_2 \rightarrow \text{CH}_4 + 2 \text{H}_2\text{O}$ is an exothermic reaction ($\Delta\text{H} = - 165.0 \text{ kJ/mol}$). The latter needs a catalytic support such as ZrO₂/Sr or Ce or Al₂O₃ with CeO_x and in every case, NiO_x or Ru sites are required to produce the reduction mechanism at low temperatures (300-350 °C). At higher temperatures, the formation of CO decreases the selectivity and produces a poisoning effect of the catalytic sites.

Hydrogen adsorption sites on various catalysts can be classified as follows, as has been shown in a variety of works in the literature in the field:



The main reaction steps from the gas mixture of CO₂ and H₂ are:

- | | | | |
|----|---|---|---|
| 1) | $\text{CO}_2 + 4 \text{H}_2 = \text{CH}_4 + 4 \text{H}_2\text{O}$ | $\Delta\text{H} = - 165 \text{ kJ/mol}$ | $200 \text{ }^\circ\text{C} \leq T \leq 400 \text{ }^\circ\text{C}$ |
| 2) | $\text{CO}_2 + \text{H}_2 = \text{CO} + \text{H}_2\text{O}$ | $\Delta\text{H} = 41 \text{ kJ/mol}$ | $300 \text{ }^\circ\text{C} \leq T \leq 600 \text{ }^\circ\text{C}$ |
| 3) | $\text{CO} + 3 \text{H}_2 = \text{CH}_4 + \text{H}_2\text{O}$ | $\Delta\text{H} = - 206 \text{ kJ/mol}$ | $200 \text{ }^\circ\text{C} \leq T \leq 400 \text{ }^\circ\text{C}$ |



The most studied materials are Ni supported catalysts. Supports such as ZrO₂, due to its acidic/basic features and its CO₂ adsorption abilities, can also play an important role [207, 208].

As CeO₂ N-type semiconductor can supply labile oxygen, it is commonly used in Ce-Zr binary oxides. For instance, with a 10%NiCe_{0.72}Zr_{0.28}O₂ catalyst, a CO₂ conversion of 75,9 % and a CH₄ selectivity of 99,1 % were obtained [19]. The high oxygen storage capacity and its ability to enhance nickel dispersion is one of the reasons behind these high performances. The incorporation of nickel cations into the Ce_{0.72}Zr_{0.28}O₂ structure combined to a high dispersion of nickel improves the redox properties of the material and thus, restrains the metal sintering. Ni/ZrO₂ catalysts doped with Ce or Samarium (Sm), with a 30 % mol. nickel loading, have the maximum porous volume and size, and exhibit a higher catalytic activity (1.5 s⁻¹ turnover frequency (TOF) at 573 K) [142]. The mesoporous structure of the support (i.e. a high volume and size of pores) leads to the insertion of nickel particles into the pores. Research on the Pd-Mg/SiO₂ bi-functional catalyst showed a CO₂ conversion of 59 % and a CH₄ selectivity higher than 95 % at 723 K, whereas, in the absence of Mg, only CO was produced. Moreover, the use of Mg/SiO₂ as a catalyst did not result in a catalytic activity [37].

The methanation mechanism is not yet clear because it strongly depends on the nature of catalyst/support used. However, two mechanisms were proposed in the literature [1, 4, 19, 37, 89, 141, 142, 207, 208]: one occurs through the formation of CO while the other, occurs through the formation of formate as an intermediate.

According to the literature, oxygen vacancy on the surface of CeO₂ is one of the most interesting catalytic structures in the heterogeneous catalysis field and in particular in the CO₂ methanation reaction. This is owing to its high capacity for storing and releasing oxygen. CeO₂ is a promising catalyst in this reaction because it can greatly increase the reaction rate by adsorbing and activating the carbon-oxygen bond. Hydrogen is dissociatively adsorbed on Ni⁰. The methanation of CH₄ can occur by two pathways [1, 19]. The first one is the dissociation of CO₂ to CO as an intermediate and the second is its direct hydrogenation. The formation of CO is dependent on the nature of the catalyst and temperature. Regarding the temperature in all catalysts, the formation of CO begins above 350 °C. Above 400 °C, CO becomes the main product (WGS reaction). As only CH₄ is produced, the reaction mechanism

shall be considered without CO as an intermediate. According to this mechanism, in thermal catalysis, hydrogen molecules are activated and dissociated into atomic H on the nickel metal sites. Carbon dioxide is adsorbed on the oxide support leading to the formation of monodentate type carbonates. Then, the carbonates become formates through the hydrogencarbonates. Finally, formates are reduced to formaldehyde type species such as methoxides and methane [21] (Fig. 89).

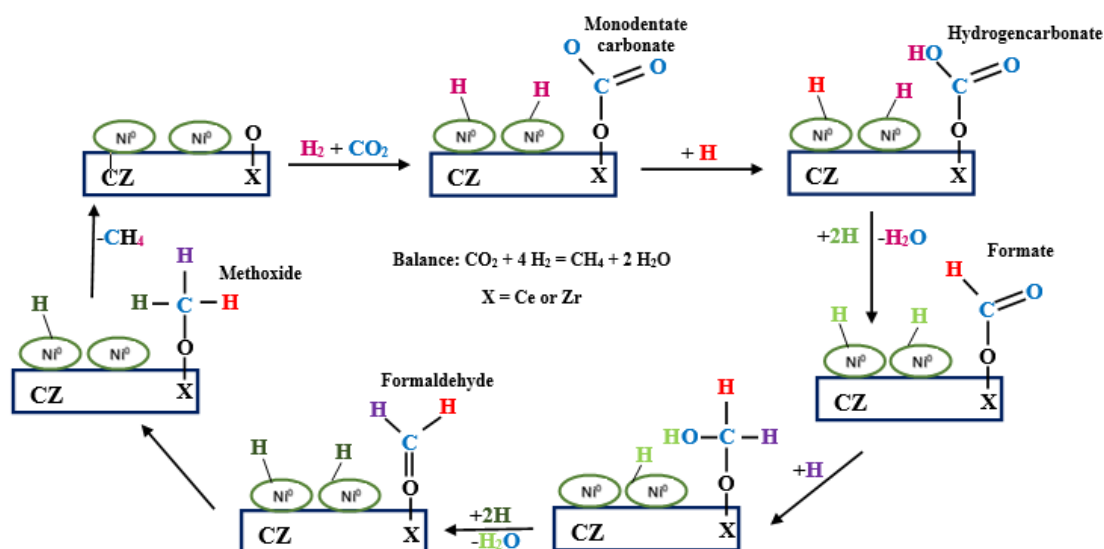


Fig. 89. Mechanism of CO_2 methanation under thermal catalysis conditions (adapted and modified from Ocampo Thesis) [209].

CO_2 prefers to be adsorbed on surface oxygen sites adjacent to Ce(III) compared to those adjacent to Ce(IV), Zr or surface hydroxyl sites. The formate species, which are derived from the hydrogenation of hydrogen carbonates and monodentate carbonates, are the main intermediate species during the reaction. The Ce(III) sites are active sites for their hydrogenation [210]. The introduction of divalent cations in the structure leads to the creation of oxygen vacancies, which improves the ionic conductivity and enhances its reducibility. Thus, the insertion of Ni^{2+} cations into the CeZrO_2 structure improved the redox properties of the material and restricted the Ni sintering, leading thus to a further improvement in their catalytic performance [21]. The incorporation of NiO in the CeZrO_2 structure modifies the chemical environment of nickel particles. As a result, a lower reducibility of NiO can be exploited in providing oxygen atoms for the removal of carbon. Therefore, the activity and the stability of the catalyst are enhanced. The enhanced activity of the catalyst depends on the preparation

method and the size of crystallites [211]. Ni particles with 5-6 nm size have a good activity and stability, while larger Ni particles (10 nm) showed a deactivation due to the formation of carbon deposit and sintering. Finally, the deactivation of the catalyst is mainly due to the rejection of the NiO from the bulk to the surface. The high mobility of oxygen in the CeZrO₂ structure, that enables an efficient re-oxidation of carbon, is reduced. As a result, the transformation of carbon into CO₂ is ineffective.

Another direct hydrogenation mechanism of CO₂ to CH₄ on Ni (110), without the formation of a CO intermediate was also proposed by Vesselli et al. [212]. According to the latter, at low temperatures, CO₂ is negatively charged and gets chemically bonded mainly via the carbon atom. The CO₂ molecule receives an electronic charge from the metal bonds, and binds to the surface with the carbon atom in a “V” configuration. As a result, the energy barrier (0.43 eV) becomes smaller for the CO₂ hydrogenation. Moreover, the energy barrier becomes smaller for the CO₂ dissociation into CO and O, as well as for the CO₂ desorption, both of were found to have an activation barrier of 0.60 eV. When adsorbed hydrogen approaches the CO₂ molecule, the formed H-CO₂ complex flips and binds to the surface with two oxygen atoms with hydrogen binding to the carbon atom. As a result, a formate intermediate is formed. Therefore, the presence of hydrogen prevents the formation of CO.

The role of the water produced by the methanation reactions is very important. Indeed, previous research [213] in the RWGS reaction ($\text{CO}_2 + \text{H}_2 \rightarrow \text{CO} + \text{H}_2\text{O}$), on an acidic catalyst (Al₂O₃) showed that when water is removed, the limiting step is the decomposition of the formate intermediate specie (HCOO⁻). However, when water is not removed, the limiting step is the formation of the formate ion; water molecules blocking the sites of CO₂ adsorption. Carbon dioxide, water and formate ions share the active sites of the catalyst. In more recent works utilizing the so-called sorption enhanced catalysis, researchers have managed to remove the water produced by the methanation of CO₂ as illustrated in Figure 90. Using catalysts that have a sorption function with a high affinity to water, can actively remove it from the reaction centers [214-216]. Comparing such a zeolite catalyst with a commercial one (without having a sorption function) resulted in a higher CO₂ conversion and a negligible CO production [216]. From a thermodynamic point of view, the Sabatier reaction is more favorable on a sorption catalyst. However, the water sorption depends on the storage capacity of the catalyst and when the sorption function is saturated, it should be regenerated. In any case, the water desorption from the catalysts can be performed by heating. However, a temperature increase leads to the

deposition of carbon on the catalyst and to its further deactivation. An alternative to avoid this carbon deposition resides in the use of a non-thermal plasma.

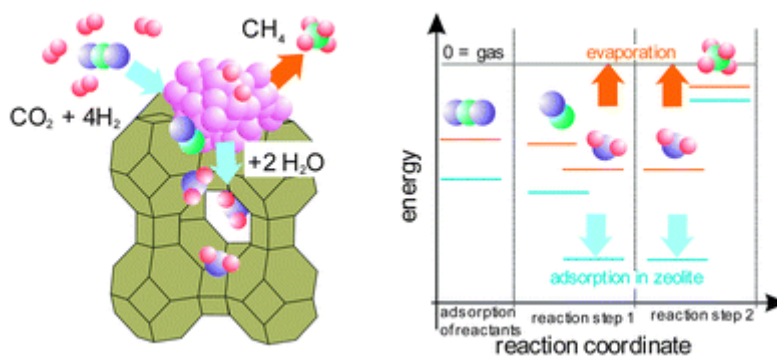


Fig. 90. Left: model structure of a sorption catalyst based on Ni particles on zeolites; right: sketch of the free energy of reactants and products of the Sabatier reaction on the conventional metal catalyst (orange) and a sorption catalyst (blue), respectively (adapted from [216]).

3.5.2. Plasma-Enhanced Water Desorption

Historically speaking, electrical discharges have been used for the charging and separation of particulates from gases in electrostatic precipitators. Experimental studies have shown that the evaporation rate of moisture from various porous dielectric absorbents can be greatly enhanced when the absorbents undergo an electrical discharge [217]. The enhancement of water desorption was attributed to the “corona wind” effect. Work performed in quartz micro-capillaries filled with water gave similar results when they were subjected to a point-plane corona discharge [218]. One possible explanation to elucidate this behavior could reside in an electro-convective flow caused by the diffusion of polar water vapor molecules in the presence of a highly non-uniform electric field, combined to a reduction of the vapor pressure above the capillary in the discharge zone. Another explanation may reside in a screening of the capillary charge of high density, or by the sorption of vapor molecules on nuclei (ions) produced in the discharge. A fundamental study of the corona discharge effect on the adsorption-desorption of water vapor on microporous silica and mesoporous fly ash, performed by Someshwar and Peshori [219], showed a significant decrease of the water adsorption capacity for both materials. According to the authors, this was due to the alteration of the thermodynamic

equilibrium. Indeed, at a non-zero potential, interfacial charges increase the electrochemical potential leading to a decrease of the adsorption capacity. Corona discharge was also used to regenerate water vapor absorbers in air condition devices [220]. For non-thermal plasmas, the water vapor desorption was estimated at 72 mg/kJ per unit power with a desorption time of 9 min, whereas for the conventional thermal desorption, it was respectively of 63 mg/kJ and 29 min. According to the authors, these values were primarily due to the high-energy electrons and excited molecules that impact the adsorbent surface.

Water desorption can usually be observed by Optical Emission Spectroscopy or Mass Spectroscopy. In the previously cited works, water vapor is physisorbed whereas, in the case of a chemical reaction; water vapor is chemisorbed. Nevertheless, when an object is immersed into a plasma, it gets negatively charged by the electrons because of their high mobility. Being a Lewis base, physisorbed or chemisorbed water will be consequently repelled.

3.5.3. Plasma-Enhanced Catalysis

Besides the water desorption, non-thermal-plasmas associated to heterogeneous catalysis allow optimal working temperatures for the catalyst. As the main function of the catalyst is the activation of the reactants generally obtained at high temperatures, the association of non-thermal plasmas decreases this temperature. As a consequence, the use of non-thermal plasmas and catalysts results in an increase of the energy efficiency as well as in an increase of the time of stream of the catalyst; reactions taking place at low temperatures.

Plasma driven catalysis was first used for the decomposition of NH_3 on Fe, Ag, Cu, Pt, Pd and Ni, with a yield for the catalytic process of 20 times higher compared to the non-catalytic one [221-223]. The enhancement of the NO_x yield with the use of a catalyst in the direct low-pressure plasma synthesis from air, has been pointed out in previous works from our laboratory [224, 225].

More recently, the production of CH_4 has been investigated by plasma-catalysis from a mixture of CO and H_2 [191]. The DBD plasma investigation has proved all the potential of the synergy between excited species through the plasma activation and the catalyst activity. The CO conversion into CH_4 has been increased from 50 % to 95 % at 280 °C with a Ni- Al_2O_3

catalyst. Furthermore, 95 % of the CO conversion was obtained at 280 °C with plasma activation, whereas the same conversion was achieved at 320 °C without plasma. The CH₄ selectivity remains constant with plasma. If CO is considered as an intermediate specie in the carbon cycle (CO₂→CO→CH₄) then CO can be obtained by the direct reduction of CO₂ as mentioned in the following equation: CO₂ → CO + ½ O₂. However, in this work [191], Y.S. Mok does not make any hypothesis on the reaction mechanisms.

In another work [226], the use of dielectric-catalysts with a high permittivity leads to high CO₂ conversions. With the Li₂Si₂O₅/Ca_{0.7}Sr_{0.3}TiO₃ dielectric, the CO₂ conversion is of about 13 %, while with Al₂O₃ and SiO₂, the conversion is only of 5 %. In addition, the arcing voltage is much higher for high dielectric strength materials and the latter results can be explained by a high density of micro-discharges obtained with Li₂Si₂O₅/Ca_{0.7}Sr_{0.3}TiO₃.

In addition to activation species, plasma can induce the water desorption from the catalyst and shifts the equilibrium towards the formation of methane. This concept can be used in all the reactions in which plasma driven catalysts produce water.

The activation of the catalyst by plasma is the key of our current process. The electrical power supplied to the fixed bed, described as a sinusoidal high voltage (~14kV), creates multiple streamers on the HV carrier waves, during the positive and negative polarization.

These streamers from hundreds of picoseconds to tenths of nanoseconds, corresponding to a frequency of a few MHz, are responsible for either negative or positive polarization of the catalyst sites. This polarization induces adsorption and desorption reactions at low temperatures (100-200 °C). Without polarization (conventional process), the working temperature is 200 °C higher than the mean one used between 300 °C to 400 °C.

The internal discharges increase the conductivity of the dielectric that leads to a spreading of the surface charge. The resulting streamers are shorter but their number significantly increase that leads to an increase of the injected power in the reactor.

However, it seems that the polarization of the adsorbed species on the catalyst sites is one of the concealed phenomena which can explain the modification of the kinetic rate. Nevertheless, the question that remains to be answered does not only concern the inlet species, CO₂ and H₂ which are non-polar molecules, but also the outlet species such as the CH₃· radical, CH₄ and the H₂O polar species.

3.5.4. Methanation of CO₂ (Plasma catalysis)

As previously mentioned, the difference in the methanation process between thermal catalysis and gas phase plasma catalysis is that the former, is obtained at a relatively high temperature (300-350 °C), whereas in the latter, the process begins at room temperature thanks to the electrons generated by the discharge and, after 10 minutes the temperature is stabilized at 130-150 °C.

In the methanation of CO₂, plasma will probably accelerate the global process but the steps should remain unchanged. Therefore, the remaining questions to be answered are: in which steps is the plasma involved and what is its action?

The reaction mechanism occurs without CO as an intermediate, as only CH₄ is produced. There are three possible ways where we can show the plasma action. The first one is presented in Figure 91.

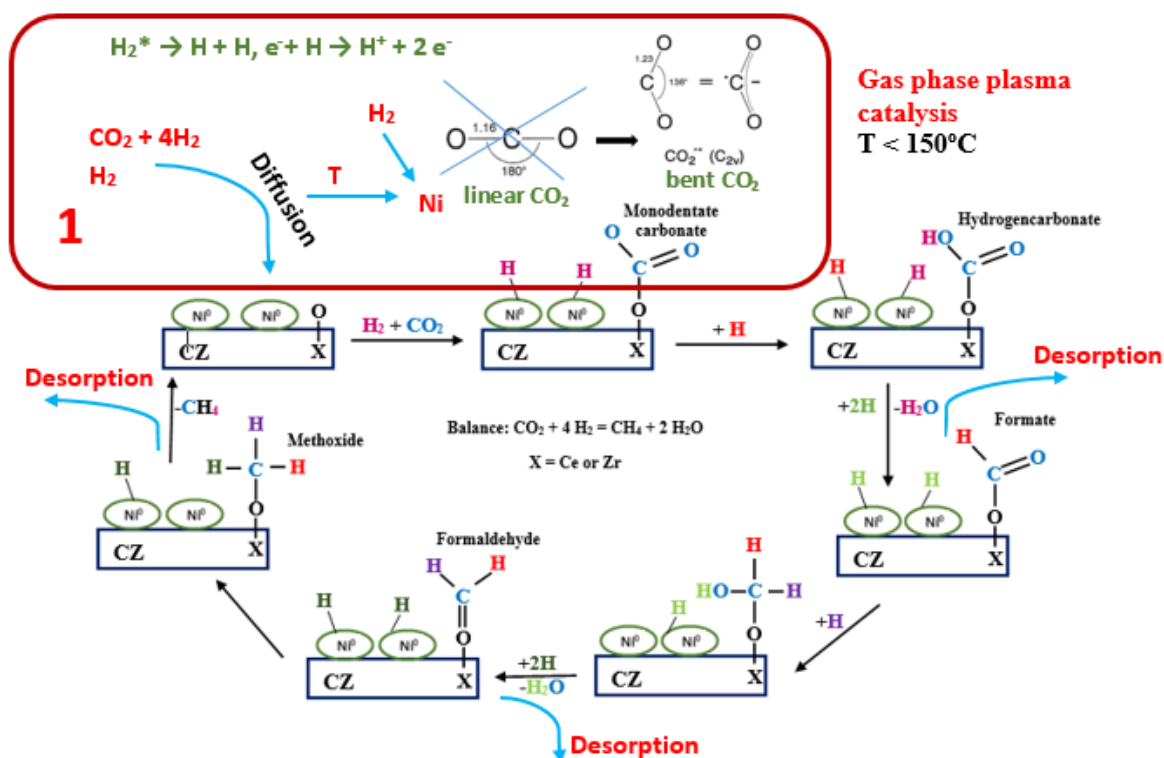
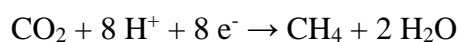


Fig. 91. Mechanism of CO₂ methanation under plasma catalysis conditions - the activation of CO₂ and H₂ in the gas phase.

In the first step of the CO₂ methanation (Fig. 91), which concerns the diffusion of the reactants, the plasma indirectly influences the process. Indeed, plasma does not affect the diffusion, but enables the activation of reactants before they reach the catalyst. The “task” of the catalyst is to weaken the strength of the bond of the molecule. For this purpose, the catalyst must be at a temperature compatible with the activation energy for the adsorption of the molecule. CO₂ has a linear configuration in the ground state and is a non-polar molecule containing two polar C=O bonds. The carbon atom (LUMO orbitals) has a Lewis acid character, whereas the oxygen atoms (HOMO orbitals) are weak Lewis bases. When the LUMO orbitals of CO₂ are occupied, via electron transfers or by electronic excitations, the lowest energy state corresponds to a bent geometry with an angle of 138°. Thus, any interaction of CO₂ with the catalyst is bound to induce a loss of linearity and leads to the formation of a carbon dioxide radical anion (CO₂^{δ-}) [227]. Plasma, by electron-molecule collisions activates vibrationally the molecules, reducing the strength bond, before they reach the catalyst surface. Thus, the activation energy for the adsorption decreases and the catalyst can operate at a lower temperature. The activation by plasma occurs at room temperature.

The quantum energy for symmetric deformation vibration ν_2 is only of 0.085 eV. In other words, that means that with an average electron energy of 1 eV in a DBD plasma, high vibrational levels can be reached. Even the symmetric and asymmetric vibrations ν_1 and ν_2 have a relatively low quanta energy, respectively of 0.17 and 0.3 eV (0.1eV corresponding to 1100 K in a thermal activated process). The vibrational excitation of molecular hydrogen by electron impact is also very effective at electron temperatures around $T_e = 1-2$ eV. Therefore, the vibrational temperature in non-thermal H₂ discharges can be very high and can significantly increase the H₂ dissociation rate [104].

Thus, both molecules in the methanation reaction under plasma conditions are activated at room temperature, whereas in thermal catalysis, the temperature needs to be set at 350 °C. The following electro-catalytic reaction:



take place in the NiCeZrO₂ bifunctional catalyst.

Plasma can also help to increase the desorption of the water produced by the methanation reaction as shown in Figure 92.

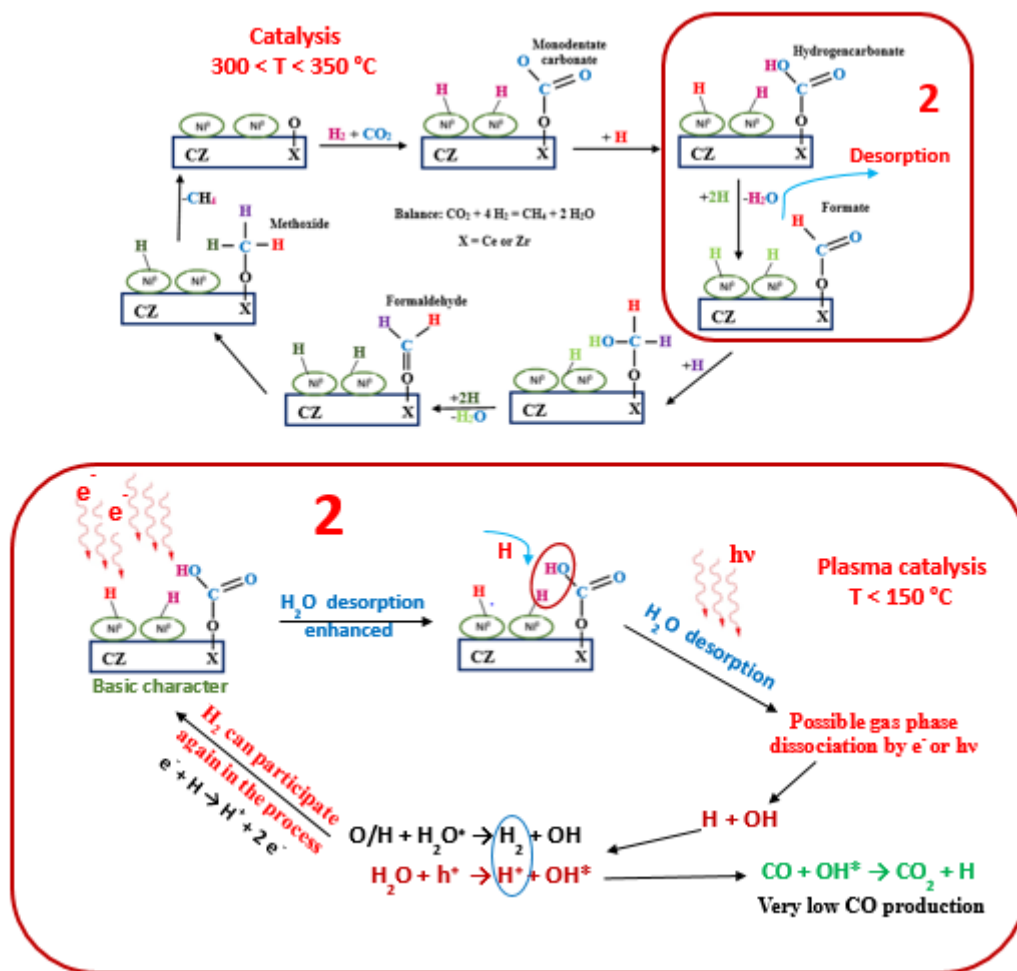
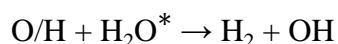


Fig. 92. Mechanism of CO₂ methanation under plasma catalysis conditions - the desorption of the water.

As NiCeZrO₂ catalyst has a basic character, electrons which are generated by the discharge enhanced this character and water being a Lewis base will be consequently repelled (Fig. 92).

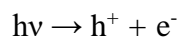
The dissociation of water, under plasma can be considered in the gas phase when water is already desorbed. Indeed in the gas phase H₂ and OH can be produced from the dissociation of vibrationally excited water by the following equation:



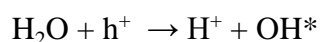
Therefore, these reactions occurring only under plasma conditions at room temperature can increase the CO₂ conversion and the production of H₂ that can participate again in the process.

Another point to be considered is the production of UV radiation produced by the electric discharge. These photons can contribute to the formation of H^+ and also to electrons that are needed for the reduction of CO_2 to CH_4 . As electrical discharges produce UV photons, there is an additional effect of electrons and UV radiation in the vibrational excitation of the species and the dissociative adsorption on the catalyst.

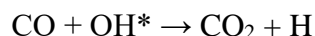
When a photocatalyst receives a radiation ($h\nu$), an electron and a h^+ are produced as mentioned in the following equation:



The h^+ can dissociate water and can give H^+ and OH^* :



This last reaction can supply additional hydrogen atom ions but also OH radicals that can remove CO:



This last reaction can explain the very low CO production what is in agreement with thermodynamics of the reaction.

The last point to be taken into consideration is the action of the polarization of the support/catalyst by the electric field (Fig. 93). The catalyst used here has two specific sites, one for each species. Indeed, one concerns the CeO_2/ZrO_2 (N-type semiconductor) site for the adsorption of CO_2 while the other one, regards the NiO (P-type semiconductor) site for the adsorption of H_2 . The polarization and their P-N junction could both explain the results with high CO_2 conversions at a low temperature.

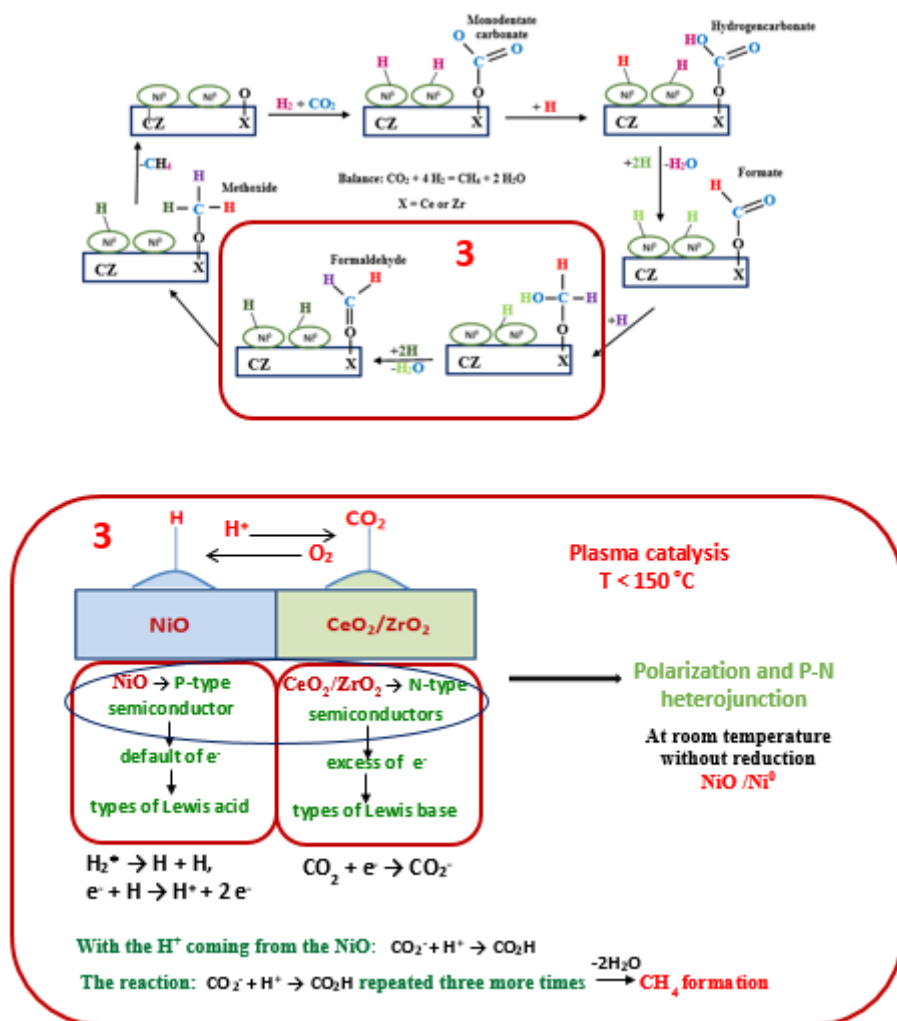


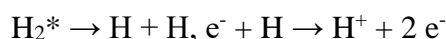
Fig. 93. Mechanism of CO_2 methanation under plasma catalysis conditions - polarization and P-N heterojunction.

The catalyst, without an initial reduction, at least initially, was in the form of $\text{NiO-CeO}_2\text{ZrO}_2$. Later, during the process the catalyst could be found to occur in the form of a Ni/NiO mixture.

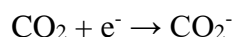
In thermal catalysis, CO_2 is adsorbed in CeZrO_2 while H_2 is dissociated in the Ni^0 after reduction of NiO at 470°C . Under plasma conditions, when the reaction is started with NiO and CeZrO_2 , it is possible to have a significant part of nickel such as Ni^{2+} during the reaction. Therefore, it can be considered that during the process, nickel is present under the form of Ni^0 as well as Ni^{2+} . The catalyst/support has two kinds of sites. The first ones, NiO sites, are P-type semiconductor (which means that there is a default of electrons in the conductive band), can be the anode and are Lewis acid. The other ones, $\text{CeO}_2/\text{ZrO}_2$ are N-type semiconductors (which

means that there is an excess of electrons in the conductive band), can be the cathode and are Lewis base. As a first step, NiO is partially reduced by H atoms formed in the gas phase of electrical discharge. Then CO₂ can be adsorbed on a bidentate position, which means that the carbon of the CO₂ on the CZ and oxygen on the nickel. These two types of sites (P and N), can form a P-N junction, that under a polarization can lead to a transfer of H⁺ from NiO to CZ and of O₂ from CZ to NiO.

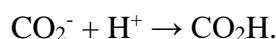
The reactions in the NiO can be written as:



As it was previously mentioned, in the CZ, collisions of the linear CO₂ with electrons lead to a bent configuration allowing its adsorption on CZ, and to the formation of carbonates and formates:



Then, with the H⁺ coming from the NiO:



This last step is repeated three more times leading to the CH₄ formation. The remaining four hydrogen atoms with the two oxygen atoms from the CO₂ form two molecules of water. As water is a very strong polar species with a dipole of 1.85 D, its desorption, is enhanced by the plasma leading to an increase of the methane formation.

Last but not least, an advantage of using plasma is that in thermal catalysis, at temperature below 200 °C Ni(CO)₄ is produced, which leads to the blocking of the sites for the H₂ dissociation, while under plasma, this carbonyl is decomposed. Indeed, this reaction is used for the deposition of thin films of Ni in plasma reactors.

Thus, we can conclude that the plasma contributes to the process of methanation of CO₂ in three ways:

- 1) via enhanced adsorption of excited CO₂ molecules (activated in gas phase by the plasma) inside the micropores of the catalyst.
- 2) via control of the water molecule desorption from the active sites of the pore and an increase of the rate of methane production at lower temperature. Furthermore, the desorbed water can be dissociated by electron collision producing H₂ that can contribute again to the process.

3) via electrochemical promotion of the catalyst by the transfer of the labile oxygen (O_2), in the N-type semiconductor CeO_2 , at room temperature.

3.5.4.1. Isothermal Conditions: Temperature Range Between 250-450 °C at Atmospheric Pressure

From the statements previously described, the two limited steps are:

- 1) water desorption
- 2) energy transfer from the N/P-type sites of the semiconductors in order to develop the reduction of CO_2 .

Therefore, a large difference between plasma and non-plasma studies at low temperatures can be evidenced as the evolution of the global conversion rate increases. However, only a small difference at high temperatures can be observed, resulting mainly in the production of CO.

At a temperature of 200 °C, the thermal effect of the catalytic reactor is limited by a low H_2O desorption process without plasma. In addition, the conversion is also limited, and depends of the catalyst properties and on the nature of the semi-conductor sites.

With a plasma excitation, at 200 °C, the conversion rate raises up to 80-85 % depending of the nature of the catalyst.

In this temperature range, it seems that some catalysts are not able to be activated by plasma. On a closer look at such catalysts, cerium oxide seems to be the key to explain such differences. In addition, some species such as Na, K, Ca, which are introduced in the bulk in order to modify the acid/basic properties of the surface, can only work at high temperatures with a poor selectivity.

Between 350 and 400 °C, the difference in the conversion rate is less than the difference in the methane selectivity, meaning that CO is produced instead. With plasma, an enhancement of the CO_2 conversion of 10-20 % is reached.

This is an interesting result which points out that the CO specie only appears at low temperatures with a DBD plasma excitation (300 °C). Moreover, this means that the competition between the CO desorption and the CO reduction is modified with an increasing CO desorption.

Without plasma, the thermal effect produces the H₂O desorption and at a higher temperature, a competition between the CO reduction and CO desorption occurs.

3.5.4.2. Adiabatic Conditions: Results at Room Temperature at Atmospheric Pressure

In this section, the main results described are the enhancement of the electron transfer in the NP-type junction semiconductors at low temperatures.

Apparently, the conversion rate is close to zero at room temperature, as there is no ignition of the reduction of CO₂ and there is no knowledge if the CO₂ is adsorbed with or without H₂O on the catalyst sites, as it could not be measured. The results are the same for all catalysts.

When the plasma DBD excitation process starts, the reduction occurs as the switching of an electric circuit. Starting from 20 °C, the mechanism clearly appears along with the water production and at the same time, an increase of the temperature due to the exothermic reaction, occurs. As a result, from the thermal production and H₂O production, the best information is obtained on each type of catalysts. The reaction rate reaches 85 to 90 % of the CO₂ reduction without any production of CO.

It seems that an electrical process opens as a double phenomenon. One occurs on the semiconductor which moves an electron from the P site to the N site for the reduction of CO₂, whereas the other one, an electron moves of oxygen atom or ions from CO₂ to H-NiO_x resulting in the H₂O formation.

Such formulated proposal points out the electronic ignition of the reaction by the DBD discharge. This means that the electron motion and the oxygen ions are the support for the mass exchanges on the surface of the catalyst.

4. Conclusions

In the present work, a hybrid catalytic plasma system for CO₂ methanation based on the combination of a DBD plasma and Ni/CeZrO_x catalysts has been presented. It was clearly demonstrated that the hybrid plasma catalytic process was active at low temperature (<260 °C) on the selective conversion of CO₂ into methane. At low temperature and in the absence of plasma, the conversions of CO₂ were lower than 15 %, but they were drastically enhanced and in the presence of plasma reaching 80 % at temperatures between 100 and 300 °C, whereas for plasma alone conversions of 5 % were observed. In the presence of plasma the CO₂ is activated in both CO* and O*, even at low temperatures, leading to higher conversion rates in the presence of the catalysts. Almost no difference in catalyst activity was found for Ni catalysts prepared using different ceria-zirconia supports. On the contrary, in absence of plasma, the 15NiCZ5842 showed enhanced methanation activity due to the presence of low and medium strength basicity together with a better dispersion of Ni-species, at high ZrO₂ contents on the mixed oxide support.

Our works have pointed out that the energy exchanges of a redox mechanism that characterizes the Paul Sabatier reaction can be developed at room temperature with N-P type semiconductor catalysis with electro-conductive properties of the bulk. The key step is to polarize the substrate with a high frequency and high voltage pulses in order to produce the electron mobility from the N-P type semiconductor as it is usually done in an electronic circuit. This opens up the field of redox process at room temperature as the thermal energy of the reaction is stored in the gas phase and in the bulk of the catalyst. In other words, these results open the field of energy storage using the chemical energy from CO₂ using a DBD process which transform CO₂ and electrons into CH₄ with hydrogen as the reducer.

The great advantage of this room temperature process is the high selectivity and the stability of the catalyst without the formation of CO, which is a poison of the catalyst.

Chapter 5: Hydrotalcite Catalysts for Hybrid Plasma Methanation Process

1. Introduction

In the present work, the CO₂ methanation activity of Ce and/or Zr promoted Ni-Mg-Al hydrotalcite-derived catalysts was assayed in the absence and in the presence of a dielectric barrier discharge (DBD) plasma. With the aim to further modify the basicity of HT derived catalysts, Ce and Zr were added, either together with the Ni, Mg and Al precursors or, in the case of Ce, through ion exchange from a solution containing [Ce(EDTA)]-complexes.

High methane yields, around 80 %, were measured under hybrid plasma-catalytic conditions, even at very low temperatures (110 °C, adiabatic conditions). In the absence of plasma, acceptably high CO₂ conversions and methane yields were observed only at temperatures higher than 330 °C. The presence of completely reduced Ni-crystallites of intermediate size, more readily available on the non-promoted catalysts was found to enhance the methanation reaction. Ce and Zr addition did not result in any noticeable improvement of the catalytic activity

Hydrotalcite materials started to be interesting for their application in CO₂ methanation and in catalysis due to the ability to exchange interlayer anions, their particular basic features and the possibility of introducing different type of divalent (Mg²⁺, Co²⁺, Ni²⁺, Mn²⁺, Zn²⁺) and trivalent (Al³⁺, Fe³⁺, Cr³⁺) cations into their brucite-like structure. Hydrotalcite is a naturally occurring layered mineral with chemical formula: Mg₆Al₂(OH)₁₆CO₃·4H₂O [228]. It is a mixed magnesium and aluminium hydroxycarbonate, which have the structure of brucite. Hydrotalcite layers are built of octahedral units in which divalent or trivalent cation is placed in the centre of an octahedron and six OH-groups are placed in the corners of the octahedron as shown in Figure 94 (A). Octahedral units are linked by edges, forming in this way parallel layers. Hydrotalcite structure may have rhombohedral or hexagonal symmetry (depending on the arrangement of the layers) in which the unit cell is build up from three and two hydrotalcite layers, respectively. In hydrotalcite brucite-like layers a part of divalent magnesium cations have been isomorphously exchange by trivalent aluminium cations. It is possible because of similar ionic radii of Mg²⁺ and Al³⁺. Thanks to the substitution, layers of hydrotalcite possess positive charge. This charge is compensated by carbonate anions present in the interlayer spaces

and water molecules fill the voids in the spaces between hydrotalcite layers [228-230]. A schematic hydrotalcite structure is presented in Figure 94 (B).

Ni and Ni-Ru supported on diverse porous materials are typically used as catalysts in CO₂ methanation [16, 19, 26, 35]. Ni-containing hydrotalcite-derived catalysts can be easily prepared through the incorporation of Ni-cations into their pristine brucite-like structure [145]. Such materials have already shown relatively high activity towards CO₂ methanation, at moderate temperatures, i.e. 350 °C [146]. Ce-species can be moreover ion-exchanged into such materials, resulting in an increased reducibility of the Ni-species, and in the introduction of intermediate strength basic sites (Lewis acid-base pairs), which can promote CO₂ adsorption and activate its hydrogenation [145]. The use of a Dielectric barrier discharge (DBD) plasma during the preparation of hydrotalcite-derived catalyst has been lately shown to lead to the formation of relatively small Ni particles tightly bonded to the support which, in turn, facilitated the hydrogenation of CO₂ to CH₄ [147]. The in-situ use of cold DBD plasmas can furthermore assist the catalytic hydrogenation reaction through the formation of a large variety of active species, as has been recently reported for CO methanation [25, 26].

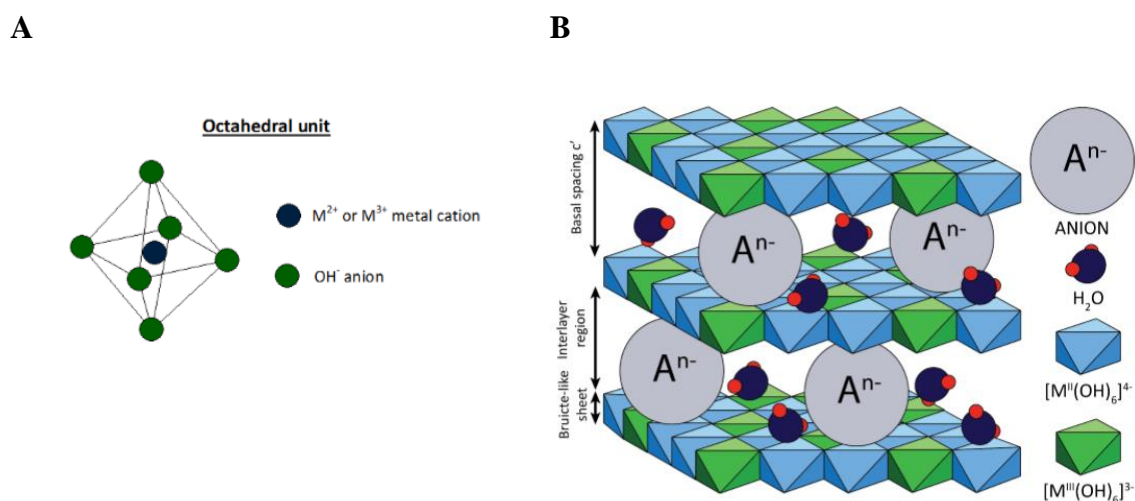


Fig. 94. The structure of hydrotalcite (A) the octahedral unit of brucite-like layers, (B) the schematic representation.

The aim of this study was to investigate the effect of combined Ni-Mg-Al hydrotalcite-derived catalysts (promoted either with Ce, Zr and CeZr) and DBD plasma in a hybrid plasma-

catalytic methanation process in order to propose low temperature operating conditions and show the differences between CO₂ conversion and CH₄ selectivity.

2. Catalyst Preparation and Characterization

Four different catalysts were prepared by a co-precipitation method (Chapter 2), HT-Ni, Ce-promoted: HTNi-Ce, Zr-promoted: HTNi-Zr, and Ce-Zr-promoted: HTNi-CeZr [145, 180].

The physic-chemical features of catalysts were evaluated by means of BET analysis of the N₂ adsorption isotherms, X-Ray Diffraction (XRD), Temperature-Programmed Reduction of H₂ (H₂-TPR) and Temperature Programmed-Desorption of CO₂ (CO₂-TPD). Conditions during these experiments were described in Chapter 2 and results are shown below.

The XRD diffractograms acquired for the reduced HTNi-catalysts (Fig. 95), evidence the typical reflections of hydroxalcite-derived mixed-oxides having a periclase-type structure (2θ : 43°, 62.5°) [231]. Several diffraction peaks corresponding to metallic nickel are also present (2θ : 44°, 51°, 76°). In the case of Ce and/or Zr promoted catalysts, additional phases of segregated ceria and/or zirconia can be observed.

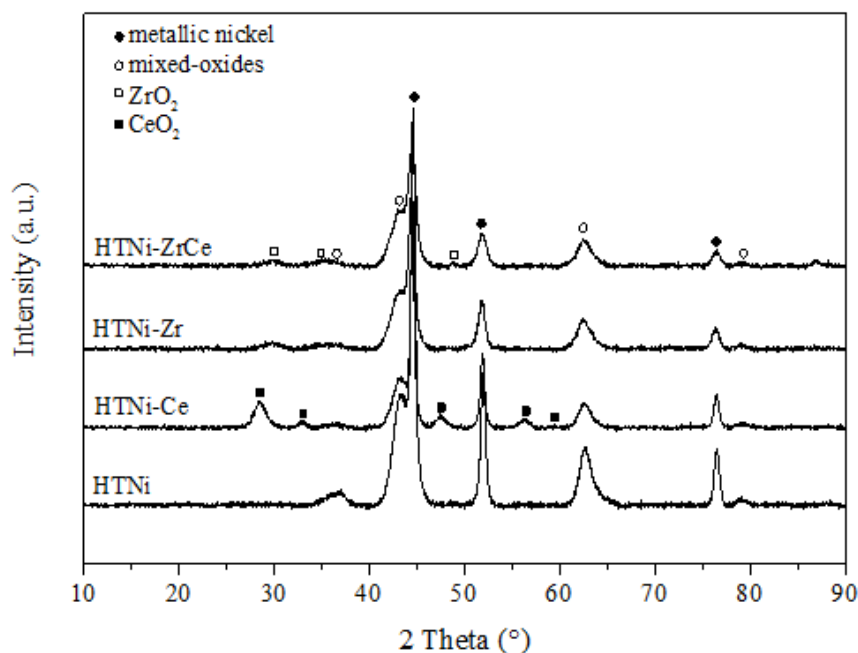


Fig. 95. X-ray diffractograms of reduced samples.

Ni crystal sizes were estimated using Scherrer equation and are presented in Table 22. Crystal size notably decreases as a consequence of the presence of Zr, i.e. from 20.7 nm in HTNi-Ce to 8.1 nm in HTNi-ZrCe. Table 22 shows as well the results of the textural characterization. The addition of Zr seems to increase the final porosity of the HT-derived mixed oxide, whereas Ce results in a certain extent of pore blockage, related to its incorporation through ion-exchange using [Ce(EDTA)]-complexes.

Table 22. Basicity (CO₂-TPD), Ni-crystal size (XRD), and textural properties for the HT-derived catalysts.

Catalyst	Total basicity [mmol/g]*	Ni crystallite size [nm]**	S _{BET} [m ² /g]	V _{total} [cm ³ /g]
HTNi	0.060	15.200	115	0.410
HTNi-Ce	0.094	20.700	102	0.330
HTNi-Zr	0.064	10.500	229	0.620
HTNi-ZrCe	0.119	8.100	158	0.560

* calculated from CO₂-TPD

** calculated from Scherrer Equation (XRD)

The H₂-TPR profiles for these catalysts, Figure 96, evidence a single wide and asymmetric reduction peak centered between 810 and 860 °C, arising from the reduction of nickel oxide in strong interaction with the MgAl mixed oxide matrix [145]. The shoulders appearing at about 600 °C can be assigned to segregated NiO-species, as already observed before [180]. For the Ce-promoted catalysts, i.e. HTNi-Ce and HTNi-ZrCe, the main reduction peak is shifted to lower temperatures, pointing to enhanced reducibility of Ni-species in the presence of this promoter. Additional reduction peaks at 300 and 415 °C arising from the reduction of Ce⁴⁺ to Ce³⁺ are also observed [145, 232]. On the contrary, in the presence of Zr a shift to higher reduction temperatures can be observed, due to further stabilization and stronger interaction between the mixed Mg-Al oxides and Ni-species. H₂-TPR experiments were repeated after reduction of the catalysts at 900 °C for 2h under 5 vol% H₂/Ar. Two small

reduction peaks at much lower temperatures are now shown, i.e. at 172 and 250-300 °C, pointing to Ni or NiO segregation from the Mg-Al mixed oxide structure upon the reduction treatment [233] and further oxidized when storing the materials under ambient conditions. Bulk NiO is normally reduced at such low temperatures [233, 234].

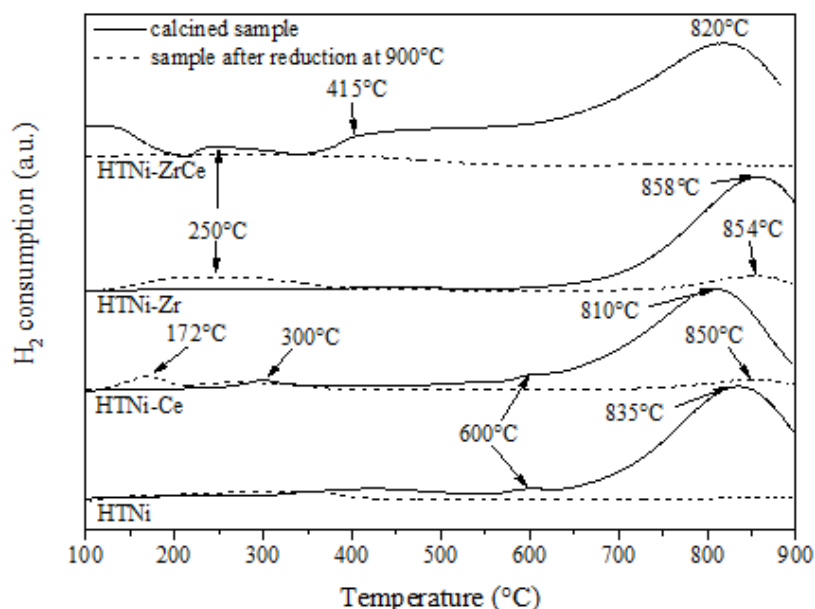


Fig. 96. TPR profiles for both calcined and reduced HT-derived catalysts.

CO₂-TPD profiles for these reduced materials, Figure 97, evidence the presence of three types of basic sites on the catalysts surface: (i) weak Brønsted OH-groups (ca. 120-130 °C), (ii) medium strength Lewis metal-oxygen pairs (175-235 °C), and (iii) strong Lewis-base oxygen anions (300-390 °C) [145, 235, 236]. The total basicity (Table 22) is remarkably influenced by the presence of Ce and/or Zr. The highest basicity corresponds to the CeZr-promoted catalyst, HTNi-CeZr. In general, the addition of both Ce and Zr results in an increased presence of medium-strength and strong basic sites, i.e. strong basic sites account for 50-51 % of total basicity in HTNi-Ce and HTNi-Zr whereas they correspond to 85 % of total basicity in HTNi-CeZr. Weak and medium strength basic sites contribute to more than 75 % of the total basicity in HTNi.

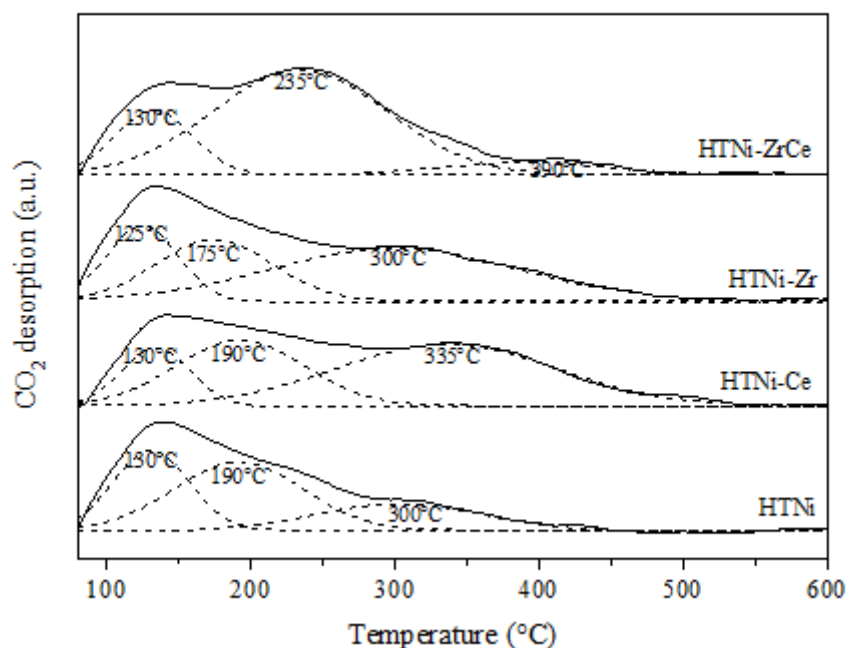


Fig. 97. CO₂-TPD profiles for the reduced HT-derived catalysts.

3. Catalysts Testing

The activity of the different catalysts in CO₂-methanation was evaluated at temperatures from 110 to 420 °C, in a dielectric barrier discharge (DBD) plasma reactor operating at atmospheric pressure.

A blank on-plasma test was performed in the absence of catalysts at 420 °C. This test yielded almost no CO₂ conversion and zero selectivity to CH₄ (Chapter 4, Fig. 79). Off-plasma experiments were performed in the presence of each catalyst, at temperatures from 130 to 420 °C. The results of these off-plasma experiments are discussed in detail below.

3.1. Activity Towards Methanation in the Absence of Plasma (Plasma Off)

The results of the off-plasma methanation experiments are shown in Figure 98, in the presence of the four different catalysts and at temperatures from 130 to 420 °C. In the absence

of the DBD plasma, CO₂ conversion only becomes significant at temperatures higher than 320 °C. It increases rapidly with increasing temperature, tending towards the thermodynamically forecasted values [158, 193]. The non-promoted catalyst, HTNi, shows the highest off-plasma activity within this series of catalysts. The addition of Ce results in much lower activity and selectivity towards the production of methane, with CO yields reaching almost 7 % (Fig. 98B). Off-plasma activity seems to be directly related to the size and availability of Ni⁰ particles on the catalyst's surface. The 15 nm-size Ni⁰ particles in HTNi seem to be more active towards off-plasma methanation than far too small (8.1 nm in HTNi-CeZr) or incompletely reduced NiO-particles (see TPR profiles for the reduced catalysts in Fig. 96). The influence of basicity on catalytic activity remains unclear, since the off-plasma CO₂ conversion and methane selectivity are not directly related to the total basicity measured for these catalysts. The increased presence of low-strength basic sites in HTNi may, however, enhance a weak-type adsorption of CO₂, resulting in easier CH₄ desorption upon its hydrogenation by the H₂ adsorbed on nearby Ni⁰ sites.

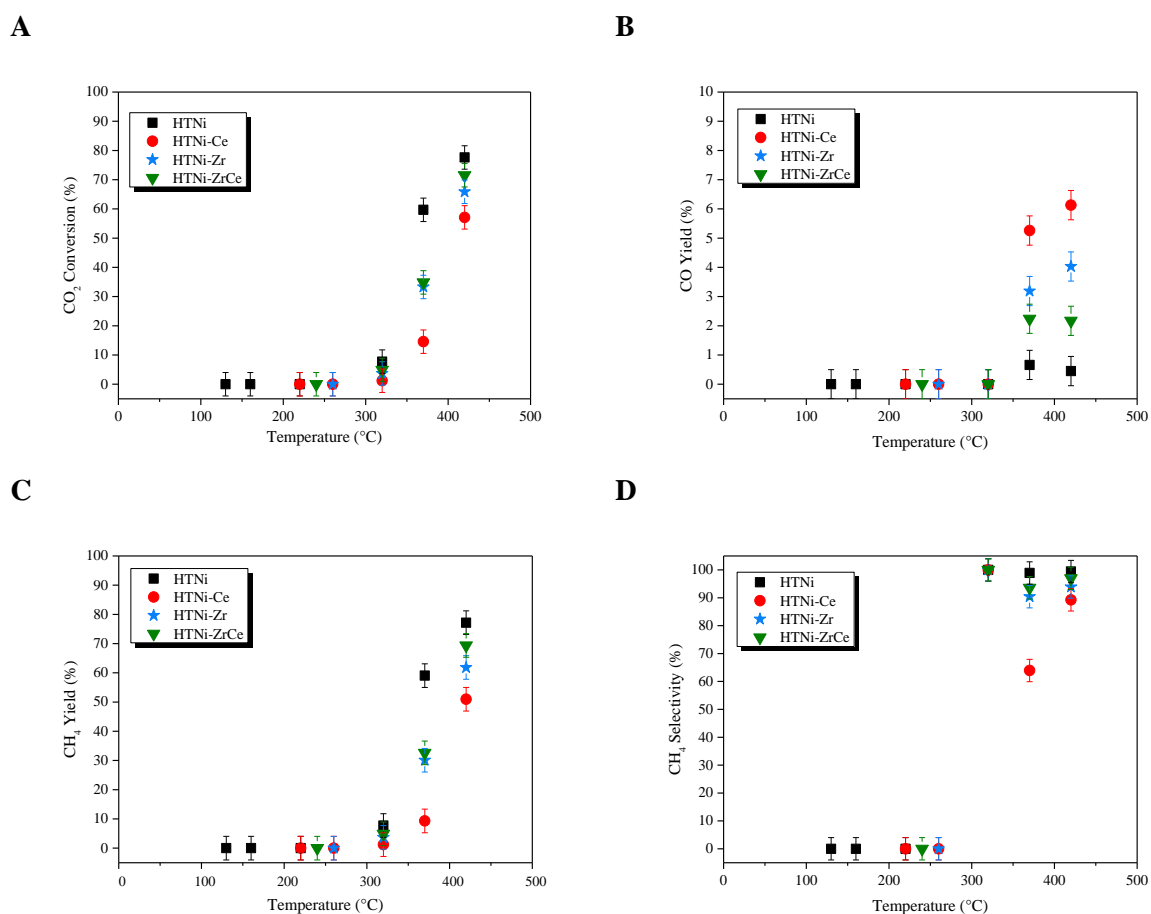


Fig. 98. Off-plasma catalytic methanation experiments: (A) CO₂ conversion, (B) CO yield, (C) CH₄ yield and (D) CH₄ selectivity versus temperature over HTNi; HTNi-Zr; HTNi-ZrCe and HTNi-Ce

catalysts. Reaction conditions: 20 vol% CO₂, 80 vol% H₂, GHSV = 20,000 h⁻¹, voltage = 15 kV, f = 41 kHz.

3.2. Hybrid Plasma-Catalytic Methanation (Plasma On)

Figure 99 presents the results obtained during the on-plasma catalytic methanation experiments. Whereas in the absence of a DBD plasma almost zero CO₂ conversion was measured at temperatures below 270 °C, the on-plasma experiments evidence that it is possible to convert CO₂ into methane even at very low temperatures, within the range of 110-420 °C, and, at temperatures between 110 and 270 °C, even without external heating, i.e. under adiabatic conditions (note that the methanation reaction is exothermic, $H_r^{298K} = -165$ kJ/mol). In the presence of the DBD plasma, the Zr-promoted catalysts show higher activity at lower temperatures than those measured during the off-plasma methanation experiments, i.e. around 70 % CO₂ conversion was measured at 240-250 °C for both HTNi-Zr and HTNi-ZrCe whereas these catalysts evidenced zero or almost zero CO₂ conversion in the absence of plasma. Ce-promoted catalysts only show interestingly high activities at relatively high temperatures. In any case, the non-doped HTNi catalyst maintains its activity (around 80 % conversion with almost 100 % selectivity to methane) within the entire temperature window. Even in presence of a DBD plasma, the highest availability of zero-valent Ni⁰ sites of intermediate crystal size might be responsible for the enhanced activity evidenced for this HTNi catalyst. The influence of basicity remains unclear. Though discussed before in the existing literature, there is no general agreement about the type of basic sites leading to enhanced catalytic activity [40, 237]. At the sight of the results obtained in the presence of plasma, it seems that low or medium-strength basic sites are still needed in order to boost the methanation reaction. On the contrary, the presence of too strong basic sites introduced by means of Ce and Zr doping does not seem to be beneficial for the overall reaction mechanism. Note here that the spent catalysts were characterized by means of transition electron microscopy (TEM) and X-ray diffraction. The micrographs, histograms and diffraction patterns obtained do not evidence any important change in the morphology and structure of the catalyst upon plasma methanation. Crystal sizes remained practically unchanged.

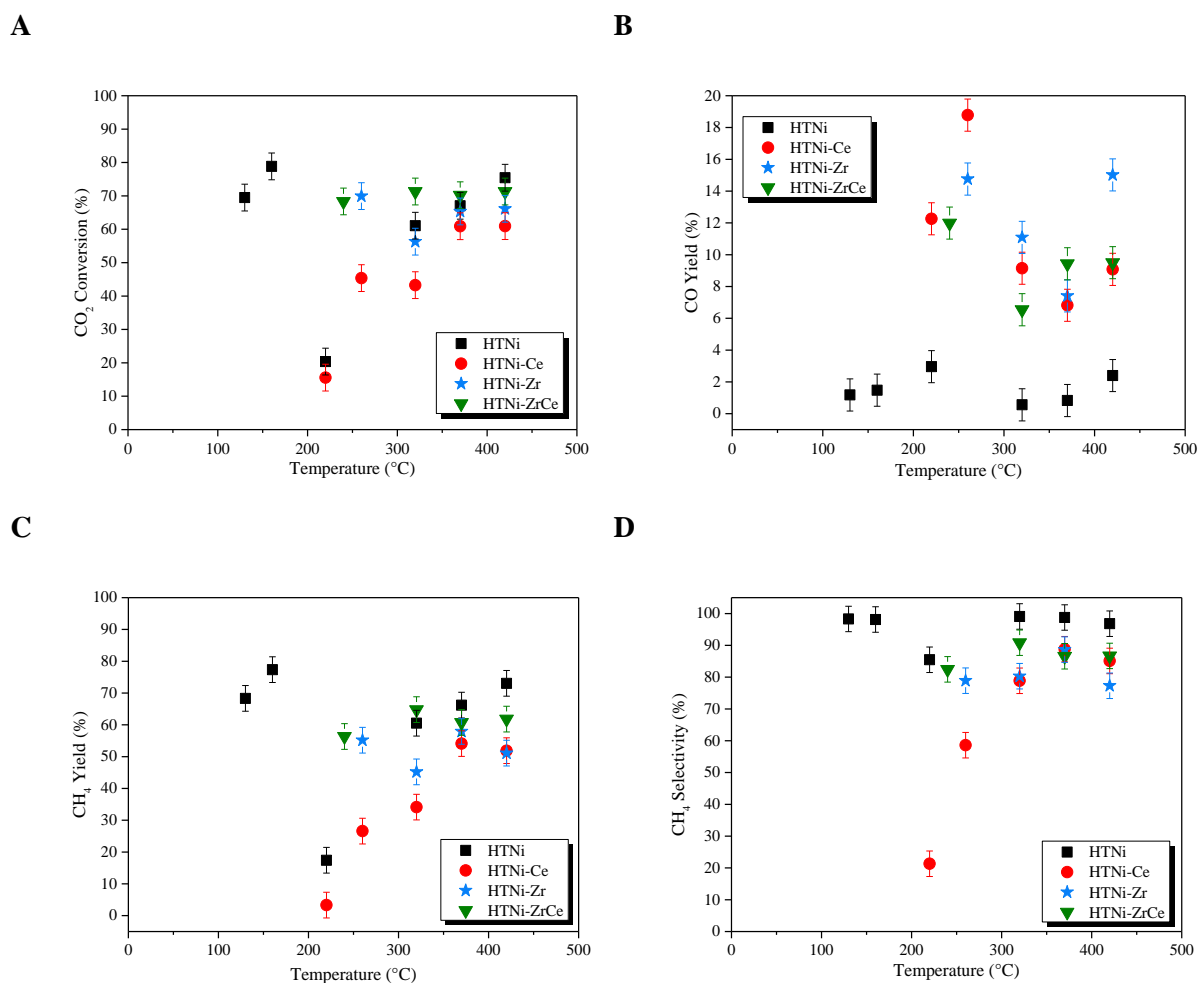


Fig. 99. Hybrid plasma-catalytic methanation experiments: (A) CO₂ conversion, (B) CO yield, (C) CH₄ yield and (D) CH₄ selectivity versus temperature over HTNi; HTNi-Zr; HTNi-ZrCe and HTNi-Ce catalysts. Reaction conditions: 20 vol% CO₂, 80 vol% H₂, GHSV = 20,000 h⁻¹, voltage = 15 kV, f = 41 kHz.

4. Conclusions

Ni-containing hydrothermal-derived catalysts were prepared using Ce and/or Zr as promoters. Their activity in the methanation of CO₂ was assayed both in the absence and in the presence of a DBD plasma. Off-plasma CO₂ methanation sets off at temperatures higher than 320 °C. However, CO₂ conversions as high as 80 % were measured in the presence of the DBD plasma, even at very low reaction temperatures, i.e. 110 °C under adiabatic conditions. The on-plasma catalytic methanation was found to be almost completely selective to methane, corresponding to CO yields lower than 2 %. The addition of either Ce or Zr did not improve the

catalytic activity of the hydrotalcite-derived materials. Zr-containing catalysts showed higher activity than those promoted only with Ce, especially in the presence of the plasma. The presence of medium size zero-valent Ni-crystallites, more readily available in the non-promoted catalyst, was found to enhance the methanation reaction, whereas the influence of the basicity of this series of catalysts on their activity remains relatively unclear.

References

1. Fechete, I. and J. Vadrine, Nanoporous Materials as New Engineered Catalysts for the Synthesis of Green Fuels. *Molecules*, 2015. 20(4): p. 5638.
2. Aresta, M., A. Dibenedetto, and A. Angelini, Catalysis for the Valorization of Exhaust Carbon: from CO₂ to Chemicals, Materials, and Fuels. *Technological Use of CO₂*. *Chemical Reviews*, 2014. 114(3): p. 1709-1742.
3. Xiaoding, X. and J.A. Moulijn, Mitigation of CO₂ by Chemical Conversion: Plausible Chemical Reactions and Promising Products. *Energy & Fuels*, 1996. 10(2): p. 305-325.
4. Wang, W., et al., Recent advances in catalytic hydrogenation of carbon dioxide. *Chemical Society Reviews*, 2011. 40(7): p. 3703-3727.
5. S. Solomon, D.Q., M. Manning, Z. Chen, M. Marquis, K.B. Averyt, M. Tignor, H.L. Miller, *Climate Change 2007: The Physical Science Basics (WGI)*. 2007.
6. Utilisation and Storage of CO₂. Position Paper, DECHEMA, 2009.
7. Sakakura, T., J.-C. Choi, and H. Yasuda, Transformation of Carbon Dioxide. *Chemical Reviews*, 2007. 107(6): p. 2365-2387.
8. Raudaskoski, R., et al., Catalytic activation of CO₂: Use of secondary CO₂ for the production of synthesis gas and for methanol synthesis over copper-based zirconia-containing catalysts. *Catalysis Today*, 2009. 144(3-4): p. 318-323.
9. Song, C., Global challenges and strategies for control, conversion and utilization of CO₂ for sustainable development involving energy, catalysis, adsorption and chemical processing. *Catalysis Today*, 2006. 115(1-4): p. 2-32.
10. Aresta, M. and I. Tommasi, Carbon dioxide utilisation in the chemical industry. *Energy Conversion and Management*, 1997. 38, Supplement: p. S373-S378.
11. Sudiro, M. and A. Bertucco, Production of synthetic gasoline and diesel fuel by alternative processes using natural gas and coal: Process simulation and optimization. *Energy*, 2009. 34(12): p. 2206-2214.
12. Kolbe, H., Ueber Synthese der Salicylsäure. *Justus Liebigs Annalen der Chemie*, 1860. 113: p. 125-127.
13. Solvay, E., Manufacture of Soda by the Ammonia Process. U.S. Patent 263,981, 1882.
14. G. Bosch, M.W., Process of Manufacturing Urea. U.S. Patent 1,429,483, 1922.
15. Krier, C., et al., Improving the Methanation Process. *Chemie Ingenieur Technik*, 2013. 85(4): p. 523-528.
16. Sharma, S., et al., CO₂ methanation on Ru-doped ceria. *Journal of Catalysis*, 2011. 278(2): p. 297-309.
17. Janke, C., et al., Catalytic and adsorption studies for the hydrogenation of CO₂ to methane. *Applied Catalysis B: Environmental*, 2014. 152-153: p. 184-191.
18. Abelló, S., C. Berruero, and D. Montané, High-loaded nickel-alumina catalyst for direct CO₂ hydrogenation into synthetic natural gas (SNG). *Fuel*, 2013. 113: p. 598-609.
19. Ocampo, F., B. Louis, and A.-C. Roger, Methanation of carbon dioxide over nickel-based Ce_{0.72}Zr_{0.28}O₂ mixed oxide catalysts prepared by sol-gel method. *Applied Catalysis A: General*, 2009. 369(1-2): p. 90-96.
20. Cai, M., et al., Methanation of carbon dioxide on Ni/ZrO₂-Al₂O₃ catalysts: Effects of ZrO₂ promoter and preparation method of novel ZrO₂-Al₂O₃ carrier. *Journal of Natural Gas Chemistry*, 2011. 20(3): p. 318-324.

21. Ocampo, F., et al., Effect of Ce/Zr composition and noble metal promotion on nickel based $Ce_xZr_{1-x}O_2$ catalysts for carbon dioxide methanation. *Applied Catalysis A: General*, 2011. 392(1-2): p. 36-44.
22. Karelavic, A. and P. Ruiz, Mechanistic study of low temperature CO_2 methanation over Rh/TiO₂ catalysts. *Journal of Catalysis*, 2013. 301: p. 141-153.
23. Andersson, M.P., et al., Structure sensitivity of the methanation reaction: H₂-induced CO dissociation on nickel surfaces. *Journal of Catalysis*, 2008. 255(1): p. 6-19.
24. J. Amouroux, S.C., M. Nizio, S. Ognier, T. Andreu, J.R. Morante, C.M.F.d.B. Henriques, J.M. Lopes, M.F. Ribeiro, M.d.C. Bacariza, I. Graça, Process for the carbon dioxide reduction to methane by DBD plasma activated catalyst. UPMC Paris VI, IREC, Univ. de Lisboa, Univ. de Barcelona, 2015. EP3050865A1.
25. Song, H.K., et al., Synthesis gas production via dielectric barrier discharge over Ni/ γ -Al₂O₃ catalyst. *Catalysis Today*, 2004. 89(1-2): p. 27-33.
26. Jwa, E., et al., Plasma-assisted catalytic methanation of CO and CO₂ over Ni-zeolite catalysts. *Fuel Processing Technology*, 2013. 108: p. 89-93.
27. A. Samimi, S.Z., Reduction of Greenhouse gases emission and effect on environment. *Journal of American Science*, 2012. 8: p. 1011-1015.
28. Chapter 8 Energy-Related Carbon Dioxide Emissions. U.S. Energy Information Administration/International Energy Outlook 2010, 18/02/2016.
29. Srivastava, R., D. Srinivas, and P. Ratnasamy, Zeolite-based organic-inorganic hybrid catalysts for phosgene-free and solvent-free synthesis of cyclic carbonates and carbamates at mild conditions utilizing CO₂. *Applied Catalysis A: General*, 2005. 289(2): p. 128-134.
30. Y. Li, B.M., A.R. Mohan, V. Rodriguez-Santiago, D. Thompson, D.V. Niekerk, Utilization of carbon dioxide from coal-fired power plant for the production of value-added products. *Design Engineering of Energy and Geo-Environmental Systems (EGEE 580)*, 27/04/2016.
31. Arakawa, H., et al., Catalysis Research of Relevance to Carbon Management: Progress, Challenges, and Opportunities. *Chemical Reviews*, 2001. 101(4): p. 953-996.
32. B.P. Sullivan, K.K., H.E. Guard, *Electrochemical and Electrocatalytic Reactions of Carbon Dioxide*. Elsevier Science Publishers, Amsterdam,, 1993.
33. Zhang, G., et al., A comparison of Ni/SiC and Ni/Al₂O₃ catalyzed total methanation for production of synthetic natural gas. *Applied Catalysis A: General*, 2013. 462-463: p. 75-81.
34. Zangeneh, F.T., S. Sahebdehfar, and M.T. Ravanchi, Conversion of carbon dioxide to valuable petrochemicals: An approach to clean development mechanism. *Journal of Natural Gas Chemistry*, 2011. 20(3): p. 219-231.
35. Ma, J., et al., A short review of catalysis for CO₂ conversion. *Catalysis Today*, 2009. 148(3-4): p. 221-231.
36. Behr, A., *The Synthesis of Organic Chemicals by Catalytic Reactions of Carbon Dioxide*. *Bulletin des Sociétés Chimiques Belges*, 1985. 94(9): p. 671-683.
37. Park, J.-N. and E.W. McFarland, A highly dispersed Pd-Mg/SiO₂ catalyst active for methanation of CO₂. *Journal of Catalysis*, 2009. 266(1): p. 92-97.
38. Brooks, K.P., et al., Methanation of carbon dioxide by hydrogen reduction using the Sabatier process in microchannel reactors. *Chemical Engineering Science*, 2007. 62(4): p. 1161-1170.
39. Müller, K., et al., Sabatier based CO₂-methanation of Flue Gas Emitted by Conventional Power Plants. *Energy Procedia*, 2013. 40: p. 240-248.
40. Aziz, M.A.A., et al., Highly active Ni-promoted mesostructured silica nanoparticles for CO₂ methanation. *Applied Catalysis B: Environmental*, 2014. 147: p. 359-368.

41. Takenaka, S., T. Shimizu, and K. Otsuka, Complete removal of carbon monoxide in hydrogen-rich gas stream through methanation over supported metal catalysts. *International Journal of Hydrogen Energy*, 2004. 29(10): p. 1065-1073.
42. Rahmani, S., M. Rezaei, and F. Meshkani, Preparation of highly active nickel catalysts supported on mesoporous nanocrystalline γ -Al₂O₃ for CO₂ methanation. *Journal of Industrial and Engineering Chemistry*, 2014. 20(4): p. 1346-1352.
43. Gao, J., et al., A thermodynamic analysis of methanation reactions of carbon oxides for the production of synthetic natural gas. *RSC Advances*, 2012. 2(6): p. 2358-2368.
44. Beuls, A., et al., Methanation of CO₂: Further insight into the mechanism over Rh/ γ -Al₂O₃ catalyst. *Applied Catalysis B: Environmental*, 2012. 113-114: p. 2-10.
45. Graça, I., et al., CO₂ hydrogenation into CH₄ on NiHNaUSY zeolites. *Applied Catalysis B: Environmental*, 2014. 147: p. 101-110.
46. Li, G., L. Hu, and J.M. Hill, Comparison of reducibility and stability of alumina-supported Ni catalysts prepared by impregnation and co-precipitation. *Applied Catalysis A: General*, 2006. 301(1): p. 16-24.
47. Savva, P.G., et al., Benzene hydrogenation over Ni/Al₂O₃ catalysts prepared by conventional and sol-gel techniques. *Applied Catalysis B: Environmental*, 2008. 79(3): p. 199-207.
48. Li, H., et al., Crystallization Deactivation of Ni-P/SiO₂ Amorphous Catalyst and the Stabilizing Effect of Silica Support on the Ni-P Amorphous Structure. *Journal of Catalysis*, 2000. 194(2): p. 211-221.
49. Wambach, J., A. Baiker, and A. Wokaun, CO₂ hydrogenation over metal/zirconia catalysts. *Physical Chemistry Chemical Physics*, 1999. 1(22): p. 5071-5080.
50. Duan, X., et al., Tuning the size and shape of Fe nanoparticles on carbon nanofibers for catalytic ammonia decomposition. *Applied Catalysis B: Environmental*, 2011. 101(3-4): p. 189-196.
51. Hwang, S., et al., Methane production from carbon monoxide and hydrogen over nickel-alumina xerogel catalyst: Effect of nickel content. *Journal of Industrial and Engineering Chemistry*, 2011. 17(1): p. 154-157.
52. Chang, F.-W., et al., Hydrogenation of CO₂ over nickel catalysts on rice husk ash-alumina prepared by incipient wetness impregnation. *Applied Catalysis A: General*, 2003. 247(2): p. 309-320.
53. Kustov, A.L., et al., CO methanation over supported bimetallic Ni-Fe catalysts: From computational studies towards catalyst optimization. *Applied Catalysis A: General*, 2007. 320: p. 98-104.
54. Reddy, B.M., et al., Silica supported transition metal-based bimetallic catalysts for vapour phase selective hydrogenation of furfuraldehyde. *Journal of Molecular Catalysis A: Chemical*, 2007. 265(1-2): p. 276-282.
55. Hartley, F.R., *Supported Metal Complexes*. D. Reidel Publishing Company, Dordrecht, 1985.
56. Canning, A.S., S.D. Jackson, and S. Mitchell, Identification, by selective poisoning, of active sites on Ni/Al₂O₃ for hydrogenation and isomerisation of cis-2-pentenenitrile. *Catalysis Today*, 2006. 114(4): p. 372-376.
57. Pinna, F., et al., Consecutive hydrogenation of benzaldehyde over Pd catalysts: Influence of supports and sulfur poisoning. *Applied Catalysis A: General*, 2001. 219(1-2): p. 195-200.
58. Chen, S.L., et al., Effect of alumina supports on the properties of supported nickel catalysts. *Applied Catalysis*, 1991. 73(2): p. 289-312.
59. Bartholomew, C.H., Mechanisms of catalyst deactivation. *Applied Catalysis A: General*, 2001. 212(1-2): p. 17-60.

60. Bhatia, S., J. Beltramini, and D.D. Do, Deactivation of Zeolite Catalysts. *Catalysis Reviews*, 1989. 31(4): p. 431-480.
61. Disdale, W., An Experimental and Computational Investigation of the Time Dependency of Automotive Catalyst Deactivation. Ph.D. Thesis, Coventry University, 2007.
62. Moulijn, J.A., A.E. van Diepen, and F. Kapteijn, Catalyst deactivation: is it predictable?: What to do? *Applied Catalysis A: General*, 2001. 212(1-2): p. 3-16.
63. Forzatti, P. and L. Lietti, Catalyst deactivation. *Catalysis Today*, 1999. 52(2-3): p. 165-181.
64. Zhu, X.D. and H. Hofmann, Deactivation of Ni/SiO₂/Al₂O₃-catalyst in hydrogenation of 3-hydroxypropanal solution. *Applied Catalysis A: General*, 1997. 155(2): p. 179-194.
65. Albers, P., J. Pietsch, and S.F. Parker, Poisoning and deactivation of palladium catalysts. *Journal of Molecular Catalysis A: Chemical*, 2001. 173(1-2): p. 275-286.
66. Menon, P.G., Coke on catalysts-harmful, harmless, invisible and beneficial types. *Journal of Molecular Catalysis*, 1990. 59(2): p. 207-220.
67. Quincoces, C.E., N.E. Amadeo, and M.G. González, Effects of reduction and regeneration conditions on the activity of CuO-ZnO catalysts, in *Studies in Surface Science and Catalysis*, C.H. Bartholomew and G.A. Fuentes, Editors. 1997, Elsevier. p. 535-541.
68. Besson, M. and P. Gallezot, Deactivation of metal catalysts in liquid phase organic reactions. *Catalysis Today*, 2003. 81(4): p. 547-559.
69. Kopyscinski, J., T.J. Schildhauer, and S.M.A. Biollaz, Production of synthetic natural gas (SNG) from coal and dry biomass - A technology review from 1950 to 2009. *Fuel*, 2010. 89(8): p. 1763-1783.
70. Schaaf, T., et al., Methanation of CO₂ - storage of renewable energy in a gas distribution system. *Energy, Sustainability and Society*, 2014. 4(1): p. 2.
71. Helmeth Project, <http://www.helmeth.eu/index.php/technologies/methanation-process>, 17/07/2016.
72. Höhlelein, B., et al., Methane from synthesis gas and operation of high-temperature methanation. *Nuclear Engineering and Design*, 1984. 78(2): p. 241-250.
73. Höhlelein, B., R. Menzer, and J. Range, High temperature methanation in the long-distance nuclear energy transport system. *Applied Catalysis*, 1981. 1(3): p. 125-139.
74. Fedders, H. and B. Höhlelein, Operating a pilot plant circuit for energy transport with hydrogen-rich gas. *International Journal of Hydrogen Energy*, 1982. 7(10): p. 793-800.
75. J. H. Jensen, J.M.P., N.U. Andersen, From Coal to Clean Energy. Technical Report, Haldor Topsoe, 2011.
76. Kopyscinski, J., T.J. Schildhauer, and S.M.A. Biollaz, Employing Catalyst Fluidization to Enable Carbon Management in the Synthetic Natural Gas Production from Biomass. *Chemical Engineering & Technology*, 2009. 32(3): p. 343-347.
77. Falconer, J.L. and A.E. Zağli, Adsorption and methanation of carbon dioxide on a nickel/silica catalyst. *Journal of Catalysis*, 1980. 62(2): p. 280-285.
78. Marwood, M., R. Doepper, and A. Renken, In-situ surface and gas phase analysis for kinetic studies under transient conditions The catalytic hydrogenation of CO₂. *Applied Catalysis A: General*, 1997. 151(1): p. 223-246.
79. Lapidus, A.L., et al., The mechanism of carbon dioxide hydrogenation on copper and nickel catalysts. *Petroleum Chemistry*, 2007. 47(2): p. 75-82.
80. Peebles, D.E., D.W. Goodman, and J.M. White, Methanation of carbon dioxide on nickel (100) and the effects of surface modifiers. *The Journal of Physical Chemistry*, 1983. 87(22): p. 4378-4387.

81. Weatherbee, G.D. and C.H. Bartholomew, Hydrogenation of CO₂ on group VIII metals. *Journal of Catalysis*, 1982. 77(2): p. 460-472.
82. Fujita, S., et al., Methanation of carbon monoxide and carbon dioxide over nickel catalyst under the transient state. *Reaction Kinetics and Catalysis Letters*, 1987. 33(1): p. 179-184.
83. Schild, C., A. Wokaun, and A. Baiker, On the mechanism of CO and CO₂ hydrogenation reactions on zirconia-supported catalysts: a diffuse reflectance FTIR study. *Journal of Molecular Catalysis*, 1990. 63(2): p. 243-254.
84. Sehested, J., et al., Methanation of CO over Nickel: Mechanism and Kinetics at High H₂/CO Ratios. *The Journal of Physical Chemistry B*, 2005. 109(6): p. 2432-2438.
85. Oki, S. and R. Mezaki, Identification of rate-controlling steps for the water-gas shift reaction over an iron oxide catalyst. *The Journal of Physical Chemistry*, 1973. 77(4): p. 447-452.
86. Oki, S. and R. Mezaki, Mechanistic structure of the water-gas shift reaction in the vicinity of chemical equilibrium. *The Journal of Physical Chemistry*, 1973. 77(13): p. 1601-1605.
87. Lunde, P.J. and F.L. Kester, Rates of methane formation from carbon dioxide and hydrogen over a ruthenium catalyst. *Journal of Catalysis*, 1973. 30(3): p. 423-429.
88. Doehlemann, E., Über den Mechanismus der Wassergasreaktion an Eisen als Katalysator. *Zeitschrift für Elektrochemie und angewandte physikalische Chemie*, 1938. 44(3): p. 178-183.
89. Jacquemin, M., A. Beuls, and P. Ruiz, Catalytic production of methane from CO₂ and H₂ at low temperature: Insight on the reaction mechanism. *Catalysis Today*, 2010. 157(1-4): p. 462-466.
90. Watwe, R.M., et al., Theoretical Studies of Stability and Reactivity of CH_x Species on Ni (111). *Journal of Catalysis*, 2000. 189(1): p. 16-30.
91. Ackermann, M., et al., Hydrogenation of carbon monoxide on Ni (111) investigated with surface X-ray diffraction at atmospheric pressure. *Surface Science*, 2004. 557(1-3): p. 21-30.
92. Fujita, S.-i., et al., Mechanisms of methanation of carbon dioxide and carbon monoxide over nickel/alumina catalysts. *Applied Catalysis A: General*, 1993. 104(1): p. 87-100.
93. S. J. Choe, H.J.K., S-J. Kim, S-B. Park, D. H. Park, D.S. Huh, Adsorbed Carbon Formation and Carbon Hydrogenation for CO₂ Methanation on the Ni(111) Surface: ASED-MO Study. *Bulletin of the Korean Chemical Society*, 2005. 26: p. 1682-1688.
94. Solymosi, F., A. Erdöhelyi, and T. Bánsági, Methanation of CO₂ on supported rhodium catalyst. *Journal of Catalysis*, 1981. 68(2): p. 371-382.
95. Ibraeva, Z.A., et al., Kinetics of methanation of carbon dioxide on a nickel catalyst. *Theoretical and Experimental Chemistry*, 1991. 26(5): p. 584-588.
96. Kim, H.Y., H.M. Lee, and J.-N. Park, Bifunctional Mechanism of CO₂ Methanation on Pd-MgO/SiO₂ Catalyst: Independent Roles of MgO and Pd on CO₂ Methanation. *The Journal of Physical Chemistry C*, 2010. 114(15): p. 7128-7131.
97. Fisher, I.A. and A.T. Bell, A Comparative Study of CO and CO₂ Hydrogenation over Rh/SiO₂. *Journal of Catalysis*, 1996. 162(1): p. 54-65.
98. Leitenburg, C.d., A. Trovarelli, and J. Kašpar, A Temperature-Programmed and Transient Kinetic Study of CO₂ Activation and Methanation over CeO₂ Supported Noble Metals. *Journal of Catalysis*, 1997. 166(1): p. 98-107.
99. Sanchez-Escribano, V., et al., On the mechanisms and the selectivity determining steps in syngas conversion over supported metal catalysts: An IR study. *Applied Catalysis A: General*, 2007. 316(1): p. 68-74.
100. Trovarelli, A., C. de Leitenburg, and G. Dolcetti, CO and CO₂ hydrogenation under transient conditions over Rh-CeO₂: novel positive effects of metal-support interaction on catalytic activity and selectivity. *Journal of the Chemical Society, Chemical Communications*, 1991(7): p. 472-473.

101. Trovarelli, A., et al., CO₂ Methanation Under Transient and Steady-State Conditions over Rh/CeO₂ and CeO₂-Promoted Rh/SiO₂: The Role of Surface and Bulk Ceria. *Journal of Catalysis*, 1995. 151(1): p. 111-124.
102. Tada, S., et al., Ni/CeO₂ catalysts with high CO₂ methanation activity and high CH₄ selectivity at low temperatures. *International Journal of Hydrogen Energy*, 2012. 37(7): p. 5527-5531.
103. Bogaerts, A., et al., Gas discharge plasmas and their applications. *Spectrochimica Acta Part B: Atomic Spectroscopy*, 2002. 57(4): p. 609-658.
104. Fridman, A., *Plasma Chemistry*. Cambridge University Press, 2008.
105. Alexander F., K.L.A., *Plasma Physics and Engineering*. CRC press, 2004: p. 8-10.
106. Eliasson, B. and U. Kogelschatz, Nonequilibrium volume plasma chemical processing. *IEEE Transactions on Plasma Science*, 1991. 19(6): p. 1063-1077.
107. Tonks, L., The Birth of "Plasma". *American Journal of Physics*, 1967. 35(9): p. 857-858.
108. Bill, G., Technological plasmas. *Physics World*, 2001. 14(3): p. 31.
109. Tendero, C., et al., Atmospheric pressure plasmas: A review. *Spectrochimica Acta Part B: Atomic Spectroscopy*, 2006. 61(1): p. 2-30.
110. Petitpas, G., et al., A comparative study of non-thermal plasma assisted reforming technologies. *International Journal of Hydrogen Energy*, 2007. 32(14): p. 2848-2867.
111. Eric, M., Airflow control by non-thermal plasma actuators. *Journal of Physics D: Applied Physics*, 2007. 40(3): p. 605.
112. Raizer, Y.P., *Gas Discharge Physics*. Springer-Verlag Berlin Heidelberg, 1991.
113. Chang, J.S., P.A. Lawless, and T. Yamamoto, Corona discharge processes. *IEEE Transactions on Plasma Science*, 1991. 19(6): p. 1152-1166.
114. Lee, Y.-H., et al., Application of Pulsed Corona Induced Plasma Chemical Process to an Industrial Incinerator. *Environmental Science & Technology*, 2003. 37(11): p. 2563-2567.
115. Liu, C., et al., Methane conversion to higher hydrocarbons in a corona discharge over metal oxide catalysts with OH groups. *Applied Catalysis A: General*, 1997. 164(1): p. 21-33.
116. Li, D., et al., CO₂ reforming of CH₄ by atmospheric pressure glow discharge plasma: A high conversion ability. *International Journal of Hydrogen Energy*, 2009. 34(1): p. 308-313.
117. Whitmell, D.S. and R. Williamson, The deposition of hard surface layers by hydrocarbon cracking in a glow discharge. *Thin Solid Films*, 1976. 35(2): p. 255-261.
118. Cheng, D.-g., et al., Carbon dioxide reforming of methane over Ni/Al₂O₃ treated with glow discharge plasma. *Catalysis Today*, 2006. 115(1-4): p. 205-210.
119. Wang, J.-g., et al., Partial oxidation of methane to syngas over glow discharge plasma treated Ni-Fe/Al₂O₃ catalyst. *Catalysis Today*, 2004. 89(1-2): p. 183-191.
120. https://en.wikipedia.org/wiki/File:Electric_glow_discharge_schematic.png, 22/02/2016.
121. U. Kogelschatz, B.E., W. Egli, From Ozone Generators to Flat Television Screens: History and Future Potential of Dielectric-Barrier Discharges. *Pure and Applied Chemistry*, 1999. 71: p. 1819-1828.
122. Kogelschatz, U., B. Eliasson, and W. Egli, Dielectric-Barrier Discharges. Principle and Applications. *J. Phys. IV France*, 1997. 07(C4): p. C4-47-C4-66.
123. Kogelschatz, U., Dielectric-Barrier Discharges: Their History, Discharge Physics, and Industrial Applications. *Plasma Chemistry and Plasma Processing*, 2003. 23(1): p. 1-46.
124. Kogelschatz, U., Filamentary, patterned, and diffuse barrier discharges. *IEEE Transactions on Plasma Science*, 2002. 30(4): p. 1400-1408.
125. Sarmiento, B., et al., Hydrogen production by reforming of hydrocarbons and alcohols in a dielectric barrier discharge. *Journal of Power Sources*, 2007. 169(1): p. 140-143.

126. Salge, J., Plasma-Assisted Deposition at Atmospheric Pressure. *J. Phys. IV France*, 1995. 05(C5): p. C5-583-C5-592.
127. Conrads, H. and M. Schmidt, Plasma generation and plasma sources. *Plasma Sources Science and Technology*, 2000. 9(4): p. 441.
128. R.J. Farrauto, C.H.B., *Fundamentals of Industrial Catalytic Processes*. John Wiley & Sons, Hoboken, New Jersey, 1997.
129. Whitehead, J.C., Plasma catalysis: A solution for environmental problems, in *Pure and Applied Chemistry*. 2010. p. 1329.
130. Chen, H.L., et al., Removal of Volatile Organic Compounds by Single-Stage and Two-Stage Plasma Catalysis Systems: A Review of the Performance Enhancement Mechanisms, Current Status, and Suitable Applications. *Environmental Science & Technology*, 2009. 43(7): p. 2216-2227.
131. Chen, H.L., et al., Review of plasma catalysis on hydrocarbon reforming for hydrogen production-Interaction, integration, and prospects. *Applied Catalysis B: Environmental*, 2008. 85(1-2): p. 1-9.
132. Wen, Y. and X. Jiang, Decomposition of CO₂ Using Pulsed Corona Discharges Combined with Catalyst. *Plasma Chemistry and Plasma Processing*, 2001. 21(4): p. 665-678.
133. Boutonnet Kizling, M. and S.G. Järås, A review of the use of plasma techniques in catalyst preparation and catalytic reactions. *Applied Catalysis A: General*, 1996. 147(1): p. 1-21.
134. Jogan, K., et al., The effect of residence time on the CO₂ reduction from combustion flue gases by an AC ferroelectric packed bed reactor. *IEEE Transactions on Industry Applications*, 1993. 29(5): p. 876-881.
135. Ji-Jun Zou, C.-J.L., *Utilization of Carbon Dioxide through Nonthermal Plasma Approaches. Carbon Dioxide as Chemical Feedstock*, 2010.
136. Liu, C.-j., G.P. Vissokov, and B.W.L. Jang, Catalyst preparation using plasma technologies. *Catalysis Today*, 2002. 72(3-4): p. 173-184.
137. Jwa, E.J., Y.S. Moks, and S.B. Lee, Conversion of carbon oxides into methane in a nonthermal plasma-catalytic reactor. *Eur. Phys. J. Appl. Phys.*, 2011. 56(2): p. 24025.
138. Panagiotopoulou, P., D.I. Kondarides, and X.E. Verykios, Selective methanation of CO over supported noble metal catalysts: Effects of the nature of the metallic phase on catalytic performance. *Applied Catalysis A: General*, 2008. 344(1-2): p. 45-54.
139. Galletti, C., et al., CO-selective methanation over Ru- γ -Al₂O₃ catalysts in H₂-rich gas for PEM FC applications. *Chemical Engineering Science*, 2010. 65(1): p. 590-596.
140. Zhang, J., et al., Synthesis, characterization and properties of anti-sintering nickel incorporated MCM-41 methanation catalysts. *Fuel*, 2013. 109: p. 693-701.
141. Yamasaki, M., et al., Effect of tetragonal ZrO₂ on the catalytic activity of Ni/ZrO₂ catalyst prepared from amorphous Ni-Zr alloys. *Catalysis Communications*, 2006. 7(1): p. 24-28.
142. Perkass, N., et al., Methanation of Carbon Dioxide on Ni Catalysts on Mesoporous ZrO₂ Doped with Rare Earth Oxides. *Catalysis Letters*, 2009. 130(3): p. 455-462.
143. Yan, X., et al., Enhanced sulfur resistance of Ni/SiO₂ catalyst for methanation via the plasma decomposition of nickel precursor. *Physical Chemistry Chemical Physics*, 2013. 15(29): p. 12132-12138.
144. Xavier, K.O., et al., Doping effects of cerium oxide on Ni/Al₂O₃ catalysts for methanation. *Catalysis Today*, 1999. 49(1-3): p. 17-21.
145. Dębek, R., et al., Ni-containing Ce-promoted hydrotalcite derived materials as catalysts for methane reforming with carbon dioxide at low temperature - On the effect of basicity. *Catalysis Today*, 2015. 257, Part 1: p. 59-65.

146. He, L., et al., Unique catalysis of Ni-Al hydrotalcite derived catalyst in CO₂ methanation: cooperative effect between Ni nanoparticles and a basic support. *Journal of Energy Chemistry*, 2014. 23(5): p. 587-592.
147. Fan, Z., et al., Improved activity of Ni/MgAl₂O₄ for CO₂ methanation by the plasma decomposition. *Journal of Energy Chemistry*, 2015. 24(5): p. 655-659.
148. Du, G., et al., Methanation of carbon dioxide on Ni-incorporated MCM-41 catalysts: The influence of catalyst pretreatment and study of steady-state reaction. *Journal of Catalysis*, 2007. 249(2): p. 370-379.
149. Cheng, D., et al., Computational Approaches to the Chemical Conversion of Carbon Dioxide. *ChemSusChem*, 2013. 6(6): p. 944-965.
150. Liu, C., T.R. Cundari, and A.K. Wilson, Reaction Mechanism of the Reverse Water-Gas Shift Reaction Using First-Row Middle Transition Metal Catalysts L'M (M = Fe, Mn, Co): A Computational Study. *Inorganic Chemistry*, 2011. 50(18): p. 8782-8789.
151. Cai, W., Q. Zhong, and Y. Zhao, Fractional-hydrolysis-driven formation of non-uniform dopant concentration catalyst nanoparticles of Ni/Ce_xZr_{1-x}O₂ and its catalysis in methanation of CO₂. *Catalysis Communications*, 2013. 39: p. 30-34.
152. Shang, S., et al., Research on Ni/γ-Al₂O₃ catalyst for CO₂ reforming of CH₄ prepared by atmospheric pressure glow discharge plasma jet. *Catalysis Today*, 2009. 148(3-4): p. 268-274.
153. Y.S. Mok, H.C.K., D.J. Koh, D.N. Shin, J.H. Baik, Nonthermal plasma-enhanced catalytic methanation of CO over Ru/TiO₂/Al₂O₃. *Journal of the Korean Physical Society*, 2010. 57: p. 451-457.
154. Oshima, K., et al., Low temperature catalytic reverse water gas shift reaction assisted by an electric field. *Catalysis Today*, 2014. 232: p. 27-32.
155. Ando, H., et al., Methanation of carbon dioxide over LaNi₄X type catalysts. *Energy Conversion and Management*, 1995. 36(6-9): p. 653-656.
156. Liu, H., et al., Effect of CeO₂ addition on Ni/Al₂O₃ catalysts for methanation of carbon dioxide with hydrogen. *Journal of Natural Gas Chemistry*, 2012. 21(6): p. 703-707.
157. Song, H., et al., Methanation of Carbon Dioxide over a Highly Dispersed Ni/La₂O₃ Catalyst. *Chinese Journal of Catalysis*, 2010. 31(1): p. 21-23.
158. Aldana, P.A.U., et al., Catalytic CO₂ valorization into CH₄ on Ni-based ceria-zirconia. Reaction mechanism by operando IR spectroscopy. *Catalysis Today*, 2013. 215: p. 201-207.
159. Zhi, G., et al., Effect of La₂O₃ modification on the catalytic performance of Ni/SiC for methanation of carbon dioxide. *Catalysis Communications*, 2011. 16(1): p. 56-59.
160. Yaccato, K., et al., Competitive CO and CO₂ methanation over supported noble metal catalysts in high throughput scanning mass spectrometer. *Applied Catalysis A: General*, 2005. 296(1): p. 30-48.
161. Alstrup, I., On the Kinetics of CO Methanation on Nickel Surfaces. *Journal of Catalysis*, 1995. 151(1): p. 216-225.
162. Yadav, R. and R.G. Rinker, Steady-state methanation kinetics over a Ni/Al₂O₃ catalyst. *The Canadian Journal of Chemical Engineering*, 1993. 71(2): p. 202-208.
163. Manley, T.C., The Electric Characteristics of the Ozonator Discharge. *Journal of Electrochemical Society*, 1943. 84: p. 83-96.
164. Feng, R., G.S.P. Castle, and S. Jayaram, Automated system for power measurement in the silent discharge. *IEEE Transactions on Industry Applications*, 1998. 34(3): p. 563-570.
165. Valdivia-Barrientos, R., et al., Analysis and electrical modelling of a cylindrical DBD configuration at different operating frequencies. *Plasma Sources Science and Technology*, 2006. 15(2): p. 237.

166. Wagner, H.E., et al., The barrier discharge: basic properties and applications to surface treatment. *Vacuum*, 2003. 71(3): p. 417-436.
167. Laux, C.O., et al., Optical diagnostics of atmospheric pressure air plasmas. *Plasma Sources Science and Technology*, 2003. 12(2): p. 125.
168. Aragón, C. and J.A. Aguilera, Characterization of laser induced plasmas by optical emission spectroscopy: A review of experiments and methods. *Spectrochimica Acta Part B: Atomic Spectroscopy*, 2008. 63(9): p. 893-916.
169. Zhang, J.-F., et al., Diagnosis of Methane Plasma Generated in an Atmospheric Pressure DBD Micro-Jet by Optical Emission Spectroscopy. *Chinese Physics Letters*, 2009. 26(3): p. 035203.
170. Herzberg, G., *Atomic Spectra and Atomic Structure*. Dover Publications, New York, 1944.
171. A. G. Gaydon, R.W.B.P., *The Identification of Molecular Spectra*. Wiley, 1976.
172. Baugh, P.J., *Gas Chromatography A Practical Approach*. Oxford: Oxford University Press., 1993.
173. Cruz, D., et al., Microfabricated thermal conductivity detector for the micro-ChemLab™. *Sensors and Actuators B: Chemical*, 2007. 121(2): p. 414-422.
174. Derenne, A., O. Vandersleyen, and E. Goormaghtigh, Lipid quantification method using FTIR spectroscopy applied on cancer cell extracts. *Biochimica et Biophysica Acta (BBA) - Molecular and Cell Biology of Lipids*, 2014. 1841(8): p. 1200-1209.
175. Dilek Yalçın Duygu, T.B., İlkay Açikgoz, K. Yildiz, Fourier Transform Infrared (FT-IR) Spectroscopy for Biological Studies(Review). *G.U. Journal of Science*, 2009. 22: p. 117-121.
176. Joly, L., et al., Development of a compact CO₂ sensor open to the atmosphere and based on near-infrared laser technology at 2.68 μm. *Applied Physics B*, 2007. 86(4): p. 743-748.
177. C. Banwell, E.M., *Fundamentals of Molecular Spectroscopy*. McGraw-Hill International Ltd, 4th ed.1994.
178. Herzberg, G., *Infrared and Raman Spectra of Polyatomic Molecules*. New York: D.Van Nostrand Company, 1945.
179. Nizio, M., et al., Hybrid plasma-catalytic methanation of CO₂ at low temperature over ceria zirconia supported Ni catalysts. *International Journal of Hydrogen Energy*, 2016. 41(27): p. 11584-11592.
180. Dębek, R., et al., Low temperature dry methane reforming over Ce, Zr and CeZr promoted Ni-Mg-Al hydrotalcite-derived catalysts. *International Journal of Hydrogen Energy*, 2016. 41(27): p. 11616-11623.
181. Choi, J.-G., Reduction of supported cobalt catalysts by hydrogen. *Catalysis Letters*, 1995. 35(3): p. 291-296.
182. Nizio, M., et al., Low temperature hybrid plasma-catalytic methanation over Ni-Ce-Zr hydrotalcite-derived catalysts. *Catalysis Communications*, 2016. 83: p. 14-17.
183. Abecassis-Wolfovich, M., et al., Catalytic Wet Oxidation of Phenol with Mn-Ce-Based Oxide Catalysts: Impact of Reactive Adsorption on TOC Removal. *Industrial & Engineering Chemistry Research*, 2004. 43(17): p. 5089-5097.
184. World energy, technology and, climate policy outlook 2030, WETO report CO₂ Emissions from fuel combustion. I E A - Statistics 2010 Edition.
185. Ivy, J., Summary of Electrolytic Hydrogen Production Milestone Completion Report 2004.
186. Breck, D., *Zeolite Molecular Sieves*. 1974: p. 92-95.
187. Gao, J., et al., Methanation of carbon dioxide over the LaNiO₃ perovskite catalysts activated under the reactant stream. *Journal of Fuel Chemistry and Technology*, 2009. 37(5): p. 573-577.

188. D. Zhao, J.F., Q. Huo, N. Melosh, G.H. Fredrickson, B.F. Chmelka, G.D. Stucky, Triblock Copolymer Syntheses of Mesoporous Silica with Periodic 50 to 300 Angstrom Pores. *Science*, 1998. 279: p. 548-552.
189. Rodríguez-Carvajal, J., Recent advances in magnetic structure determination by neutron powder diffraction. *Physica B: Condensed Matter*, 1993. 192(1): p. 55-69.
190. Jiang, T., et al., Effect of Ni-doping on the pore structure of pure silica MCM-41 mesoporous molecular sieve under microwave irradiation. *Colloids and Surfaces A: Physicochemical and Engineering Aspects*, 2008. 315(1-3): p. 299-303.
191. Mok, Y.S., et al., Effect of Nonthermal Plasma on the Methanation of Carbon Monoxide over Nickel Catalyst. *Plasma Chemistry and Plasma Processing*, 2010. 30(4): p. 437-447.
192. Jwa, E., Y.S. Mok, and S.B. Lee, Nonthermal plasma-assisted catalytic methanation of CO and CO₂ over nickel-loaded alumina. *WIT Transactions on Ecology and the Environment*, WIT Press: UK, 2011. 143: p. 361-368.
193. Pan, Q., et al., Insight into the reaction route of CO₂ methanation: Promotion effect of medium basic sites. *Catalysis Communications*, 2014. 45: p. 74-78.
194. Taufiq-Yap, Y.H., et al., CeO₂-SiO₂ supported nickel catalysts for dry reforming of methane toward syngas production. *Applied Catalysis A: General*, 2013. 468: p. 359-369.
195. Reddy, B.M., et al., Catalytic Efficiency of Ceria-Zirconia and Ceria-Hafnia Nanocomposite Oxides for Soot Oxidation. *Catalysis Letters*, 2008. 123(3): p. 327-333.
196. García-Vargas, J.M., et al., Precursor influence and catalytic behaviour of Ni/CeO₂ and Ni/SiC catalysts for the tri-reforming process. *Applied Catalysis A: General*, 2012. 431-432: p. 49-56.
197. Rao, P.V.R., et al., Vapor phase selective hydrogenation of acetone to methyl isobutyl ketone (MIBK) over Ni/CeO₂ catalysts. *Catalysis Science & Technology*, 2012. 2(8): p. 1665-1673.
198. Gao, J., et al., Production of syngas via autothermal reforming of methane in a fluidized-bed reactor over the combined CeO₂-ZrO₂/SiO₂ supported Ni catalysts. *International Journal of Hydrogen Energy*, 2008. 33(20): p. 5493-5500.
199. Sun, N., et al., Catalytic performance and characterization of Ni-CaO-ZrO₂ catalysts for dry reforming of methane. *Applied Surface Science*, 2011. 257(21): p. 9169-9176.
200. Radlik, M., et al., Dry reforming of methane over Ni/Ce_{0.62}Zr_{0.38}O₂ catalysts: Effect of Ni loading on the catalytic activity and on H₂/CO production. *Comptes Rendus Chimie*, 2015. 18(11): p. 1242-1249.
201. Krämer, M., et al., The impact of dopants on the activity and selectivity of a Ni-based methanation catalyst. *Applied Catalysis A: General*, 2009. 369(1-2): p. 42-52.
202. Men, Y., et al., Selective methanation of carbon oxides in a microchannel reactor-Primary screening and impact of gas additives. *Catalysis Today*, 2007. 125(1-2): p. 81-87.
203. Alessandro Trovarelli, P.F.E., *Catalysis by ceria and related materials*. Catalytic science series (2nd ed.), 12 (World Scientific 2013).
204. Kraus, M., et al., Investigation of mechanistic aspects of the catalytic CO₂ reforming of methane in a dielectric-barrier discharge using optical emission spectroscopy and kinetic modeling. *Physical Chemistry Chemical Physics*, 2002. 4(4): p. 668-675.
205. Database and spectral simulation program LIFBASE.
206. Sarah, N.G., E.F. John, and C.G. Maria, An investigation of an underwater steam plasma discharge as alternative to air plasmas for water purification. *Plasma Sources Science and Technology*, 2015. 24(5): p. 055005.
207. Chang, F.-W., T.-J. Hsiao, and J.-D. Shih, Hydrogenation of CO₂ over a Rice Husk Ash Supported Nickel Catalyst Prepared by Deposition-Precipitation. *Industrial & Engineering Chemistry Research*, 1998. 37(10): p. 3838-3845.

208. Chang, F.-W., M.-T. Tsay, and S.-P. Liang, Hydrogenation of CO₂ over nickel catalysts supported on rice husk ash prepared by ion exchange. *Applied Catalysis A: General*, 2001. 209(1-2): p. 217-227.
209. Ocampo, F., Développement de catalyseurs pour la réaction de méthanation du dioxyde de carbone. Université de Strasbourg, 2011.
210. Pan, Q., et al., In situ FTIR spectroscopic study of the CO₂ methanation mechanism on Ni/Ce_{0.5}Zr_{0.5}O₂. *Catalysis Science & Technology*, 2014. 4(2): p. 502-509.
211. Dong, W.-S., et al., Methane reforming over Ni/Ce-ZrO₂ catalysts: effect of nickel content. *Applied Catalysis A: General*, 2002. 226(1-2): p. 63-72.
212. Vesselli, E., et al., Carbon Dioxide Hydrogenation on Ni(110). *Journal of the American Chemical Society*, 2008. 130(34): p. 11417-11422.
213. Amenomiya, Y., Active sites of solid acidic catalysts. *Journal of Catalysis*, 1979. 57(1): p. 64-71.
214. Carvill, B.T., et al., Sorption-enhanced reaction process. *AIChE Journal*, 1996. 42(10): p. 2765-2772.
215. Habazaki, H., et al., Co-methanation of carbon monoxide and carbon dioxide on supported nickel and cobalt catalysts prepared from amorphous alloys. *Applied Catalysis A: General*, 1998. 172(1): p. 131-140.
216. A. Borgschulte, N.G., B. Probst, R. Suter, E. Callini, D. Ferri, Y. Arroyo, R. Erni, H. Geerlings, A. Züttel, Sorption enhanced CO₂ methanation. *Physical Chemistry Chemical Physics*, 2013. 15: p. 9620-9625.
217. Sadek, S.E., R.G. Fax, and M. Hurwitz, The Influence of Electric Fields on Convective Heat and Mass Transfer from a Horizontal Surface under Forced Convection. *Journal of Heat Transfer*, 1972. 94(2): p. 144-148.
218. Kulacki, F.A. and J.A. Daumenmier, A preliminary study of electrohydrodynamic augmented baking. *Journal of Electrostatics*, 1978. 5: p. 325-336.
219. Someshwar, A.V. and D.L. Peshori, Corona Discharge Effects In Gas-Solid Adsorption: Water Vapor On Silica Gel And Fly Ash. *Chemical Engineering Communications*, 1987. 50(1-6): p. 331-345.
220. Yamamoto, T., et al., Water vapor desorption and adsorbent regeneration for air conditioning unit using pulsed corona plasma. *Journal of Electrostatics*, 2007. 65(4): p. 221-227.
221. E.N. Eremin, A.N.B., *Russian Journal of Physical Chemistry*, 1962. 36: p. 1266.
222. Eremin, E.N., *Russian Journal of Physical Chemistry*, 1974. 48: p. 1229.
223. E.N. Eremin, V.L.S., *Russian Journal of Physical Chemistry*, 1975. 49: p. 587.
224. Rapakoulias, D., S. Cavadias, and J. Amouroux, Processus catalytiques dans un réacteur à plasma hors d'équilibre II. Fixation de l'azote dans le système N₂-O₂. *Rev. Phys. Appl. (Paris)*, 1980. 15(7): p. 1261-1265.
225. Gicquel, A., S. Cavadias, and J. Amouroux, Heterogeneous catalysis in low-pressure plasmas. *Journal of Physics D: Applied Physics*, 1986. 19(11): p. 2013.
226. Li, R., et al., Plasma catalysis for CO₂ decomposition by using different dielectric materials. *Fuel Processing Technology*, 2006. 87(7): p. 617-622.
227. Joëlle, M., "Carbon dioxide Coordination Chemistry and Reactivity of Coordinated CO₂" in *Carbon Dioxide as a Feedstock*. in: Michelele Aresta, W.-V.V.G.C. KGaA (Eds.), 2010.
228. Cavani, F., F. Trifirò, and A. Vaccari, Hydrotalcite-type anionic clays: Preparation, properties and applications. *Catalysis Today*, 1991. 11(2): p. 173-301.

229. Evans, D.G. and R.C.T. Slade, Structural Aspects of Layered Double Hydroxides, in Layered Double Hydroxides, X. Duan and D.G. Evans, Editors. 2006, Springer Berlin Heidelberg: Berlin, Heidelberg. p. 1-87.
230. Rives, V., D. Carriazo, and C. Martín, Heterogeneous Catalysis by Polyoxometalate-Intercalated Layered Double Hydroxides, in Pillared Clays and Related Catalysts, A. Gil, et al., Editors. 2010, Springer New York: New York, NY. p. 319-397.
231. Rives, V., Characterisation of layered double hydroxides and their decomposition products. *Materials Chemistry and Physics*, 2002. 75(1-3): p. 19-25.
232. Daza, C.E., et al., CO₂ reforming of methane over Ni/Mg/Al/Ce mixed oxides. *Catalysis Today*, 2008. 133-135: p. 357-366.
233. Li, C. and Y.-W. Chen, Temperature-programmed-reduction studies of nickel oxide/alumina catalysts: effects of the preparation method. *Thermochimica Acta*, 1995. 256(2): p. 457-465.
234. Mile, B., et al., The location of nickel oxide and nickel in silica-supported catalysts: Two forms of "NiO" and the assignment of temperature-programmed reduction profiles. *Journal of Catalysis*, 1988. 114(2): p. 217-229.
235. Di Cosimo, J.I., et al., Structure and Surface and Catalytic Properties of Mg-Al Basic Oxides. *Journal of Catalysis*, 1998. 178(2): p. 499-510.
236. Gac, W., Acid-base properties of Ni-MgO-Al₂O₃ materials. *Applied Surface Science*, 2011. 257(7): p. 2875-2880.
237. Toemen, S., W.A.W. Abu Bakar, and R. Ali, Effect of ceria and strontia over Ru/Mn/Al₂O₃ catalyst: Catalytic methanation, physicochemical and mechanistic studies. *Journal of CO₂ Utilization*, 2016. 13: p. 38-49.
238. Leofanti, G., et al., Catalyst characterization: characterization techniques. *Catalysis Today*, 1997. 34(3): p. 307-327.
239. Albarazi, A., Development of Ni-based catalysts for methane dry reforming application. Univesite Pierre et Marie Curie, Paris, France, 2013.
240. Jellinek, M.H. and I. Fankuchen, The Application of X-Ray Diffraction to the Study of Solid Catalysts, in *Advances in Catalysis*, V.I.K. W.G. Frankenburg and E.K. Rideal, Editors. 1948, Academic Press. p. 257-289.
241. Smart L, M.E., *Solid state chemistry: an introduction*. 4. ed. Boca Raton: CRC Press, 2012.
242. http://www.wikiwand.com/en/X-ray_crystallography. 15/03/2016.
243. Datye, A.K. and D.J. Smith, The Study of Heterogeneous Catalysts by High-Resolution Transmission Electron MicroscopY. *Catalysis Reviews*, 1992. 34(1-2): p. 129-178.

General Conclusions and Perspectives

The studies performed in this thesis were mainly focused on the interactions between a DBD plasma discharge and Ni-Ce_xZr_{1-x}O₂ catalysts in a combined system for the hydrogenation of carbon dioxide (CO₂) into methane (methanation) at atmospheric pressure and low temperatures.

In the first chapter, information about carbon dioxide valorization processes and the catalytic methanation, as well as the information about catalysis, reactors and reaction mechanisms for CO₂ methanation were described. From the literature review, Ni was identified as the best optional candidate from other catalysts due to its high selectivity for methane production. The role of the support prevails on the choice of the catalyst in order to develop an efficient methanation catalyst, mainly with respect to ensure an enhanced metal dispersion and a long catalyst lifetime. Therefore, ceria-zirconia oxides have been recently considered as promising catalyst supports in the preparation of active and selective catalytic systems for the CO₂ methanation. However, even more in presence of a plasma, the methanation mechanisms are not yet clear as they strongly depend of the nature of catalyst/support used. Nevertheless, two mechanisms were proposed in the literature: one occurs through the formation of CO while the other one occurs through the formation of formate (methanoate) as an intermediate. This chapter gave a short overview of the different types and applications of plasmas as well as the description of the main physical processes occurring during a plasma. Special attention was taken to describe the generation of a Dielectric Barrier Discharge (DBD) plasma and the plasma conditions needed for an efficient dissociation. From the literature review, hybrid plasma-catalyst systems present the advantages and uses of catalyst material when combined with plasma systems. The potential of non-thermal plasma technologies for the methanation of CO₂ has been also described. Non-thermal plasmas exhibit many advantages over conventional catalysis, as they can be generated under ambient conditions (at room temperature). Therefore, the addition of catalyst material may help to increase conversion rate and shift temperature of the process to much lower, leading to a more energy efficient reaction than with plasma alone.

In Chapter 2, information about the experimental setup was presented with a description of the experimental parameters used with/without plasma. In this chapter, the catalysts characterization techniques were described as well as in-situ methods such as Optical Emission Spectroscopy (OES).

Chapter 3 presented a short overview about the CEOPS project and the results obtained in this study. For CO₂ conversion to CH₄, two DBD catalysts 20%Ni-30%Ce/Cs-USY and Ce_{0.9}Zr_{0.1}O₂-15% Ni SBA-15 presents a synergy with a DBD plasma below 200 °C on the CO₂ hydrogenation with a conversion rate about 80 %. For the catalyst 15%Ni-Ce_{0.9}Zr_{0.1}O₂ SBA-15 (IREC), the experiments under adiabatic (120-170 °C, without external heating) and isothermal (220-420 °C with external heating) conditions were performed. The results show a very low (less than 1 %) production of CO for all temperatures except at 420 °C and large amounts of CH₄ and water. It was found that this catalyst is active under adiabatic conditions (120-170 °C, without external heating) in the presence of plasma, producing only CH₄ with conversions ranging from 75 to 90 %. Without plasma and with an external heating up to 170 °C, the Ce_{0.9}Zr_{0.1}O₂-15% Ni catalyst is totally inactive. It was expected an increase of total conversion with the plasma at 250-300 °C but not at 140 °C and without external heating. The experiments were repeated at least 3 times and confirmed the effect of the DBD plasma on the CO₂ conversion at low temperatures. With all catalysts, an increase of the CO₂ total conversion was observed when plasma operates. In addition, with some catalysts, especially those containing Ce, at a low temperature (150 °C) and without external heating, a total conversion ranging between 60 and 70 % was obtained with plasma with a CH₄ selectivity around 100 %.

Chapter 4 presents results obtained during the methanation experiments at atmospheric pressure and low temperatures using a DBD plasma reactor packed with Ni-Ce_xZr_{1-x}O₂ catalysts. Experiments were carried out in the temperature range of 90-420 °C. The obtained results clearly demonstrated that the hybrid plasma-catalytic process is active at low temperatures (<260 °C) on the selective conversion of CO₂ into methane. At low temperatures and in the absence of plasma, the conversions of CO₂ were found to be lower than 15 %, but they were drastically enhanced. However, in the presence of plasma, the conversion was found to reach 80 % at temperatures ranged between 100 and 300 °C, whereas for plasma alone (without catalyst), conversions around 5 % were observed. Almost no difference in the catalytic activity was found for Ni catalysts prepared using different ceria-zirconia supports. On the contrary, in the absence of plasma, the 15NiCZ5842 showed an enhanced methanation activity due to the presence of low and medium strength basicity, combined to a better dispersion of Ni-species on the mixed oxide support at high ZrO₂ contents. As a conclusion, reaction mechanisms of the CO₂ methanation was proposed and discussed. The action of the plasma on the methanation process is especially presented.

Chapter 5 presents the results obtained from the study of the activity of Ceria and Zirconia-promoted Ni-containing hydrotalcite-derived catalysts performed in a hybrid plasma-catalytic process. High methane yields, around 80 %, were measured under hybrid plasma-catalytic conditions, even at low temperatures (110 °C, adiabatic conditions). In the absence of plasma, high CO₂ conversions (>70 %) and methane yields (>70 %) were only observed at temperatures higher than 330 °C. The presence of completely reduced Ni-crystallites (15.2 nm) on the non-promoted catalysts was found to enhance the methanation reaction. In addition, Ce and Zr did not result in an improvement of the catalytic activity.

As a result, a few promising perspectives for future research can be drawn from the present studies performed in this thesis:

- The understanding of the plasma chemistry for the CO₂ methanation reactions in hybrid DBD plasma-catalytic reactors needs to be investigated. Indeed, the reaction mechanisms and kinetics still remain unclear since the chemistry of non-thermal plasmas is very complex. Moreover, the electronic properties of the catalysts, due to the modification of the surface by electrically charges, should also be further studied.
- In situ FT-IR studies on the surface of the catalysts could offer answers in order to understand the detailed reaction mechanisms of CO₂ methanation over the Ni-Ce_xZr_{1-x}O₂ hybrid plasma-catalyst system.
- Mass Spectroscopy could be used in order to validate the proposed set of reaction mechanisms, especially the effect of plasma on water desorption.
- The discharge power of the high voltage generator should be decreased in order to achieve a low energy consumption. This could be achieved through the decrease of the frequency used (to about 2-5 kHz) and/or the discharge voltage (to about 5-10 kV) simultaneously using a pulsed plasma.

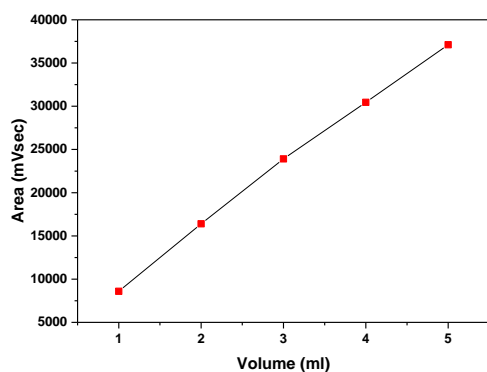
Appendix A

Gas Chromatograph Analysis

Calibration of Gas Chromatograph

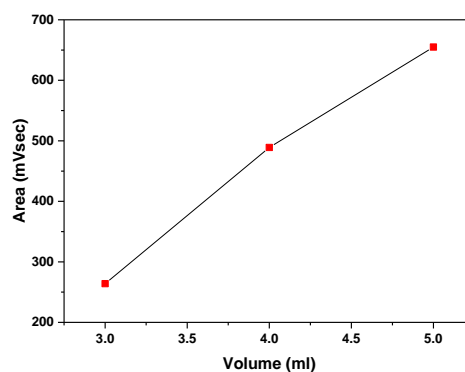
Below shows the results of gas chromatograph calibration in terms of area versus concentration plots for each gas and their corresponding parameters of goodness of fit.

Carbon Dioxide



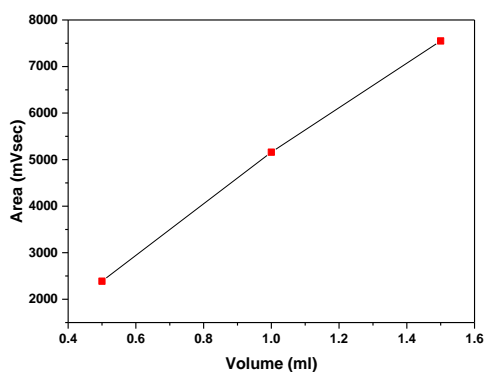
$$Y = aX + b$$
$$a = 7108.2$$
$$b = 1968.4$$
$$R^2 = 0.9984$$
$$R = 0.9992$$

Hydrogen



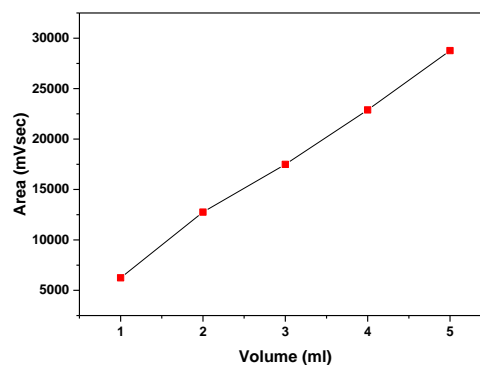
$$Y = aX + b$$
$$a = 195.5$$
$$b = -312.67$$
$$R^2 = 0.9925$$
$$R = 0.9962$$

Air (O₂ + N₂)



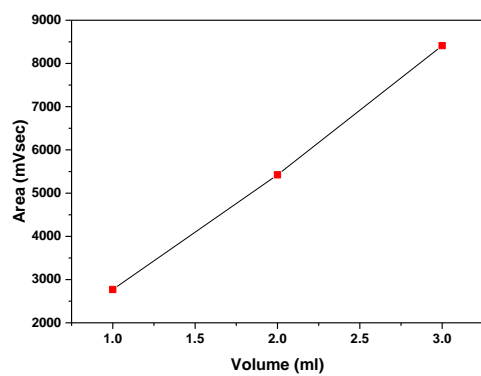
$$Y = aX + b$$
$$a = 5160.7$$
$$b = -127.8$$
$$R^2 = 0.9982$$
$$R = 0.9991$$

Methane



$$Y = aX + b$$
$$a = 5518.6$$
$$b = 1072.4$$
$$R^2 = 0.9979$$
$$R = 0.9989$$

Carbon Monoxide



$$Y = aX + b$$

$$a = 2821$$

$$b = -106.33$$

$$R^2 = 0.9988$$

$$R = 0.9994$$

Appendix B

To characterize the catalysts the following techniques were used:

- **Hydrogen Temperature Programmed Reduction (H₂-TPR)**

This technique leads to identification of the different species present during the reduction [238]. The amount of H₂ consumed was well correlated with the number of reacting sites existing in the catalyst.

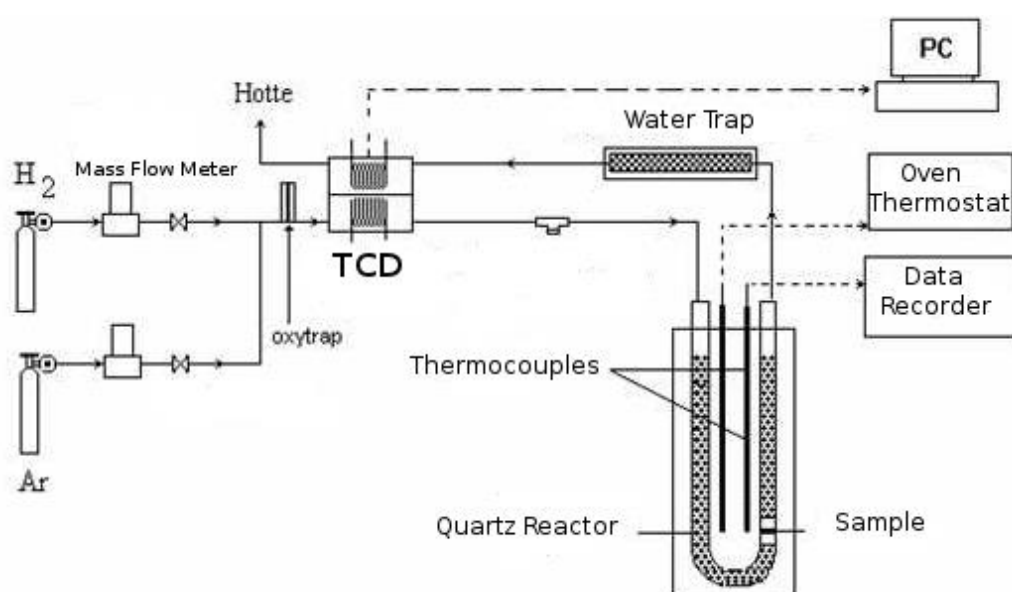


Fig. 100. Schematic diagram of TPR instrument (BEL Japan BELCAT-M) equipped with TCD detector [239].

- **X-Ray Diffraction (XRD)**

X-ray diffraction is a technique used to determine the bulk structure and crystalline structure composition of the catalysts surface [240], where a beam of X-rays strikes a crystal and scatters into many various directions. X-rays of various wavelength are made when electrons return to vacancies in the deepest shell by bombarding copper with electrons. These vacancies are generated by electron excitation. The X-ray wavelength depends on from which shell the electron descends back to the deepest shell. For radiation cleaning a nickel filter is

used to get uniform $K\alpha$ radiation with a wavelength of 0.15418 nm. The distance between crystalline atoms is in the same range as this wavelength [241].

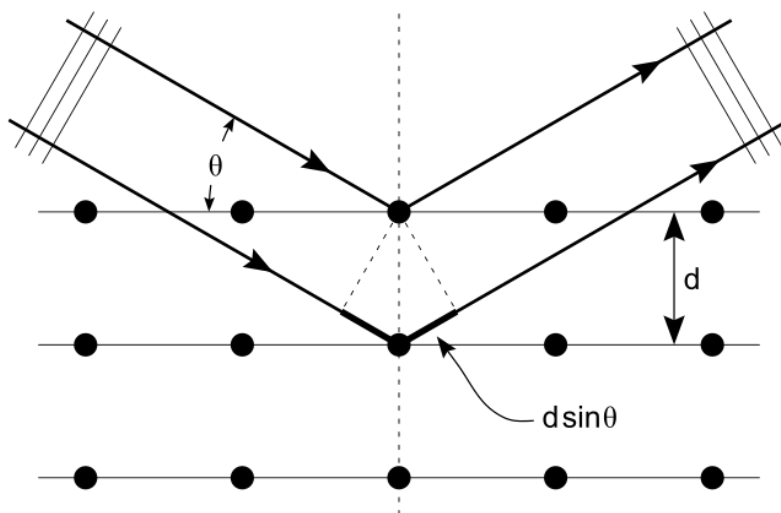


Fig. 101. Illustration of mechanism of X-Ray diffraction on atoms array [242].

At specific angles the crystalline powder diffract the X-ray in such a manner that constructive interference gives rise to a diffraction pattern for the sample. The scattering is spherical and each peak corresponds to a single 2θ angle. The peaks contain information about the distance between atomic planes named miller indices (hkl) in the crystal structure.

The Bragg equation (1) is used to establish the crystal structure of the catalyst and to characterise active metals present on the support.

$$n \lambda = 2 * d_{hkl} * \sin \theta_{hkl} \quad (1)$$

d_{hkl} - distance between crystal planes,

λ - fixed X-ray wavelength,

n - any integer,

θ_{hkl} - Bragg angles reflecting atom planes.

Diffraction patterns are usually presented as a plot of intensity versus 2θ . The smallest Bragg angle to the left in the plot is caused by the largest d_{hkl} spacing. X-ray diffraction comparison of various catalysts with each other and achievable standardized diffraction pattern ensure important information about the sample preparation and metal-support interaction. It is a fast analysis technique that contributes to better understanding of the catalyst.

- **Brunauer-Emmett-Teller (BET) Surface Area**

Brunauer, Emmett and Teller (BET) once derived a method to measure specific surface area (SSA). Their method is based on N_2 physisorption which take place on almost all kind of surfaces at 77 K and low pressure. At the beginning, a monolayer of adsorbed molecules is assumed to be formed when N_2 gas is added. The instrument device inserts measured parameters in the BET equation (2) and extrapolates the slope to the intercept, which contains the monolayer volume (V_m) term. The surface area can be calculated according to equation (3) where A_m is the area of a nitrogen molecule and N_A/V_A is Avogadro's number per cubic meter. Specific surface area is calculated by dividing SA with the weight of the catalyst.

$$\frac{p}{V(p_0 - p_1)} = \frac{1}{V_m * C} + \frac{(C - 1)}{V_m * C} * \frac{p}{p_0} \quad (2)$$

$$SA = V_m * A_m * \frac{N_A}{V_A} \quad (3)$$

- **High-Resolution Transmission Electron Microscopy (HRTEM)**

Electron microscopy (EM) is considered as a developed technique which uses a beam of electrons to examine the solid catalyst morphology and particles sizes. Transmission electron microscopy (TEM) is the modes of electron microscopy, used in catalysts characterization, to give a direct view of the solid under study, and is good for imaging catalyst particles with nanometer dimensions (down to 0.1 nm).

High-resolution TEM (HRTEM) facilitates imaging individual planes in crystalline particles, to provide more detailed structural information on the surface of the catalysts [243].

Appendix C

Results obtained for all tested catalysts from CEOPS project:

Catalyst Name	Support	Active phase	Promotor	WITHOUT PLASMA					WITH PLASMA				
				Temperature (°C)	CO ₂ Conversion (%)	CO Yield (%)	CH ₄ Yield (%)	CH ₄ Selectivity (%)	Temperature (°C)	CO ₂ Conversion (%)	CO Yield (%)	CH ₄ Yield (%)	CH ₄ Selectivity (%)
5%Ni 3%Ce IST		5% Ni	3% Ce	20	0	0	0	0	20 PL	0	0	0	0
				100	0	0	0	0	100 PL	0	0	0	0
				160	0	0	0	0	160 PL	0	0	0	0
				220	0	0	0	0	220 PL	0.96	0	0.96	100
				320	4.12	3.25	0.88	21.25	320 PL	11.52	9.00	2.53	21.92
				370	16.79	6.88	9.91	59.02	370 PL	39.16	20.48	18.68	47.70
				420	31.46	14.62	16.84	53.52	420 PL	69.76	41.20	28.56	40.95
5%Ni Ce _{0.8} Zr _{0.2} O ₂ IREC	SBA15	5% Ni	Ce _{0.8} Zr _{0.2} O ₂	20	0	0	0	0	70 PL (adiabatic conditions)	14.42	7.36	7.06	48.95
				370	39.28	10.97	28.31	72.07	370 PL	50.11	30.85	19.26	38.44
				420	42.03	17.85	24.19	57.54	420 PL	49.34	33.57	15.76	31.95
				20	0	0	0	0					

5%Ni Ce_{0.9}Zr_{0.1} O₂ IREC	SBA15	5% Ni	Ce_{0.9}Zr_{0.1} O₂	80	0	0	0	0	80 PL	5.78	4.68	1.10	19.04
				100	0	0	0	0	100 PL	8.56	5.26	3.30	38.51
				110	0	0	0	0	110 PL (adiabatic conditions)	33.36	10.39	22.98	68.87
				140	0	0	0	0	140 PL (adiabatic conditions)	77.58	10.37	67.21	86.63
				160	0	0	0	0	160 PL (adiabatic conditions)	76.66	9.48	67.18	87.63
				180	0	0	0	0	180 PL	38.52	9.07	29.44	76.44
				200	1.46	0	1.46	100	200 PL	53.27	12.16	41.12	77.18
				220	2.73	0	2.73	100	220 PL	41.42	10.73	30.69	74.09
				240	8.49	1.30	7.18	84.63	240 PL	57.65	11.97	45.68	79.23
				260	21.87	3.14	18.73	85.66	260 PL	60.12	11.84	48.28	80.31
				280	33.93	5.60	28.33	83.51	280 PL	56.54	14.67	41.87	74.06
				320	38.00	6.76	31.25	82.22	320 PL	82.60	22.55	60.05	72.70
				370	63.82	14.31	49.51	77.57	370 PL	89.92	22.24	67.68	75.26
				420	72.09	19.83	52.26	72.50	420 PL	91.18	30.42	60.76	66.63

5%Ni CeO ₂ IREC	SBA15	5% Ni	CeO ₂	20	0	0	0	0	100 PL (adiabatic conditions)	74.72	14.59	60.14	80.48
				220	5.65	3.92	1.73	30.67	220 PL	62.95	15.96	46.99	74.64
				280	22.53	3.84	18.69	82.96	280 PL	75.63	18.12	57.51	76.04
				320	79.39	8.59	70.80	89.19	320 PL	85.69	11.64	74.05	86.41
				370	79.27	16.48	62.79	79.21	370 PL	86.22	20.34	65.89	76.41
				420	83.01	20.25	62.76	75.61	420 PL	87.30	33.95	53.35	61.11
5%Ni HNaUSY IST	HNaUS Y	5% Ni		20	0	0	0	0	20 PL	0	0	0	0
				320	2.11	1.51	0.60	28.63	320 PL	18.70	14.61	4.10	21.91
				370	10.12	7.66	2.45	24.26	370 PL	56.15	41.24	14.91	26.56
				420	24.45	18.75	5.71	23.34	420 PL	73.49	47.14	26.35	35.85
				500	58.68	49.40	9.28	15.82	500 PL	79.66	70.36	9.30	11.68
7%Mg 5%Ni HNaUSY IST	HNaUS Y	5% Ni	7% Mg	20	0	0	0	0	20 PL	0	0	0	0
				320	6.06	4.57	1.50	24.68	320 PL	38.43	29.17	9.26	24.10
				370	20.04	15.44	4.60	22.94	370 PL	50.34	36.64	13.70	27.22
				420	44.70	34.47	10.23	22.88	420 PL	76.04	56.78	19.26	25.33
				20	0	0	0	0	20 PL (adiabatic conditions)	9.24	9.24	0	0

15%Ce 14%Ni HNaUSY IST	HNaUS Y	14% Ni	15% Ce	200		0	0	0	200 PL	2.32	1.08	1.24	53.51
				320	13.86	3.14	10.72	77.34	320 PL	48.36	11.64	36.73	75.94
				370	38.16	9.12	29.05	76.11	370 PL	70.26	12.61	57.66	82.06
				420	61.64	17.19	44.46	72.12	420 PL	75.08	18.57	56.52	75.27
15%Ni Ce_{0.9}Zr_{0.1} O₂ SBA15 IREC	SBA15	15% Ni	Ce_{0.9}Zr_{0.1} O₂	20	0	0	0	0	140 PL (adiabatic conditions)	86.67	0	86.67	100
				140	0	0	0	0					
				150	0	0	0	0	150 PL (adiabatic conditions)	92.76	0	92.76	100
				160	0	0	0	0	160 PL (adiabatic conditions)	90.60	0	90.60	100
									160 PL	82.12	0	82.12	100
				220	8.80	0	8.80	100	220 PL	96.62	0	96.62	100
				320	75.36	0.48	74.88	99.36	320 PL	88.81	0.58	88.22	99.34
				370	78.34	1.15	77.19	98.53	370 PL	81.64	4.13	77.51	94.94
420	71.33	2.20	69.13	96.91	420 PL	69.83	22.09	47.74	68.37				
Ni-Al₂O₃ from CEA	Al₂O₃	Ni		20	0	0	0	0	20 PL	0	0	0	0
			150	0	0	0	0	150 PL	5.35	3.01	2.33	43.68	
			220	0.66	0	0.66	100	220 PL	18.97	3.55	15.42	81.29	

				320	32.12	6.58	25.55	79.53	320 PL	74.83	3.47	71.36	95.36
				370	67.53	2.65	64.88	96.07	370 PL	71.64	4.23	67.41	94.09
15% Ni Ce _{0.9} Zr _{0.1} O ₂ SBA15 IREC sample without removal of tamplate	SBA15	15% Ni	Ce _{0.9} Zr _{0.1} O ₂	20	0	0	0	0	20 PL (adiabatic conditions)	12.26	7.90	4.36	35.54
				140	0	0	0	0	140 PL	0.79	0.79	0	0
				170	0	0	0	0	170 PL	3.11	3.11	0	0
				220	0	0	0	0	220 PL	6.72	4.89	1.84	27.33
				320	5.09	1.75	3.34	65.64	320 PL	37.18	19.65	17.54	47.16
				370	16.33	7.73	8.60	52.68	370 P L	62.89	32.86	30.04	47.76
				420	31.96	19.39	12.57	39.32	420P L	88.69	23.78	64.91	73.19
15% Ni Ce _{0.9} Zr _{0.1} O ₂ KIT6 IREC sample without removal of tamplate	KIT6	15% Ni	Ce _{0.9} Zr _{0.1} O ₂	20	0	0	0	0	150 PL (adiabatic conditions)	7.58	4.83	2.75	36.33
				320	32.46	4.19	28.27	87.09	320 PL	62.94	10.56	52.38	83.22
				20	0	0	0	0	120 PL (adiabatic conditions)	61.93	6.87	55.06	88.91

20%Ni-30%Ce/Cs-USY IST	USY IST	20% Ni	30% Ce/Cs						140 PL (adiabatic conditions)	67.47	4.33	63.13	93.58
				220	1.77	0	1.77	100	220 PL	60.47	3.75	56.72	93.80
				320	60.17	3.87	56.30	93.56	320 PL	61.36	14.30	47.06	76.70
				370	60.40	5.94	54.46	90.17	370 PL	62.52	21.65	40.87	65.38
				420	60.25	11.97	48.27	80.13	420 PL	68.63	41.01	27.62	40.24
30% from sample 5 in alumina Pural SB IST	alumina Pural SB			20	0	0	0	0	160 PL (adiabatic conditions)	6.06	2.00	4.05	66.91
				220	0	0	0	0	220 PL	4.07	0.79	3.28	80.59
				320	0	0	0	0	320 PL	24.11	5.82	18.29	75.85
				370	6.22	1.25	4.97	79.91	370 PL	58.72	16.98	41.74	71.08
ISTCEA01 in alumina Pural SB	alumina Pural SB	20% Ni	30% Ce	20	0.00	0.00	0.00	0.00	120 PL (adiabatic conditions)	3.98	2.47	1.50	37.78
				220	0.00	0.00	0.00	0.00	220 PL	14.60	2.38	12.22	83.71
				320	14.45	0.00	14.45	100.00	320 PL	61.45	2.88	58.57	95.31
IBERCA T 10%Ni	IBERC AT Support	10% Ni	20% Ce	20	0.00	0.00	0.00	0.00	48 PL (adiabatic conditions)	0.00	0.00	0.00	0.00

20%Ce				220	0.00	0.00	0.00	0.00	220 PL	0.00	0.00	0.00	0.00
				320	5.45	1.41	4.04	74.15	320 PL	16.09	4.94	11.15	69.32
				370	36.30	2.95	33.35	91.87	370pl	55.23	4.22	51.01	92.35
				420	58.91	5.10	53.81	91.34	420PL	69.54	3.85	65.68	94.46
CEOPS 28 La	$Ce_{0.9}Zr_{0.1}O_2$	15%Ni	1% La	220	0.00	0.00	0.00	0.00	220 (adiabatic conditions)	69.18	7.11	62.07	89.72
				320	7.90	4.39	3.51	44.40	320	71.14	6.91	64.23	90.29
				370	42.45	6.34	36.11	85.07	370	69.8	10.41	59.39	85.09
				420	68.12	2.76	65.36	95.95	420	68.34	17.31	51.04	74.68
IBERCA T 2	IBERC AT Support	10% Ni	20% Ce 5% Zr	220	0.00	0.00	0.00	0.00	220 (adiabatic conditions)	61.18	19.98	41.2	67.34
				320	1.6	0.00	1.6	100	320	66.56	11.51	55.05	82.7
				370	5.6	0.00	5.6	100	370	66.1	14.44	51.65	78.15
				420	15.6	3.2	12.3	79.2	420	65.6	20.57	45.02	68.63

Appendix D

Summary of results from Figure 86.

NiCZ5842 (0.3 g, volume 0.23 cm³)									
Temperature (°C)	Frequency (kHz)	Voltage (kV)	Power (W)	CO₂ Conversion (%)	CO Yield (%)	CH₄ Yield (%)	CH₄ Selectivity (%)	Specific Input energy (power/flow rate) (kJ/L)	Power density(power/volume) (W/cm³)
28	2	15	0.2	0	0	0	0	0.06	0.9
34	5	15	0.6	0	0	0	0	0.18	2.6
70	41	11	2	0	0	0	0	0.6	8.7
110	41	13	4	3	0	3	100	1.2	17.4
160	41	15	7	82.61	0.7	81.9	99.15	2.1	30.4
210	41	18	13	62.76	29.33	33.43	53.27	3.9	56.5

Summary of results from Figure 87.

NiCZ5842 (0.3 g, volume 0.23 cm³) Temperature 160 °C									
Frequency (kHz)	Voltage (kV)	Power (W)	CO₂ Conversion (%)	CO Yield (%)	CH₄ Yield (%)	CH₄ Selectivity (%)	Specific Input energy (power/flow rate) (kJ/L)	Power density(power/volume) (W/cm³)	
5	15	1	0	0	0	0	0.3	4.3	
41	13	4	1.48	0	1.48	100	1.2	17.4	
41	15	7	80.65	0.26	80.39	99.68	2.1	30.4	
41	18	13	61.73	15.95	45.78	74.17	3.9	56.5	

Abstract

The limited resources of oil and natural gas, together with an increasing energy demand, forces us to seek more and more efficient and cleaner energy production alternatives. Hydrogen has been recently considered as a promising energy carrier. However, there are several inherent problems to the utilization of H₂, from its transportation to its distribution. Transformation of the H₂ molecule by fixing into a carbon-containing compound, i.e. CH₄, will offer the possibility of using the conventional transportation network. Indeed, the Sabatier reaction, which is highly exothermic, involves the reaction of carbon dioxide and hydrogen gas in order to produce methane and water. This process, called methanation, represents a feasible approach contributing to the reduction of the CO₂ emissions in our atmosphere, through a closed carbon cycle involving the valorization of CO₂, i.e. from capture. However, below a temperature of 250 °C, the conversion becomes practically close to 0 %, whereas at higher temperatures, i.e., (>300 °C), the co-existence of secondary reactions favours the formation of CO and H₂. This is the reason why new catalysts and process conditions are continuously being investigated in order to maximize the methane selectivity at low reaction temperatures at atmospheric pressure. Therefore, by using catalysts combined to Dielectric Barrier Discharge plasmas (DBD), the activation of the methanation reaction can be enhanced and overcome the drawbacks of existing conventional processes. Several Ni-containing catalysts were prepared using various ceria-zirconia oxides as supports, with different Ce/Zr ratios. The results obtained in the adiabatic conditions at low temperatures (ranging between 100-150 °C), in the presence of catalysts activated by plasma, are promising. Indeed, the conversion of CO₂ to CH₄ is about 85 % with a selectivity close to 100 %. The same conversion in the absence of the plasma activation of the catalyst is observed at 350 °C. At low temperatures (120-150 °C) and without plasma, conversion is almost close to zero. This low consumption energy system helps reduce the cost of production of synthetic methane together with an extended life of the catalyst.

Résumé

Combiné à une demande en énergie croissante, les ressources limitées de pétrole et de gaz naturel nous obligent à rechercher des alternatives plus propres et de plus en plus efficaces pour la production d'énergie. L'hydrogène (H₂) est considéré comme un vecteur énergétique prometteur. Cependant, il existe plusieurs problèmes liés à l'utilisation de H₂, depuis son transport jusqu'à sa distribution. La transformation de la molécule de H₂ peut s'effectuer par la synthèse d'un composé contenant du carbone, à savoir du méthane (CH₄), offrant ainsi la possibilité d'utiliser le réseau de transport existante. En effet, la réaction de Sabatier, qui est fortement exothermique, implique la réaction du dioxyde de carbone (CO₂) et du dihydrogène afin de produire du méthane et de l'eau. Ce procédé, appelé méthanation, représente une approche réalisable contribuant à la réduction des émissions de CO₂ dans l'atmosphère, à travers un cycle fermé du carbone impliquant la valorisation du CO₂. Cependant, en dessous d'une température de 200 °C, la conversion devient proche de zéro, tandis qu'à des températures plus élevés (>300 °C), des réactions secondaires favorisant la formation du CO et d'H₂ apparaissent. C'est une des raisons pour laquelle de nouveaux types de catalyseurs doivent être étudiés dans le but de maximiser la sélectivité du méthane à des basses températures et à pression atmosphérique. Par conséquent, en utilisant des catalyseurs associés aux plasmas DBD, l'activation de la réaction de méthanation peut ainsi être améliorée. Plusieurs catalyseurs contenant du Ni ont donc été synthétisés en utilisant différents oxydes de Ce-Zr en tant que supports, avec un ratio Ce-Zr variable. Les résultats obtenus dans des conditions adiabatiques à basses températures (comprises entre 120 et 150 °C), en présence de catalyseurs activés par plasma, sont prometteurs. La conversion du CO₂ en CH₄ est d'environ 85 % avec une sélectivité proche de 100 %. En l'absence de catalyseurs activés par plasma, cette même conversion est observée à 350 °C, tandis qu'à basses températures et sans plasma, celle-ci est presque nulle. Ce système à basse consommation d'énergie permet donc de diminuer le coût de production du méthane synthétique avec une durée de vie du catalyseur prolongée.